The Sheer Stress of Shear Stress
Responses of the Vascular Wall to a Haemodynamic Force

Caroline (Ka Lai) Cheng

1

The Sheer Stress of Shear Stress
Responses of the Vascular Wall to a Haemodynamic Force

De Zware Spanning van Afschuifspanning
Responsen van de Vaatwand op een Haemodynamische Kracht

Thesis

To obtain the degree of Doctor from the
Erasmus University Rotterdam
By command of the Rector Magnificus

Prof.dr. S.W.J. Lamberts

And according to the decision of the Doctoral Board
The public defense shall be held on

Wednesday 1th February 2006 at 11.45 hours

by

Ka Lai Cheng
Born at Hong Kong - China

Doctoral Committee

Promotor:	Prof.dr.ir. A.F.W. van der Steen
Copromotors:	Dr. R. Krams
	Dr. M.P.G. de Crom
Other members:	Prof.dr. F.G. Grosveld
	Prof.dr. R.E. Poelmann
	Prof.dr. M.L. Simoons

Say if I only could
I would make a deal with God
And get Him to swap our places

Be running up that road
Be running up that hill
With no problems

-Kate Bush-

To mom, dad, Kawah, Wing and Poeki

Thank you

Contents:

Chapter 1: Introduction

1.1 Background

In the Western world, approximately one third of all disease-related mortality is directly or indirectly related to atherosclerosis. Intense research over several decades has identified several risk factors in relation to the progression of the disease. Most if not all risk factors have in common that they act systemically, while it is a well-known fact that atherosclerosis manifests itself at certain predilection sites, like side branches and curvatures [1-4]. Consequently, an as yet unexplained factor must be involved in the process.

Wall shear stress or shear stress is defined as the tractive force per unit area applied by the flowing blood on the endothelium. Several studies provided evidence for a role of this haemodynamic force as the factor linking atherosclerotic plaque formation to these predilection sites. This force is transmitted from sensors located at the cell membrane to the cell nucleus, affecting the gene expression, cellular metabolism, and cellular morphology [5,6].

In most studies, association of shear stress with atherosclerosis has been limited to investigations *in vitro* or in post mortem human material. Our group has developed a novel method based on angiography, Intra Vascular Ultrasound (IVUS), and Computational Fluid Dynamics (CFD), to calculate shear stress *in vivo*. Using this method, we could show that in curved atherosclerotic coronary arteries of living humans, plaque is located predominantly in the inner curvature where local shear stress is low [7-13]. In several other studies, it could also be shown that low shear stress regions were coupled to in stent restenosis and vascular remodeling after balloon angioplasty [9,11-13]. In addition, a more recent study indicated that local increase of shear stress (by instrumentation of an intra-vascular device) in the stented areas reduced in stent restenosis, independent of other confounding factors, such as injury and inflammation [14].

Although these results clearly indicate an important modulating role of shear stress in plaque progression, the precise relation between changes in the shear stress field and the underlying mechanism in atherosclerosis is currently unknown. This thesis will discuss some of the profound effects of shear stress on the biology of the vascular wall related to the development of atherosclerosis. The studies described in this thesis are all performed using a newly in-house developed device that can induce alterations in shear stress *in vivo*, thereby providing an opportunity to examine the effects of shear stress in a cause-effective manner. The development and the validation of this device will be further discussed in the next chapters. In this first chapter, a short outline of the process of atherosclerosis is given, followed by an overview of the different conditions of the shear stress that relates this haemodynamic force to this disease. Two (related) mechanisms for coupling shear stress to the occurrence of predilection sites in atherosclerosis are also presented. We will discuss the effect of different shear stress conditions on the expression of genes that influence vascular biology, and the effect of different shear stress parameters on triggering inflammation during the development of athersclerosis. The definition of the problem, the

hypothesis, the aims of the research and the outline of this thesis, are also described in this chapter.

1.2 Atherosclerosis

Atherosclerosis is a degenerative disease of large and medium sized arteries, characterized by lipid accumulation and collagen deposition. It is known as a major cause of ischaemia (e.g. myocardial infarction), leading to the high morbidity and mortality rate in cardiovascular disease. The exact initiator is unclear, but a number of risk factors (e.g. age, smoking, high levels of plasma cholesterol, diabetes mellitus, and hypertension) and inflammation are strongly associated to the initiation of atherosclerosis. It is conceivable that all these factors contribute to the onset and the progression of the disease, mutually amplifying the effects via triggering of the immune response. However, as stated previously, these *systemic* risk factors cannot explain the *locality* of the onset of the disease. It is also known that atherogenesis (i.e. development of atherosclerosis) starts at the level of the endothelial cells (ECs). Damage or stimulation of the endothelium by components induced by risk factors, such as nicotine by smoking, activates the ECs to express pro-inflammatory molecules, attracting leukocytes (mainly monocytes) into the area between the endothelium and internal elastic lamina (i.e. intima). The permeability of the endothelium is also affected, resulting in the increased influx of macro-molecules including low density lipoproteins (LDL) that will become trapped in the vessel wall as they bind to the extra cellular matrix. Oxidation of these bound LDL particles (oxLDL) by superoxides, hydroxyl radicals or peroxynitrites provide yet another stimulus to boost the already on-going inflammatory response of the endothelial cells. The oxLDL is scavenged by macrophages via scavenger receptors such as CD36 and Scavenger Receptor A (SRA), activating them to become lipid-laden cells (foam cells). Following the by the American Heart Association (AHA) provided histological classifications of atherosclerotic lesions [15], this initial pathology can be classified as Type I (initial) lesions, consisting mainly of isolated macrophages and foam cells located in the intima. As the lesion further progresses into Type II (fatty streaks) and Type III (intermediate) lesions, multiple layers of macrophages and foam cells are formed, and continuing lipid accumulation in the vessel wall result in the accumulation of lipid droplets outside the cells, eventually leading to the formation of a lipid core. The lipid core is an extensive accumulation of extracellular lipid localized in the intima that characterizes Type IV (atheroma) lesions. In type II lesions, vascular smooth muscle cells (VSMCs) also start to migrate into the intima in response to chemoattractants secreted by activated macrophages and ECs. In addition, proliferation of these VSMCs due to stimulation by secreted growth factors

and cytokines (e.g. tumor growth factor-β (TGF-β), interleukin 1 (IL1), and tumor necrosis factor α (TNF-α)) contributes to the progression of the disease. The Type IV is the first lesion considered advanced by histological criteria, whereas the term early lesions is also used for Type I and II lesions.

As atherosclerosis continues to develop, disarrangement of intimal structure by the lipid core is followed by thickening of the intima, caused by increased formation of fibrous connective tissue layers that consists of VSMCs and collagen. This contributes to the progression of the plaques into Type V lesions. Three subtypes of Type V lesions can be distinguished: Type Va (fibroatheroma) lesions are characterized by the presence of these fibrous layers, also called the fibrous cap, covering to one or more lipid cores. Type Vb (calcific) lesions show extended calcification in the intima, and Type Vc (fibrotic) lesions are characterized by fibrous tissue layers without or with only minimal lipid (no core) and minimal or no calcium accumulation. Later adjustments to the AHA classification classify Type Vb and Type Vc as possible later phases of Type IV-VI lesions as a result of plaque stabilization due to regression of the lipid component. Therefore, Type Vb is also listed after the update as type VII and Type Vc as Type VIII lesions [16].

In addition to Type IV, Type V lesions are also considered advanced lesions. Type IV and type V lesions in which disruptions of the lesion surface, haemorrhage, or thrombotic deposition have occurred are classified as Type VI or complicated lesions. Different subtypes of Type VI lesions can also be distinguished: Type VIa are characterized by disruption of the plaque surface, Type VIb by the occurrence of hemorrhage, and type VIc by thrombosis. Type VIabc indicates the presence of all three of these features. From all these lesion types, mainly Type V and VI lesions are clinically relevant: Type VI lesions often obstruct the vessel lumen (i.e. lumen stenosis), causing ischaemia in the down stream tissues as a result of the diminished blood flow. This could lead to serious clinical syndromes of cardiovascular disease, such as myocardial infarction (heart attack), pulmonary embolism (blockage in an artery of the lungs), and stroke (blockage in an artery of the brain). Type V lesions may be silent or with clinical complications, depending on the degree of the obstruction. Depending on its morphology and its composition, the atherosclerotic lesion can be more or less susceptible to the disruption of the plaque surface that could lead to acute vessel closure. This pathological event is called plaque rupture, and is often considered as the onset to the progression of plaques to a Type VI lesion. The most common specific type of plaque susceptible to rupture is the inflamed thin cap fibro-atheroma (TCFA), which is a Type Va lesion with increased inflammation and a thin fibrous cap covering a lipid-rich, necrotic core. These lesions contain little VSMCs and collagen, the two main stabilizing components of an atherosclerotic lesion. TCFAs are considered vulnerable or high risk plaques, a term used to describe atherosclerotic lesions that are at increased risk of thrombosis and rapid stenosis

progression. Two additional types of atherosclerotic lesions are also considered as vulnerable plaques: The eroded plaque, which is often a Type Vc (VII) lesion with loss and/or dysfunction of the lumenal endothelial cells leading to thrombosis, and lesions with calcified nodules, which are type Vb lesions with heavy calcifications and loss and/or dysfunction of endothelial cells covering the calcified nodules, resulting in loss of the fibrous cap. In relation to these three types of vulnerable lesions, plaque erosion and plaque rupture of TCFAs account for most of the sudden coronary deaths, claiming 6 per 100,000 and 17 per 100,000 men per year in the elderly population respectively [17]. In young victims of sudden coronary deaths, plaque rupture account for 60% of thrombi, and plaque erosion for the remaining 40% [18]. In recent years, early detection of vulnerable plaques has therefore become an important research goal, encouraging the development of novel imaging methods [19,20], as it would result in a major decrease in the morbidity and mortality of cardiovascular disease. In addition, potential plaque stabilization therapies are being developed, based on the knowledge acquired from the findings in patients. However, the mechanism of vulnerable plaque development remains unclear as no animal model of vulnerable plaque or plaque rupture is currently established.

In atherosclerosis research, mice are commonly used. The use of inbred strains kept under similar housing and dietary conditions reduces genetic variability and the effects of environmental factors, which could affect the outcome of atherosclerosis studies in patients. Furthermore, the pathology of the disease can be investigated at multiple time points, and (surgical) interventions can easily be introduced in these animals. However, wild-type mice are highly resistant to atherosclerosis due to their low levels of cholesterol in plasma. In addition, the main class of plasma lipoprotein in mice is the anti-atherogenic (high density lipoprotein) HDL. This is in contrast to the lipoprotein profile of humans, in which the main portion of plasma lipoproteins consists of pro-atherogenic very low density lipoprotein (VLDL) and LDL. Indeed, atherosclerosis can only develop in the relatively susceptible C57BL6 mouse strain after feeding the animals an extremely atherogenic diet for a prolonged period of time [21]. Several mouse models have been generated in which genetic modifications (i.e. overexpression or deficiency of specific genes) have made them more susceptible to the disease. The most commonly used models in atherosclerosis research are mice deficient in ApoE [22,23] or the LDL-receptor [24], both capable of developing advanced atherosclerotic lesions. Recent developments in studies using ApoE deficient mice have also indicated that they might be useful for assessing the mechanism involved in the progression of vulnerable plaque.

1.3 Flow patterns affecting vascular biology

As stated previously, ECs play a crucial role in the onset of atherosclorosis, and they are responsive to a large number of different stimuli. However, most of the factors associated with the initiation of atherosclerosis have a systemic effect. An additional stimulus is needed to clarify the specific localization of atherogenesis in the vasculature. A large body of evidence demonstrated that shear stress is this localizing factor. Wall shear stress or shear stress is defined as the tractive force per unit area applied by the flowing blood on the endothelium. Endothelial cells throughout the vasculature experience a variety of flow conditions with large differences in shear stress level (which is the actual force expressed in dynes, 1 dyne = 0.1 N/m^2), and in shear stress gradients (which are changes in shear stress direction and/or shear stress levels over time). In the venous system, shear stress levels are low (between 0.76 and 7.6 dynes/cm^2) with minimal gradients because of the non-pulsatile nature of the flow. In the straight vessel segments, flow conditions are generally laminar and pulsatile, with higher shear stress levels (averages are between 11.4 and 30.4 dynes/cm^2 for large arteries, and between 19.0 and 60.8 dynes/cm^2 for arterioles (reviewed in [25])). In the relatively high flow environment of the arterial system, blood is a suspension of particles that behaves approximately as a Newtonian fluid. Shear stress (σ) can therefore be determined by flow rate (Q), fluid viscosity (μ) and radial distance of the vessel lumen (d) according to the relationship: $\sigma = 4\mu Q/\pi d^3$, under the additional conditions that the vessel is a circular tube with a constant diameter, and the blood flow is stationary, resulting in a parabolic profile of blood velocity (i.e. assuming Poisseuille flow conditions)(reviewed in [26]). Shear stress levels are actively maintained in the arterial circulation as vascular tissues respond to shear stress changes with acute adjustments in vascular tone and with chronic structural remodeling, resulting in adjustments of vessel diameter. Shear stress gradients are dependent on specific flow conditions. Flow conditions in the artery are specified by the Reynolds number (Re), which is a ratio of inertial over viscous effects. It can be described by the following formula: $Re = 4\rho Q/\pi \mu D$, where ρ is the density of blood, D the vessel diameter, μ the blood viscosity and Q is the flow rate. At very low flow rates, Re is low (below 1). This means that the force due to the viscosity of the blood (viscous force) dominate over the force dependent from flow rate (inertial force). As a result, blood flow follows the geometry of the vessel. When Re become larger, and viscous forces and inertial forces become comparable, secondary flows (vortices and non-axial flow profiles) arise. These secondary flows develop at arterial bends and bifurcations. When Re becomes even larger (larger than 2000), the blood flow becomes turbulent, with fully randomized lateral motion of the blood. Turbulence is dependent on vascular geometries, such as the presence of lumen stenosis, and on flow pulsality as a result of the cardiac cycle. Transient turbulence has been shown to occur in the human aorta at peak systole, during heavy dynamic exercise in much of the central arterial system and distal to arterial lumenal stenosis and aneurysms [26].

Shear stress has been related to atherosclerosis for several decades, and a large body of studies in both patients and animal models have provided evidence in particular for a role of low shear stress (<1.5 N/m^2) in this disease [5,12,27-32]. However, additional studies have also indicated that oscillations in shear stress with time dependent gradients correlate to plaque localization [33]. Oscillations with time dependent gradients are changes in shear stress levels during the cardiac cycle. They are the result of the occurrence of secondary flow at vessel regions where viscous and inertial forces are comparable. Recent improvements of imaging techniques confirmed these early findings in patients *in vivo* [34,35]. Additionally, recent experiments showed that besides temporal gradients in shear stress, spatial gradients in shear stress predict plaque location and macrophage accumulation in the rabbit aorta [36-39]. Spatial gradients in shear stress are changes in shear stress at different locations and are mainly due to secondary flow. Temporal gradients of shear stress are mainly due to pulsatile variations of vortices. These two last observations are of particular importance as they introduce dynamics in place and in time to the biology of fluid dynamics.

Extensive studies on particle behavior near the vessel wall indicated that the predicted locations of macrophage accumulation coincide with regions where particles come in close contact with the endothelium. In addition, specific localization of other atherogenic events correlated with the above mentioned shear stress gradients [36-39]. From these studies, we conclude that besides the mean shear stress levels other parameters derived from the velocity field potentially affect the localization of inflammation and plaque formation.

In summary, given the complexity of shear stress fields, the search for specific shear stress conditions that predict plaque location and plaque inflammation is still under debate. In general, besides low shear stress, changes in the direction of the shear stress near the vessel wall over time leading to spatial gradients in shear stress is the most obvious condition. The latter will be further indicated as oscillatory shear stress in this thesis. The effects of low shear stress and oscillatory shear stress on the pathology of the vascular wall will be examined in the studies described in the next chapters.

1.4 Shear stress and gene expression

The molecular mechanisms by which shear stress acts on the vessel wall by stimulating the endothelium have been extensively studied *in vitro*. Studies from different laboratories reported between 40 and 125 genes to be modulated by shear stress in cultured endothelial cells [3,40-49]. Excellent reviews have been published regarding the number and interaction between shear stress responsive genes, and the role of transcription factors [3-6]. Studies on individual genes *in vitro* (Table 1) and *in vivo* (Table 2) indicated that, in general, low shear stress is associated with an pro-atherosclerotic phenotype and high shear stress with an athero-protective phenotype (Tables 1 and 2). The studies that evaluated oscillatory shear stress *in vitro* also suggest a more atherogenic effect for this type of shear stress than shear stress under laminar flow conditions, as they indicate that eNOS is downregulated [50,51], endothelin-1 is upregulated [50,51], and adhesion factors (e.g. vascular adhesion molecule-1 (VCAM-1 [52]), intercellular adhesion molecule-1 (ICAM-1 [52]), and E-selectin [52]) are upregulated, resulting in an increase in the adhesion of monocytes. In addition to these data, more than 40-120 genes have been associated with shear stress by gene-profiling studies; Table 3. From Table 3 it is clear that most of these studies have been performed in cultures, and that there is a great variability between laboratories despite close similarity of the protocols and cell types used. Although the reasons for these discrepancies are presently unknown, it has been postulated that the isolation of the endothelial cells might induce changes in the phenotype of these cells. Furthermore, only one study concentrated on the differential gene expression in conditions of laminar shear stress and disturbed shear stress *in vitro* [47]. Disturbed flow regulates a different set of genes than laminar shear stress, which may explain the relation between shear stress oscillations and predilection sites for atherosclerosis. Therefore, this study extends earlier studies on single genes (see above). However, most studies relating gene expression to shear stress are performed *in vitro* only and extrapolation to *in vivo* conditions may be problematic. Also, interpretation of these results with respect to atherosclerosis remains difficult. Atherosclerosis in humans and animal models need respectively years and months to develop, a time span that can hardly be maintained in cell cultures. In addition, the pathology of atherosclerosis involves too many factors (involved in e.g. lipid metabolism and inflammation) and too many different cell types (ECs, VSMCs, macrophages and T-cells), to be successfully mimicked in an *in vitro* situation. Furthermore, atherosclerosis related genes that have been identified to be shear stress responsive *in vitro* may not have an overall (pro-atherosclerotic) effect as complex feedback mechanisms active in the vessel wall could act to preserve homeostasis. Davies *et al.* also studied the effect of shear stress on gene expression of the vascular endothelium, but used a more sophisticated approach by obtaining ECs located in areas of the porcine aorta that are naturally exposed to different shear stress conditions for mRNA analysis. They selected the aortic arch as a region of disturbed flow (secondary flow and turbulence), and the descending thoracic aorta as a region of undisturbed flow, and

16

compared the expression and activity of endothelial protein kinase C (PKC) in these areas [56]. Furthermore, studies in mice using the natural sites of disturbed flow in the aorta for validation of *in vitro* findings could show increased activation of NFκ-B [57] (indicated by translocation of this transcription factor to the nuclei), and upregulation of ICAM-1 and VCAM-1 [58]. These types of studies provide crucial insight for the role of shear stress in the development of pathologies in the vessel wall. However, these studies of predeliction sites for atherosclerosis associated to certain shear stress conditions do not provide direct causal evidence.

In conclusion, the effect of low shear stress and oscillatory shear stress on gene expression in cultured ECs has been extensively studied. However, relevance of these mechanisms in the pathology of atherosclerosis is still largely unclear. This is due to the lack of a method capable of inducing these shear stress parameters under pro-atherosclerotic *in vivo* conditions.

Table 1: Shear stress and gene expression in ECs *in vitro*.

Gene	Function	SS level	duration (hours)	Result	Cell type	Ref.
VCAM-1	Adhesion	Low	6	Up	EC	[59]
ICAM-1	Adhesion	Low	6	Up	HUVEC	[60]
TF	Clotting	High	1-3	Up	EC	[60]
ET-1	Constrict	High	6	Down	EC	[61]
COX-1 COX-2	Dilator Constrict	High	12	Up	HUVEC	[62]
LOX-1	Lipid	Low	8	Up	BAEC	[63]
SOD	Anti-oxidant	Low	N.A.	Up	HUAC	[64]
eNOS	Dilator	High	4	Up	HUVEC	[65]
CNP	Dilator	High	3-8	Up	HUVEC	[62]
PDGF A/B	Growth	Low	1-2	Up	HUVEC	[66]
βFGF	Growth	High	9	Up	BAEC	[5]
TGF-β1	Growth	High	3	Up	EC	[67]
ACE	Growth	Low	18	Up	EC	[68]

EC: endothelial cell; HUVEC: human umbilical vascular endothelial cell; BAEC: bovine arterial endothelial cell; VCAM: vascular adhesion molecule; ICAM: intercellular adhesion molecule; TF: tissue factor; ET-1: endothelin-1; COX cyclo-oxygenase; LOX-1: lecitine-like ox-LDL receptor; SOD: superoxide dismutase; eNOS: endothelial nitric oxide synthase; CNP: C-natriuretic protein; PDGF: platelet derived growth factor; βFGF: basic fibroblast growth factor TGF-β1: transforming growth factor β1; ACE: angiotensin converting enzyme. Shear stress values are given with reference to the normal value of 1.5 N/m^2. The response is expressed with respect to a housekeeping gene. N.A.: not available.

Table 2: Shear stress related gene expression in blood vessels *in vivo*.

Gene	Function	Flow	Duration (weeks)	Result	Tissue	Ref.
VCAM-1	Adhesion	Down	5	Up	Carotid Artery	[69]
ICAM-1	Adhesion	Down	5	Up	Carotid Artery	[69]
TF	Clotting	Up	<1	Up	Carotid Artery	[60]
β-FGF	Growth	Up	1-7	Up	Carotid Artery	[70]
PDGF-A	Growth	Up	1	Up	Mesenteric Artery	[71]
PDGF-B	Growth	Up	7	Up	Mesenteric Artery	[71]
TGF-β	Growth	Up	7	Up	Mesenteric Artery	[71]
MMP-2 and MMP-9	Matrix degradation	Up	1	Up	Carotid Artery	[72]
MMP-2 and MMP-9	Matrix degradation	Down	1	Up	Carotid Artery	[72]

VCAM: vascular adhesion molecule; ICAM: intercellular adhesion molecule; TF: tissue factor; ET-1: endothelin-1; βFGF: basic fibroblast growth factor; PDGF: platelet derived growth factor; TGF-β1: transforming growth factor β1; MMP: metallo-proteinase. The response is expressed with respect to a housekeeping gene.

Table 3: Review of literature studying the effect of shear stress on gene expression

Ref.	Cell type	SS (N/m^2)	Method	Up	Down	Time (hours)	Control
[47]	HAEC	0.001	Microarray	11	19	24	Static
[47]	HAEC	1.3	Microarray	9	50	24	Static
[47]	HAEC	1.3	Microarray	7	7	24	Laminar flow
[46]	HAEC	1.2	Microarray	15	53	24	Static
[3]	HUVEC	1.2	Microarray	32	20	24	Static
[73]	HUVEC	Turbulent	Subtraction	63	-	0-20	Static
[73]	HUVEC	1.2	Subtraction	5	-	N.A.	Static
[74]	HUVEC	0.6	Diff display	13	20	0-48	Static
[75]	HUVEC	1.5	Gene calling	60	47	6,24	Static
[48]	HAEC	1.2	Microarray	27	33	1-24	Static
[49]	HAEC	1.5	Microarray	19	91	1	Static
[49]	HAEC	4.5	Microarray	25	25	1	Static
[46]	HAEC	2	Diff.display	8	-	48	Static
[45]	HUVEC	2.5	Diff. display	12	-	24	Static

HAEC: human endothelial cells; HUVEC: human umbilical vascular endothelial cells
N.A.: not available.

1.5 Shear stress and inflammation

Accumulating evidence demonstrates that atherosclerosis is modulated by chronic inflammation [76,77]. As stated previously, atherosclerotic plaques contain inflammatory infiltrates, mainly consisting of macrophages and T-cells. Of the entire T-cell population, the majority consists of CD4 (+) cells (70-80%), while the rest consists of CD8 (+) cells and natural killer cells [78,79]. Co-localization studies and the cytokine secretion pattern indicate that these T-cells are activated and belong predominantly to the Th1 cell type [79,80]. In addition, it has recently been shown that CD40, the counterpart of CD40L, is expressed on ECs, dendritic cells (DCs), VSMCs and macrophages. As CD40L is expressed on the surface of active T-cells [81], the T-cells in the plaque may regulate the activity of these cell types. Recent intervention experiments that either inhibit CD40-CD40L ligation or immunize animals with ox-LDL showed large effect upon plaque progression and plaque composition [78]. These studies indicate an important modulating role of an activated immune system in plaque composition.

In order to investigate the role of inflammation in the formation of the predilection sites for atherosclerosis, one has to postulate that shear stress modulates inflammation *in vivo*. In healthy vessels, immuno-competent and antigen-presenting cells have been identified at the well-known predilection sites [82]. As a result of these findings, Gozales and co-workers proposed the existence of vascular-associated lymphoid tissue (VALT) in accordance with the resemblance with mucosa-associated lymphoid tissue (MALT), and gut-associated lymphoid tissue (GALT). These regions are highly organized immunological regions within tissues, consisting of non-encapsulated lymphoid tissue with germinal centers. Due to this organization, DCs and macrophages may come in close contact with B- and T-cells allowing their maturation after antigen presentation. In atherosclerosis, the number of DCs at these sites increases and the immature DC transforms into mature DCs [83]. Although it is presently unknown why VALTs are located on the predilection sites, this may be due to the shear stress dependency of the expression of adhesion factors and pro-inflammatory mediators on the endothelium, described above [52,84-87]. Recently in a rare *in vivo* analysis of vascular regions exposed to disturbed blood flow, it was shown that altered shear stress can prime the endothelium to respond to pro-atherosclerotic stimuli through upregulation of the inflammatory transcription factor NF-κB [57]. In contrast, laminar flow with normal shear stress levels (laminar shear stress) promotes an anti-inflammatory and anti-oxidative expression profile, acting through promoter elements identified as shear stress responsive elements (SSREs), antioxidant responsive elements (ARE) and PPARγ-responsive elements[57]. Conversely, low shear stress triggers adhesion of leukocytes to activated endothelium through enhanced expression of ICAM-1, VCAM-1, and E-selectin. Oscillatory shear stress has recently been shown to upregulate the expression of bone morphogenic

protein (BMP-4), a member of the TGF-β family of cytokines, which was associated with increased ICAM-1 expression through an NF-κB-dependent mechanism[88]. These findings may explain the specific and local accumulation of immuno-competent cells at predilection sites and provide evidence for an immunological mechanism underlying the role of (oscillatory) shear stress and atherosclerotic predilection sites.

While the above mentioned studies indicated a role of inflammation in early atherosclerosis, it has recently been shown that accumulation of inflammatory cells causes plaque rupture in advanced atherosclerotic lesions. It has been postulated that during the progression of atherosclerotic lesions towards a more vulnerable plaque phenotype, activated T-cells, either directly or by CD40 ligation, amplify the activation of macrophages. These activated macrophages secrete matrix metallo proteinases (MMPs) that locally weaken the extracellular matrix, thereby causing a malignant progression of the plaque to vulnerability to rupture. Recently, inflammatory cells were detected predominantly upstream of human carotid plaques [89] at the location where plaque ruptures are frequently observed. While these authors have implied that shear stress could play a role in the distribution of inflammatory cells, a direct relationship was not shown. In order to study this phenomenon, we have developed an experimental rabbit model that mimics the findings reported in patients (Figure 1). With a modification of our numerical techniques [10-12] we could correlate **local** shear stress to **local** macrophage accumulation. These experiments clearly show that regions upstream of the plaque contained more macrophages and are associated with higher shear stress values (Figure 1). Accumulation of macrophages not necessarily implies that these cells are active. In order to evaluate the activity of macrophages we measured the MMP activity upstream and downstream of the plaque. We tested the hypothesis that stimulated macrophages increase the production of metalloproteinases, which will induce collagen breakdown and provide possible local weak spots in the plaque, creating a state of plaque vulnerability [90-93]. To evaluate if (oscillatory) shear stress is related to MMP activity, we performed a study in rabbits. In figure 2 an image depicts a relationship between MMP9 location and shear stress, indicating that at high shear stress regions upstream of the plaque the MMP9 levels are high. MMP9 has been identified in human ruptured plaques and has been associated with macrophage accumulation [92,93]. Hence, the association of shear stress with MMP9 activity may favour a rheological effect underlying vulnerable plaque. We propose that the secondary flow induced by the (abrupt) narrowing of the blood vessel upstream of the plaque may favour the contact of particles in the bloodstream and the vessel wall. As a result, the occupancy of the adhesion factors upstream of the plaque increases, allowing a selective uptake of inflammatory cells upstream of the plaque. Alternatively the haemodynamic environment resulting from the curved streamlines may induce uptake of lipids and as a result create a region of endothelial dysfunction, adhesion factor expression and uptake of macrophages.

In summary, we conclude that shear stress oscillations, via direct or indirect induction of adhesion factors, may be associated with secondary lymphoid tissue in normal and atherosclerotic tissue (VALT). These findings make it plausible that the relation between shear stress and predilection sites is due to an immunological mechanism. In addition, our own data provide evidence that existing plaques, and specifically advanced lesions, can also be affected by shear stress variations via triggering of an immunological response.

1.6 Problem definition and hypothesis

The mechanisms by which shear stress influence the biology of the vascular wall and induce atherosclerosis are still largely unclear. Although the effect of low shear stress and oscillatory shear stress on gene expression in cultured ECs has been examined extensively, the relevance of these findings for the progression of atherosclerosis has not been shown. This is due to the lack of a reproducible method capable of inducing these shear stress conditions *in vivo* under pro-atherosclerotic conditions. Shear stress may influence the vessel wall by inducing the expression of atherogenic genes by the endothelium. These atherogenic compounds contribute to an inflammatory response, which triggers the development of atherosclerotic plaques. By developing and validating a new device that can induce different shear stress conditions in an *in vivo* animal model, we are able to examine this mechanism, and provide data that show the relevance of the biological effects of shear stress on the vessel wall.
Therefore, we have the following hypothesis:

Shear stress affects the biology of the vascular wall and can induce the expression of atherogenic genes, making it susceptible to atherosclerosis.

The experiments performed to test this hypothesis are described in the next chapters.

1.7 Research objectives and thesis outline

In this thesis, studies are described that focus on the relationship between different shear stress conditions and their biological effects on the vessel wall leading to atherosclerosis. The lack of a method that can induce different shear stress conditions in laboratory animals hampers the design of studies *in vivo* that could determine the role of shear stress in vascular biology.
Therefore, the aims of the studies described in this thesis were:

> I)   *To develop and validate a new shear stress altering device (referred to as the cast) that is capable of inducing physiological and biological changes in an in vivo animal model.*
>
> II)   *To study the in vivo response of shear stress related genes (e.g. eNOS) to low shear stress and oscillatory shear stress.*
>
> III)   *To study the effects of low shear stress and oscillatory shear stress in vivo on the development of atherosclerosis and plaque stability.*
>
> IV)   *To examine the effects of low shear stress and oscillatory shear stress on inflammation in the vessel wall.*

The cast is described in chapter 3. The physiological effect of this device on shear stress is tested by Doppler measurements and CFD. The biological response of alterations in shear stress on the endothelium is validated by studying the response of the shear stress responsive gene eNOS. We used an in-house developed transgenic mouse model in which a human eNOS gene fused to a green fluorescent protein (GFP) is driven by the humane NOS promoter. This mouse model is described in chapter 2. After the cast model was successfully validated, this method was used in all the subsequent studies described in this thesis. Regulation of eNOS protein levels and activity is very complex and occurs both at transcriptional and post-transcriptional levels [94]. Post-translational modification of eNOS by myristoylation and palmitoylation that targets the protein to the Golgi complex and the lipid rich domains of the cell membrane are both necessary for proper eNOS activation. We therefore studied the effect of shear stress on the cellular localization of eNOS. The findings of these experiments are described in chapter 4. Furthermore, influence of the drug rapamycin on eNOS responsiveness to shear stress is evaluated in chapter 5. As shear stress is strongly related to the onset of atherosclerosis, we tested the atherogenic properties of low shear stress and oscillatory shear stress in a mouse model for atherosclerosis (ApoE -/-). In addition, we examined the effect of these two different shear stress conditions on plaque vulnerability. The findings of this study are described in chapter 6. The immunological mechanism by which these shear stress conditions induce atherosclerosis and define plaque vulnerability is studied by examining the effect on expression of chemoattractants (chemokines) in chapter 7. Finally, the results obtained in these studies are summarized and discussed in chapter 8 of this thesis.
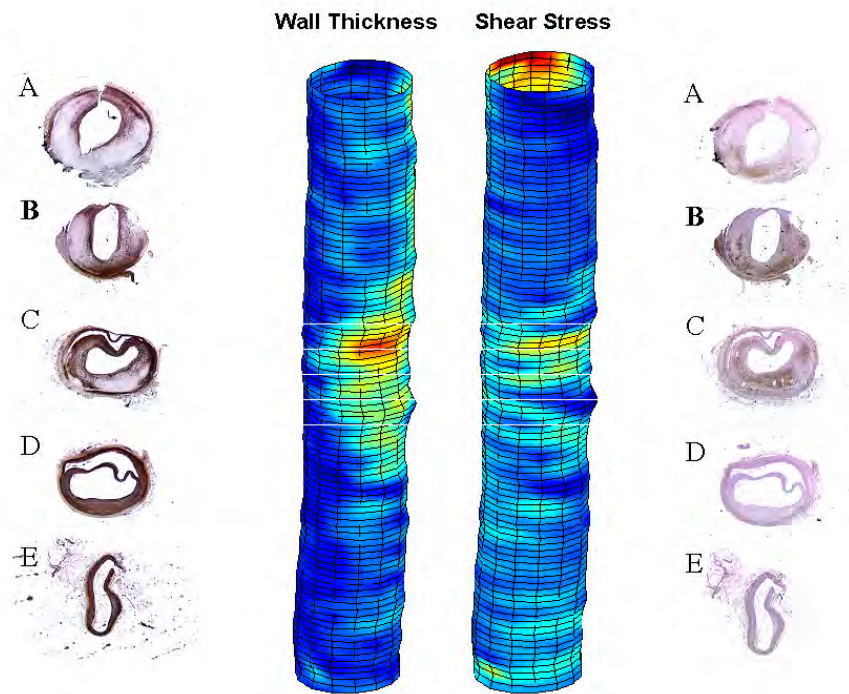
Figure 1: 3D reconstruction of an atherosclerotic rabbit aorta with IVUS, allowing the projection of wall thickness on the 3D lumen reconstruction. Indicated is also the shear stress distribution obtained by CFD. Atherosclerosis was induced in New Zealand White rabbits by a combination of denudation (surgical removal of the endothelium) and high cholesterol diet for two months. CFD modeling was based upon a commercially available finite element package as described before [7-9]. On the left and right sides are indicated the macrophage distribution and the smooth muscle cell distribution. Lines in the figure indicate the approximate location of the histological cross sections. The position of these cross sections was determined by measurement at sacrifice. Note that upstream, where the shear stress is high, the macrophages accumulate. Full colour image of this figure is available in the colour section.
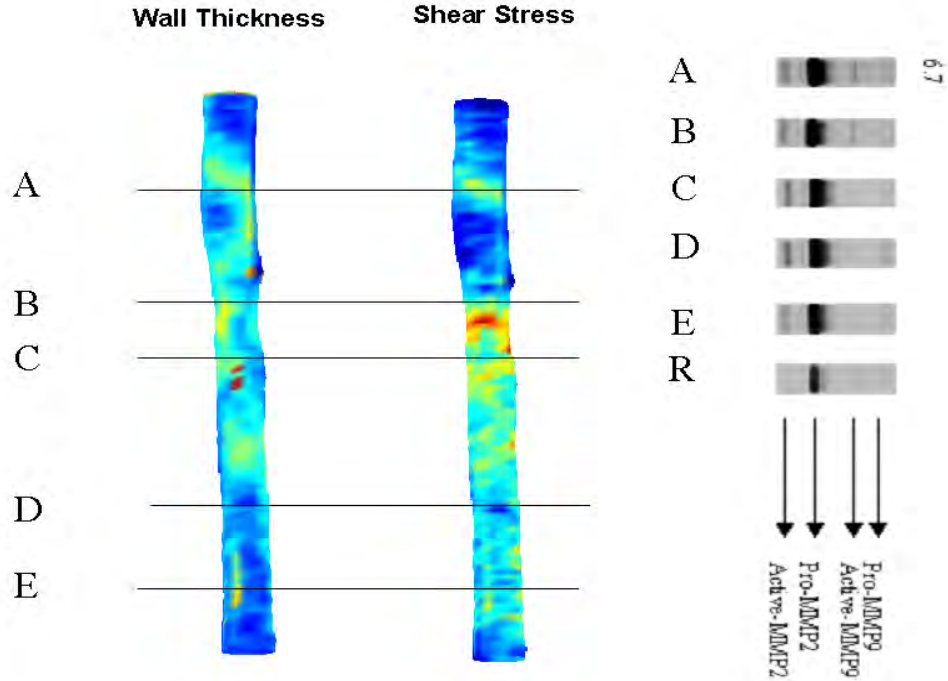
Figure 2: Relationship between metalloproteinase activity as determined by zymography [92], plaque location and shear stress distribution mapped upon the 3D reconstruction of the blood vessel. CFD was used as described in figure 1. Mapping of location was performed by selection on basis of shear stress distribution and correction for shrinkage after dissection. Note that the location of MMP9 activity is upstream of the plaque and associates with high shear stress values. MMP-2 is activated through the entire plaque region. A-E represent samples from the sections in different locations of the atherosclerotic vessel. R stands for the control sample. Full colour image of this figure is available in the colour section.

1.8 References

1. Shaaban AM, Duerinckx AJ. Wall shear stress and early atherosclerosis: a review. *AJR Am J Roentgenol*. 2000;174:1657-65.
2. Barakat A, Lieu D. Differential responsiveness of vascular endothelial cells to different types of fluid mechanical shear stress. *Cell Biochem Biophys*. 2003;38:323-43.
3. McCormick SM, Frye SR, Eskin SG, Teng CL, Lu CM, Russell CG, Chittur KK, McIntire LV. Microarray analysis of shear stressed endothelial cells. *Biorheology*. 2003;40:5-11.
4. Shyy JY, Chien S. Role of integrins in endothelial mechanosensing of shear stress. *Circ Res*. 2002;91:769-75.
5. Malek AM, Izumo S. Control of endothelial cell gene expression by flow. *J Biomech*. 1995;28:1515-28.
6. Takahashi M, Ishida T, Traub O, Corson MA, Berk BC. Mechanotransduction in endothelial cells: temporal signaling events in response to shear stress. *J Vasc Res*. 1997;34:212-9.
7. Wentzel JJ, Kloet J, Andhyiswara I, Oomen JA, Schuurbiers JC, de Smet BJ, Post MJ, de Kleijn D, Pasterkamp G, Borst C, Slager CJ, Krams R. Shear-stress and wall-stress regulation of vascular remodeling after balloon angioplasty: effect of matrix metalloproteinase inhibition. *Circulation*. 2001;104:91-6.
8. Wentzel JJ, Krams R, Schuurbiers JC, Oomen JA, Kloet J, van Der Giessen WJ, Serruys PW, Slager CJ. Relationship between neointimal thickness and shear stress after Wallstent implantation in human coronary arteries. *Circulation*. 2001;103:1740-5.
9. Wentzel JJ, Whelan DM, van der Giessen WJ, van Beusekom HM, Andhyiswara I, Serruys PW, Slager CJ, Krams R. Coronary stent implantation changes 3-D vessel geometry and 3-D shear stress distribution. *J Biomech*. 2000;33:1287-95.
10. Krams R, Wentzel JJ, Cespedes I, Vinke R, Carlier S, van der Steen AF, Lancee CT, Slager CJ. Effect of catheter placement on 3-D velocity profiles in curved tubes resembling the human coronary system. *Ultrasound Med Biol*. 1999;25:803-10.
11. Krams R, Wentzel JJ, Oomen JA, Schuurbiers JC, Andhyiswara I, Kloet J, Post M, de Smet B, Borst C, Slager CJ, Serruys PW. Shear stress in atherosclerosis, and vascular remodelling. In: *Semin Interv Cardiol*; 1998:39-44.
12. Krams R, Wentzel JJ, Oomen JA, Vinke R, Schuurbiers JC, de Feyter PJ, Serruys PW, Slager CJ. Evaluation of endothelial shear stress and 3D geometry as factors determining the development of atherosclerosis and remodeling in human coronary arteries in vivo. Combining 3D reconstruction

from angiography and IVUS (ANGUS) with computational fluid dynamics. *Arterioscler Thromb Vasc Biol*. 1997;17:2061-5.

13. Bom N, de Korte CL, Wentzel JJ, Krams R, Carlier SG, van der Steen AW, Slager CJ, Roelandt JR. Quantification of plaque volume, shear stress on the endothelium, and mechanical properties of the arterial wall with intravascular ultrasound imaging. *Z Kardiol*. 2000;89:105-11.

14. Carlier SG, van Damme LC, Blommerde CP, Wentzel JJ, van Langehove G, Verheye S, Kockx MM, Knaapen MW, Cheng C, Gijsen F, Duncker DJ, Stergiopulos N, Slager CJ, Serruys PW, Krams R. Augmentation of wall shear stress inhibits neointimal hyperplasia after stent implantation: inhibition through reduction of inflammation? *Circulation*. 2003;107:2741-6.

15. Stary HC, Chandler AB, Dinsmore RE, Fuster V, Glagov S, Insull W, Jr., Rosenfeld ME, Schwartz CJ, Wagner WD, Wissler RW. A definition of advanced types of atherosclerotic lesions and a histological classification of atherosclerosis. A report from the Committee on Vascular Lesions of the Council on Arteriosclerosis, American Heart Association. *Circulation*. 1995;92:1355-74.

16. Stary HC. Natural history and histological classification of atherosclerotic lesions: an update. *Arterioscler Thromb Vasc Biol*. 2000;20:1177-8.

17. Burke AP, Farb A, Pestaner J, Malcom GT, Zieske A, Kutys R, Smialek J, Virmani R. Traditional risk factors and the incidence of sudden coronary death with and without coronary thrombosis in blacks. *Circulation*. 2002;105:419-24.

18. Farb A, Burke AP, Tang AL, Liang TY, Mannan P, Smialek J, Virmani R. Coronary plaque erosion without rupture into a lipid core. A frequent cause of coronary thrombosis in sudden coronary death. *Circulation*. 1996;93:1354-63.

19. Schaar JA, de Korte CL, Mastik F, Baldewsing R, Regar E, de Feyter P, Slager CJ, van der Steen AF, Serruys PW. Intravascular palpography for high-risk vulnerable plaque assessment. *Herz*. 2003;28:488-95.

20. Tearney GJ, Yabushita H, Houser SL, Aretz HT, Jang IK, Schlendorf KH, Kauffman CR, Shishkov M, Halpern EF, Bouma BE. Quantification of macrophage content in atherosclerotic plaques by optical coherence tomography. *Circulation*. 2003;107:113-9.

21. Paigen B, Morrow A, Holmes PA, Mitchell D, Williams RA. Quantitative assessment of atherosclerotic lesions in mice. *Atherosclerosis*. 1987;68:231-40.

22. Plump AS, Smith JD, Hayek T, Aalto-Setala K, Walsh A, Verstuyft JG, Rubin EM, Breslow JL. Severe hypercholesterolemia and atherosclerosis in apolipoprotein E-deficient mice created by homologous recombination in ES cells. *Cell*. 1992;71:343-53.

23. Zhang SH, Reddick RL, Piedrahita JA, Maeda N. Spontaneous hypercholesterolemia and arterial lesions in mice lacking apolipoprotein E. *Science*. 1992;258:468-71.

24. Ishibashi S, Goldstein JL, Brown MS, Herz J, Burns DK. Massive xanthomatosis and atherosclerosis in cholesterol-fed low density lipoprotein receptor-negative mice. *J Clin Invest*. 1994;93:1885-93.

25. Kroll MH, Hellums JD, McIntire LV, Schafer AI, Moake JL. Platelets and shear stress. *Blood*. 1996;88:1525-41.

26. Cunningham KS, Gotlieb AI. The role of shear stress in the pathogenesis of atherosclerosis. *Lab Invest*. 2005;85:9-23.

27. Doroudi R, Gan LM, Selin Sjogren L, Jern S. Effects of shear stress on eicosanoid gene expression and metabolite production in vascular endothelium as studied in a novel biomechanical perfusion model. *Biochem Biophys Res Commun*. 2000;269:257-64.

28. Galbraith CG, Skalak R, Chien S. Shear stress induces spatial reorganization of the endothelial cell cytoskeleton. *Cell Motil Cytoskeleton*. 1998;40:317-30.

29. Gan L, Miocic M, Doroudi R, Selin-Sjogren L, Jern S. Distinct regulation of vascular endothelial growth factor in intact human conduit vessels exposed to laminar fluid shear stress and pressure. *Biochem Biophys Res Commun*. 2000;272:490-6.

30. Honda HM, Hsiai T, Wortham CM, Chen M, Lin H, Navab M, Demer LL. A complex flow pattern of low shear stress and flow reversal promotes monocyte binding to endothelial cells. *Atherosclerosis*. 2001;158:385-90.

31. Hsiai TK, Cho SK, Reddy S, Hama S, Navab M, Demer LL, Honda HM, Ho CM. Pulsatile flow regulates monocyte adhesion to oxidized lipid-induced endothelial cells. *Arterioscler Thromb Vasc Biol*. 2001;21:1770-6.

32. Ishibashi H, Sunamura M, Karino T. Flow patterns and preferred sites of intimal thickening in end-to-end anastomosed vessels. *Surgery*. 1995;117:409-20.

33. Ku DN, Giddens DP, Zarins CK, Glagov S. Pulsatile flow and atherosclerosis in the human carotid bifurcation. Positive correlation between plaque location and low oscillating shear stress. *Arteriosclerosis*. 1985;5:293-302.

34. Cheng CP, Herfkens RJ, Taylor CA. Abdominal aortic hemodynamic conditions in healthy subjects aged 50-70 at rest and during lower limb exercise: in vivo quantification using MRI. *Atherosclerosis*. 2003;168:323-31.

35. Cheng CP, Herfkens RJ, Taylor CA. Comparison of abdominal aortic hemodynamics between men and women at rest and during lower limb exercise. *J Vasc Surg*. 2003;37:118-23.

36. Buchanan JR, Jr., Kleinstreuer C, Truskey GA, Lei M. Relation between non-uniform hemodynamics and sites of altered permeability and lesion growth at the rabbit aorto-celiac junction. *Atherosclerosis*. 1999;143:27-40.

37. Kanai AJ, Strauss HC, Truskey GA, Crews AL, Grunfeld S, Malinski T. Shear stress induces ATP-independent transient nitric oxide release from vascular endothelial cells, measured directly with a porphyrinic microsensor. *Circ Res*. 1995;77:284-93.

38. Malinauskas RA, Sarraf P, Barber KM, Truskey GA. Association between secondary flow in models of the aorto-celiac junction and subendothelial macrophages in the normal rabbit. *Atherosclerosis*. 1998;140:121-34.

39. Truskey GA, Herrmann RA, Kait J, Barber KM. Focal increases in vascular cell adhesion molecule-1 and intimal macrophages at atherosclerosis-susceptible sites in the rabbit aorta after short-term cholesterol feeding. *Arterioscler Thromb Vasc Biol*. 1999;19:393-401.

40. Ando J, Tsuboi H, Korenaga R, Takahashi K, Kosaki K, Isshiki M, Tojo T, Takada Y, Kamiya A. Differential display and cloning of shear stress-responsive messenger RNAs in human endothelial cells. *Biochem Biophys Res Commun*. 1996;225:347-51.

41. Bongrazio M, Baumann C, Zakrzewicz A, Pries AR, Gaehtgens P. Evidence for modulation of genes involved in vascular adaptation by prolonged exposure of endothelial cells to shear stress. *Cardiovasc Res*. 2000;47:384-93.

42. Topper JN, Cai J, Qiu Y, Anderson KR, Xu YY, Deeds JD, Feeley R, Gimeno CJ, Woolf EA, Tayber O, Mays GG, Sampson BA, Schoen FJ, Gimbrone MA, Jr., Falb D. Vascular MADs: two novel MAD-related genes selectively inducible by flow in human vascular endothelium. *Proc Natl Acad Sci U S A*. 1997;94:9314-9.

43. Topper JN, Cai J, Falb D, Gimbrone MA, Jr. Identification of vascular endothelial genes differentially responsive to fluid mechanical stimuli: cyclooxygenase-2, manganese superoxide dismutase, and endothelial cell nitric oxide synthase are selectively up-regulated by steady laminar shear stress. *Proc Natl Acad Sci U S A*. 1996;93:10417-22.

44. McCormick SM, Eskin SG, McIntire LV, Teng CL, Lu CM, Russell CG, Chittur KK. DNA microarray reveals changes in gene expression of shear stressed human umbilical vein endothelial cells. *Proc Natl Acad Sci U S A*. 2001;98:8955-60.

45. Dekker RJ, van Soest S, Fontijn RD, Salamanca S, de Groot PG, VanBavel E, Pannekoek H, Horrevoets AJ. Prolonged fluid shear stress induces a distinct set of endothelial cell genes, most specifically lung Kruppel-like factor (KLF2). *Blood*. 2002;100:1689-98.

46. Chen BP, Li YS, Zhao Y, Chen KD, Li S, Lao J, Yuan S, Shyy JY, Chien S. DNA microarray analysis of gene expression in endothelial cells in response to 24-h shear stress. *Physiol Genomics*. 2001;7:55-63.

47. Brooks AR, Lelkes PI, Rubanyi GM. Gene expression profiling of human aortic endothelial cells exposed to disturbed flow and steady laminar flow. *Physiol Genomics*. 2002;9:27-41.

48. Zhao Y, Chen BP, Miao H, Yuan S, Li YS, Hu Y, Rocke DM, Chien S. Improved significance test for DNA microarray data: temporal effects of shear stress on endothelial genes. *Physiol Genomics*. 2002;12:1-11.

49. Peters DG, Zhang XC, Benos PV, Heidrich-O'Hare E, Ferrell RE. Genomic analysis of immediate/early response to shear stress in human coronary artery endothelial cells. *Physiol Genomics*. 2002;12:25-33.

50. Ziegler T, Bouzourene K, Harrison VJ, Brunner HR, Hayoz D. Influence of oscillatory and unidirectional flow environments on the expression of endothelin and nitric oxide synthase in cultured endothelial cells. *Arterioscler Thromb Vasc Biol*. 1998;18:686-92.

51. Silacci P, Formentin K, Bouzourene K, Daniel F, Brunner HR, Hayoz D. Unidirectional and oscillatory shear stress differentially modulate NOS III gene expression. *Nitric Oxide*. 2000;4:47-56.

52. Chappell DC, Varner SE, Nerem RM, Medford RM, Alexander RW. Oscillatory shear stress stimulates adhesion molecule expression in cultured human endothelium. *Circ Res*. 1998;82:532-9.

53. Takada Y, Kato C, Kondo S, Korenaga R, Ando J. Cloning of cDNAs encoding G protein-coupled receptor expressed in human endothelial cells exposed to fluid shear stress. *Biochem Biophys Res Commun*. 1997;240:737-41.

54. Resnick N, Yahav H, Khachigian LM, Collins T, Anderson KR, Dewey FC, Gimbrone MA, Jr. Endothelial gene regulation by laminar shear stress. *Adv Exp Med Biol*. 1997;430:155-64.

55. Garcia-Cardena G, Comander J, Anderson KR, Blackman BR, Gimbrone MA, Jr. Biomechanical activation of vascular endothelium as a determinant of its functional phenotype. *Proc Natl Acad Sci U S A*. 2001;98:4478-85.

56. Magid R, Davies PF. Endothelial protein kinase C isoform identity and differential activity of PKCzeta in an athero-susceptible region of porcine aorta. *Circ Res*. 2005;97:443-9.

57. Tzima E, Irani-Tehrani M, Kiosses WB, Dejana E, Schultz DA, Engelhardt B, Cao G, DeLisser H, Schwartz MA. A mechanosensory complex that mediates the endothelial cell response to fluid shear stress. *Nature*. 2005;437:426-31.

58. Nakashima Y, Raines EW, Plump AS, Breslow JL, Ross R. Upregulation of VCAM-1 and ICAM-1 at atherosclerosis-prone sites on the endothelium in the ApoE-deficient mouse. *Arterioscler Thromb Vasc Biol*. 1998;18:842-51.

59. Mohan S, Mohan N, Valente AJ, Sprague EA. Regulation of low shear flow-induced HAEC VCAM-1 expression and monocyte adhesion. *Am J Physiol*. 1999;276:C1100-7.

60. Houston P, Dickson MC, Ludbrook V, White B, Schwachtgen JL, McVey JH, Mackman N, Reese JM, Gorman DG, Campbell C, Braddock M. Fluid shear stress induction of the tissue factor promoter in vitro and in vivo is mediated by Egr-1. *Arterioscler Thromb Vasc Biol*. 1999;19:281-9.

61. Malek AM, Greene AL, Izumo S. Regulation of endothelin 1 gene by fluid shear stress is transcriptionally mediated and independent of protein kinase C and cAMP. *Proc Natl Acad Sci U S A*. 1993;90:5999-6003.

62. Okahara K, Sun B, Kambayashi J. Upregulation of prostacyclin synthesis-related gene expression by shear stress in vascular endothelial cells. *Arterioscler Thromb Vasc Biol*. 1998;18:1922-6.

63. Murase T, Kume N, Korenaga R, Ando J, Sawamura T, Masaki T, Kita T. Fluid shear stress transcriptionally induces lectin-like oxidized LDL receptor-1 in vascular endothelial cells. *Circ Res*. 1998;83:328-33.

64. Inoue N, Ramasamy S, Fukai T, Nerem RM, Harrison DG. Shear stress modulates expression of Cu/Zn superoxide dismutase in human aortic endothelial cells. *Circ Res*. 1996;79:32-7.

65. Harrison DG, Sayegh H, Ohara Y, Inoue N, Venema RC. Regulation of expression of the endothelial cell nitric oxide synthase. *Clin Exp Pharmacol Physiol*. 1996;23:251-5.

66. Resnick N, Collins T, Atkinson W, Bonthron DT, Dewey CF, Jr., Gimbrone MA, Jr. Platelet-derived growth factor B chain promoter contains a cis-acting fluid shear-stress-responsive element. *Proc Natl Acad Sci U S A*. 1993;90:4591-5.

67. Ohno M, Cooke JP, Dzau VJ, Gibbons GH. Fluid shear stress induces endothelial transforming growth factor beta-1 transcription and production. Modulation by potassium channel blockade. *J Clin Invest*. 1995;95:1363-9.

68. Rieder MJ, Carmona R, Krieger JE, Pritchard KA, Jr., Greene AS. Suppression of angiotensin-converting enzyme expression and activity by shear stress. *Circ Res*. 1997;80:312-9.

69. Walpola PL, Gotlieb AI, Cybulsky MI, Langille BL. Expression of ICAM-1 and VCAM-1 and monocyte adherence in arteries exposed to altered shear stress. *Arterioscler Thromb Vasc Biol*. 1995;15:2-10.

70. Singh TM, Abe KY, Sasaki T, Zhuang YJ, Masuda H, Zarins CK. Basic fibroblast growth factor expression precedes flow-induced arterial enlargement. *J Surg Res*. 1998;77:165-73.

71. Tulis DA, Prewitt RL. Medial and endothelial platelet-derived growth factor A chain expression is regulated by in vivo exposure to elevated flow. *J Vasc Res*. 1998;35:413-20.

72. Bassiouny HS, Song RH, Hong XF, Singh A, Kocharyan H, Glagov S. Flow regulation of 72-kD collagenase IV (MMP-2) after experimental arterial injury. *Circulation*. 1998;98:157-63.

73. Yoshisue H, Suzuki K, Kawabata A, Ohya T, Zhao H, Sakurada K, Taba Y, Sasaguri T, Sakai N, Yamashita S, Matsuzawa Y, Nojima H. Large scale

isolation of non-uniform shear stress-responsive genes from cultured human endothelial cells through the preparation of a subtracted cDNA library. *Atherosclerosis*. 2002;162:323-34.

74. Bongrazio M, Baumann C, Zakrzewicz A, Pries AR, Gaehtgens P. Evidence for modulation of genes involved in vascular adaptation by prolonged exposure of endothelial cells to shear stress. *Cardiovasc Res*. 2000;47:384-93.

75. Wasserman SM, Mehraban F, Komuves LG, Yang RB, Tomlinson JE, Zhang Y, Spriggs F, Topper JN. Gene expression profile of human endothelial cells exposed to sustained fluid shear stress. *Physiol Genomics*. 2002;12:13-23.

76. Libby P, Ridker PM, Maseri A. Inflammation and atherosclerosis. *Circulation*. 2002;105:1135-43.

77. Berk BC, Abe JI, Min W, Surapisitchat J, Yan C. Endothelial atheroprotective and anti-inflammatory mechanisms. *Ann N Y Acad Sci*. 2001;947:93-109; discussion 109-11.

78. Hansson GK. Regulation of immune mechanisms in atherosclerosis. *Ann N Y Acad Sci*. 2001;947:157-65; discussion 165-6.

79. Frostegard J, Ulfgren AK, Nyberg P, Hedin U, Swedenborg J, Andersson U, Hansson GK. Cytokine expression in advanced human atherosclerotic plaques: dominance of pro-inflammatory (Th1) and macrophage-stimulating cytokines. *Atherosclerosis*. 1999;145:33-43.

80. de Boer OJ, Hirsch F, van der Wal AC, van der Loos CM, Das PK, Becker AE. Costimulatory molecules in human atherosclerotic plaques: an indication of antigen specific T lymphocyte activation. *Atherosclerosis*. 1997;133:227-34.

81. Mach F, Schonbeck U, Libby P. CD40 signaling in vascular cells: a key role in atherosclerosis? *Atherosclerosis*. 1998;137 Suppl:S89-95.

82. Wick G, Perschinka H, Xu Q. Autoimmunity and atherosclerosis. *Am Heart J*. 1999;138:S444-9.

83. Bobryshev YV, Lord RS. Mapping of vascular dendritic cells in atherosclerotic arteries suggests their involvement in local immune-inflammatory reactions. *Cardiovasc Res*. 1998;37:799-810.

84. Korenaga R, Ando J, Kosaki K, Isshiki M, Takada Y, Kamiya A. Negative transcriptional regulation of the VCAM-1 gene by fluid shear stress in murine endothelial cells. *Am J Physiol*. 1997;273:C1506-15.

85. Tsao PS, Buitrago R, Chan JR, Cooke JP. Fluid flow inhibits endothelial adhesiveness. Nitric oxide and transcriptional regulation of VCAM-1. *Circulation*. 1996;94:1682-9.

86. Ishida T, Takahashi M, Corson MA, Berk BC. Fluid shear stress-mediated signal transduction: how do endothelial cells transduce mechanical force into biological responses? *Ann N Y Acad Sci*. 1997;811:12-23; discussion 23-4.

87. Gonzales RS, Wick TM. Hemodynamic modulation of monocytic cell adherence to vascular endothelium. *Ann Biomed Eng*. 1996;24:382-93.

88. Sorescu GP, Song H, Tressel SL, Hwang J, Dikalov S, Smith DA, Boyd NL, Platt MO, Lassegue B, Griendling KK, Jo H. Bone morphogenic protein 4 produced in endothelial cells by oscillatory shear stress induces monocyte adhesion by stimulating reactive oxygen species production from a nox1-based NADPH oxidase. *Circ Res*. 2004;95:773-9.

89. Dirksen MT, van der Wal AC, van den Berg FM, van der Loos CM, Becker AE. Distribution of inflammatory cells in atherosclerotic plaques relates to the direction of flow. *Circulation*. 1998;98:2000-3.

90. Aikawa M, Rabkin E, Okada Y, Voglic SJ, Clinton SK, Brinckerhoff CE, Sukhova GK, Libby P. Lipid lowering by diet reduces matrix metalloproteinase activity and increases collagen content of rabbit atheroma: a potential mechanism of lesion stabilization. *Circulation*. 1998;97:2433-44.

91. Fukumoto Y, Libby P, Rabkin E, Hill CC, Enomoto M, Hirouchi Y, Shiomi M, Aikawa M. Statins alter smooth muscle cell accumulation and collagen content in established atheroma of watanabe heritable hyperlipidemic rabbits. *Circulation*. 2001;103:993-9.

92. Galis ZS, Sukhova GK, Lark MW, Libby P. Increased expression of matrix metalloproteinases and matrix degrading activity in vulnerable regions of human atherosclerotic plaques. *J Clin Invest*. 1994;94:2493-503.

93. Galis ZS, Khatri JJ. Matrix metalloproteinases in vascular remodeling and atherogenesis: the good, the bad, and the ugly. *Circ Res*. 2002;90:251-62.

94. Fulton D, Gratton JP, Sessa WC. Post-translational control of endothelial nitric oxide synthase: why isn't calcium/calmodulin enough? *J Pharmacol Exp Ther*. 2001;299:818-24.

Chapter 2:
Functional Expression of Endothelial Nitric Oxide Synthase Fused to Green Fluorescent Protein in Transgenic Mice

R. van Haperen, C. Cheng, B. Mees, E. van Deel, M. de Waard, L.C.A. van Damme,
T. van Gent, T. van Aken, R. Krams, D. J. Duncker, R. de Crom,

2.1 Abstract

The activity of endothelial nitric oxide synthase (eNOS) is subject to complex transcriptional and post-translational regulation including the association with several proteins and variations in subcellular distribution. In the present study we describe a transgenic mouse model expressing eNOS fused to green fluorescent protein (GFP), which allows the study of localization and regulation of eNOS expression. We tested the functionality of eNOS in the eNOS–GFP mice. Expression of eNOS was restricted to the endothelial lining of blood vessels in various tissues tested, without appreciable expression in non-endothelial cells. Activity of the enzyme was confirmed by essaying the conversion of L-arginine to L-citrulline. NO production in isolated vessels was increased in transgenic mice when compared to non-transgenic control animals 4.88± 0.59 and 2.48± 0.47 μM NO, respectively, P<0.005) . Both the mean aortic pressure and the pulmonary artery pressure were reduced in eNOS–GFP mice (both ~30%, P<0.05). Plasma cholesterol levels were also slightly reduced (~20%, P<0.05). In conclusion, eNOS–GFP mice express functional eNOS and provide a unique model to study regulation of eNOS activity or eNOS mediated vascular events, including response to ischemia, response to differences in shear stress, angiogenesis and vasculogenesis, and to study the subcellular distribution in relation with functional responses to these events.

2.2 Introduction

In endothelial cells, nitric oxide (NO) is generated by the enzyme endothelial nitric oxide synthase (eNOS) via the conversion of L-arginine to L-citrulline. NO produced by eNOS affects a number of biological processes in the vessel wall. It is important for the regulation of blood pressure and plays an important role in the aggregation of blood platelets, adhesion of leukocytes to the vessel wall and migration of vascular smooth muscle cells [1]. A decrease in NO availability is one of the hallmarks of endothelial dysfunction, which can occur in a number of cardiovascular disorders, including hypertension, heart failure, diabetes and atherosclerosis [2]. It has been shown in animal models that a decrease in eNOS activity results in accelerated atherosclerosis [3,4]. Conversely, stimulation of eNOS activity by statin treatment has been implicated in the protective actions of these drugs [5-7].

For these reasons, the regulation of eNOS activity is considered to be of major physiological and pathophysiological importance. Although eNOS was originally termed endothelial *constitutive* NOS (ecNOS) [8-10], several laboratories have found that its protein expression and enzymatic activity is under tight regulation [10-13]. In addition to regulation at the transcriptional level, protein activity is controlled in several ways. Regulatory processes include *N*-myristoylation and cysteine palmitoylation, serine/threonine phosphorylation, and protein-protein interactions. These events affect the intracellular localization of eNOS which might influence its enzymatic activity. Normally, eNOS is localized in two subcellular compartments: the Golgi complex and the plasma membrane [14]. Although it has been suggested that translocation between these two compartments is important in the regulation of the enzymatic activity, it has been demonstrated that eNOS in both pools can be phosphorylated and activated [14]. In vitro studies of cells transfected with eNOS cDNA fused to DNA encoding green fluorescent protein (GFP) have provided valuable information of eNOS localization and regulation. However, to date such studies have not been performed in vivo. Consequently, we developed a transgenic mouse model in which an eNOS–GFP fusion protein is expressed. The results indicate that the eNOS fusion protein is functionally intact. These eNOS–GFPtg mice can be used to study vascular reactions in which eNOS is involved, including angiogenesis or response to variations in shear stress.

2.3 Materials and Methods

Generation of eNOS–GFP transgenic mice
A genomic DNA fragment was isolated from a home made human cosmid library. It included 6 kb of 5' sequence, the complete eNOS gene, and 3 kb of 3' sequence. At the STOP codon of the eNOS gene, a linker was introduced that allowed the in frame insertion of a BamHI-NotI DNA fragment encoding eGFP which was derived from the pEGFP-N1 plasmid (BD-Sciences Clontech, Palo Alto CA). Fertilized oocytes from FVB mice were microinjected with a solution of 1-2 µg/ml in 8 mM Tris-HCl, 0.1 mM EDTA and transplanted into the oviducts of pseudopregnant B10xCBA mice. Founder mice and offspring were genotyped by PCR on DNA isolated from tail biopsies. Primers used were: 5'-GTCCTGCAGACCGTGCAGC-3' (sense) and 5'-GGCTGTTGGTGTCTGAGCCG-3' (antisense). Mice were backcrossed to C57Bl6 for at least 5 generations (>96% C57Bl6). Transgenic mice used in the present study were hemizygous. All animal experiments were performed in compliance with institutional and national guidelines.

Immunohistochemistry, fluorescence microscopy, confocal microscopy
Immunohistochemistry experiments were performed according to Bakker et al. [15] on 7 µm paraffin sections. The antibodies used were raised against the carboxy terminus of eNOS (Santa Cruz Biotechnology Inc., Santa Cruz, CA, cat.nr. sc-654). For confocal microscopy, mice were sacrificed using an overdose of isoflurane (1-chloro-2,2,2-trifluoroethyl-difluoromethyl-ether). Subsequently, in situ perfusion fixation was performed by flushing 20 ml PBS through a cardiac puncture followed by 20 ml 4% (v/v) paraformaldehyde in PBS. The common carotid arteries were then harvested, fixed in 4% paraformaldehyde in PBS at 4 °C, and mounted in Vectashield® (Vector Laboratories, Inc, Burlingame, CA) between glass slides. Samples were examined under a Zeiss LSM inverted laser scanning confocal fluorescence microscope. Images of GFP fluorescence were acquired after excitation with a 488-nm argon laser and after filtering the fluorescence with a 500-550 nm bandpass barrier filter. The thickness of the optical slice images is 0.6 µm.

Western blotting
Western blotting experiments were performed as described previously [16]. The antibodies used were directed against human eNOS or human eNOS phosphorylated at Ser-1177, both obtained from Santa Cruz Biotechnology Inc., Santa Cruz, CA (cat.nr. sc-654 and sc-12972, respectively).

eNOS enzyme activity and nitric oxide measurements
eNOS activity was measured in the L-arginine to L-citrulline conversion assay using a nitric oxide synthase assay kit (Calbiochem, La Jolla, CA; cat.no. 482700) as described previously [16]. For NO measurements, mice were anaesthetised with 0.2 ml i.p. sodium pentobarbital (Apharmo BV, Arnhem, The Netherlands) and

intracardially perfused with 10 ml Krebs Henseleit buffer solution (118 mM NaCl, 4.7 mM KCl, 3.0 mM $CaCl_2$, 1.2 mM KH_2PO_4, 1.2 mM $MgSO_4$, 25 mM $NaHCO_3$, 0.5 mM EDTA, 10 mM D-glucose and 0.1 mM L-arginine, equilibrated with 95% air and 5% CO_2 at room temperature resulting in a pH of 7.4). The aorta was dissected and in situ cannulated with two metal cannulas, proximal at the level of aortic arch and distal at the level of the diaphragm. The cannulas were connected to a homemade device keeping the vessel at its original length. Next, the vessel was transported to the set-up, where the cannulas were fixed to two holders. The two holders were placed in a chamber filled with Krebs buffer. The cannula at the proximal end of the vessel was connected to Tygon® tubing coming out of a reservoir with Krebs buffer. Between the reservoir and the cannula a flow pump (Watson Marlow, UK) and an infusion pump (Perfusor VI, B.Braun, Germany) were positioned. The settings of the pump were adjusted to perfuse the aorta with a constant flow of 10 ml/min, measured by an EMF flow sensor. This value was based on measurements of the cardiac output of our mice with a clinical Doppler device (Prosound 4000, Aloka, Japan) or by a transit-time flow probe (see below). Next, the aorta vessel was equilibrated by perfusing it for 30 minutes. During that period the experimental set up was switched to its calibration state and the NO-sensor was calibrated by infusing known NO concentrations through a tube mounted in parallel to the vessel (0.1 to 30 µM). Then, L-arginine (0.1 M) in Krebs buffer was added to the perfusate via the infusion pump. The NO-sensitive electrode was positioned at the distal end of the aorta, in order to measure the NO-production by the vessel. The electrode was connected to an NO measurement system (Iso-NO mark II, World Precision Instruments, USA). All data, including temperature, pressure drop, flow and NO measurements were stored in a PC equipped with a AD converter and analysis software (Acodas, Dataq Instruments, Natick, MA).

Hemodynamics and heart weights
Hemodynamic measurements were performed as described [16]. Shortly, blood pressure measurements were performed in mice anesthetized with ketamine (100 mg/kg ip) and xylazine (20 mg/kg ip), intubated and ventilated with a mixture of O_2 and N_2 (1/2 vol/vol). A flame stretched PE 50 polyethylene catheter was inserted into the right carotid artery and advanced into the aortic arch for measurement of aortic pressure and connected to a pressure transducer (Braun). For infusion of L-NAME, a second catheter was introduced into the right external jugular vein and advanced into the superior caval vein. After thoracotomy through the second right intercostal space, the ascending aorta was exposed and a transit-time flow probe (ID 1.5 mm; Transonics systems T206) was placed around the aorta for measuring aorta flow. Ten min after a second intraperitoneal bolus of 100 mg/kg ketamine and 20 mg/kg xylazine, baseline recordings were obtained. Then, a continuous 10 min intravenous infusion of L-NAME (100 mg/kg) was started and measurements were continued until 10 min after completion of the infusion. For the measurements of pulmonary artery pressure, the second left intercostal space was opened and a 30G needle connected to a PE 10

polyethylene catheter was directly inserted into the pulmonary artery. Hemodynamic data were recorded and digitized using an on-line 4 channel data acquisition program (ATCODAS, Dataq Instruments, Akron, OH). Ten consecutive beats were selected for determination of heart rate, aortic and pulmonary artery pressures, and aortic blood flow. For determination of ventricular weights the heart was removed and the ventricles were separated from the atria, the aorta and the pulmonary artery. The right ventricle was carefully separated from the left ventricle (incl. septum) and the right and left ventricle were weighed on a microbalance (Sartorius AG Göttingen). For the measurements of dry weights, tissue fluids were removed by lyophilization.

Cholesterol and Lipoprotein analysis
Blood was collected by orbital puncture after an overnight fast. Plasma from 6-10 mice was pooled and subjected to gel filtration analysis on two HR10/30 FPLC columns in tandem (Superdex 200 and Superose 6, both prepgrade, Pharmacia Biotech., Uppsala, Sweden) [17]. Cholesterol concentrations were measured with the free cholesterol C kit (WAKO, Neuss, Germany) after hydrolysis of cholesterol esters with cholesterol esterase from *Candida cylindracea*.

Data analysis
Analysis of data was performed using two-way or one-way analysis of variance followed by Scheffé's test, as appropriate. Statistical significance was accepted when $P<0.05$ (two-tailed). Data are presented as mean ± SEM.

2.4 Results

eNOS–GFP transgenic mice

We aimed to create mice transgenic for human eNOS, in which the expression resembled that of the endogenous gene as much as possible, both with respect to the expression pattern as well as the regulation. Therefore, we used a DNA fragment to generate transgenic mice that comprised the complete human eNOS genomic sequence, including the natural promoter. This fragment was isolated from a human cosmid library. In addition to the eNOS gene, the DNA fragment contained ~6 kb of 5' sequence, including the endothelial enhancer sequence identified by Laumonnier et al. [18], and ~3 kb of 3' sequence. At the STOP codon of the eNOS gene, a DNA fragment encoding enhanced GFP was inserted in frame with the eNOS gene, in order to obtain a DNA construct encoding an eNOS–GFP fusion protein. This fragment (Fig. 1a) was used for the generation of eNOS–GFP transgenic (eNOS–GFPtg) mice. Fig. 1b shows sections from mouse aorta, taken from eNOS–GFPtg mice or wild type littermates (controls). Immunohistochemistry studies on these sections using an antibody directed against human eNOS revealed a strong staining of the endothelial layer of the aorta in the eNOS–GFPtg mice, while there was no staining in the media of the aorta (Fig. 1b, lower left panel). Sections from non-transgenic controls showed virtually no staining (Fig. 1b, upper left panel). Inspection with fluorescence microscopy showed a strong fluorescent signal in the endothelial layer of the aorta from eNOS–GFPtg mice (Fig. 1b, lower right panel), which is much higher than the autofluorescence from the elastic lamellae that is present in both eNOS–GFPtg mice and in wild type controls (Fig. 1b, upper right panel). The subcellular localization was studied by confocal microscopy in the carotid artery (Fig. 1c). The expression pattern exactly matches the sites where eNOS is known to be primarily located: in the Golgi complex and at the plasma membrane. We performed Western blotting experiments with aorta and lung tissue from eNOS–GFPtg mice and non-transgenic controls (Fig. 1d). Using an antibody directed against human eNOS, both the endogenous murine eNOS is detected, caused by cross-reactivity of the antibody, as well as the eNOS–GFP fusion protein, which has a slightly higher molecular mass caused by the GFP moiety (approximately 130 kDa and 155 kDa, respectively; Fig. 1d, left panels). In addition, we used an antibody that recognizes eNOS that is phosphorylated on serine 1177 (P-eNOS), which is the activated form of the enzyme. P-eNOS–GFP is present in both aorta and lung tissue from eNOS–GFPtg mice (Fig. 1d, right panels). In order to determine whether the expressed eNOS–GFP fusion protein is catalytically active, enzymatic activity was measured in aorta and lung tissue from eNOS–GFPtg mice and non-transgenic controls. As shown in Fig. 1e, the transgenic mice show an increase in eNOS activity of approximately 35-fold in aorta and 27-fold in lung tissue. In addition, NO production was measured in isolated vessels ex vivo, using an NO sensor. Aortas from eNOS–GFP transgenic mice showed an increased NO production compared with aortas from control mice (Fig 1f). The data could be described by a first order

kinetic reaction, which was confirmed by a Lineweaver-Burke transformation (data not shown).
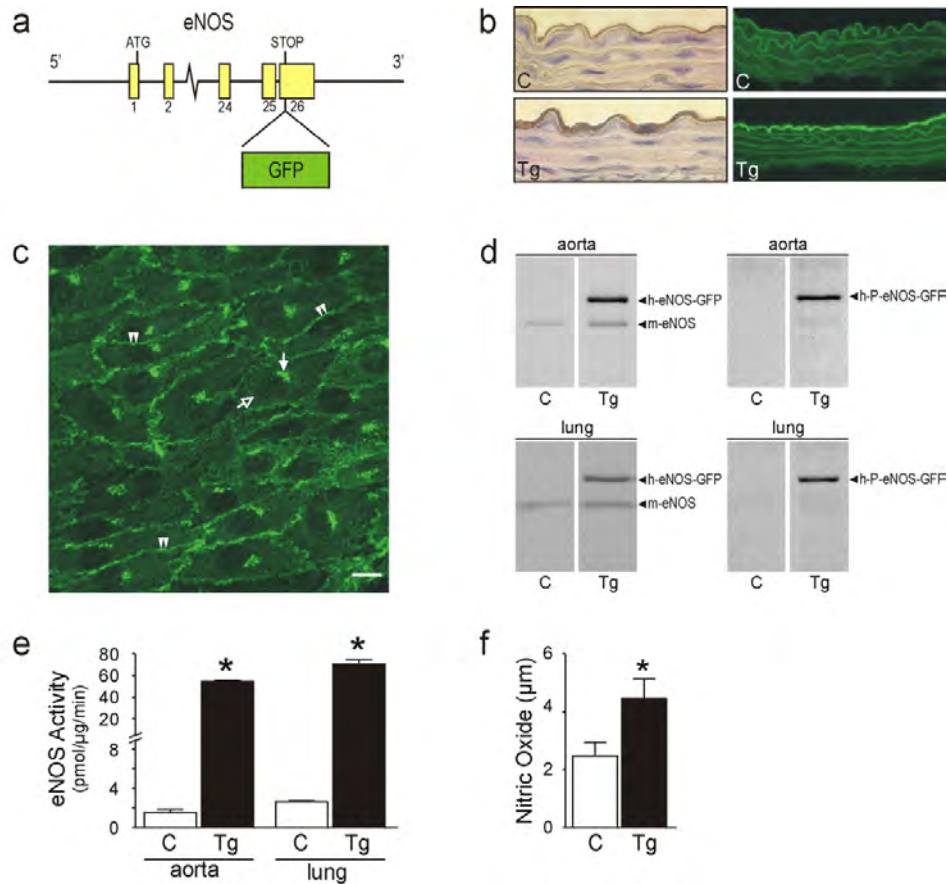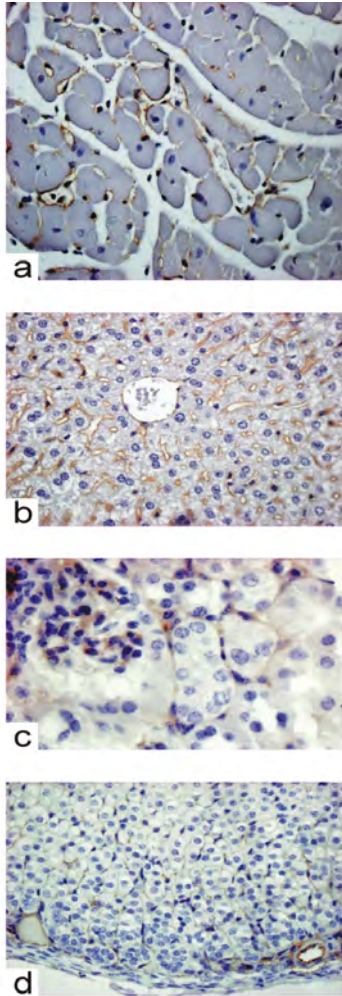

Figure 1. Transgenic mice expressing eNOS–GFP. a. The DNA construct used for the generation of eNOS–GFPtg mice consisted of the complete eNOS gene in which an eGFP encoding cassette was cloned in frame at the position of the eNOS STOP codon. The natural flanking sequences of the eNOS gene were left intact. b. Sections of aorta from control mice or eNOS–GFP transgenic mice, inspected with immunohistochemistry using an antibody directed against human eNOS (left panels) or by fluorescent microscopy (right panels). Original magnifications: 630x. c. Green fluorescence in endothelial cells from an intact carotid artery inspected with confocal microscopy. Double arrowheads point at fluorescence at the position of the plasma membrane, the white arrow at fluorescence at the position of the Golgi complex. The non-filled arrow points at the cell nucleus. Scale bar: 10 μm. d. Immunoblotting of

aorta (upper panels) or lung (lower panels) homogenates with antibodies directed against human eNOS (left panels), which show cross-reactivity with endogenous mouse eNOS, or antibodies directed against phosphorylated Ser-1177 from human eNOS (right panels). e. eNOS activity measured in aorta or lung homogenates by the L-arginine to L-citrulline conversion assay. n=9. *P<0.001. f. NO production in isolated aortas measured with an NO-sensitive electrode. n=11 (C), n=8 (Tg). *P<0.005. b, d-f: C: control mice, Tg: eNOS–GFP transgenic mice.

Localization of eNOS–GFP

In order to investigate the cell specificity of the expression of the transgene, sections from organs of eNOS–GFPtg mice were inspected by immunohistochemistry using an antibody directed against human eNOS (Fig. 2). eNOS immunoreactivity was detected in small blood vessels in the heart (Fig. 2a), in the sinusoids in the liver (Fig. 2b), in the peritubular capillaries and in the endothelial cells in the glomeruli in the kidney (Fig. 2c) and in the capillary sinusoids in the adrenal (Fig. 2d). eNOS protein was not found in the parenchymal cells of these organs. Sections from non-transgenic controls showed no immunoreactivity (not shown). This expression pattern was confirmed by fluorescence microscopy. Fig. 3 shows micrographs from heart (Fig. 3a,b), liver (Fig. 3c,d), kidney (Fig. 3e,f) and adrenal gland (Fig. 3g,h). The lining of the larger vessels was clearly fluorescent (Fig. 3c). A dense capillary network was fluorescent in the heart, surrounding the cardiomyocytes, and in the adrenal. The sinusoids in the liver, as well as the peritubular capillaries in the kidney showed a positive signal, just like the capillaries of the glomeruli in the kidney. The parenchymal cells of none of these organs showed appreciable expression. In sections from non-transgenic controls, no fluorescent signal was detected (not shown).

Figure 2. Localization of eNOS–GFP in various organs from eNOS–GFPtg mice visualized by immunohistochemistry using an antibody directed against human eNOS. a. heart, b. liver, c. kidney, d. adrenal. Original magnifications: 400x. Full color version of this figure is available in the color section.
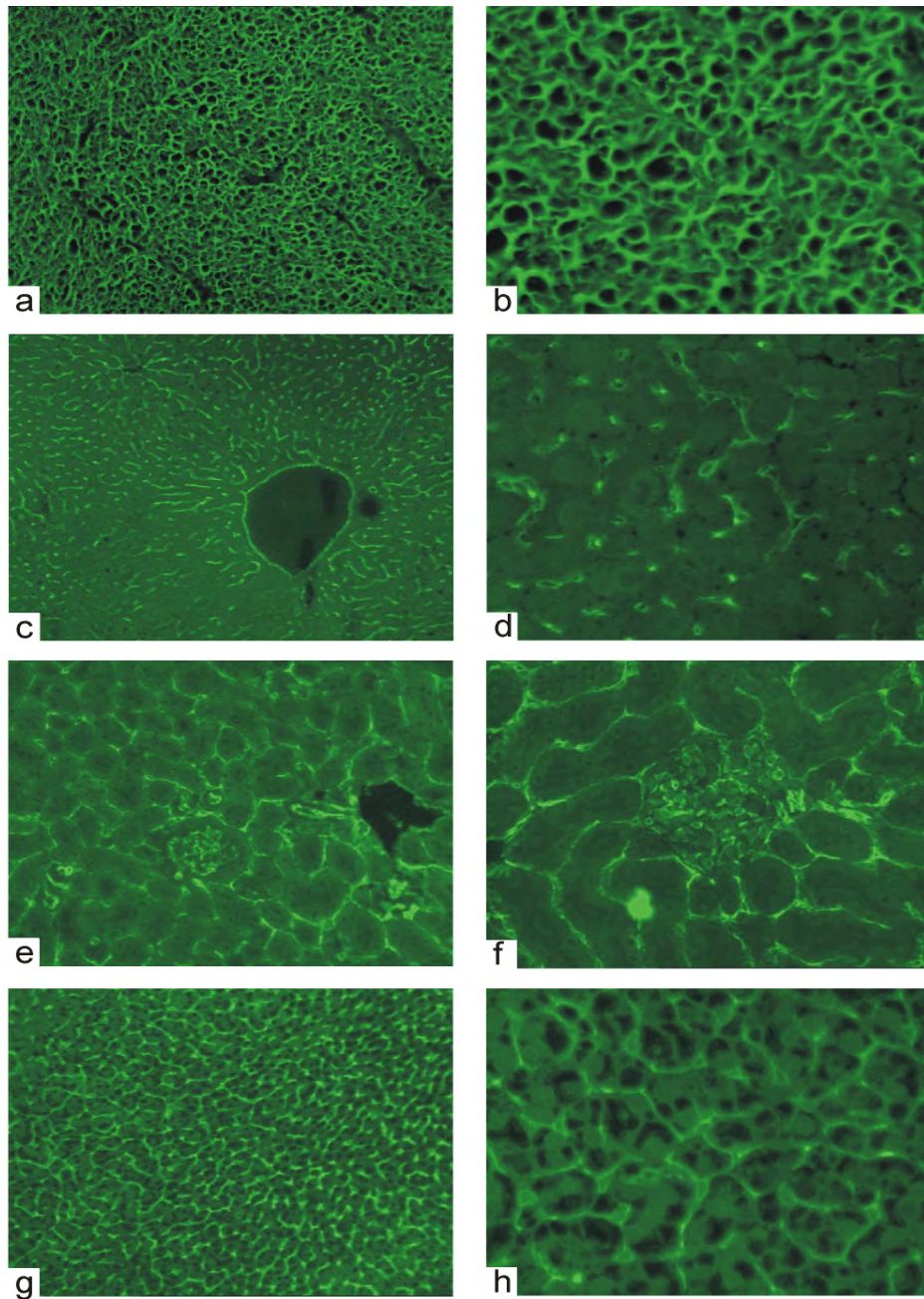
Figure 3. Localization of eNOS–GFP in various organs from eNOS–GFPtg mice visualized by fluorescence microscopy. a.,b.: heart, c.,d. liver, e.,f. kidney, g.,h. adrenal. Original magnifications: 100x (a.,c.,e.,g.), 400x (b.,d.,f.,h.).

Hemodynamic properties of eNOS–GFPtg mice

We performed hemodynamic measurements in eNOS–GFPtg mice compared to non-transgenic control mice. This was done in order to establish the functional activity of the eNOS–GFP fusion protein, as eNOS derived NO is an important modulator of vascular tone. As shown in figure 4a, the mean aortic pressure (MAP) was decreased in eNOS–GFP expressing mice compared to wild type litter mates by approximately 29%. Treatment with the NO synthase inhibitor N^G nitro-L-arginine methyl ester (L-NAME) resulted in an increase of the MAP and abolished the difference between transgenic mice and wild type littermates. The increase in the MAP (ΔMAP) caused by L-NAME treatment was greater in transgenic mice than in non-transgenic controls. There were no differences found in heart rate (Fig. 4b) or mean aortic blood flow (Fig. 4c) between transgenic or control mice, with or without treatment with L-NAME. Consequently, the difference in MAP can be attributed to a difference in systemic vascular resistance (Fig. 4d). In addition to a lower pressure in the systemic bed, we also observed a lower mean pulmonary artery pressure in eNOS–GFPtg mice of 30% (Fig. 4e). We also analyzed the heart weights of the transgenic mice in comparison with controls. No differences were found (Fig. 4f).

Plasma cholesterol levels in eNOS–GFPtg mice

Finally, we measured levels of plasma cholesterol in eNOS–GFPtg mice with different genetic backgrounds as models for variations in plasma cholesterol levels. We compared wild type background, heterozygous low density lipoprotein receptor deficient background, which results in a condition of slight hypercholesterolemia, and apolipoprotein E deficient background, which results in a condition of more severe hypercholesterolemia. We found a slight decrease in cholesterol levels in all backgrounds when comparing eNOS–GFP transgenic animals with animals without this transgene (Fig. 5a). Next, we analyzed the lipoprotein profile in two of these backgrounds. In wild type background, plasma cholesterol is predominantly found in high density lipoproteins (HDL) [19]. Thus, the cholesterol lowering observed in eNOS–GFP transgenic animals is found in HDL (Fig. 5b). In apolipoprotein E deficient background however, plasma cholesterol is present in the atherogenic lipoproteins, very low density lipoproteins (VLDL) and low density lipoproteins (LDL) [16]. In this background, expression of eNOS–GFP results in a decrease in both VLDL+LDL and HDL (Fig. 5c).
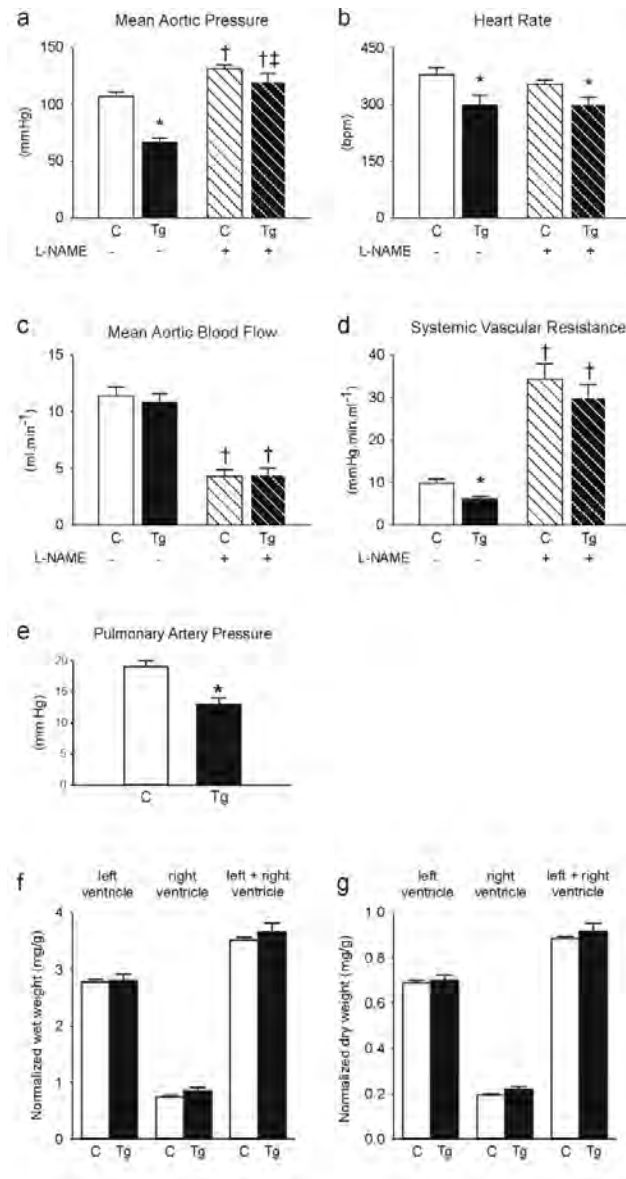
45

Figure 4. Hemodynamics and ventricular weights were measured in control mice (C) or eNOS–GFPtg mice (Tg) before and after addition of L-NAME. a. Mean aortic pressure; b. heart rate; c. mean aortic blood flow; d. systemic vascular resistance; e. pulmonary artery pressure; f. ventricular wet weights; g. ventricular dry weights. a-d: n=10 (C), n=9 (Tg), e: n=8 (C), n=6 (Tg), f-g: n=20 (C), n=12 (Tg). *: $P<0.05$ versus controls; †: $P<0.05$ versus controls before addition of L-NAME; ‡: $P<0.05$ Δ in C versus Δ in Tg (before and after addition of L-NAME).
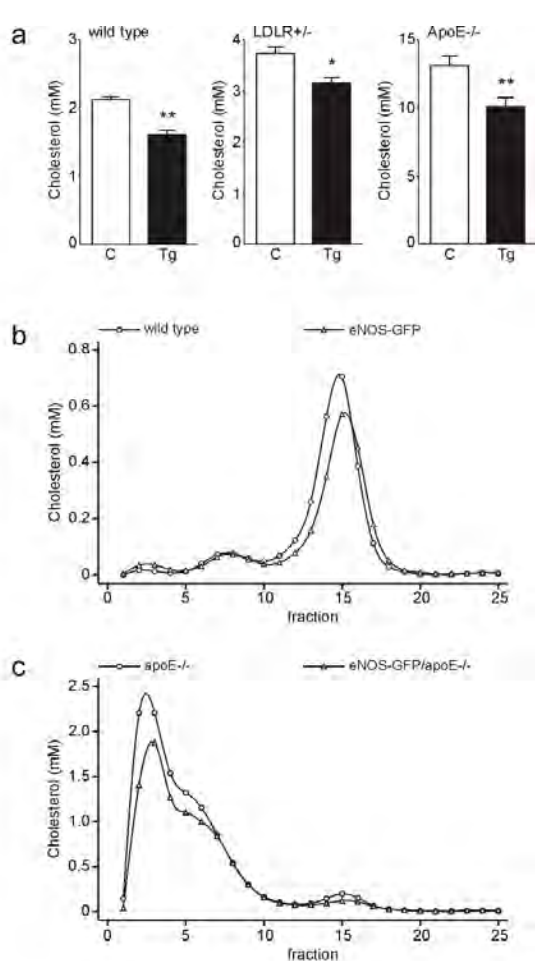
Figure 5. a. Plasma cholesterol concentrations of wild type, LDLR heterozygous knock out (LDLR+/-) and apolipoprotein E homozygous knock out (ApoE-/-) mice with (Tg) or without (C) the eNOS–GFP transgene. *: P<0.01 versus controls; **: P<0.001 versus controls. b.,c. Fractionation of lipoproteins by gel filtration of plasma from mice with wild type background (b) or apolipoprotein E knock out background (c). Fraction 1-5 contain VLDL, 6-11 contain LDL and 12-20 contain HDL.

47

2.5 Discussion

We generated transgenic mice that express human eNOS in fusion with GFP. In order to preserve transcriptional regulation, we used a genomic construct which contains the intronic sequences as well as the natural flanking sequences, including the previously identified endothelial enhancer located 4.9 kilobases upstream of the transcription initiation site [18]. The expression pattern was visualized either indirectly, via immunohistochemistry using antibodies directed against eNOS, or directly via fluorescence microscopy. Both techniques showed virtually the same distribution of the eNOS–GFP transgene in a variety of organs: endothelial cells of smaller and larger vessels in various organs are positive, while the parenchymal cells are not. These results indicate that the DNA construct used for microinjections resulted in expression of the transgene predominantly, if not exclusively, in endothelial cells.

The functionality of the eNOS–GFP fusion protein was demonstrated in two different ways. Using the L-arginine to L-citrulline conversion assay, it was shown that eNOS enzyme activity is ~30 fold higher in eNOS–GFP transgenic animals compared with non-transgenic controls. In ex vivo measurements with an NO sensor, NO production by endothelial cells in isolated blood vessels was shown to be 1.8 fold higher when vessels from eNOS–GFP transgenic mice were used.

The apparent discrepancy between these measurements can be explained by the difference between the methods that were used. In the L-arginine to L-citrulline conversion assay, a homogenate of aortic tissue was used. Cofactors and reagents are added to the assay in order to optimize the conditions for the enzymatic reaction. Therefore, the actual measurement represents the maximal eNOS activity, thereby reflecting the total amount of enzyme present. In contrast, the ex vivo measurements with the NO sensor were performed in intact blood vessels. As a consequence, the cellular regulation of the activity of the enzyme is still intact. In this system, the actual NO production is measured. This is much lower than the maximal enzymatic activity, probably because post-translational control of eNOS activity is intact.

In addition, blood pressure measurements showed that the mean aortic pressure was lower in eNOS–GFP transgenic animals compared with non-transgenic controls. This is in agreement with findings in other transgenic models of eNOS overexpression [16,20]. In the latter models, pulmonary pressures have not been measured. However, these are expected to be decreased as well, as the pulmonary vasodilator response following NO inhalation in patients is well known [21,22]. Indeed, we found lower pulmonary pressure in eNOS–GFP transgenic animals compared with non-transgenic controls.

GFP expression has been used in various transgenic mouse models and in numerous in vitro studies using cultured cells. It is generally assumed that the GFP protein itself does not interfere with any biological function of other proteins studied. However, specific expression in cardiomyocytes has been reported to result in hypertrophy [23]. Although the transgene in our mouse model is expressed in endothelial cells and not in cardiomyocytes, we measured the ventricular weights of transgenic and control

mice. No differences were found, demonstrating that hypertrophy probably does not occur in eNOS–GFPtg mice.

Previously, we generated and studied transgenic mice overexpressing eNOS without GFP [16]. In addition to a lower blood pressure, these animals displayed a decrease in plasma levels of cholesterol. Thus, we measured plasma cholesterol in eNOS–GFP transgenic mice and found a decrease of ~20% compared with non-transgenic mice (Fig. 5a). Plasma cholesterol in mice is for the larger part in HDL, which is generally believed to be atheroprotective [19]. Therefore, atherosclerosis in mouse models is usually studied in a genetic background with increased cholesterol in atherogenic very low density lipoproteins (VLDL) and low density lipoproteins (LDL). We crossbred eNOS–GFPtg mice with two of these models. In the first place, we crossbred them to low density lipoprotein receptor deficient mice, resulting in a background of heterozygous deficiency. This genetic background causes mild hypercholesterolemia [24]. In addition, we crossbred the mice in a apolipoprotein E deficient background, which causes more severe hypercholesterolemia [16]. In both of these backgrounds, we found that expression of eNOS–GFP results in lower levels of plasma cholesterol (Fig. 5a). While in wild type background a reduction in HDL-cholesterol was found (Fig. 5b), the effect in apolipoprotein E deficient mice was primarily in VLDL+LDL cholesterol (Fig. 5c). This is in agreement with our previous work, in which it was tentatively concluded that this effect contributed to the anti-atherogenic properties of elevated eNOS expression [16].

The mouse model described in the present study can be used to study the unusually complex regulation of eNOS [11,13]. Regulation takes place at the transcriptional level [25-27], and is responsive to variations in shear stress [28,29]. In addition, extensive regulation of eNOS activity at the post-translational level exists. These pathways are probably also active in the eNOS–GFPtg mice, as these are most likely responsible for the remarkable discrepancy between the level of protein overexpression and the physiological level of NO production (compare Fig. 1d,e with Fig. 1f). The post-translational regulatory mechanisms include protein–protein interactions, some of which affect the subcellular localization of the protein. eNOS is primarily located in the Golgi complex and in the caveolae in the plasma membrane, which were shown to be two pools of active enzyme [14], although others have suggested that active eNOS is largely restricted to caveolae [30-32]. A number of proteins have been shown to interact with eNOS and affect its activity. Caveolin, the structural protein of the caveolae, forms an inhibitory complex with eNOS [32], for which further evidence was provided by studies in caveolin deficient mice [33]. Upon activation by calcium, calmodulin can activate eNOS by displacing it from caveolin [34,35]. Another protein that binds to eNOS and subsequently activates it is heat shock protein 90 [36]. The latter protein appears to play a role in the caveolin–calmodulin regulatory complex [37]. Recently identified proteins that interact with eNOS have been termed NOSIP and NOSTRIN [38,39]. The functions of these proteins have not been established yet. Still another way of post-translational regulation of eNOS activity is protein modification,

like palmitoylation and myristoylation [40,41], or phosphorylation, especially of the serine at position 1177 (human eNOS) [42,43].

The eNOS–GFPtg mice described in the present study are particularly suited to study various aspects of the complex regulation of eNOS activity. Subcellular localization under various conditions or dynamic changes in this pattern upon various stimuli can be studied, as well as interactions with other proteins or with the cytoskeleton [44]. Valuable information has been achieved by studying expression of eNOS–GFP cDNA in transfected cells [45,46]. Our model also allows ex vivo and in vivo studies, including real time imaging by intravital microscopy. These type of studies will be useful to further assess the impact of eNOS activity in processes like reactivity to variations in shear stress or angiogenesis under conditions of ischemia or in tumor growth.

2.6 References:

1. Li H, Forstermann U: Nitric oxide in the pathogenesis of vascular disease. J Pathol 2000, 190:244-254.
2. Harrison DG: Cellular and molecular mechanisms of endothelial cell dysfunction. J Clin Invest 1997, 100:2153-2157.
3. Knowles JW, Reddick RL, Jennette JC, Shesely EG, Smithies O, Maeda N: Enhanced atherosclerosis and kidney dysfunction in eNOS(-/-)Apoe(-/-) mice are ameliorated by enalapril treatment. J Clin Invest 2000, 105:451-458.
4. Kuhlencordt PJ, Gyurko R, Han F, Scherrer-Crosbie M, Aretz TH, Hajjar R, Picard MH, Huang PL: Accelerated atherosclerosis, aortic aneurysm formation, and ischemic heart disease in apolipoprotein E/endothelial nitric oxide synthase double-knockout mice. Circulation 2001, 104:448-454.
5. Laufs U, La Fata V, Plutzky J, Liao JK: Upregulation of endothelial nitric oxide synthase by HMG CoA reductase inhibitors. Circulation 1998, 97:1129-1135
6. Kano H, Hayashi T, Sumi D, Esaki T, Asai Y, Thakur NK, Jayachandran M, Iguchi A: A HMG-CoA reductase inhibitor improved regression of atherosclerosis in the rabbit aorta without affecting serum lipid levels: possible relevance of up-regulation of endothelial NO synthase mRNA. Biochem Biophys Res Commun 1999, 259:414-419.
7. Sessa WC: Can modulation of endothelial nitric oxide synthase explain the vasculoprotective actions of statins? Trends Mol Med 2001, 7:189-191.
8. Nishida K, Harrison DG, Navas JP, Fisher AA, Dockery SP, Uematsu M, Nerem RM, Alexander RW, Murphy TJ: Molecular cloning and characterization of the constitutive bovine aortic endothelial cell nitric oxide synthase. J Clin Invest 1992, 90:2092-2096
9. Marsden PA, Heng HH, Scherer SW, Stewart RJ, Hall AV, Shi XM, Tsui LC, Schappert KT: Structure and chromosomal localization of the human constitutive endothelial nitric oxide synthase gene. J Biol Chem 1993, 268:17478-17488
10. Forstermann U, Boissel JP, Kleinert H: Expressional control of the 'constitutive' isoforms of nitric oxide synthase (NOS I and NOS III). Faseb J 1998, 12:773-790.
11. Fulton D, Gratton JP, Sessa WC: Post-translational control of endothelial nitric oxide synthase: why isn't calcium/calmodulin enough? J Pharmacol Exp Ther 2001, 299:818-824.
12. Govers R, Rabelink TJ: Cellular regulation of endothelial nitric oxide synthase. Am J Physiol Renal Physiol 2001, 280:F193-206.
13. Marletta MA: Another activation switch for endothelial nitric oxide synthase: why does it have to be so complicated? Trends Biochem Sci 2001, 26:519-521.

14. Fulton D, Fontana J, Sowa G, Gratton JP, Lin M, Li KX, Michell B, Kemp BE, Rodman D, Sessa WC: Localization of endothelial nitric-oxide synthase phosphorylated on serine 1179 and nitric oxide in Golgi and plasma membrane defines the existence of two pools of active enzyme. J Biol Chem 2002, 277:4277-4284

15. Bakker CE, de Diego Otero Y, Bontekoe C, Raghoe P, Luteijn T, Hoogeveen AT, Oostra BA, Willemsen R: Immunocytochemical and biochemical characterization of FMRP, FXR1P, and FXR2P in the mouse. Exp Cell Res 2000, 258:162-170

16. Van Haperen R, De Waard M, Van Deel E, Mees B, Kutryk M, Van Aken T, Hamming J, Grosveld F, Duncker DJ, De Crom R: Reduction of blood pressure, plasma cholesterol, and atherosclerosis by elevated endothelial nitric oxide. J Biol Chem 2002, 277:48803-48807

17. Lie J, de Crom R, van Gent T, van Haperen R, Scheek L, Lankhuizen I, van Tol A: Elevation of plasma phospholipid transfer protein in transgenic mice increases VLDL secretion. J Lipid Res 2002, 43:1875-1880

18. Laumonnier Y, Nadaud S, Agrapart M, Soubrier F: Characterization of an upstream enhancer region in the promoter of the human endothelial nitric-oxide synthase gene. J Biol Chem 2000, 275:40732-40741.

19. van Haperen R, van Tol A, Vermeulen P, Jauhiainen M, van Gent T, van den Berg P, Ehnholm S, Grosveld F, van der Kamp A, de Crom R: Human plasma phospholipid transfer protein increases the antiatherogenic potential of high density lipoproteins in transgenic mice. Arterioscler Thromb Vasc Biol 2000, 20:1082-1088.

20. Ohashi Y, Kawashima S, Hirata K, Yamashita T, Ishida T, Inoue N, Sakoda T, Kurihara H, Yazaki Y, Yokoyama M: Hypotension and reduced nitric oxide-elicited vasorelaxation in transgenic mice overexpressing endothelial nitric oxide synthase. J Clin Invest 1998, 102:2061-2071.

21. Hurford WE: Inhaled nitric oxide. Respir Care Clin N Am 2002, 8:261-279

22. Sitbon O, Humbert M, Simonneau G: Primary pulmonary hypertension: Current therapy. Prog Cardiovasc Dis 2002, 45:115-128

23. Huang WY, Aramburu J, Douglas PS, Izumo S: Transgenic expression of green fluorescence protein can cause dilated cardiomyopathy. Nat Med 2000, 6:482-483

24. van Haperen R, van Tol A, van Gent T, Scheek L, Visser P, van der Kamp A, Grosveld F, de Crom R: Increased risk of atherosclerosis by elevated plasma levels of phospholipid transfer protein. J Biol Chem 2002, 277:48938-48943

25. Zhang R, Min W, Sessa WC: Functional analysis of the human endothelial nitric oxide synthase promoter. Sp1 and GATA factors are necessary for basal transcription in endothelial cells. J Biol Chem 1995, 270:15320-15326

26. Karantzoulis-Fegaras F, Antoniou H, Lai SL, Kulkarni G, D'Abreo C, Wong GK, Miller TL, Chan Y, Atkins J, Wang Y, Marsden PA: Characterization of

the human endothelial nitric-oxide synthase promoter. J Biol Chem 1999, 274:3076-3093

27. Wu KK: Regulation of endothelial nitric oxide synthase activity and gene expression. Ann N Y Acad Sci 2002, 962:122-130

28. Topper JN, Cai J, Falb D, Gimbrone MA, Jr.: Identification of vascular endothelial genes differentially responsive to fluid mechanical stimuli: cyclooxygenase-2, manganese superoxide dismutase, and endothelial cell nitric oxide synthase are selectively up-regulated by steady laminar shear stress. Proc Natl Acad Sci U S A 1996, 93:10417-10422

29. Go YM, Boo YC, Park H, Maland MC, Patel R, Pritchard KA, Jr., Fujio Y, Walsh K, Darley-Usmar V, Jo H: Protein kinase B/Akt activates c-Jun NH(2)-terminal kinase by increasing NO production in response to shear stress. J Appl Physiol 2001, 91:1574-1581

30. Blair A, Shaul PW, Yuhanna IS, Conrad PA, Smart EJ: Oxidized low density lipoprotein displaces endothelial nitric-oxide synthase (eNOS) from plasmalemmal caveolae and impairs eNOS activation. J Biol Chem 1999, 274:32512-32519

31. Uittenbogaard A, Shaul PW, Yuhanna IS, Blair A, Smart EJ: High density lipoprotein prevents oxidized low density lipoprotein-induced inhibition of endothelial nitric-oxide synthase localization and activation in caveolae. J Biol Chem 2000, 275:11278-11283

32. Everson WV, Smart EJ: Influence of caveolin, cholesterol, and lipoproteins on nitric oxide synthase: implications for vascular disease. Trends Cardiovasc Med 2001, 11:246-250

33. Schubert W, Frank PG, Woodman SE, Hyogo H, Cohen DE, Chow CW, Lisanti MP: Microvascular hyperpermeability in caveolin-1 (-/-) knock-out mice. Treatment with a specific nitric-oxide synthase inhibitor, L-name, restores normal microvascular permeability in Cav-1 null mice. J Biol Chem 2002, 277:40091-40098

34. Michel JB, Feron O, Sase K, Prabhakar P, Michel T: Caveolin versus calmodulin. Counterbalancing allosteric modulators of endothelial nitric oxide synthase. J Biol Chem 1997, 272:25907-25912

35. Michel T, Feron O: Nitric oxide synthases: which, where, how, and why? J Clin Invest 1997, 100:2146-2152

36. Garcia-Cardena G, Fan R, Shah V, Sorrentino R, Cirino G, Papapetropoulos A, Sessa WC: Dynamic activation of endothelial nitric oxide synthase by Hsp90. Nature 1998, 392:821-824

37. Gratton JP, Fontana J, O'Connor DS, Garcia-Cardena G, McCabe TJ, Sessa WC: Reconstitution of an endothelial nitric-oxide synthase (eNOS), hsp90, and caveolin-1 complex in vitro. Evidence that hsp90 facilitates calmodulin stimulated displacement of eNOS from caveolin-1. J Biol Chem 2000, 275:22268-22272

38. Dedio J, Konig P, Wohlfart P, Schroeder C, Kummer W, Muller-Esterl W: NOSIP, a novel modulator of endothelial nitric oxide synthase activity. Faseb J 2001, 15:79-89

39. Zimmermann K, Opitz N, Dedio J, Renne C, Muller-Esterl W, Oess S: NOSTRIN: a protein modulating nitric oxide release and subcellular distribution of endothelial nitric oxide synthase. Proc Natl Acad Sci U S A 2002, 99:17167-17172

40. Robinson LJ, Michel T: Mutagenesis of palmitoylation sites in endothelial nitric oxide synthase identifies a novel motif for dual acylation and subcellular targeting. Proc Natl Acad Sci U S A 1995, 92:11776-11780

41. Sakoda T, Hirata K, Kuroda R, Miki N, Suematsu M, Kawashima S, Yokoyama M: Myristoylation of endothelial cell nitric oxide synthase is important for extracellular release of nitric oxide. Mol Cell Biochem 1995, 152:143-148

42. Fulton D, Gratton JP, McCabe TJ, Fontana J, Fujio Y, Walsh K, Franke TF, Papapetropoulos A, Sessa WC: Regulation of endothelium-derived nitric oxide production by the protein kinase Akt. Nature 1999, 399:597-601.

43. Dimmeler S, Fleming I, Fisslthaler B, Hermann C, Busse R, Zeiher AM: Activation of nitric oxide synthase in endothelial cells by Akt- dependent phosphorylation. Nature 1999, 399:601-605.

44. Venema VJ, Marrero MB, Venema RC: Bradykinin-stimulated protein tyrosine phosphorylation promotes endothelial nitric oxide synthase translocation to the cytoskeleton. Biochem Biophys Res Commun 1996, 226:703-710

45. Liu J, Hughes TE, Sessa WC: The first 35 amino acids and fatty acylation sites determine the molecular targeting of endothelial nitric oxide synthase into the Golgi region of cells: a green fluorescent protein study. J Cell Biol 1997, 137:1525-1535

46. Sowa G, Liu J, Papapetropoulos A, Rex-Haffner M, Hughes TE, Sessa WC: Trafficking of endothelial nitric-oxide synthase in living cells. Quantitative evidence supporting the role of palmitoylation as a kinetic trapping mechanism limiting membrane diffusion. J Biol Chem 1999, 274:22524-22531

Chapter 3:
Shear Stress Alterations Induce eNOS Response: Direct Demonstration by a Novel *in vivo* Technique

3.1 Abstract

The focal location of atherosclerosis in the vascular tree is correlated with local variations in shear stress. We developed a method to induce defined variations in shear stress in a straight vessel segment of a mouse. To this end, a cylinder with a tapered lumen is placed around the carotid artery, inducing a high shear stress field. Concomitantly, regions of low shear stress and oscillatory shear stress are created upstream and downstream of the device, respectively. This device was used in mice transgenic for an eNOS-GFP fusion gene. We observed a strong induction of eNOS-GFP mRNA expression in the high shear stress region compared with the other regions ($P<0.05$). Quantification of eNOS-GFP fluorescence showed an S-like relation between eNOS-GFP levels and shear stress that could be described by a hill equation, thereby providing direct evidence that eNOS expression is shear stress responsive in an *in vivo* situation. In addition, we demonstrate *in vivo* shear stress responses of ET-1, ACE, SOD, and ACE. This model provides the opportunity to study the relation between shear stress alterations, gene expression and atherosclerosis.

3.2 Introduction

Wall shear stress is the drag force acting on the endothelial cells as a result of the blood flow. In straight arteries, laminar flow with an average shear stress level of 1.5 N/m^2 prevail and this level is actively maintained by adjusting the vascular tone and by structural remodelling in response to shear stress[1,2].

The relation between low wall shear stress and the occurrence of atherosclerotic lesions in the vascular tree has been recognized since several decades [3,4], but the mechanism underlying this relation is unknown. Furthermore, it is not clear whether low shear stress (<1.5 N/m^2) or oscillatory shear stress (exhibiting directional change) is more important for the development of atherosclerosis [5,6]. It has been postulated that altered shear stress results in changes in gene expression and protein function [7,8]. This was confirmed in experiments studying endothelial cells in flow chambers under well-controlled shear stress conditions *in vitro* [9] [10]. Such changes can underlie the observed susceptibility to atherosclerosis of the affected vascular regions. Indeed, endothelial cells located at athero-susceptible sites show a specific pattern of gene expression *in vivo* [11,12], indicating a relationship with shear stress. However, this relation has not been substantiated by direct causal *in vivo* evidence. Moreover, there is no *in vivo* model that generates oscillations in shear stress. Therefore, we developed a new method by which low and oscillatory shear stress is introduced in different segments of a straight vessel. The first aim of the present study is to demonstrate that the proposed method induces a complex shear stress field *in vivo*.

To evaluate whether these changes in shear stress affect gene expression, we chose to monitor one of the best-characterized shear stress responsive genes, endothelial nitric oxide synthase (eNOS) [13,14]. This was studied in an in-house developed transgenic mouse model in which eNOS expression and distribution can be easily monitored by virtue of a fusion of the protein with green fluorescent protein[15]. An additional selection of genes that have been reported to be shear stress responsive *in vitro* (endothelin (ET)-1[16-21], cyclo-oxygenase (COX)-1[22,23], angiotensin converting enzyme (ACE)[24] and super oxide dismuthase (SOD)[25,26]) were also studied in the cast model using quantitative PCR techniques.

3.3 Materials and Methods

Animals
Mice expressing an eNOS-GFP fusion protein were generated as described before [15]. Mice were bred to C57BL/6 background for at least 10 generations (>99% C57BL/6), and were 15-20 weeks of age. Animal care and experiments complied with institutional and national guidelines.

In vivo alteration of shear stress
In order to induce standardized changes in shear stress, we designed a shear stress modifier, which was manufactured of the thermoplastic, polyetherketon. The device is referred to as *cast* throughout the study. The cast consists of two longitudinal halves of a cylinder with a cone shaped lumen (Figure 1a). The geometry of the cast has been designed with computational flow dynamics software [27] to produce vortices downstream of the cast when placed around the common carotid artery (Figure 1b). This downstream region will therefore be exposed to oscillations in shear stress (oscillatory shear stress region). The upstream inner diameter is 500 μm (non-constrictive) and gradually declines to 250 μm at the downstream side of the cast (constrictive). This tapering induces a gradual increase in shear stress (high shear stress region). In addition, the constrictive stenosis decreases the blood flow, resulting in a low shear stress region upstream from the cast. Control casts consist of a cylinder with a continuous non-constrictive diameter of 500 μm. Adequacy of the cast design was evaluated by Doppler measurements. For surgery, the mice were anesthetized with isoflurane. Both halves of the cast were placed around the right common carotid artery and fixed with a suture. Animals with cast implants were sacrificed at 1-6 days after surgery by *in situ* fixation.

Instrumentation of rabbits
Two groups of rabbits were studied. In the first group (n= 5), the immediate effect of cast placement was studied while in the second group (n = 5) the chronic effect of a two-week period of cast placement was evaluated. Two separate groups were studied, as we did not want to introduce catheters during instrumentation in the chronic group. In both groups, the rabbits were premedicated with a mixture of fentanyl (0.3 mg/ml) and fluanisone (0.6 mg/ml) (Hypnorm® 0.5 ml/kg i.m.) and anesthetized with an infusion of fentanyl (infusion rate: 0.3 mg/kg/hr) and a 2:1 mixture of N_2O and O_2. Subsequently, the rabbits were intubated and the respirator (Infant Respirator, Hoek Loos, Schiedam, The Netherlands) was adjusted to achieve and maintain physiological blood gas levels (7.35< pH <7.45; 35 mmHg<PCO_2< 45 mmHg; PO2>100 mmHg). The marginal ear artery was cannulated for arterial pressure measurement with a fluid filled catheter (Amatek Inc, Paoli, PA), for arterial blood withdrawal and for the infusion of fentanyl. During instrumentation of group I and after two weeks in group II, the iliac artery was dissected and a 4 French (Fr) sheet (Fast Cath®, Daig inc. Minnetonka, MN) was placed for the advancement of guide wires and guiding catheters. In 50% of the cases the

diameter of the iliac arteries was too small and the aorta was directly punctured. After performing angiography (see below), the carotid artery was surgically exposed and dissected from its surrounding tissue. After a stabilization period of 30 minutes, recordings of baseline hemodynamics were performed. Next, in the acute group, a guiding catheter (Fast Cath®, Daig inc. Minnetonka, MN) was advanced into the entrance of one of the two carotid arteries, which was randomly selected. Thirty to sixty seconds after a bolus of nitroglycerine (0.5 mg; Cedocard®; Dyk inc., The Netherlands), injected through the guiding catheter, contrast material (Iodixanol, Nicomed b.v., Breda, The Netherlands) was injected and angiography was performed with an X-ray system (Cardioskop-U, Siemens Nederland b.v., The Haque, The Netherlands). Following this, the other carotid artery was imaged in the same way. Subsequently, in both groups, one of the carotid arteries was dissected and a 20 mHz range-gated Doppler sensor (model VF-1, Crystal Biotech, Hopkinton, Mass) was placed at an angle of 45 degrees. The range gating properties allowed us to determine minimal and maximal velocities over the cross section of the vessel lumen. The other carotid artery was used as a control vessel.

As a next step, the cast was placed around the carotid artery and recordings of systemic hemodynamics and Doppler velocities downstream of the cast were repeated, followed by angiography as described above. The Doppler measurements distally from the constrictor were intended for the detection of velocity reversal. To that end, we carefully positioned the Doppler sensor to place the sample volume near the expected location of the vortex.

In the acute group, the animal was terminated at the end of the measurement protocol. In the chronic group, after the placement of the constrictor around the carotid artery, the incision in the neck was closed with a two-layer suture. At the end of each procedure, acetylsalicylic acid (10 mg/kg i.m., Aspegic®, Lorex Synthelabo, Maarsen, The Neherlands) and Amoxicillin (25 mg/kg i.m., Clamoxyl®, SmithKline Beecham, Rijswijk, The Netherlands) were given to prevent trombocyte aggregation and wound infection, respectively. During the two-week follow-up period, clopidogrel (25 mg, p.o., Plavix®, Sanofi Winthrop, The Netherlands) and acetylsalicylic acid (Aspegic, 10 mg/kg, p.o.) were given daily. After two weeks all hemodynamic and angiographic measurements as described for the acute group were performed.

Doppler measurements in mice.
Mice were anesthetized with isoflurane, intubated, and ventilated with a 1:2 mixture of O_2/N_2O to which 2.3% of isoflurane was added. The animals were maintained at 37°C on a heating-pad during the whole experiment, a neck incision was made and both the left and right common carotid arteries were dissected from connective tissue. Calibrated digital images were taken in order to measure vessel diameters. Doppler velocity signals were measured on both carotid arteries using a 20 MHz range-gated Doppler probe at a 45° angle from the vessel wall. The cast was then placed around the carotid artery

upstream of the Doppler probe, and the measurement was repeated. Additionally, the Doppler signal in the left carotid artery after cast placement was recorded.

Confocal microscopy
Tissue samples were examined under a Zeiss LSM510LNO inverted laser scanning confocal fluorescence microscope (Carl Zeiss, Thornwood, USA). Images of GFP fluorescence were acquired by excitation with a 488 nm argon laser and were detected using a 500-550 bandpass barrier filter. Background fluorescence was corrected for by subtracting the image that was acquired after filtering the emission spectrum with a 560 nm longpass filter. To obtain an image of an intact whole mounted vessel, an optical slice of 40 μm thickness and 500 μm x 500 μm in cross sectional area was obtained using the 10x Axiovert lens. Next, the position of the table was changed in order to image several adjacent vessel sections encompassing the entire vessel segment under study. Individual images were fused to form a tile (Figure 1d) in order to provide a complete picture of the vessel.

Quantitative PCR
Carotid arteries treated with casts were divided into three different regions: 1 mm of the low shear stress region upstream of the cast, 1 mm of the high shear stress region in the cast, and 1 mm of the oscillatory shear stress region downstream of the cast. Similar 1 mm sections of the untreated contra-lateral carotid arteries from the same animals were isolated to serve as controls. Total RNA from each region was obtained using the RNAeasy kit (Qiagen, Cologne, Germany), treated with DNA-ase and cDNA was obtained by reverse transcription reaction. Primers were designed for the studied genes: mouse SOD, ACE, COX-1 and ET-1, and for human eNOS. Tissue samples of each region from 5 individual mice were pooled and mRNA expression levels were analysed by real time PCR using the iCycler iQ Detection System (Biorad, Veenendaal, The Netherlands) in three separate experiments. The hypoxanthine guanine phosphoribosyl transferase (HPRT) gene was used as a house keeping gene.

Computational fluid dynamics
In order to estimate the augmentation in wall shear stress distribution after cast placement, a 3-D computational fluid dynamical technique (CFD) was used [39]. The CFD needed the vessel geometry as input, which was obtained from the contours of the GFP images, assuming a circular geometry and constant circumference of the intact vessel (Figure 1c). On the basis of this geometry a mesh was generated, which consisted of approximately 20.000 nodes. The boundary conditions for the calculations were: no slip conditions at the wall, stationary parabolic inflow at the entrance with a maximal velocity equivalent to a shear stress of 1.5 N/m^2 and zero stress outflow. The combination of the mesh geometry and boundary conditions were used to solve the Navier-Stokes equations, applying a well-validated finite element software package (Sepran, Sepra, Delft, The Netherlands) in order to calculate shear

stress (Figure 1d,e). The accuracy of the calculations was set at 10^{-4} m/sec, which resulted in a numerical error of wall shear stress of approximately 1%.

Analysis and statistics
In order to relate the GFP signal to the shear stress calculations the in-house developed software automatically selected the same region as used for the CFD analyses. The centre-line of the vessel was generated using an iterative optimisation method. Lines of integration perpendicular to this centre-line served to average the GFP signal at similar positions as the shear stress calculations (Figure 1f). The relationship between shear stress and eNOS-GFP was described for each individual vessel by a sigmoid curve, applying an iterative algorithm. After setting initial parameters an optimal data set was selected on basis of a line search algorithm and a steepest decline algorithm.

Diameters of the blood vessels were determined for the entire arterial segment under study before, immediately after, and 6 days after cast placement, using a high-resolution digital camera coupled to the dissection microscope. Diameter analysis was performed of 2 mm segments immediately upstream and downstream of the cast. Vessel wall thickness was measured in cross-sections of the *in situ* fixated vessels.

Statistical analyses were performed using one-way ANOVA followed by Dunnett's ad-hoc test (SigmaStat, version 2.03, Systat Software Inc., Richmond, California, USA). The Student's *t*-test was used in the Doppler evaluations. Data are presented as mean ± SEM. *P* values <0.05 were considered statistically significant.
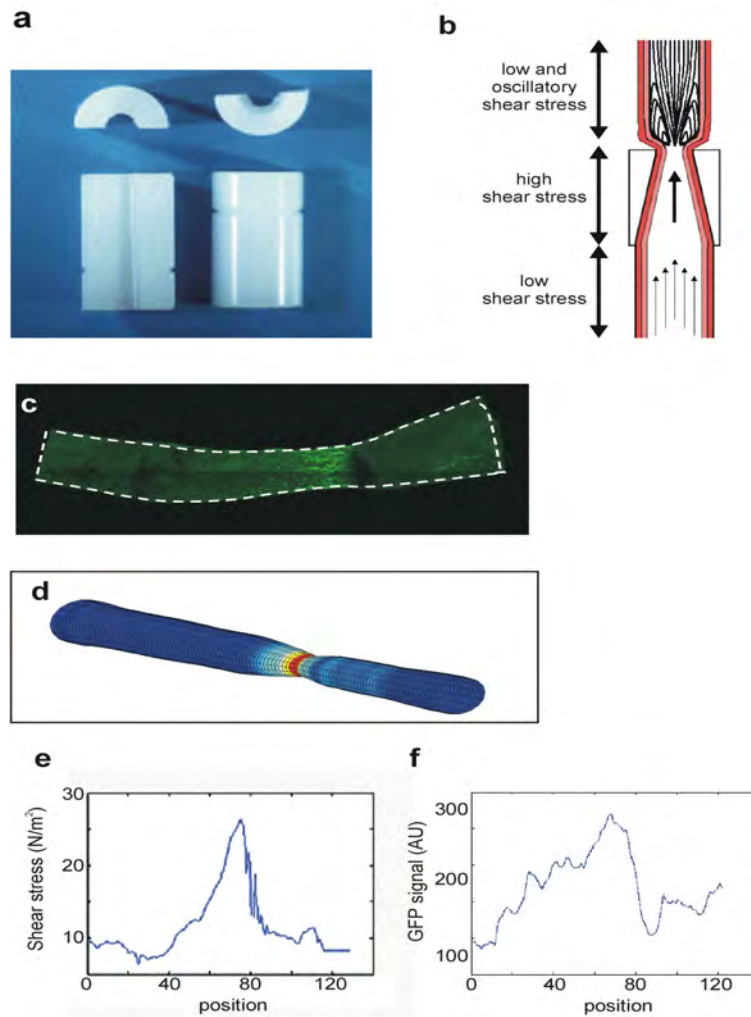
Figure 1: Design of the shear stress modifier: cast model. (a) The cast consists of two longitudinal halves of a cylinder with a conical lumen. (b) The theoretical design with induction of large vortices downstream of the cast in the carotid artery. Additionally, the conical lumen induces a stenosis of the vessel, causing a gradual increase in vascular shear stress in the cast area. Because of the stenosis, a region of low shear stress is created upstream of the cast. (c) Contours were obtained of GFP images, assuming a circular geometry of the vessel. (d) The computer generated 3 D mesh of the vessel lumen in which the shear stress was calculated. (e) The distribution of shear stress (N/m^2) along the vessel. (f) Quantification of the GFP signal using the same images: The distribution of eNOS-GFP (in arbitrary units) along the vessel wall.

3.4 Results

Cast placement in rabbits induces flow reversal in the distal region.
In a group of 10 New Zealand White rabbits, mean arterial blood pressure and heart rate were not affected, immediately and two weeks after cast placement. Average, maximal and minimal Doppler velocities were consistent with a laminar velocity profile before cast placement. However, after cast placement all animals exhibited reversal of velocity near the endothelium distal from the cast with an unchanged maximal velocity in the centre of the blood vessel (see Table 1). These reversals in velocity indicate the occurrence of vortices in the area downstream from the cast.

Table 1: Systemic hemodynamics before and after cast placement in rabbits

	Before cast placement	After cast placement	2 weeks follow up
Heart rate (beats/min)	200±13	200±12.5	196±9.8
Mean arterial pressure (mmHg)	77±1.8	73±3.6	67±2.2
Minimal velocity (cm/sec)	9.8±2.5	-9.9±1.9*	-10.4±2.8*
Maximal velocity (cm/sec)	45.5±10.7	37.1±8.3	39.0±14

N=10, * *P*<0.05 versus before cast placement.

Cast placement reduces the blood flow in the proximal region.
In a group of eNOS-GFP transgenic mice, the average blood flow was initially 2.9 ± 0.3 ml/min and 2.8 ± 0.2 ml/min in the right and left common carotid arteries, respectively (See supplemented data figure S1a). Directly after cast placement, the blood flow was significantly reduced to an average of 2.0 ± 0.2 ml/min (P<0.001) in the low shear stress region upstream to the cast in the right carotid artery. This reduction was observed in each animal. The reduction in blood flow was solely due to the increase in resistance from the stenosis caused by the cast, as vascular diameters upstream of the cast region before (538±39 μm) and immediately after (535±48 μm) cast placement remained unchanged. The vascular diameter downstream of the cast region also remained unchanged after cast placement (546±48 μm vs. 593±91 μm, respectively). In the left carotid artery, the blood flow was not affected by cast placement around the right vessel (2.75±0.21 ml/min vs. 2.88±0.18

ml/min, respectively). Placement of a non-tapering control cast around the right carotid artery did not affect the blood flow in both carotid arteries (See supplemented data figure S1a). Vascular remodeling of the carotid artery was minimal both in the upstream and downstream segments during the time period used in this study (6 days; see supplement data figure S4).

Expression of eNOS protein is shear stress responsive in vivo.
In mice instrumented with the cast, a gradual increase in fluorescence is clearly visible along the length of the vessel segment that was located in the cast (Figure 2a, arrow). Both the fluorescent signal and the shear stress were quantified along the length of the carotid artery segment, and were found to increase along the decreasing diameter of the cast (Figure 2b). Similar responses were observed in all of the treated animals. In a time series of 1, 2, 4, and 6 days of cast implantation, the response is already present after one day and remains unchanged for at least 6 days (Results shown in data supplement figure S2). To exclude other factors introduced by tapering (like damage to the vessel wall and endothelium), control experiments were performed in which the blood vessel was ligated downstream of the cast, resulting in complete obstruction of the flow and consequently in the abolishment of shear stress. In this situation the cast model does not induce variations in eNOS-GFP expression (Figure 2c), indicating that there are no direct effects of the surgical procedure or the presence of the cast. In addition, placement of the non-constrictive control-cast does not result in changes in eNOS-GFP expression (Figure 2d), indicating that the geometry of the constrictive cast, inducing variations in shear stress patterns, is responsible for the observed effects.
Next we assessed whether shear stress affects mRNA expression of the human eNOS transgene in the different regions. Both the low and oscillatory shear stress regions show a 3-fold decrease in eNOS mRNA expression compared to the control vessel (undisturbed shear stress) (Figure 2e), while the average eNOS expression in the high shear stress region is similar to control. The expression of endogenous murine eNOS was similarly affected by shear stress variations (see supplement data figure S3).

Expression of known shear stress responsive genes in vivo.
We further validated the cast model on its capacity to elicit a biological response, comparing the effect of low shear stress to oscillatory shear stress. In C57BL/6 wildtype mice we measured mRNA levels of an additional subset of shear stress responsive genes. We found that SOD, ACE, COX-1 and ET-1 expression levels are decreased with respect to the control vessel. Distally from the cast, where vortices are active, all genes are further downregulated compared to the low shear stress regions with the exception of SOD (Figure 3), which remains unchanged.
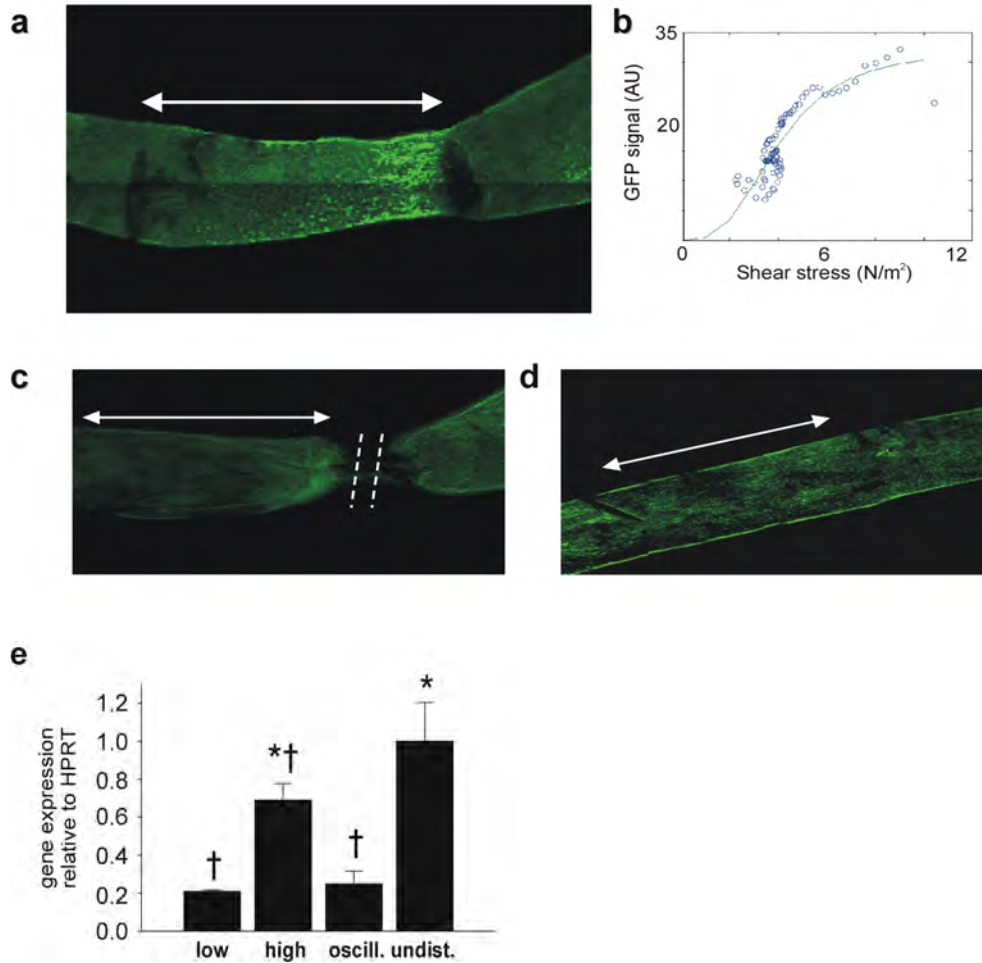
64

Figure 2: Effect of cast placement around carotid arteries on eNOS-GFP fluorescence. (a) Fluorescence of eNOS-GFP was imaged in the right carotid artery after the instalment of a tapering cast. The arrow indicates the position where the cast was situated (high shear stress region). The direction of the blood flow was from left to right. (b) Relation between shear stress and eNOS-GFP fluorescence: Representative example of the relation between the calculated shear stress and eNOS-GFP fluorescence along a linear segment of the carotid artery of an individual mouse. (c) Effect on eNOS-GFP fluorescence following downstream ligation of the carotid artery with a tapering cast, or (d) placement of a non-tapering cast. Arrows indicate the cast region, and dashed lines mark the site of ligation. (e) eNOS mRNA levels of the human transgene in the segments of the right carotid artery after the instalment of a tapering cast: 1 mm immediately upstream of the cast (low shear stress), 1 mm in the cast (high shear stress) and 1 mm immediately downstream of the cast (oscillating

shear stress), and in 1mm of the contra-lateral control carotid artery (undisturbed shear stress). n =3 groups (5 animals per group), * P<0.05 versus low shear stress, † P<0.05 versus undisturbed shear stress. Note that Figure 2a is derived from the same picture as Figure 1c.
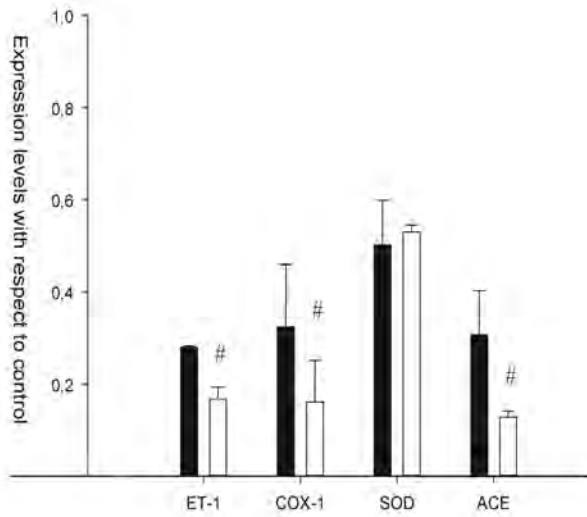

Figure 3: Expression levels for endothelin-1 (ET-1), angiotensin converting enzyme (ACE), cyclo-oxygenase (COX-1) and superoxide dismuthase (SOD) in low shear stress conditions (Panel A) and oscillatory shear stress (Panel B). All values were normalized to the contra-lateral control vessel. This implies that values smaller than one are values smaller than the value of the control vessel. # P<0.05

3.5 Discussion

In the present study, we present a novel technique to induce complex shear stress fields *in vivo*. From the results we conclude that: (a) the technique induces changes in shear stress; (b) augmentation of shear stress results in elevated eNOS gene expression and eNOS protein levels as previously suggested by *in vitro* experiments. Augmentation of shear stress up-regulates eNOS within 1 day, lasting until at least 6 days. These results are in agreement with previous findings [13,14,28]. Control experiments with a non-tapered cast or the abolishment of shear stress in the tapered cast by blood flow arrest indicate that variations in local shear stress induce the observed responses in eNOS expression. Induction of oscillatory shear stress in the downstream area from the cast is demonstrated by Doppler sonography as well as by the loss of the alignment of endothelial cells with the flow direction. In addition, responses in SOD, ACE, COX-1 and ET-1 expression levels were observed in C57BL/6 wildtype animals under stimulation of the different shear stress parameters. These results demonstrate that the new cast model is effective in triggering responses in gene expression caused by variations in shear stress.

Limitations of the study
mRNA studies. Although the fluorescent signal is clearly increased in the high shear stress region compared with the undisturbed shear stress region (Figure 3a, 4a, and 6a, middle panel), the eNOS mRNA levels were similar (Figure 2e). This could be due to differences in sampling. Confocal microscopy demonstrated significant variation in eNOS-GFP signal within the high shear stress region (Figure 2a). However, for RNA measurements complete segments were collected and therefore the data represent the average eNOS expression, masking variations caused by hemodynamic differences within the segments. Part of the discrepancy might also be due to a posttranscriptional mechanism altering the half-life of eNOS mRNA [13]. When monitoring the expression of endogenous murine eNOS, we found responses in the four shear stress regions that were similar to those of eNOS-GFP, supporting our findings.
Transgenic model. Over-expression of eNOS-GFP may result in a negative feedback by the increased NO production inhibiting transcription of the gene [29]. Thus, the effect of shear stress on eNOS expression might have been underestimated in the present study. However, the expression of murine eNOS in wild type controls shows a similar response to the shear stress alterations induced by the cast. The observed effect of shear stress on eNOS-GFP is therefore not restricted to the human eNOS transgenic construct.
The change in vessel geometry by cast placement may compress fibro-elastin layers of the vessel wall and thereby increase background auto-fluorescence. This does not affect our data however, because the auto-fluorescent signal was subtracted from the total GFP signal. The tapering effect of the cast could also compress the endothelial cells to make them fit into a smaller area, increasing the number of cells per area. Co-

67

localization studies of the endothelium in the different shear stress regions do not show an increase in cell number per area or a decrease in cell size. In addition, the up-regulation of eNOS-GFP in single endothelial cells is observed, providing further evidence that the eNOS-GFP signal in the high shear vessel segment is not an artefact created by the tapered shape of the cast.

In conclusion, the present study demonstrates that complex shear stress fields can be induced in straight vessels *in vivo*. Furthermore, information about the *in vivo* regulation of eNOS by shear stress can be obtained by using the cast model. This hemodynamic model provides therefore the opportunity to examine directly the effect of low, high, and oscillatory shear stress on the initiation and development of atherosclerotic disease.
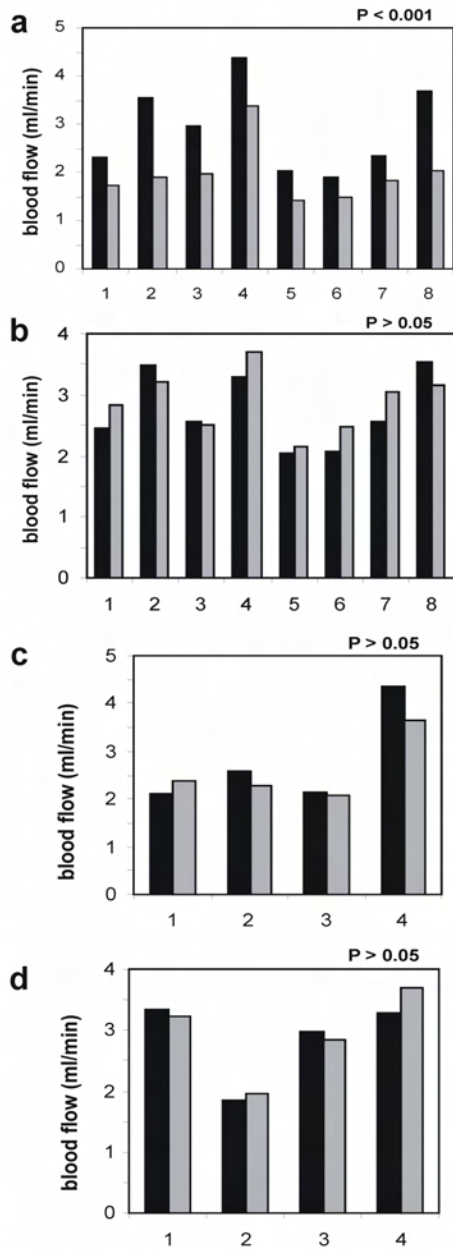
3.6 Supplemented data

Figure S1: Effect of cast placement around carotid arteries on blood flow. (a) Blood flow in the right common carotid artery and (b) left common carotid artery as measured by Doppler sonography before (black bars) and after (grey bars) cast placement in a group of eNOS-GFP transgenic mice. n =8, P<0.001 (c) In a different group, blood flow in the right carotid artery (d) and left carotid artery was measured by Doppler sonography before (black bars) and after (grey bars) placement of a non-tapering, control cast around the right carotid artery. n =4, P>0.05.
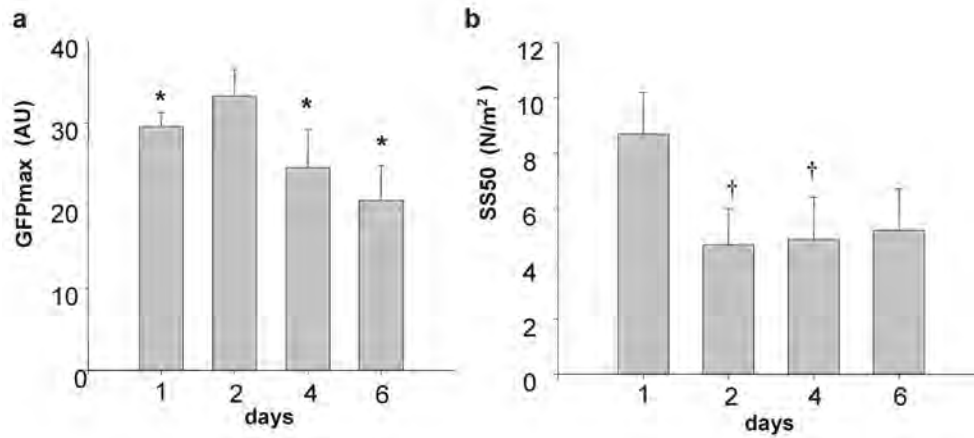
Figure S2: The time response of eNOS versus shear stress. Indicated are two parameters (of the three parameters) describing the behavior of a mathematical model (sigmoidal plot) that was fitted through the original data. It is clearly shown that; The GFP signal reaches a maximum at day 2 and slowly decreases at later time points (1 day = 30 ± 2 AU, 2 days = 33 ± 3 AU, 4 days = 4 ± 5 AU, 6 days = 20 ± 5 AU) (a). The SS50 level (level of shear stress at which the maximum GFP signal is saturated for 50%) is maximal at day 1 and decreases by 50% on day 2, after which it remains constant (1 day = 8,5 ± 2 AU, 2 days = 4,8 ± 1 AU, 4 days = 5 ± 1 AU, 6 days = 5,5 ± 1 AU) (b). From these data we conclude that the eNOS shear stress response is fast, for most of the effect is apparent after 1 day, and a steady state is reached after two days. n =5 per time point, * P<0.05 versus day 2, † P<0.05 versus day 1.
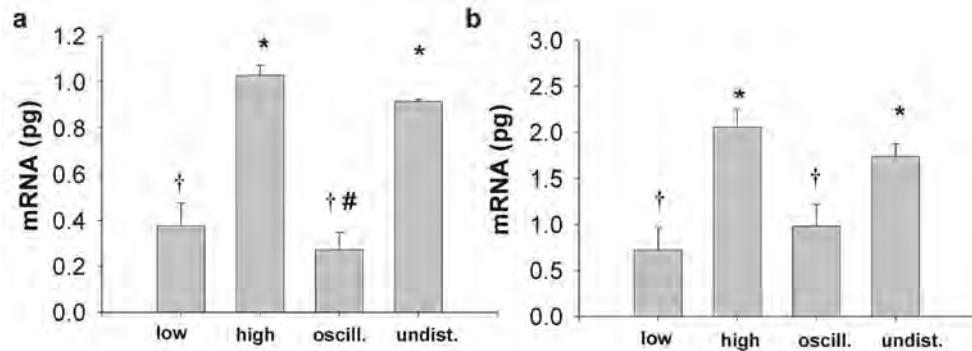
Figure S3: Shear stress induces responses in endogenous murine eNOS mRNA expression of transgenic (eNOS-GFP) (a) and wildtype (c57bl6) (b) animals. These responses are similar to those observed in eNOS-GFP mRNA. n =5, * $P<0.05$ versus low shear stress, † $P<0.05$ versus undisturbed shear stress, # $P<0.05$ versus high shear stress.
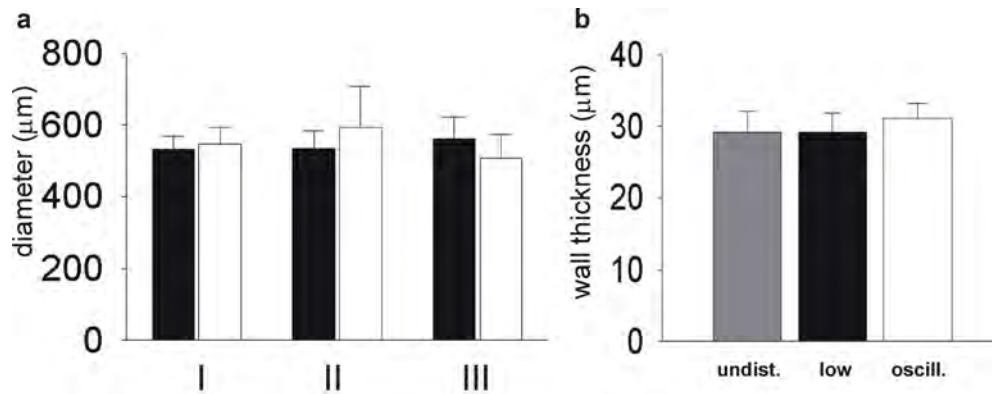

Figure S4: Vascular diameter changes before (I), immediately after (II) and after 6 days of cast placement (III) in low shear stress (black bar) or oscillatory shear stress (white bar) region (a). As outer diameters were measured, wall thickness was measured at the day of sacrifice in control (gray bar), low shear stress (black bar) and oscillatory shear stress (white bar) segments (b). Note that no difference in diameters or wall thickness before, immediately after, and after 6 days follow up was measured. N=8.

3.7 References:

1.   Kamiya A, Togawa T. Adaptive regulation of wall shear stress to flow change in the canine carotid artery. *Am J Physiol*. 1980;239:H14-21.
2.   Kubis N, Checoury A, Tedgui A, Levy BI. Adaptive common carotid arteries remodeling after unilateral internal carotid artery occlusion in adult patients. *Cardiovasc Res*. 2001;50:597-602.
3.   Caro CG, Fitz-Gerald JM, Schroter RC. Arterial wall shear and distribution of early atheroma in man. *Nature*. 1969;223:1159-60.
4.   VanderLaan PA, Reardon CA, Getz GS. Site specificity of atherosclerosis: site-selective responses to atherosclerotic modulators. *Arterioscler Thromb Vasc Biol*. 2004;24:12-22.
5.   Gimbrone MA, Jr. Vascular endothelium, hemodynamic forces, and atherogenesis. *Am J Pathol*. 1999;155:1-5.
6.   Cooke JP. Flow, NO, and atherogenesis. *Proc Natl Acad Sci U S A*. 2003;100:768-70.
7.   Stone PH, Coskun AU, Kinlay S, Clark ME, Sonka M, Wahle A, Ilegbusi OJ, Yeghiazarians Y, Popma JJ, Orav J, Kuntz RE, Feldman CL. Effect of endothelial shear stress on the progression of coronary artery disease, vascular remodeling, and in-stent restenosis in humans: in vivo 6-month follow-up study. *Circulation*. 2003;108:438-44.
8.   Buchanan JR, Jr., Kleinstreuer C, Truskey GA, Lei M. Relation between non-uniform hemodynamics and sites of altered permeability and lesion growth at the rabbit aorto-celiac junction. *Atherosclerosis*. 1999;143:27-40.
9.   Shyy JY, Chien S. Role of integrins in endothelial mechanosensing of shear stress. *Circ Res*. 2002;91:769-75.
10.   Ohura N, Yamamoto K, Ichioka S, Sokabe T, Nakatsuka H, Baba A, Shibata M, Nakatsuka T, Harii K, Wada Y, Kohro T, Kodama T, Ando J. Global analysis of shear stress-responsive genes in vascular endothelial cells. *J Atheroscler Thromb*. 2003;10:304-13.
11.   Porat RM, Grunewald M, Globerman A, Itin A, Barshtein G, Alhonen L, Alitalo K, Keshet E. Specific Induction of tie1 Promoter by Disturbed Flow in Atherosclerosis-Prone Vascular Niches and Flow-Obstructing Pathologies. *Circ Res*. 2003.
12.   Passerini AG, Polacek DC, Shi C, Francesco NM, Manduchi E, Grant GR, Pritchard WF, Powell S, Chang GY, Stoeckert CJ, Jr., Davies PF. Coexisting proinflammatory and antioxidative endothelial transcription profiles in a disturbed flow region of the adult porcine aorta. *Proc Natl Acad Sci U S A*. 2004.
13.   Ziegler T, Silacci P, Harrison VJ, Hayoz D. Nitric oxide synthase expression in endothelial cells exposed to mechanical forces. *Hypertension*. 1998;32:351-5.

14. Tuttle JL, Nachreiner RD, Bhuller AS, Condict KW, Connors BA, Herring BP, Dalsing MC, Unthank JL. Shear level influences resistance artery remodeling: wall dimensions, cell density, and eNOS expression. *Am J Physiol Heart Circ Physiol*. 2001;281:H1380-9.

15. van Haperen R, Cheng C, Mees BM, van Deel E, de Waard M, van Damme LC, van Gent T, van Aken T, Krams R, Duncker DJ, de Crom R. Functional expression of endothelial nitric oxide synthase fused to green fluorescent protein in transgenic mice. *Am J Pathol*. 2003;163:1677-86.

16. Malek AM, Zhang J, Jiang J, Alper SL, Izumo S. Endothelin-1 gene suppression by shear stress: pharmacological evaluation of the role of tyrosine kinase, intracellular calcium, cytoskeleton, and mechanosensitive channels. *J Mol Cell Cardiol*. 1999;31:387-99.

17. Gan LM, Selin-Sjogren L, Doroudi R, Jern S. Temporal regulation of endothelial ET-1 and eNOS expression in intact human conduit vessels exposed to different intraluminal pressure levels at physiological shear stress. *Cardiovasc Res*. 2000;48:168-77.

18. Zhu ZG, Li HH, Zhang BR. Expression of endothelin-1 and constitutional nitric oxide synthase messenger RNA in saphenous vein endothelial cells exposed to arterial flow shear stress. *Ann Thorac Surg*. 1997;64:1333-8.

19. Morawietz H, Talanow R, Szibor M, Rueckschloss U, Schubert A, Bartling B, Darmer D, Holtz J. Regulation of the endothelin system by shear stress in human endothelial cells. *J Physiol*. 2000;525 Pt 3:761-70.

20. Malek AM, Greene AL, Izumo S. Regulation of endothelin 1 gene by fluid shear stress is transcriptionally mediated and independent of protein kinase C and cAMP. *Proc Natl Acad Sci U S A*. 1993;90:5999-6003.

21. Qiu Y, Tarbell JM. Interaction between wall shear stress and circumferential strain affects endothelial cell biochemical production. *J Vasc Res*. 2000;37:147-57.

22. Okahara K, Sun B, Kambayashi J. Upregulation of prostacyclin synthesis-related gene expression by shear stress in vascular endothelial cells. *Arterioscler Thromb Vasc Biol*. 1998;18:1922-6.

23. Doroudi R, Gan LM, Selin Sjogren L, Jern S. Effects of shear stress on eicosanoid gene expression and metabolite production in vascular endothelium as studied in a novel biomechanical perfusion model. *Biochem Biophys Res Commun*. 2000;269:257-64.

24. Rieder MJ, Carmona R, Krieger JE, Pritchard KA, Jr., Greene AS. Suppression of angiotensin-converting enzyme expression and activity by shear stress. *Circ Res*. 1997;80:312-9.

25. Woodman CR, Muller JM, Rush JW, Laughlin MH, Price EM. Flow regulation of ecNOS and Cu/Zn SOD mRNA expression in porcine coronary arterioles. *Am J Physiol*. 1999;276:H1058-63.

26. Inoue N, Ramasamy S, Fukai T, Nerem RM, Harrison DG. Shear stress modulates expression of Cu/Zn superoxide dismutase in human aortic endothelial cells. *Circ Res*. 1996;79:32-7.

27. Wentzel JJ, Kloet J, Andhyiswara I, Oomen JA, Schuurbiers JC, de Smet BJ, Post MJ, de Kleijn D, Pasterkamp G, Borst C, Slager CJ, Krams R. Shear-stress and wall-stress regulation of vascular remodeling after balloon angioplasty: effect of matrix metalloproteinase inhibition. *Circulation*. 2001;104:91-6.

28. Davis ME, Cai H, Drummond GR, Harrison DG. Shear stress regulates endothelial nitric oxide synthase expression through c-Src by divergent signaling pathways. *Circ Res*. 2001;89:1073-80.

29. Abu-Soud HM, Ichimori K, Presta A, Stuehr DJ. Electron transfer, oxygen binding, and nitric oxide feedback inhibition in endothelial nitric-oxide synthase. *J Biol Chem*. 2000;275:17349-57.

Chapter 4: Shear Stress affects the *in vivo* Intracellular Distribution of eNOS

4.1 Abstract

The specific location of atherosclerosis in the vascular tree is correlated with local variations in shear stress. We developed a method to induce defined variations in shear stress in a straight vessel segment of a mouse. To this end, a cylinder with a tapered lumen is placed around the carotid artery, inducing a high shear stress field. Concomitantly, regions of low shear stress and oscillatory shear stress are created upstream and downstream of the device, respectively. This device was used in mice transgenic for an eNOS-GFP fusion gene. We observed a strong induction of eNOS-GFP levels in the high shear stress region compared with the other regions ($P<0.05$). Quantification of eNOS-GFP fluorescence or of immuno-reactivity to the Golgi complex or to PECAM-1 showed an increase in the high shear stress region ($P<0.05$) compared with non-treated carotid arteries. Co-localization of eNOS-GFP with either the Golgi complex or PECAM-1 also responded to alterations of shear stress.
We showed that intracellular distribution and phosphorylation of eNOS is responsive to high and oscillatory shear *in vivo*; and these shear stress conditions result in eNOS redistribution with a relatively lower association to the Golgi complex.

4.2 Introduction

Regulation of eNOS protein levels and activity is unusually complex and occurs both at transcriptional and post-transcriptional levels [1,2]. Post-translational modification of eNOS by myristoylation and palmitoylation that targets the protein to the Golgi complex and to the lipid rich domains of the cell membrane are both necessary for proper eNOS activation. Shear stress activates eNOS predominantly through Akt dependent phosphorylation of eNOS at serine1177 [3,4]. Recently, it was shown that the fraction of eNOS localized in the Golgi complex is responsive to phosphorylation by Akt [5]. This implies that shear stress activates eNOS when it is located in certain compartments of the endothelial cells. At present, it is unknown how shear stress affects the intracellular distribution of eNOS *in vivo* [6]. Using the previously validated cast model and combining this with an in-house developed quantitative method to analyse intracellular components, we conducted a study on the effect of shear stress on eNOS cellular localization. We analysed the distribution of eNOS over the Golgi and cell membrane compartments in relation to the serine1177 phosphorylation of eNOS, in vessel regions exposed to different shear stress parameters.

4.3 Materials and Methods

Animals
Mice expressing an eNOS-GFP fusion protein were generated as described before [7]. Mice were bred to C57BL/6 background for at least 10 generations (>99% C57BL/6), and were 15-20 weeks of age. Animal care and experiments complied with institutional and national guidelines.

In vivo alteration of shear stress
In order to induce standardized changes in shear stress, we designed a shear stress modifier, which was manufactured of the thermoplastic, polyetherketon. The device is referred to as *cast* throughout the study. The cast consists of two longitudinal halves of a cylinder with a cone shaped lumen. The geometry of the cast has been designed with computational flow dynamics software [8] to produce vortices downstream of the cast when placed around the common carotid artery. This downstream region will therefore be exposed to oscillations in shear stress (oscillatory shear stress region). The upstream inner diameter is 500 μm (non-constrictive) and gradually declines to 250 μm at the downstream side of the cast (constrictive). This tapering induces a gradual increase in shear stress (high shear stress region). In addition, the constrictive stenosis decreases the blood flow, resulting in a low shear stress region upstream from the cast. Control casts consist of a cylinder with a continuous non-constrictive diameter of 500 μm. For surgery, the mice were anesthetized with isoflurane. Both halves of the cast were placed around the right common carotid artery and fixed with a suture. Animals with cast implants were sacrificed at 1-6 days after surgery by *in situ* fixation.

Confocal microscopy
Tissue samples were examined under a Zeiss LSM510LNO inverted laser scanning confocal fluorescence microscope (Carl Zeiss, Thornwood, USA). To study eNOS-GFP expression on a cellular level, stacks of optical slices (0.5 μm by 20 μm by 20 μm) were obtained using the 40x water immersion Axiovert lens. To investigate the location of serine1177-phosphorylated eNOS, PECAM-1 and the Golgi complex, images of Rhodamine fluorescence were taken applying a 543-nm excitation from a NeHe-laser, using a 560 nm longpass filter for detection. Images of GFP fluorescence were acquired by excitation with a 488 nm argon laser and were detected using a 500-550 bandpass barrier filter.

Fluorescence immunohistochemistry
Following *in situ* perfusion and overnight fixation, common carotid arteries were washed in PBS and treated with 0.2% Triton X-100 (Sigma Chemical Co., Zwijndrecht, The Netherlands) in PBS. The arteries were subsequently incubated with 2.5% horse serum in PBS/0.2% BSA for 30 minutes, washed again in PBS/0.2% BSA, and incubated with rabbit polyclonal antibodies against phospho-eNOS

(serine1177) (New England Biolabs, Leusden, The Netherlands), PECAM-1 (Sigma Chemical Co., Zwijndrecht, The Netherlands), or mouse monoclonal antibodies against P115 (BD Biosciences Pharmingen, San Diego, USA) in PBS/0.2% BSA overnight at 4 C°. After washing in PBS/0.05% Tween-20 (Sigma Chemical Co., Zwijndrecht, The Netherlands), the arteries were incubated with mouse anti-rabbit IgG conjugated to R594 (Molecular Probes, Leiden, The Netherlands) or goat anti-mouse IgG conjugated to Texas Red (Molecular Probes, Leiden, The Netherlands) in PBS/0.2% BSA for two hours at room temperature, followed by wash steps and were mounted in Vectashield.

Analysis and statistics
Localization was quantified as percentage of the total image area. Co-localization of eNOS with the Golgi complex or with the plasma membrane compartment was quantified as percentage co-localization area of the total eNOS area. In addition, phospho-eNOS was expressed in percentages of total eNOS. All software was developed in Matlab (The Mathworks, Delft, The Netherlands).
All regression analyses were performed by a commercial package (SigmaStat, version 2.03, Systat Software Inc., Richmond, California, USA). Statistical analyses were performed using one-way ANOVA followed by Dunnett's ad-hoc test. The Student's *t*-test was used in the Doppler evaluations. Data are presented as mean ± SEM. *P* values <0.05 were considered statistically significant.

4.4 Results

Shear stress alters the intracellular distribution of eNOS
We compared the intracellular distribution of eNOS-GFP in the regions with different shear stress patterns. Endothelial cells in low, high and undisturbed shear stress regions are elongated in shape and are aligned with the direction of the flow. In contrast, endothelial cells in the oscillatory shear stress region appear disorganized (Figures 1a, 2a, 4a, middle panels). At the intracellular level, eNOS-GFP is mainly located at a perinuclear site where the Golgi complex is situated, and it is present at the plasma membrane (Figure 3a, undisturbed shear stress). We investigated whether shear stress has an effect on the localization of eNOS-GFP protein in the Golgi complex by *en face* immunostaining (Figure 1a). Quantification of the fluorescent signal showed a 3-fold increase in Golgi complex area in the vessel segment with high shear stress compared to undisturbed shear stress or low shear stress (Figure 1b). The eNOS-GFP area was increased by 8-fold and 7-fold in high shear stress and oscillatory shear stress respectively, compared to either low or undisturbed shear stress (Figure 1c). High shear stress and oscillatory shear stress decrease the localization of eNOS in the Golgi complex by approximately 2-fold compared to undisturbed shear stress (Figure 1d). The difference in co-localization in the low shear stress area did not reach statistical significance.

We also studied the effect of shear stress on the localization of eNOS at the cell membrane by *en face* immuno-histochemistry using a PECAM-1 antibody (Figure 2a,). A 2-fold increase in PECAM-1 was observed in the high shear stress region (Figure 2b). The response of eNOS-GFP to the different shear stress fields was as observed before (cf. Figure 1c, 2c). More eNOS co-localized with PECAM-1 in the low and high shear stress region compared to the oscillatory shear stress region (2.5-fold difference; Figure 2d). A statistically significant correlation was found between the eNOS area and the Golgi complex area (Figure 3).
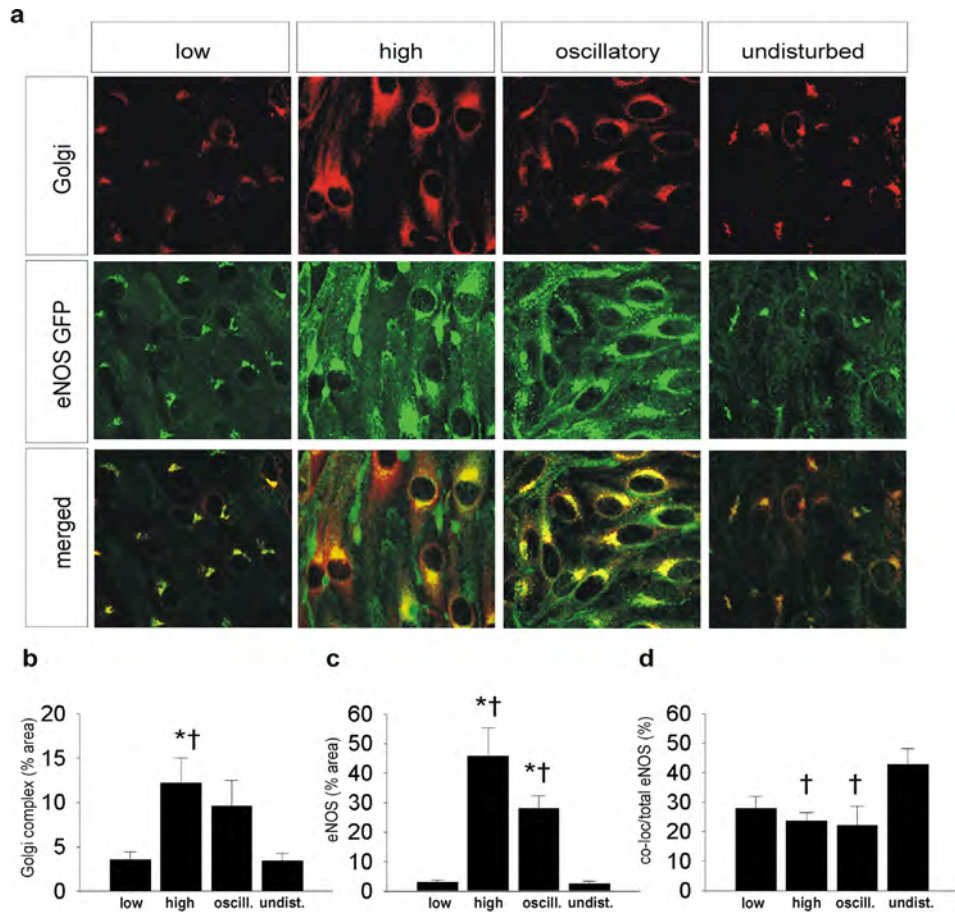
Figure 1: Intracellular localization of eNOS-GFP and Golgi complex in areas of the carotid artery experiencing different shear stress patterns after 2 days of cast placement. (a) In the upper panel: Golgi complex in corresponding vascular regions visualized by en face immunofluorescence staining. Indicated are: the low shear stress region (low), the high shear stress region (high), the oscillatory shear stress region (oscillatory), and the control region (undisturbed). Fluorescence was monitored by en face confocal microscopy in stacks of 500 μm x 500 x 40 μm each. In the middle panel: Fluorescence of eNOS-GFP in endothelial cells located in the three different shear stress regions and in the contra-lateral carotid artery. In the lower panel the upper and middle panels are merged, showing the co-localization signal in yellow. (b-d) Quantification of the localization of (b) the Golgi complex, (c) the eNOS-GFP and d) the co-localization signals in response to the different shear stress fields in percentages of the total area (b,c) or of the total eNOS-GFP signal (d). n = 4, * P<0.05 versus low shear stress. † P<0.05 versus undisturbed shear stress. Full colour image of this figure is available in the colour section.
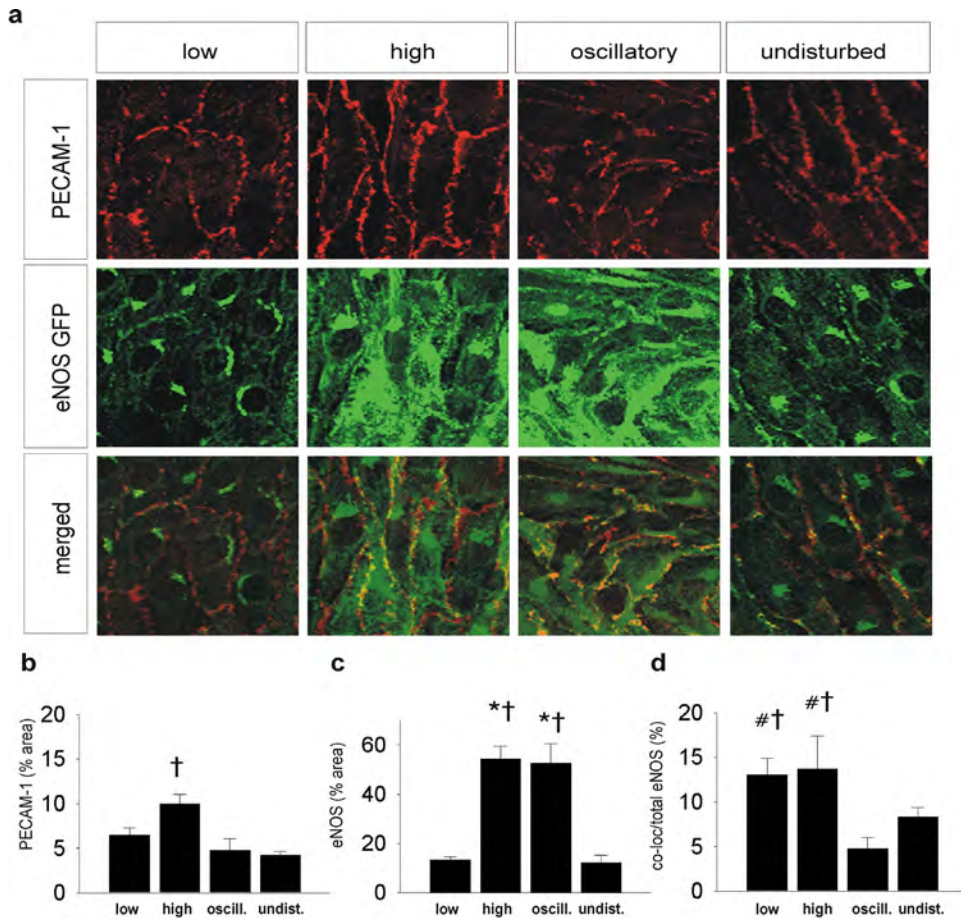
Figure 2: Intracellular localization of eNOS-GFP and PECAM-1 in regions of the carotid artery experiencing different shear stress patterns after two days cast placement. (a) In the upper panel: PECAM-1 in corresponding vascular regions visualized by en face immunofluorescence staining. Indicated are: the low shear stress region (low), the high shear stress region (high), the oscillatory shear stress region (oscillatory), and the control region (undisturbed). Fluorescence was monitored by en face confocal microscopy in stacks of 500 μm x 500 x 40 μm each. In the middle panel: Fluorescence of eNOS-GFP in endothelial cells located in the three different shear stress regions and in the contra-lateral carotid artery. In the lower panel the upper and middle panels are merged, showing the co-localization signal in yellow. (b-d) Quantification of the localization of (b) the PECAM-1, (c) the eNOS-GFP and d) the co-localization signals in response to the different shear stress fields in percentages of the total area (b,c) or of the total eNOS-GFP signal (d). n = 5, † P<0.05 versus undisturbed shear stress. # P<0.05 versus oscillatory shear stress. Full colour image of this figure is available in the colour section.
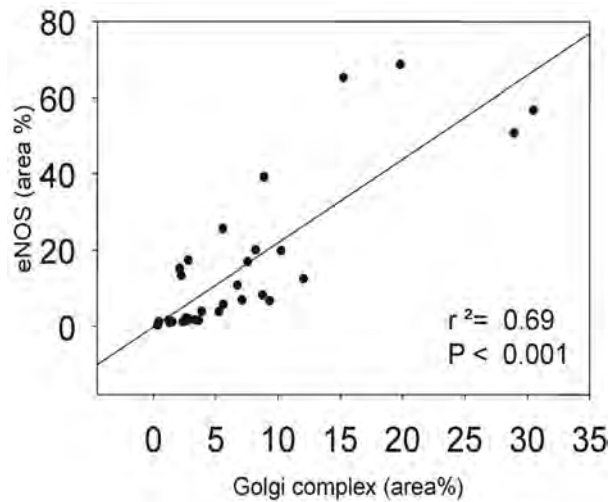
Figure 3: The correlation between the Golgi complex area versus eNOS-GFP area (both as a percentage of the total area).

Shear stress effects on eNOS phosphorylation

To investigate whether shear stress has an effect on the phosphorylation of eNOS, *en face* immunostaining on carotid arteries was performed with antibodies against phospho-eNOS (serine1177) (Figure 4a). An increase in phospho-eNOS was observed in the high shear stress region compared to regions of low or undisturbed shear stress (6-fold), and oscillatory shear stress (2-fold) (Figure 4b). Phospho-eNOS was also increased in the oscillatory shear stress area compared to regions of low or undisturbed shear stress (5-fold) (Figure 4b). The eNOS-GFP response is similar to the results obtained before (cf. Figure 1c, 2c, and 4c). The fraction of eNOS that was phosphorylated –approximately 50%– did not change by alterations in shear stress (Figure 4d).
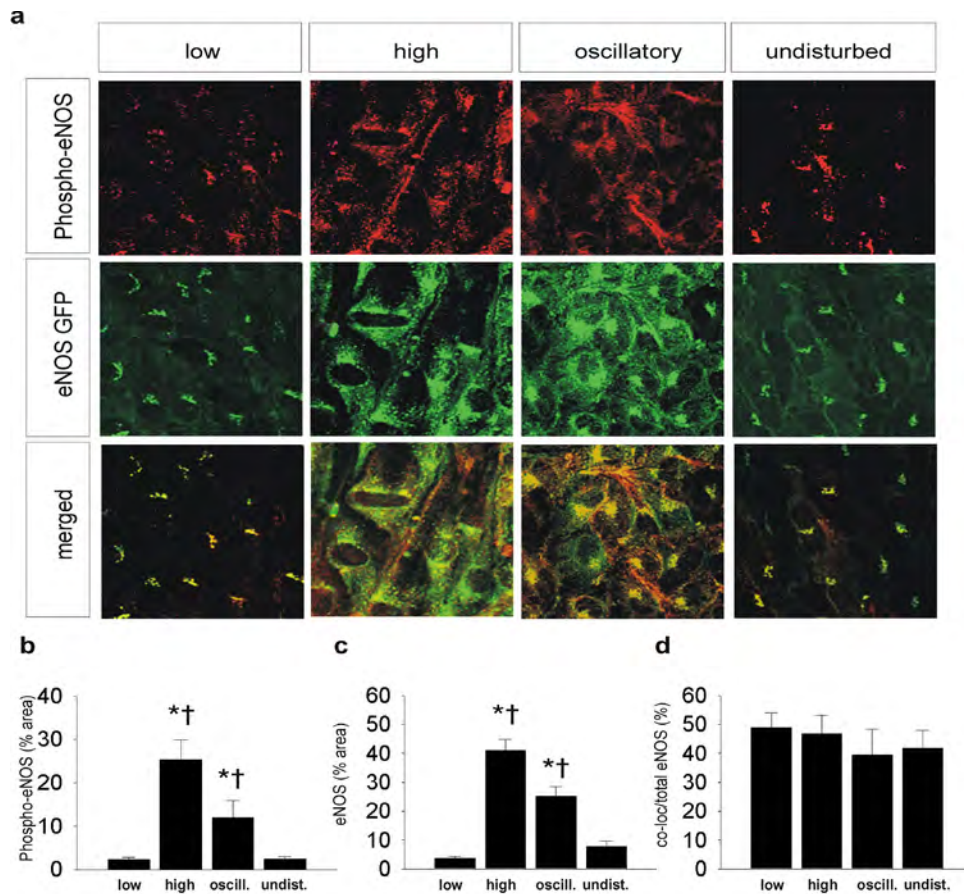
Figure 4: Intracellular localization of eNOS-GFP and phospho-eNOS in areas of the carotid artery experiencing different shear stress patterns after two days of cast placement. (a) In the upper panel: Phospho-eNOS in corresponding vascular regions visualized by en face immunofluorescence staining. Indicated are; the low shear stress region (low), the high shear stress region (high), the oscillatory shear stress region (oscillatory), and the control region (undisturbed). Fluorescence was monitored by en face confocal microscopy in stacks of 500 μm x 500 μm each. In the middle panel: Fluorescence of eNOS-GFP in endothelial cells located in the three different shear stress regions and in the contra-lateral carotid artery. In the lower panel the upper and middle panels are merged, showing the co-localization signal in yellow. (b-d) Quantification of the localization of (b) thePhospho-eNOS, (c) the eNOS-GFP and d) the co-localization signals in response to the different shear stress fields in percentages of the total area (b,c) or of the total eNOS-GFP signal (d). n = 5, * P<0.05 versus low shear stress. † P<0.05 versus undisturbed shear stress. Full colour image of this figure is available in the colour section.

4.5 Discussion

In the present study, we examined the effect of complex shear stress fields on eNOS cellular distribution and activation *in vivo*. From the results we conclude that: (a) intracellular distribution and phosphorylation of eNOS is responsive to high and oscillatory shear *in vivo*; and (b) these shear stress conditions result in eNOS redistribution with a relatively lower association to the Golgi complex. However, the fraction of eNOS that is activated by serine1177 phosphorylation is not responsive to *in vivo* changes in shear stress.

The effects of shear stress on intracellular eNOS distribution
The correct intracellular localization of eNOS is of crucial importance for its activity [9]. By using eNOS mutants which were kinetically identical to unmodified eNOS, it was demonstrated that mis-localization of the enzyme impairs the production of NO in response to agonists [10]. Activation of eNOS by shear stress involves the Akt dependent phosphorylation of eNOS at serine1177 [3,11]. It was recently shown that mainly the fraction of eNOS localized in the Golgi complex is responsive to phosphorylation by Akt [5]. Thus, the cellular distribution of eNOS in complex shear stress fields is essential for its function. To the best of our knowledge, the effect of shear stress on the intracellular re-distribution of eNOS in endothelial cells has only been evaluated once in blood vessels *in vivo* [12].
Our study shows that the Golgi complex becomes more extended in response to the augmentation of shear stress. This finding is in agreement with a previous study showing a difference in Golgi complex areas between venous endothelium (low shear stress) and arterial endothelium (high shear stress) in rats [13]. A significant part of eNOS bound to the plasma membrane is present at the cell-cell contact sites and co-localizes with PECAM-1 [13,14]. We found that PECAM-1 itself is up-regulated under high shear stress. The relative distribution of eNOS to the PECAM-1 positive cell membrane region was not influenced by shear stress, indicating that intracellular eNOS and PECAM-1 increased to similar amounts in response to shear stress. In summary, our data show that both the cell membrane and the Golgi complex compartments of the eNOS pool are increased after augmenting shear stress.

In vitro studies demonstrated that phosphorylation of serine1177 is shear stress responsive [15]. Indeed, we found increased serine1177 phosphorylation of eNOS under high and oscillatory shear stress conditions. It was recently demonstrated that the eNOS pool residing in the Golgi complex is more responsive to Akt phosphorylation of serine1177 than eNOS residing in the cell membrane [5], indicating that the shear stress responsive eNOS pool is located predominantly in the Golgi complex. Rather unexpectedly, the relative fraction of eNOS located in the Golgi complex was unchanged in the low shear stress region, but decreased in the high and oscillatory shear stress regions. The correlation found between Golgi complex area and total eNOS area (Figure 3), demonstrate a possible response by the endothelial cells to

increase the size of the Golgi complex in order to accommodate more eNOS-GFP. When only the Golgi-localized eNOS fraction was taken into account, a similar correlation was found (r^2=0.71, P<0.001). Therefore we hypothesize that chronic changes in shear stress *in vivo* induces adaptations in the extension of the Golgi complex, enabling the endothelial cells to accommodate more eNOS protein in this shear stress responsive intracellular compartment. This results in an absolute increase in eNOS phosphorylation and NO production, although the relative portion of eNOS that is phosphorylated remains unchanged.

Limitations of the study
The GFP reporter might interfere with eNOS localization. eNOS myristoylation and palmitoylation, which are both important for the localization [5], occur at the N-terminus. It is unlikely that these processes are affected, because the GFP part is fused at the C-terminus of the eNOS protein [7]. Although GFP could induce changes in protein folding, our experiments show normal localization of eNOS-GFP in the Golgi complex and plasma membrane [7]. Previous studies extensively studied the location and function of the eNOS-GFP fusion protein *in vitro* [13,14 16,17]. These studies clearly indicate that the GFP moiety does not interfere with the localization and the function of eNOS.

In conclusion, the present study demonstrates that intracellular distribution and phosphorylation of eNOS is responsive to high and oscillatory shear *in vivo*; and these shear stress conditions result in eNOS redistribution with a relatively lower association to the Golgi complex.

4.6 Supplemented data

Figure 5: Experiments showing the specificity of the antibody directed against the phosphorylation site of human eNOS. Phospho-eNOS staining using phospho-eNOS ser1177 antibody in aortas of eNOS GFP transgenic (I) and eNOS deficient (II) mice. Indicated are eNOS GFP signal, DAPI nucleus signal, Phospho-eNOS signal, and co-localization signal (yellow). In addition, control experiments were performed in aortas of eNOS GFP transgenic mice in which the first antibody was omitted (mock sample, panel III). Note that no phospho-eNOS signals in both eNOS deficient mice and mock samples were detected.

4.7 References:

1.   Fulton D, Gratton JP, Sessa WC. Post-translational control of endothelial nitric oxide synthase: why isn't calcium/calmodulin enough? *J Pharmacol Exp Ther*. 2001;299:818-24.
2.   Govers R, Rabelink TJ. Cellular regulation of endothelial nitric oxide synthase. *Am J Physiol Renal Physiol*. 2001;280:F193-206.
3.   Dimmeler S, Fleming I, Fisslthaler B, Hermann C, Busse R, Zeiher AM. Activation of nitric oxide synthase in endothelial cells by Akt-dependent phosphorylation. *Nature*. 1999;399:601-5.
4.   Fisslthaler B, Dimmeler S, Hermann C, Busse R, Fleming I. Phosphorylation and activation of the endothelial nitric oxide synthase by fluid shear stress. *Acta Physiol Scand*. 2000;168:81-8.
5.   Fulton D, Babbitt R, Zoellner S, Fontana J, Acevedo L, McCabe TJ, Iwakiri Y, Sessa WC. Targeting of endothelial nitric oxide synthase to the cytoplasmic face of the golgi or plasma membrane regulates Akt- versus calcium-dependent mechanisms for nitric oxide release. *J Biol Chem*. 2004.
6.   Davis ME, Cai H, Drummond GR, Harrison DG. Shear stress regulates endothelial nitric oxide synthase expression through c-Src by divergent signaling pathways. *Circ Res*. 2001;89:1073-80.
7.   van Haperen R, Cheng C, Mees BM, van Deel E, de Waard M, van Damme LC, van Gent T, van Aken T, Krams R, Duncker DJ, de Crom R. Functional expression of endothelial nitric oxide synthase fused to green fluorescent protein in transgenic mice. *Am J Pathol*. 2003;163:1677-86.
8.   Wentzel JJ, Kloet J, Andhyiswara I, Oomen JA, Schuurbiers JC, de Smet BJ, Post MJ, de Kleijn D, Pasterkamp G, Borst C, Slager CJ, Krams R. Shear-stress and wall-stress regulation of vascular remodeling after balloon angioplasty: effect of matrix metalloproteinase inhibition. *Circulation*. 2001;104:91-6.
9.   Shaul PW. Regulation of endothelial nitric oxide synthase: location, location, location. *Annu Rev Physiol*. 2002;64:749-74.
10.   Garcia-Cardena G, Oh P, Liu J, Schnitzer JE, Sessa WC. Targeting of nitric oxide synthase to endothelial cell caveolae via palmitoylation: implications for nitric oxide signaling. *Proc Natl Acad Sci U S A*. 1996;93:6448-53.
11.   Fulton D, Gratton JP, McCabe TJ, Fontana J, Fujio Y, Walsh K, Franke TF, Papapetropoulos A, Sessa WC. Regulation of endothelium-derived nitric oxide production by the protein kinase Akt. *Nature*. 1999;399:597-601.
12.   Rizzo V, McIntosh DP, Oh P, Schnitzer JE. In situ flow activates endothelial nitric oxide synthase in luminal caveolae of endothelium with rapid caveolin dissociation and calmodulin association. *J Biol Chem*. 1998;273:34724-9.
13.   Andries LJ, Brutsaert DL, Sys SU. Nonuniformity of endothelial constitutive nitric oxide synthase distribution in cardiac endothelium. *Circ Res*. 1998;82:195-203.

14. Govers R, Bevers L, de Bree P, Rabelink TJ. Endothelial nitric oxide synthase activity is linked to its presence at cell-cell contacts. *Biochem J*. 2002;361:193-201.
15. Rizzo V, Morton C, DePaola N, Schnitzer JE, Davies PF. Recruitment of endothelial caveolae into mechanotransduction pathways by flow conditioning in vitro. *Am J Physiol Heart Circ Physiol*. 2003;285:H1720-9.
16. Sowa G, Liu J, Papapetropoulos A, Rex-Haffner M, Hughes TE, Sessa WC. Trafficking of endothelial nitric-oxide synthase in living cells. Quantitative evidence supporting the role of palmitoylation as a kinetic trapping mechanism limiting membrane diffusion. *J Biol Chem*. 1999;274:22524-31.
17. Liu J, Hughes TE, Sessa WC. The first 35 amino acids and fatty acylation sites determine the molecular targeting of endothelial nitric oxide synthase into the Golgi region of cells: a green fluorescent protein study. *J Cell Biol*. 1997;137:1525-35.

Chapter 5: Rapamycin Reduces eNOS Sensitivity to Shear Stress

C. Cheng, D. Tempel, A. Oostlander, F. Helderman, F. Gijsen, J. Wentzel, R. van Haperen, P. W. Serruys, A. F.W. van der Steen, R. de Crom, and R. Krams,
submitted for publication

5.1 Abstract

Rapamycin reduces atherosclerosis by an unknown mechanism. Recent studies indicate that NO is involved, and that the effect is shear stress dependent. Because eNOS is anti-atherogenic and shear stress dependent, we evaluated in this study, whether rapamycin affects eNOS responsiveness to shear stress.

With an in house developed flow modifier (referred to as cast) shear stress levels were varied over a large range of values in carotid arteries of transgenic mice expressing human eNOS fused to GFP. The mice were divided in control, low dose rapamycin (3 μg/kg/day) and high dose rapamycin (3 mg/kg/day) groups. The efficacy of treatment was confirmed by measurement of rapamycin serum levels (2.0 ± 0.5 ng/ml), and of p27^{kip1} expression in vascular tissue (increased by 2.4±0.5 fold). The effect of rapamycin treatment on eNOS was evaluated by eNOS quantification of expression (qPCR) and of intracellular protein levels by *en face* confocal microscopy. The cast-induced range of shear stress levels were calculated using computional fluid dynamics. In control carotid arteries, eNOS expression increased by 1.8±0.3 fold in response to rapamycin. In the cast treated vessels, rapamycin induced at high shear stress levels (> 10 Pa) a dose-responsive reduction in maximal eNOS expression. In addition, increasing concentrations of rapamycin induced an increase in eNOS at physiological shear (1.5-3.0 Pa).

These results indicate that systemic administration of rapamycin protects the low shear stress regions from plaque initiation via an eNOS/shear stress dependent mechanism. In contrast, rapamycin decreases eNOS responsiveness to high shear stress, rendering a loss of protection via eNOS/shear stress mechanism in these regions.

5.2 Introduction

Atherosclerosis is a lipid generated inflammatory disease of the large arteries. It is the primary cause of cardiovascular disease and the underlying cause of about 30% of all deaths in the Western society. It has been widely appreciated that atherosclerosis occurs at certain predilection sites in the vascular tree, like side branches and curvatures[1,2]. These observations cannot be explained by the systemic risk factors, and it has been postulated that local haemodynamic factors like endothelial wall shear stress are involved. Wall shear stress is the force, normalized per unit area, acting in plane of the endothelium as a result of the blood flow. Numerous studies have indicated that both low and oscillatory shear stress are crucial factors in atherogenesis [3-7]. The response of the endothelium to shear stress occurs through adaptations in cell morphology, cell metabolism, and gene expression[8,9]. Among other things, this altered gene expression results in the production of vasoconstrictors and/or vasodilators, from which nitric oxide (NO) is one of the most relevant. NO is produced by nitric oxide synthase (NOS) enzymes, of which endothelial NOS (eNOS) is an isoform expressed by endothelial cells which is responsive to shear stress[10]. Therefore, changes in shear stress are partly acting through changes in eNOS expression and eNOS activity and this effect may play a role in pathological events, like atherosclerosis[10-12].

Rapamycin (sirolimus) is a macrolide antibiotic produced by the fungus *Streptomyces hygroscopicus*. In addition to immunosuppressive properties, rapamycin also prevents cell-cycle progression from the G1 to S phase, which results in the inhibition of growth factor-mediated and mitogen-induced cellular proliferation [13]. Recent studies showed that rapamycin also has anti-atherogenic properties [14]. While the mechanism is still under investigation, it has been proposed that an increased NO production as a result of increased eNOS expression and eNOS activation is involved [15,16]. As eNOS is a shear stress responsive enzyme [11,17-19], the beneficial effect of rapamycin in atherosclerosis may therefore be shear stress dependent. In a recent study we observed that the distribution of neointimal thickness in rapamycin-eluting stents is related to the shear stress pattern[20]. Therefore, we postulated that rapamycin modulates eNOS expression in response to shear stress. In order to test this hypothesis, we changed shear stress by an in house developed method that creates pre-defined patterns of shear stress in mouse carotid arteries in vivo [21]. We used a transgenic mouse model that we developed previously in which the endothelial cells express the human eNOS gene fused to eGFP[22]. The method has been well validated in previous studies[21]. The GFP allowed us to monitor the effect of rapamycin on eNOS expression in response to shear stress in mice.

5.3 Materials and Methods

Animals and experimental design
For this study eNOS-GFP transgenic (tg) male and female mice older then 25 weeks of age were used. eNOS-GFPtg mice were generated with a DNA-construct encoding human endothelial nitric oxide synthase fused to enhanced green fluorescent protein as described previously [22] Rapamycin was given orally for a period of 11 days. The eNOS-GFP tg group consisted of a control group (n=12), a group treated with a low dose of rapamycin (3.0 µg/kg/day; n=6) and a group treated with a high dose of rapamycin (3.0 mg/kg/day; n=6). In addition, a series of mice were studied in which the carotid artery was ligated without rapamycin (n=3) and with a high dose of rapamycin (n=3) treatment. The Erasmus MC review board approved all procedures. Animal care and experiments were carried out in compliance with the institutional and national guidelines.

Modification of shear stress
In order to create predefined patterns of shear stress, a perivascular shear stress modifier was used as described previously [21]. In short, the shear stress modifier, referred to as cast, was surgically positioned around the carotid artery of a mouse and immobilized with a 6/0 suture. Analyses were performed after 4 days of cast placement. This period was chosen on the basis of previous measurements showing a steady state in eNOS expression after 4 days. Thus, in rapamycin treated animals, the cast was placed at day 7 of the treatment.

Confocal Microscopy
The tissue samples were examined with a confocal laser scanning microscope system (LSM-510, Carl Zeiss Inc., Thornwood, NY, USA), equipped with an Argon laser (458, 488 nm) and two HeNe lasers (543 and 633 nm). The emission, which resulted from excitation of the tissue with a 488 nm Argon-Laser, was passed through a 560 nm longpass filter to optimise detection of the green fluorescence of eGFP. After appropriate settings of the optics (20x/0.5 Plan-neofluar objective), of the resolution (8 bits), of the pinhole (1000 µm), and of the scan mode (plane, multitrack), images were captured. Adjacent optical images from one specimen were combined to form a tile in order to provide a complete picture of the vessel segment of interest.

Computational fluid dynamics
In order to estimate the changes in wall shear stress distribution after cast placement, we applied a well-validated 3-D computational fluid package (CFD)[20,23-25]. Boundary conditions, material properties and 3D vessel geometry are essential for CFD to generate a solution. The boundary conditions for the calculations were: no slip conditions at the wall, stationary parabolic inflow at the entrance with a maximal velocity equivalent to measurements obtained in a separate group of mice (see

supplemental data for details) and zero stress outflow. Three dimensional vessel geometry was obtained from the contours of the *en face* eGFP images, assuming a circular geometry and after correction for longitudinal shrinkage of the intact vessel. On basis of this vessel geometry, a mesh was generated, which consisted of approximately 25.000 nodes. Because viscosity of the blood is dependent on shear rate, we used a non-Newtonian fluid model ('Carreau model') to estimate viscosity[25]. The accuracy of the calculations was set at 10^{-4} m/sec, which resulted in a numerical error of wall shear stress of approximately 1%.

Measurement of Rapamycin Levels
Rapamycin levels in whole blood were obtained from a commercially available immunoassay (Abbot Laboratories, Abbot Park, USA) with a detection level of 2.5 ng/ml.

Gene expression analysis
Carotid arteries were isolated from the eNOS-GFP transgenic animals untreated and treated with high concentration of rapamycin (n=5 per group). Total RNA from the samples was obtained using the RNAeasy kit (Qiagen, Cologne, Germany) and directly reversed transcribed into cDNA. PCR reactions were performed using a real-time fluorescent determination in the iCycler iQ Detection System (Biorad, Veenendaal, The Netherlands). Gene expression levels of $p27^{kip1}$ and eNOS were assessed. Target gene mRNA levels were expressed relatively hypoxanthine guanine phosphoribosyl transferase (HPRT).

Data Analysis and Statistics
The fluorescent vessel segment contours were traced manually and a bitmap was created on basis of these contours for further analysis. These regions served to reconstruct the blood vessel, generation of a 3-D mesh, performing computational fluid dynamics and for eNOS-GFP analysis. The analysis of eNOS-GFP consisted of automatic defining of lines perpendicular to the vessel centre line at location where shear stress was obtained from CFD. These lines served as a backbone for averaging eGFP thereby obtaining a longitudinal eGFP distribution. As a final step, eNOS-GFP values (y-axis) were related to local shear stress values (x-axis), and a non-linear curve fitting routine consisting of sigmoid relationship with an extra intercept was applied (see supplement data for details).
Student's t-tests were used to evaluate rapamycin serum levels, and eNOS-GFP and $P27^{kip1}$ expression levels in the control and the rapamycin treated group. The estimated parameters of the sigmoid curve fit ($eNOS_{ss=0}$, EC_{50} and $eNOS_{max}$; see supplemental data for details) were tested with a two-way ANOVA. ΔeNOS was calculated as $eNOS_{max} - eNOS_{ss=0}$. For display purposes all eNOS and shear stress data were sorted and averaged for every 10 consecutive data-points and the resulting curve was presented with a standard deviation. Statistical significance was considered at $p<0.05$. All values are reported as mean±SEM.

5.4 Results

Animal characteristics and validation of treatment adequacy
Weights of the animals for control, low and high dose rapamycin treated groups were
26.3±1.4 g, 24.9±0.7 g and 27.8±1.1 g, at the start of the experiments respectively
and did not change over time. The rapamycin plasma levels, after correction for
background, were 2.0 ± 0.5 ng/ml after treatment with the highest dosage of
rapamycin. These plasma levels were associated with a 2.4-fold increase of $p27^{kip1}$
gene expression levels in the vascular wall of the carotid arteries, as compared with
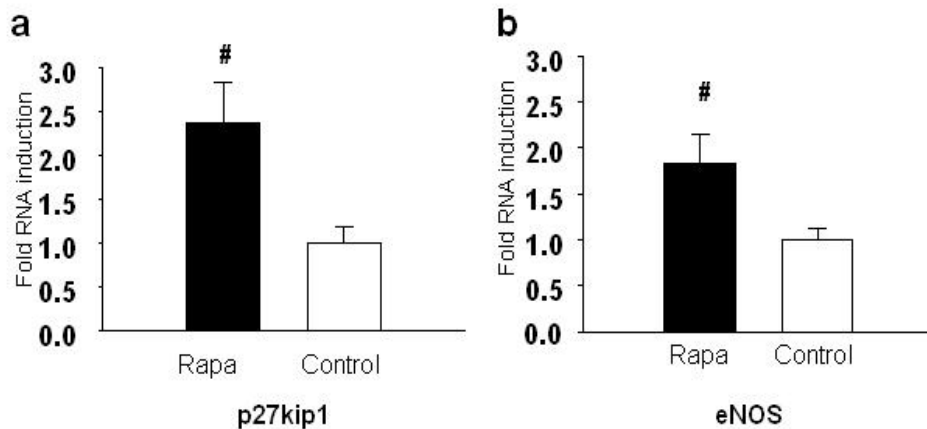the controls (Figure 1A).

Figure 1: p27kip1 (A) and (human) eNOS (B) mRNA levels obtained for control
conditions (white bars) and after rapamycin treatment (black bars) in mouse carotid
arteries of 3 mice. qPCR analysis was performed in triplicate on pooled samples from
6 animals per group. Note the upregulation of p27kip1 and (human) eNOS after
rapamycin treatement. * P<0.05 versus control.

Rapamycin affects the shear stress response of eNOS
The basal expression of the human eNOS in the contra-lateral control carotid arteries
increased by 1.8 ± 0.3 fold after treatment with the highest dose of rapamycin (Figure
1B). In the carotid arteries with shear stress modification, intracellular eNOS levels
increased in low shear stress regions after treatment with rapamycin (Figure 2, lower
panel) and in regions exposed to physiological shear stress range (1.5-3.0 Pa). In high
shear stress regions, intracellular eNOS levels decreased with increasing dosages of
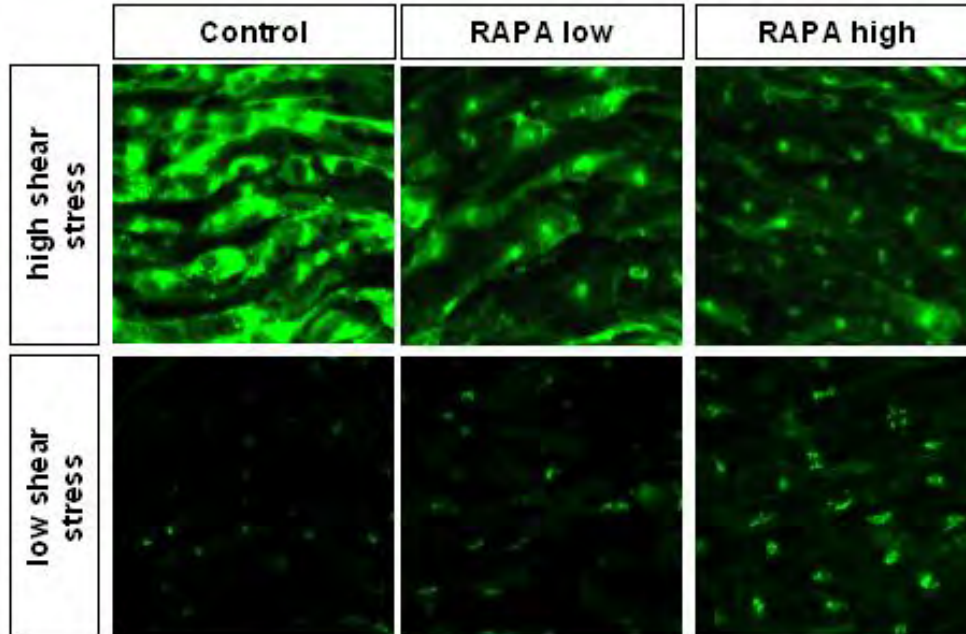rapamycin (Figure 2, upper panel).

Figure 2: eNOS-GFP images captured for high shear conditions and low shear stress conditions. All pictures are captured at equal settings of the microscope. The dose dependent effects of rapamycin at low shear stress are opposite from the effects at high shear stress: eNOS expression increased at low shear stress and decreased at high shear stress.

These observations were substantiated by the sigmoid curve fit analysis, which showed that $eNOS_{max}$ was decreased from 67.4±14.6 (Arbitrary Units or AU) to 34.1±7.7 (AU), and the EC_{50} was decreased from 10.7±2.6 N/m^2 to 4.8±0.5 N/m^2 (Figure 3A,B), while the slope and intercept remained unaffected. In figure 3C, the average curves from all three groups (control, rapamycin low dose (LD), rapamycin high dose (HD)) are displayed.

As it was difficult to obtain accurate measurements of eNOS protein at the lowest levels of the curve fit in a reliable way (Figure 3C), we also studied an extra series of mice, in which the carotid artery was ligated (i.e. zero shear stress) and eNOS protein levels were investigated (Figure 4). Ligation significantly reduced the eNOS-GFP signal in both control and the high dose rapamycin group. No significant effect of rapamycin on intracellular eNOS levels was observed in the contra-lateral control arteries (Fig. 4A, lower panels), while rapamycin treatment resulted in increased eNOS-GFP following ligation (Figure 4A, upper panels). These data clearly indicate that rapamycin increases eNOS expression at low shear stress. This effect is opposite from the response found at high shear stress levels.

97

Figure 3: Parameters derived from the sigmoid curve fit ($eNOS_{max}$, and EC_{50}) at different rapamycin dosages (in figure 3A and 3B respectively). Low dose is 3µg/kg/day, and high is 3mg/kg/day. EC_{50} is the shear stress (in N/m^2) at 50% of the maximal GFP value. $eNOS_{max}$ is the asymptote of the curve and represents the maximal eNOS-GFP level. Figure 3C: the average curve obtained from the control (C), low rapamycin dose (LD) en high rapamycin dose (HD). * $P<0.05$ *versus* control.

Figure 4: Captured eNOS-GFP images (A) and quantification of the eNOS-GFP signal under the following conditions: normal flow with rapamycin, normal flow wit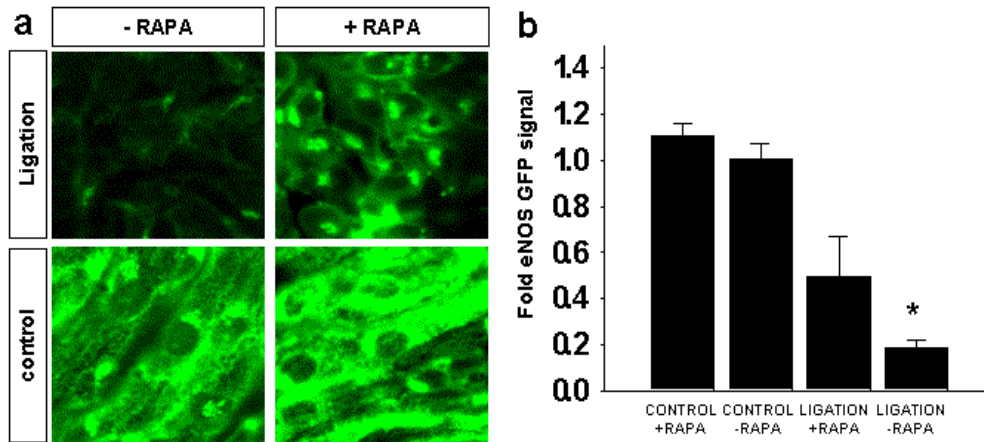hout rapamycin, ligation without rapamycin and ligation with rapamycin. Note that the effect of rapamycin is minimal during normal flow conditions, but becomes significant during ligation. Ligation reduces eNOS-GFP expression significantly in both the – rapamycin and + rapamycin groups. *$P<0.05$ *versus* ligation + rapamycin group.

The difference between minimal and maximal eNOS protein levels appeared to be dependent on rapamycin level as indicated by the relation between the difference of maximal and minimal eNOS protein levels as a function of rapamycin dosage. The relationship could be described by a linear regression line: ΔeNOS= -15*Rapa+41.4; r=0.6 (Figure 5).
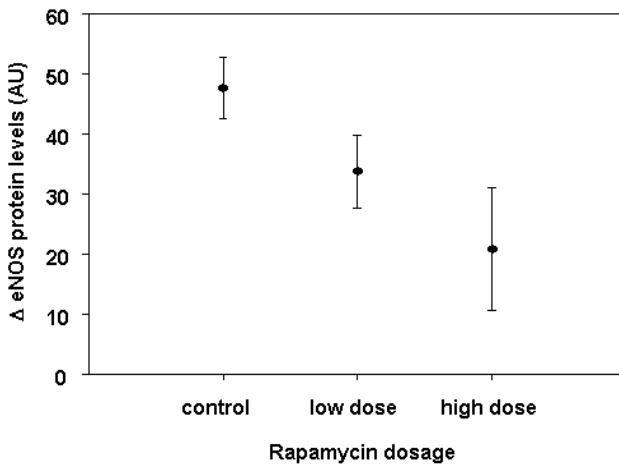

Figure 5: Relationship describing the difference of maximal and minimal eNOS protein levels as a function of rapamycin dosage. The relationship could be described by a linear regression line: ΔeNOS= -15*Rapa+41.4; r=0.6; P<0.05.

5.6 Discussion

Rapamycin has been used for treating in-stent restenosis because of its anti-proliferative, and anti-inflammatory properties[26-28]. Recently, rapamycin was shown to reduce atherosclerosis with a mechanism independent of its effects on p27^{kip1} [29]. This might be explained by a reduction in pro-atherogenic cytokines and an increase of anti-atherogenic cytokines in ApoE deficient mice treated with rapamycine found by Elloso et al.[30]. In addition, Naoum et al. showed that rapamycin increased eNOS expression in ApoE deficient mice[16] [31,32]. As the eNOS promoter is shear stress responsive[31], and we previously found that rapamycin possibly modulates the shear stress responsiveness of the vessel wall[20], we argued that rapamycin might affect the shear stress responsiveness of eNOS.

The main findings of the present study are that rapamycin treatment in aged and gender matched animals with a short protocol (11 days): 1) Increased rapamycin plasma levels and tissue p27^{kip1} expression, validating the efficacy of the treatment; 2) increased eNOS mRNA expression in carotid arteries in accordance with earlier studies; and 3) increased intracellular eNOS protein levels in cast treated carotid arteries at low shear stress levels, but decreased eNOS protein levels at high shear stress.

The present study showed that rapamycin affects eNOS expression in response to shear stress, confirming the hypothesis mentioned above. Our data indicate that intracellular eNOS protein levels increased at low shear stress levels (<1.5 Pa) in response to rapamycin. Low shear stress regions in the arterial system are notorious as initiation sites for the development of atherosclerotic lesions. The expression and activation of eNOS is severely reduced at these sites as a result of the decrease in shear stress levels. Our findings indicate that systemic administration of rapamycin will provide protection against the onset of atherosclerosis by increasing eNOS availability at these predilection sites.

Rapamycin also increased eNOS levels and expression patterns within the shear stress range, which is normally found in straight vessel segments (1.5-3.0 Pa; figure 2). This finding is consistent with previous data, showing elevated eNOS levels in straight murine aortas after administration of rapamycin [16].
The finding that eNOS levels are reduced in the high shear stress range (> 3.0 Pa) is new and implies that rapamycin might reduce the responsiveness of the putative shear stress sensor. High shear stress levels are also induced during exercise, and the vasodilatory response of the vessels in response to exercise has been reported to be due to enhanced release of NO by the endothelium. In a recent study, the coronary vessels of patients implanted with sirolimus eluting stents show impaired vasomotion in the vessel segments up- and downstream from the stented area, leading to vasoconstriction [33]. Our present study may offer an explanation for these findings, as

rapamycin reduces eNOS expression during high shear stress conditions. Diffusion of rapamycin into the peri-stent vascular regions could therefore induce endothelial dysfunction by affecting the expression of eNOS, resulting in the observed paradoxic vasocontriction.

Limitation of the method
For the calculations of the shear stress field we performed a 3-D reconstruction of the blood vessel from the flat specimen assuming a cylindrical geometry. We have tested this assumption by measuring diameter of individual mice before sacrifice and compared these measurements with 3D reconstruction diameters. The difference between prediction and measurements never exceeded the 5%. Another assumption underlying our CFD calculations was that entrance shear stress was 1.5 N/m^2.
Four days of cast placement was used throughout the experiments. This period was chosen as eNOS expression changes induced by shear stress were in a steady state and the period was too short for fibrotic tissue to interfere with the measurements.
Over-expression of eNOS-GFP may result in a negative feedback by the increased NO production inhibiting transcription of the gene. Thus, the effect of shear stress on eNOS expression might have been underestimated in the present study. However, the expression of murine eNOS in wild type controls shows a similar response to the shear stress alterations induced by the cast. The observed effect of shear stress on eNOS-GFP is therefore not restricted to the human eNOS transgenic construct.
The GFP reporter might interfere with eNOS localization. eNOS myristoylation and palmitoylation, which are both important for the localization, occur at the N-terminus. It is unlikely that these processes are affected, because the GFP part is fused at the C-terminus of the eNOS protein. Although GFP could induce changes in protein folding, our experiments show normal localization of eNOS-GFP in the Golgi complex and plasma membrane. Previous studies extensively studied the location and function of the eNOS-GFP fusion protein *in vitro*. These studies clearly indicate that the GFP moiety does not interfere with the localization and the function of eNOS.
The change in vessel geometry by cast placement may compress fibro-elastin layers of the vessel wall and thereby increase background auto-fluorescence. This does not affect our data however, because the auto-fluorescent signal was subtracted from the total GFP signal. The tapering effect of the cast could also compress the endothelial cells to make them fit into a smaller area, increasing the number of cells per area. Co-localization studies of the endothelium in the different shear stress regions do not show an increase in cell number per area or a decrease in cell size. In addition, the up-regulation of eNOS-GFP in single endothelial cells is observed, providing further evidence that the eNOS-GFP signal in the high shear vessel segment is not an artefact created by the tapered shape of the cast.

In conclusion, our results indicate that systemic administration of rapamycin protects the low shear stress regions from plaque initiation via an eNOS/shear stress dependent mechanism. In contrast, rapamycin decreases eNOS responsiveness to

high shear stress, rendering a loss of protection via eNOS/shear stress mechanism in these regions.

5.7 References

1.   Honda HM, Hsiai T, Wortham CM, et al. A complex flow pattern of low shear stress and flow reversal promotes monocyte binding to endothelial cells. *Atherosclerosis.* Oct 2001;158(2):385-390.
2.   Krams R, Wentzel JJ, Oomen JA, et al. Evaluation of endothelial shear stress and 3D geometry as factors determining the development of atherosclerosis and remodeling in human coronary arteries in vivo. Combining 3D reconstruction from angiography and IVUS (ANGUS) with computational fluid dynamics. *Arterioscler Thromb Vasc Biol.* 1997;17(10):2061-2065.
3.   Traub O, Berk BC. Laminar shear stress: mechanisms by which endothelial cells transduce an atheroprotective force. *Arterioscler Thromb Vasc Biol.* 1998;18(5):677-685.
4.   Buchanan JR, Jr., Kleinstreuer C, Truskey GA, et al. Relation between non-uniform hemodynamics and sites of altered permeability and lesion growth at the rabbit aorto-celiac junction. *Atherosclerosis.* 1999;143(1):27-40.
5.   Shaaban AM, Duerinckx AJ. Wall shear stress and early atherosclerosis: a review. *AJR Am J Roentgenol.* 2000;174(6):1657-1665.
6.   Gnasso A, Irace C, Carallo C, et al. In vivo association between low wall shear stress and plaque in subjects with asymmetrical carotid atherosclerosis. *Stroke.* 1997;28(5):993-998.
7.   Chappell DC, Varner SE, Nerem RM, et al. Oscillatory shear stress stimulates adhesion molecule expression in cultured human endothelium. *Circ Res.* 1998;82(5):532-539.
8.   Galbraith CG, Skalak R, Chien S. Shear stress induces spatial reorganization of the endothelial cell cytoskeleton. *Cell Motil Cytoskeleton.* 1998;40(4):317-330.
9.   Girard PR, Nerem RM. Shear stress modulates endothelial cell morphology and F-actin organization through the regulation of focal adhesion-associated proteins. *J Cell Physiol.* 1995;163(1):179-193.
10.   Fisslthaler B, Dimmeler S, Hermann C, et al. Phosphorylation and activation of the endothelial nitric oxide synthase by fluid shear stress. *Acta Physiol Scand.* 2000;168(1):81-88.
11.   Rizzo V, McIntosh DP, Oh P, et al. In situ flow activates endothelial nitric oxide synthase in luminal caveolae of endothelium with rapid caveolin dissociation and calmodulin association. *J Biol Chem.* 1998;273(52):34724-34729.
12.   Gloe T, Riedmayr S, Sohn HY, et al. The 67-kDa laminin-binding protein is involved in shear stress-dependent endothelial nitric-oxide synthase expression. *J Biol Chem.* 1999;274(23):15996-16002.
13.   Marks AR. Sirolimus for the prevention of in-stent restenosis in a coronary artery. *N Engl J Med.* Oct 2 2003;349(14):1307-1309.

14. Waksman R, Pakala R, Burnett MS, et al. Oral rapamycin inhibits growth of atherosclerotic plaque in apoE knock-out mice. *Cardiovasc Radiat Med.* Jan-Mar 2003;4(1):34-38.

15. Pham SM, Shears LL, Kawaharada N, et al. High local production of nitric oxide as a possible mechanism by which rapamycin prevents transplant arteriosclerosis. *Transplant Proc.* Jun 1998;30(4):953-954.

16. Naoum JJ, Zhang S, Woodside KJ, et al. Aortic eNOS expression and phosphorylation in Apo-E knockout mice: differing effects of rapamycin and simvastatin. *Surgery.* Aug 2004;136(2):323-328.

17. Li Y, Zheng J, Bird IM, et al. Mechanisms of shear stress-induced endothelial nitric-oxide synthase phosphorylation and expression in ovine fetoplacental artery endothelial cells. *Biol Reprod.* Mar 2004;70(3):785-796.

18. Boo YC, Sorescu G, Boyd N, et al. Shear stress stimulates phosphorylation of endothelial nitric-oxide synthase at Ser1179 by Akt-independent mechanisms: role of protein kinase A. *J Biol Chem.* 2002;277(5):3388-3396.

19. Ziegler T, Silacci P, Harrison VJ, et al. Nitric oxide synthase expression in endothelial cells exposed to mechanical forces. *Hypertension.* 1998;32(2):351-355.

20. Gijsen FJ, Oortman RM, Wentzel JJ, et al. Usefulness of shear stress pattern in predicting neointima distribution in sirolimus-eluting stents in coronary arteries. *Am J Cardiol.* Dec 1 2003;92(11):1325-1328.

21. Cheng C, van Haperen R, de Waard M, et al. Shear stress affects the intracellular distribution of eNOS: direct demonstration by a novel in vivo technique. *Blood.* Aug 16 2005.

22. van Haperen R, Cheng C, Mees BM, et al. Functional expression of endothelial nitric oxide synthase fused to green fluorescent protein in transgenic mice. *Am J Pathol.* Oct 2003;163(4):1677-1686.

23. Gijsen FJ, Allanic E, van de Vosse FN, et al. The influence of the non-Newtonian properties of blood on the flow in large arteries: unsteady flow in a 90 degrees curved tube. *J Biomech.* Jul 1999;32(7):705-713.

24. Gijsen FJ, Palmen DE, van der Beek MH, et al. Analysis of the axial flow field in stenosed carotid artery bifurcation models--LDA experiments. *J Biomech.* Nov 1996;29(11):1483-1489.

25. Gijsen FJ, van de Vosse FN, Janssen JD. Wall shear stress in backward-facing step flow of a red blood cell suspension. *Biorheology.* Jul-Oct 1998;35(4-5):263-279.

26. Ong AT, Serruys PW, Aoki J, et al. The unrestricted use of paclitaxel- versus sirolimus-eluting stents for coronary artery disease in an unselected population: one-year results of the Taxus-Stent Evaluated at Rotterdam Cardiology Hospital (T-SEARCH) registry. *J Am Coll Cardiol.* Apr 5 2005;45(7):1135-1141.

27. Morice MC, Serruys PW, Sousa JE, et al. A randomized comparison of a sirolimus-eluting stent with a standard stent for coronary revascularization. *N Engl J Med.* Jun 6 2002;346(23):1773-1780.

28. Regar E, Serruys PW, Bode C, et al. Angiographic findings of the multicenter Randomized Study With the Sirolimus-Eluting Bx Velocity Balloon-Expandable Stent (RAVEL): sirolimus-eluting stents inhibit restenosis irrespective of the vessel size. *Circulation.* Oct 8 2002;106(15):1949-1956.

29. Castro C, Campistol JM, Sancho D, et al. Rapamycin attenuates atherosclerosis induced by dietary cholesterol in apolipoprotein-deficient mice through a p27 Kip1 -independent pathway. *Atherosclerosis.* Jan 2004;172(1):31-38.

30. Elloso MM, Azrolan N, Sehgal SN, et al. Protective effect of the immunosuppressant sirolimus against aortic atherosclerosis in apo E-deficient mice. *Am J Transplant.* May 2003;3(5):562-569.

31. Govers R, Rabelink TJ. Cellular regulation of endothelial nitric oxide synthase. *Am J Physiol Renal Physiol.* 2001;280(2):F193-206.

32. Boo YC, Jo H. Flow-dependent regulation of endothelial nitric oxide synthase: role of protein kinases. *Am J Physiol Cell Physiol.* Sep 2003;285(3):C499-508.

33. Togni M, Windecker S, Cocchia R, et al. Sirolimus-eluting stents associated with paradoxic coronary vasoconstriction. *J Am Coll Cardiol.* Jul 19 2005;46(2):231-236.

Chapter 6: Atherosclerotic Lesion Size and Vulnerability are Determined by Patterns of Fluid Shear Stress

C. Cheng, D. Tempel, R. van Haperen A. van der Baan, F. Grosveld, M.J.A.P. Daemen, R. Krams, and R. de Crom,
Circulation, in review

6.1 Abstract

Atherosclerotic lesions are predominantly observed in curved arteries and near side branches, where low or oscillatory shear stress patterns occur, suggesting a causal connection. However, the effect of shear stress on plaque vulnerability is unknown, because the lack of an appropriate *in vivo* model precludes cause-effect studies. We developed a perivascular shear stress modifier inducing low, high, and low/oscillatory shear stress regions in mouse carotid arteries and studied plaque formation and composition. Atherosclerotic lesions developed invariably in low and/or oscillatory shear stress regions, whereas the high shear stress regions were protected. Low shear stress lesions were larger in size (intima/media: 1.38 ± 0.68 versus 0.22 ± 0.04), contained less smooth muscle cells ($1.9 \pm 1.6\%$ versus $26.3 \pm 9.7\%$) and less collagen ($15.3 \pm 1.0\%$ versus $22.2 \pm 1.0\%$), more lipids ($15.8 \pm 0.9\%$ versus $10.2 \pm 0.5\%$), and showed more outward vascular remodeling ($214 \pm 19\%$ versus $117 \pm 9\%$) than oscillatory shear stress lesions. Expression of pro-atherogenic inflammatory mediators and matrix-metalloproteinase activity was higher in the low shear stress regions. Spontaneous and angiotensin II induced intra-plaque hemorrhages occurred in the low shear stress regions only.

Low shear stress and oscillatory shear stress are both essential conditions in plaque formation. Low shear stress induces larger lesions with a vulnerable plaque phenotype, while oscillatory shear stress induces stable lesions.

6.2 Introduction

The occurrence of atherosclerosis is closely linked to local hemodynamic factors. Shear stress, the drag force acting on the endothelium as a result of blood flow, is thought to play a critical role in the development of endothelial dysfunction and atherosclerosis. This is based on the observation that atherosclerotic plaque formation occurs preferentially in areas such as the inner curvatures of coronary arteries, where the shear stress is low (<1.5 N/m^2), or near bifurcations, where shear stress is oscillatory in nature (displaying directional change and flow separation) [1-3]. Conversely, straight arterial segments with laminar flow have levels of shear stress of approximately 1.5 N/m^2 and appear to be protected from atherosclerosis. The relation between shear stress and atherosclerosis is almost exclusively based on observational studies in humans and large animals [1,4,5]. In addition, there is a large body of studies on the response of cultured endothelial cells on variations in shear stress (reviewed in [6]). While this work provides insight into the relationship between shear stress and plaque development, direct proof that deviations in shear stress induces atherosclerosis is lacking. In order to provide such evidence, an appropriate in vivo model that can generate complex shear stress fields is required. Furthermore, it is not clear whether low shear stress and oscillatory shear stress have different atherogenic properties. Therefore, our laboratory has recently developed a perivascular shear stress modifier (referred to as cast) that can induce changes in shear stress patterns in vivo in a straight vessel and in a defined manner. The cast (made of polyetheretherketon with a cone shaped lumen: 0.5 mm proximal inner diameter, 0.25 distal inner diameter) causes a tapered stenosis when placed around the carotid artery of a mouse. As a result, three regions with different shear stress patterns are created in the vessel: low shear stress (upstream from the cast), high shear stress (in the cast) and oscillatory shear stress (downstream from the cast) (see figure 1 of supplemented online data) [7]. The induction of the different shear stress conditions was validated by Doppler measurements [8], and the biological effect of the cast was validated by qPCR of shear stress responsive genes [7]. In the current study, we use this model to assess the effect of in vivo alterations of shear stress on the development of atherosclerosis in apolipoprotein E (apoE–/–) deficient mice. Our findings reveal that atherosclerotic lesions develop under both low shear stress and oscillatory shear stress conditions within 6 weeks of treatment, whereas no lesions develop in the high shear stress region.

Change in plaque composition can modify a stable atherosclerotic lesion into a plaque with a vulnerable phenotype, rendering its susceptible to rupture with dramatic consequences such as acute coronary syndrome and stroke. Therefore, it is important to understand the mechanisms that increase plaque vulnerability. While shear stress has been associated with specific plaque localization, it is presently unknown if this mechanical force has an effect on the vulnerability of the lesion. Therefore we analysed the composition of the atherosclerotic lesions that develop in the low shear stress and the oscillatory shear stress regions. Furthermore, expression of pro-

inflammatory mediators known in literature to be correlated to increased plaque instability[9,10] [11] was studied. We demonstrate that low shear stress induces the development of extensive lesions with a vulnerable plaque phenotype, whereas oscillatory shear stress induces the growth of stable lesions. Using Angiotensin II administration, we show that intra-plaque hemorrhages occur exclusively in the atherosclerotic lesions of the low shear stress regions.

6.3 Materials and Methods

Animals and diets
ApoE–/– mice in C57BL/6J background were obtained from The Jackson Laboratory, Bar Harbor, ME. Male animals 15-20 weeks of age were assigned randomly to one of the 3 time points (see supplemented data). During the experimental period, all animals were fed a Western type diet containing 15% (w/v) cacoa butter and 0.25% (w/v) cholesterol (diet W, Hope Farms, Woerden, The Netherlands). All experiments were performed in compliance with institutional (Erasmus MC, Rotterdam, The Netherlands) and national guidelines.

In vivo alteration of shear stress
In order to induce standardized changes in shear stress, we designed a shear stress modifier, which was manufactured of the thermoplastic, polyetherketon. The device is referred to as cast throughout the study. The cast consists of two longitudinal halves of a cylinder with a cone shaped lumen (see Figure 1a of supplemented data). The geometry of the cast has been designed with computational flow dynamics software to produce vortices downstream of the cast when placed around the common carotid artery (see Figure 1b of supplemented data). This downstream region will therefore be exposed to oscillations in shear stress (oscillatory shear stress region). The upstream inner diameter is 500 µm (non-constrictive) and gradually declines to 250 µm at the downstream side of the cast (constrictive). This tapering induces a gradual increase in shear stress (high shear stress region). In addition, the constrictive stenosis decreases the blood flow, resulting in a low shear stress region upstream from the cast. Control casts consist of a cylinder with a continuous non-constrictive diameter of 500 µm. The induction of the different shear stress conditions was validated by Doppler measurements [8].

Surgical procedures
After 2 weeks of Western diet, the animals were anaesthetised with isoflurane, and the anterior cervical triangles were accessed by a sagittal anterior neck incision. The right common carotid artery was dissected from circumferential connective tissues. The cast was placed around the right common carotid artery, wounds were closed and the animals were allowed to recover. Animals with cast implants were sacrificed at 6, 9, and 12 weeks after surgery. For the induction of intraplaque hemorrhages, apoE –/– mice received Western diet and were instrumented with the cast as decribed above. After 7 weeks of cast placement, the animals were treated with angiotensin II infusion of 400ng/kg/min (2 ng/µl in 200 µl volume) via a subcutaneously implanted osmotic minipump (Alzet, model 2004, Durect Corp, Maastricht, The Netherlands) for 2 weeks before they were sacrificed.

Tissue preparation and histology

Animals were anaesthetized with isoflurane and blood samples were collected by orbital puncture. Through a cardiac puncture flushing with 20 ml PBS was performed, immediately followed by in situ perfusion fixation with 20 ml 4% (w/v) paraformaldehyde (Sigma Chemical Co., Zwijndrecht, The Netherlands) in PBS at a constant perfusion pressure of 100 mm Hg. The entire aortic arch with the origins of the right and the left common carotid arteries including 5 mm of these vessels were carefully prepared. For visualization of surface area occupied by atherosclerosis, the aorta and its major branches were stained with Oil-red-O [12].

Quantification of histological data was performed on 7 µm cryosections at 140 µm intervals. In addition to standard hematoxylin/eosin staining, macrophages were detected using AIA31240 antibodies (1:3000, Accurate Chemical and Scientific, New York, USA), smooth muscle cells by antibodies against VSMC α-actin Cy3 (1:200, Sigma, Chemical Co., Zwijndrecht, The Netherlands). Antibodies against PECAM-1 (Sigma Chemical Co., Zwijndrecht, The Netherlands) were used to visualize the endothelium. Lipid deposition was analyzed with Oil-red-O staining and collagen with picrosirus red. Data analysis was performed using a microscopy image analysis system (Impak C, Clemex Technologies, Quebec, Canada).

Cholesterol analysis

Blood samples were taken by orbital puncture at the time of sacrifice. Total plasma cholesterol concentrations were measured enzymatically using a commercially available kit (Boehringer Mannheim GmbH, kit 236691)

In situ zymography

A PBS solution of DQ™ gelatin (1mg/ml) (Molecular Probes, Leiden, The Netherlands) in 1% agarose (Sigma Chemical Co., Zwijndrecht, The Netherlands) is applied to the slides and incubated for 2 hours at room temperature. Activity was detected by assessing the fluorescent signal using confocal microscopy.

Gene expression analysis

Freshly isolated carotid arteries were divided into three different regions (1 mm downstream from the cast, 1 mm in the cast, and 1 mm upstream from the cast) and these segments from 10 individual mice were pooled per region. Total RNA from the samples was isolated using the RNeasy kit (Qiagen, Venlo, The Netherlands) and linearly amplified following standard Eberwine T7 protocol [13]. Quantitative PCR reactions were performed using the iCycler iQ Detection System (Biorad, Veenendaal, The Netherlands). Primers were designed for VCAM-1, ICAM-1, IL-6, CRP, and VEGF. Target gene mRNA levels were expressed relatively to the housekeeping gene Hypoxanthine-Guanine Phosphoribosyl Transferase (HPRT). For additional material and methods section, see supplemented online data.

Statistical analysis
Statistical analysis was performed using two-way ANOVA analysis of variance (between more than two shear stress areas and between different time points). When only low shear stress and oscillatory shear stress for 1 time point were compared, the two-tailed Student t test was used. Data are presented as mean ± SEM. P values <0.05 were considered significant.

6.4 Results

Low shear stress and oscillatory shear stress both induce atherosclerotic plaque formation, whereas high shear stress protects against atherosclerosis

In order to study the effect of the 3 different shear stress fields on lesion formation, apoE–/– mice were fed an atherogenic diet, instrumented with the cast, and sacrificed at different times points (6, 9, and 12 weeks). Whole mount lipid staining of aortic arches and carotid arties showed that atherosclerotic lesions have already developed at the earliest time point (Figure 1A) in the inner curve of the aortic arch and at the beginning of the side branches. These are the natural sites of shear stress related plaque initiation [14]. In addition, lipid deposits have started to develop in the low shear stress and the oscillatory shear stress regions in the carotid artery instrumented with the cast at 6 weeks. At 9 and 12 weeks, the lesion areas grow markedly larger in the low shear stress regions (Figure 1, B and C). In the oscillatory shear stress regions, a gradual increase in lesion area can be appreciated as well (Figure 1, A-C), but these are considerably smaller than the lesions in the low shear stress regions. No atherosclerotic lesions were present in the high shear stress region at the earliest time point, and moderately sized lesions developed only in 2 out of the 7 mice (29%) at 9 weeks and in 3 out of the 6 mice (50%) at 12 weeks of cast implantation eventually, whereas all of the animals developed lesions under low and oscillatory shear stress from week 6 on. Controls included the contra-lateral, non-treated carotid arteries, sham operated animals (Figure 1D) and animals treated with a non-constrictive cast (Figure 1E). In none of these conditions, any lipid staining could be observed even after 12 weeks of cast placement. Plasma cholesterol levels were increased in animals on Western diet (6 weeks: 24.7±1.1 mmol/l; 9 weeks: 24.4±1.1 mmol/l; 12 weeks: 32.8±2.1 mmol/l) compared to animals on normal chow diet (10.9±3 mmol/l). Plasma cholesterol concentrations between animals treated with the cast or the non-constrictive cast were not different (12 weeks, cast: 32.8±2.1 mmol/l versus 12 weeks, non-constrictive cast: 31.9±0.4 mmol/l). These results indicate that the diet, the surgical procedure, or the material of the cast did not contribute to the observed atherosclerotic lesion formation in the straight segment of the carotid artery.
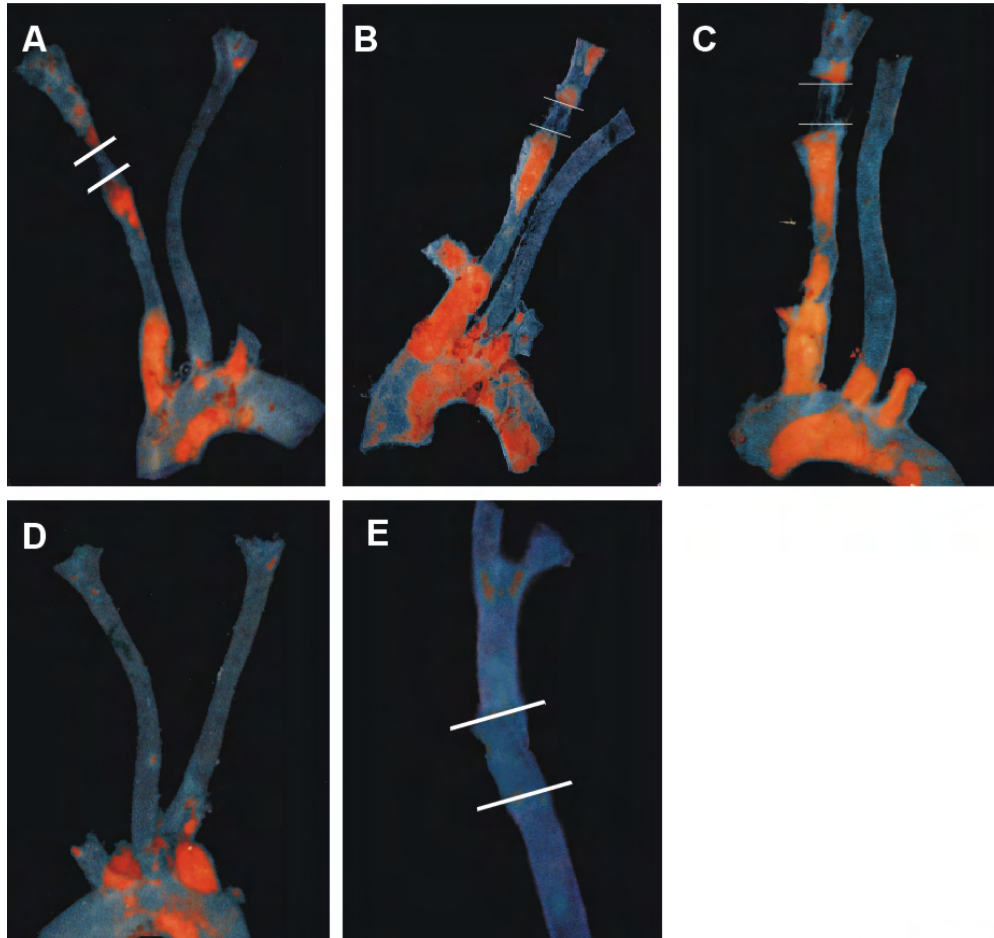
Figure 1: Low shear stress and oscillatory shear stress induce atherosclerosis in apoE −/− mice fed an atherogenic Western diet. Whole mount aortic arches and carotid arteries were stained with Oil-red-O for atherosclerotic lesions. The white lines demarcate the previous position of the cast with the high shear stress region. Upstream from the cast is the low shear stress region, and downstream from the cast is the oscillatory shear stress region. Animals were instrumented with a cast after 2 weeks of the beginning of the diet and sacrificed after 6 (A), 9 (B), or 12 (C-E) weeks of cast placement. No lesions are detected in the carotid arteries of sham operated mice (D) or in the carotid arteries of animals instrumented with a non-constrictive cast (E). Representative images are shown from groups consisting of 6-8 animals. Colour version of this figure is available in the full colour section.

Low shear stress is associated with more extensive lesions than oscillatory shear stress

Figure 2A shows micrographs of carotid artery morphology after 9 weeks of cast placement in the low, high and oscillatory shear stress regions, respectively, as well as in the contra-lateral carotid artery (undisturbed shear stress). In the high shear stress region, the appearance of the vessel is largely similar to that of the undisturbed, control region. In contrast, in the low and oscillatory shear regions atherosclerotic lesion formation is obvious. However, the lesions have a strikingly different morphology.

Platelet endothelial cell adhesion molecule-1 (PECAM-1) staining reveals an intact endothelium in all the regions studied at all time points (shown for 9 weeks in Figure 2B).

Measurements of the intima/media ratios showed that the atherosclerotic lesion areas in the low shear stress regions were much more extensive than those in the oscillatory regions (1.38 ± 0.68 versus 0.22 ± 0.04, respectively; Figure 2C). In both regions, the plaque size was significantly larger than in the undisturbed region. In contrast, no significant difference in intima/media ratios was observed between the high shear stress and undisturbed regions (Figure 2C). Vascular remodeling was evaluated by comparing the cross-sectional area of the vessel wall obtained from the low and the oscillatory shear stress regions of the instrumented carotid artery and the untreated contra-lateral carotid artery (control region). Remodeling was observed in the low shear stress region, where the relative cross-sectional vessel area was approximately 2-fold increased compared with the control region, while there was no significant change in the oscillatory shear stress region (Figure 2D). At 6 and 12 weeks, similar differences in intima/media ratios and in vascular remodeling between the different shear stress regions were found (data not shown).
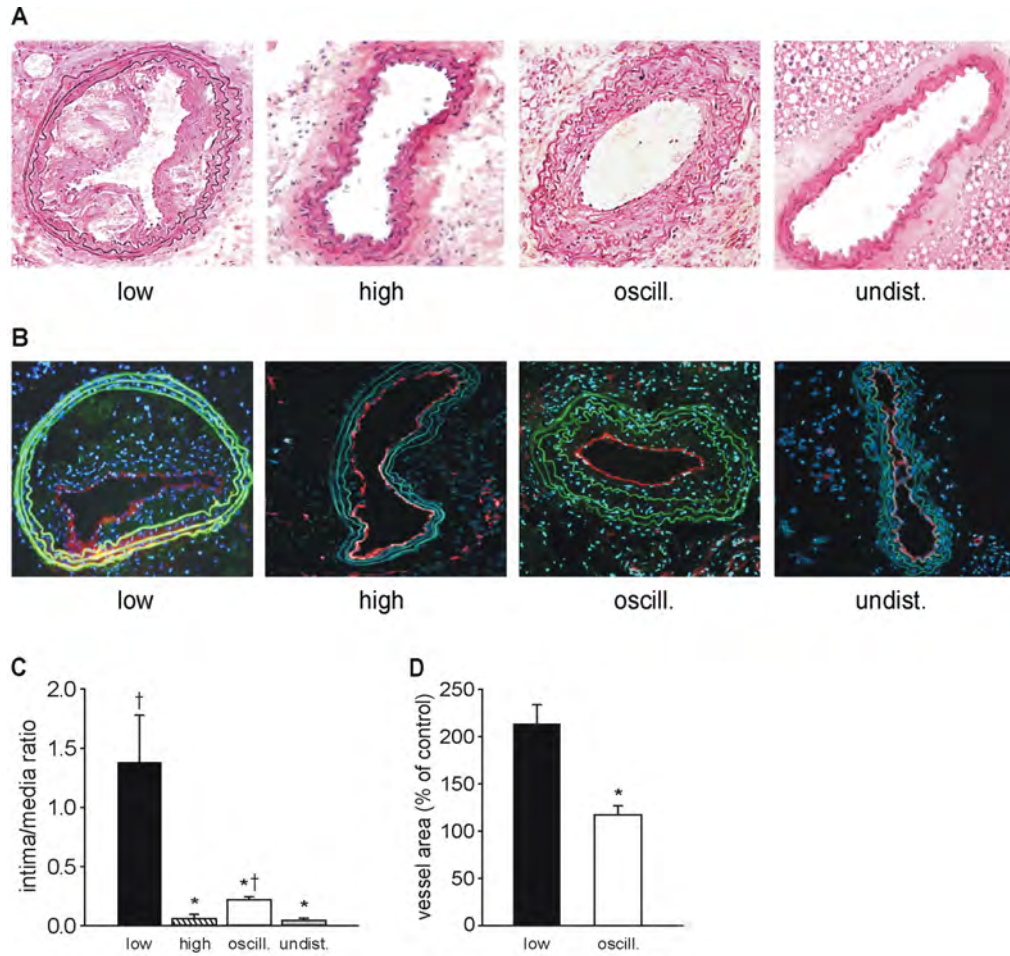
Figure 2: Histological analyses of carotid arteries at 9 weeks after cast placement in apoE–/– mice fed a Western diet. (A) Representative images are shown from the low, high, and oscillatory shear stress regions as well as from the contra-lateral non-treated carotid artery (undisturbed shear stress) (hematoxylin and eosin staining, original magnifications 100X). (B) Representative images showing PECAM-1 staining (red) of the intact endothelium in the four different shear stress regions. Auto-fluorescence of the elastic lamellae is in green and the cell nuclei stained with DAPI are in blue. Original magnifications: 100 X. Histological analyses were performed by quantification of the intima/media ratio (C), and of the relative cross-sectional area of the vessel wall (D), which was obtained by measuring the area confined by the external elastic lamina of the instrumented carotid artery and expressed as percentage of the cross-sectional area of the contra-lateral non-treated carotid artery. * $P<0.05$ versus low shear stress. † $P<0.05$ versus oscillatory shear stress. Colour version of this figure is available in the full colour section.

117

Low shear stress induces lesions with a vulnerable plaque phenotype, while oscillatory shear stress induces the development of stable lesions

In order to examine the effect of low shear stress and oscillatory shear stress on plaque composition, we performed (immuno)-histochemical analyses at 9 weeks after cast placement. As no lesions developed in the control vessels, the percentage of plaque components in the intimal area of these vessels cannot be analyzed and are therefore excluded. Macrophages and lipids were abundantly present in lesions of both low and oscillatory shear stress regions (Figure 3A). Quantification of the macrophage-positive areas showed no relative difference between lesions in the low shear stress and oscillatory shear stress regions (Figure 3B). However, the lipid content was significantly higher in the lesions located in the low shear stress regions than in the lesions located in the oscillatory shear stress regions (15.8 ± 0.9% *versus* 10.2 ± 0.5%, respectively; Figure. 3B). Further analysis of lesion components revealed that low shear stress lesions contained only thin layers of smooth muscle cells and collagen situated in the cap of the lesion, whereas in the oscillatory shear stress lesions the smooth muscle cells and collagen-positive areas were more uniformly distributed in the intima (Figure 3A). This pattern was also observed at the other time points studied (data not shown). The low shear stress lesions contained less vascular smooth muscle cells (1.9 ± 1.6% *versus* 26.3 ± 9.7%) and less collagen (15.3 ± 1.0% *versus* 22.2 ± 1.0%) than oscillatory shear stress lesions at week 9 (Figure 3B). In order to assess the observed reduction in collagen, matrix metallo-proteinase (MMP) activity was measured by DQ gelatinase assay (Figure 3A). An increase of about one third in MMP activity was found in the low shear stress region compared to the oscillatory shear stress region (Figure 3B).

Expression of pro-atherogenic inflammatory mediators is more prominent in the low shear stress region

Gene expression analysis revealed increased expression of pro-inflammatory mediators in the low shear stress region compared to the expression in the oscillatory shear stress region (Figure 4). Expression of Vascular Cell Adhesion Molecule-1 (VCAM-1) and Intercellular Adhesion Molecule-1 (ICAM-1), involved in the adhesive interactions between endothelial cells and leukocytes, were both upregulated by 3 fold in the low shear stress region compared with control, whereas only VCAM1 was 50% upregulated in the oscillatory shear stress region. Expression of the C-reactive protein (CRP) was increased by 3 fold in the low and by 2 fold the oscillatory shear stress region compared with control. The expression levels of the pro-atherogenic growth factor, vascular endothelial growth factor (VEGF), were increased by 5 fold in the low shear stress lesions exclusively. Finally, expression of the pro-inflammatory cytokine interleukin 6 (IL-6) was increased by 14 fold in the low shear stress and by 2 fold in the oscillatory shear stress region, compared with control.
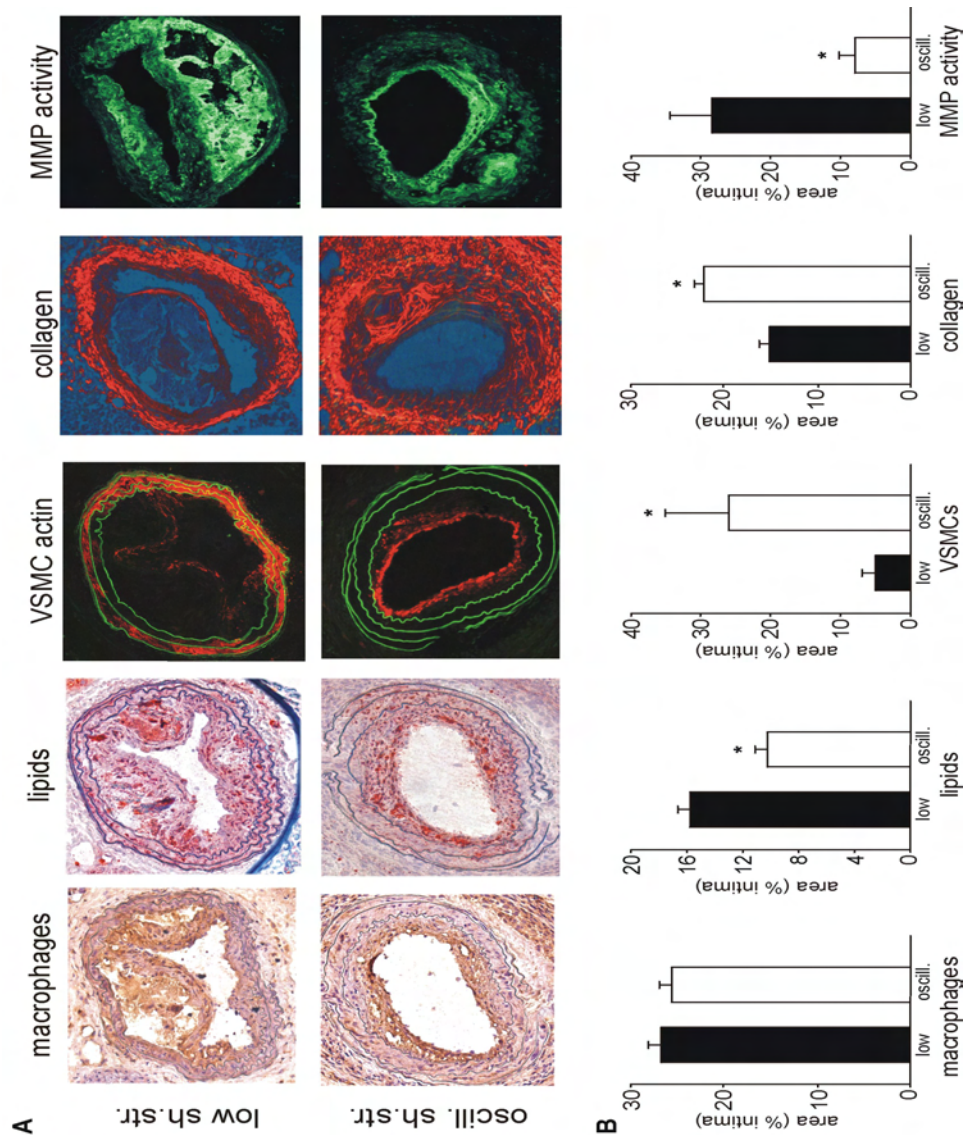
Figure 3: (A) Cross-sections of carotid arteries 9 weeks after cast placement in apoE–/– mice on a Western diet (100X magnification) stained for macrophages [15], lipids (Oil red-O), vascular smooth muscle cells (anti α-actin), or collagen (picrosirius red) in the low shear stress and the oscillatory shear stress region. MMP activity was studied by DQ gelatinase assay. (B) Quantification of macrophages, lipids, vascular smooth muscle cells, and collagen in the intimal area of the low shear stress and the oscillatory shear stress region, and of MMP activity. Data are the average values of sections from 5 different animals. * P<0.05 versus low shear stress. Colour version of this figure is available in the full colour section.
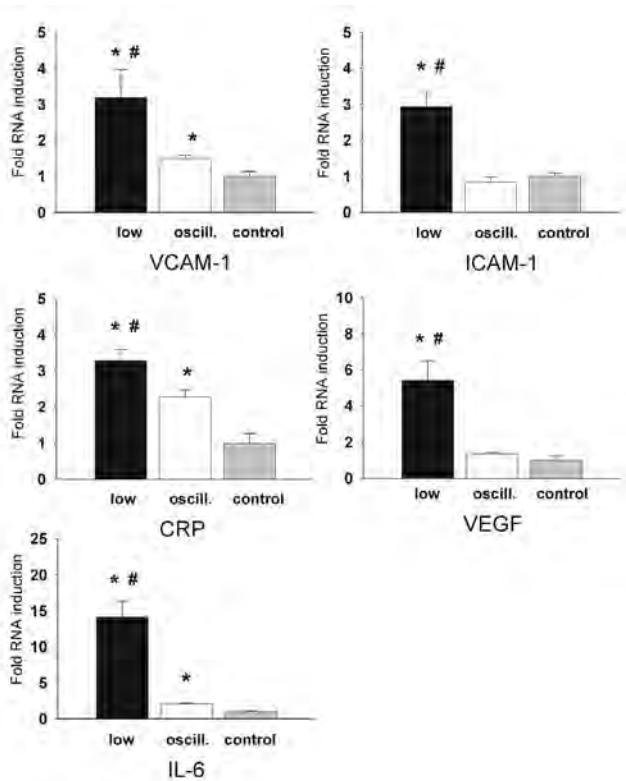
Figure 4: Vascular gene expression levels of pro-inflammatory mediators involved in the progression of atherosclerosis in carotid arteries 9 weeks after cast placement in apoE–/– mice fed a Western diet. Shown are the effects of low shear stress versus oscillatory shear stress on the expression of VCAM-1, ICAM-1, CRP, VEGF, and IL-6 measured by quantitative PCR. Data are obtained from a pool of 10 animals from four different PCRs. * $P<0.05$ versus low shear stress.

Intra-plaque hemorrhages are exclusively observed in lesions in the low shear stress region

In order to obtain further evidence of plaque instability in the low shear stress region, the more extensive group of mice was studied after 9 weeks of cast placement. Intra-plaque hemorrhages, an established sign of plaque vulnerability, could be observed in 4 out of 14 animals (28%). Traces of blood plasma and (partly degraded) erythrocytes were found in the basal region of the plaque close to the internal elastic lamina or in the necrotic core, while plaque integrity was preserved (Table 1 and Figure 5, A and B). Intra-plaque hemorrhages were never observed in lesions of the oscillatory shear stress region. We tested whether an increase in blood pressure would give rise to an even more pronounced vulnerable plaque phenotype [16,17]. To this end, Angiotensin II was chronically administrated to the mice via osmotic mini-pumps (400ng/kg/min) during the last two weeks of a 9 weeks period of cast placement. Efficacy of the treatment was validated by a raise in mean blood pressure (from 95 ± 3 mmHg to 127 ± 3 mmHg; $P<0.001$). More extended intra-plaque hemorrhages were observed in atherosclerotic lesions in the low shear stress region with an increased frequency of 6 out of 8 animals (75%) compared to the control group (Table 1 and Figure 5, C, E, F). Angiotensin II stimulation did not induce intra-plaque hemorrhages in the lesions initiated by oscillatory shear stress (Figure 5, D).

Deposition of iron, the product of degraded hemoglobin and suggestive for the presence of intramural thrombi, is detected by Prussian blue reaction (Figure 5, F). In several cases, atherosclerotic lesions became detached from the vascular wall, causing a false lumen (Figure 5, G and H). Plaque rupture or erosion could not be detected, even with angiotensin II stimulation.
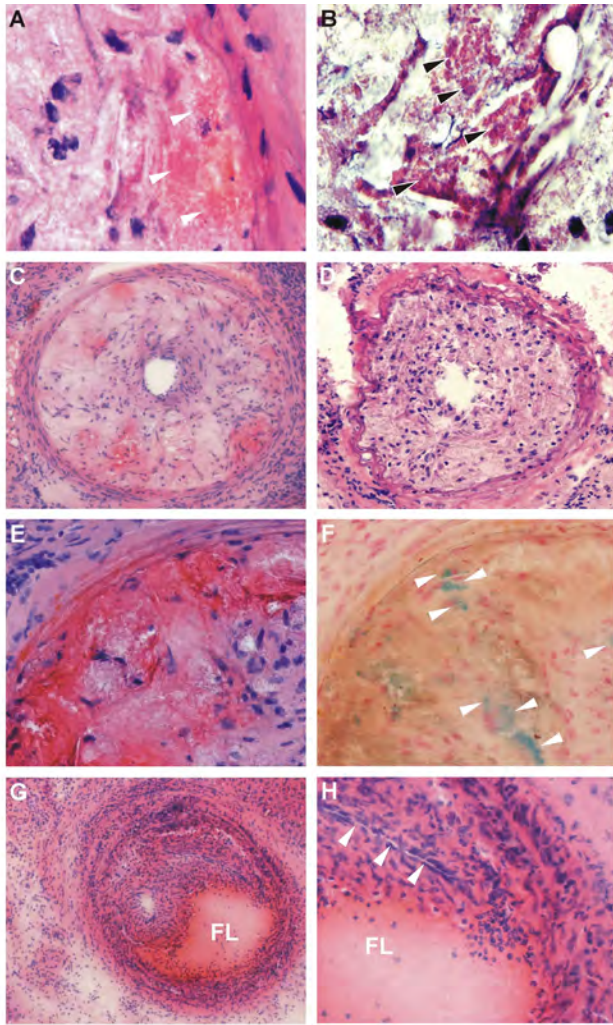

Figure 5: Intra-plaque hemorrhages in the lesions located in the low shear stress region. ApoE–/– mice were fed a Western diet and instrumented with a cast around the carotid artery. (A,B) After nine weeks, intra-plaque hemorrhages were found in approximately 28% of the animals analyzed. Arrowheads point at accumulations of red blood cells near the internal elastic lamina (A) or in the necrotic core (B). (C-H) After 7 weeks of cast placement, the animals were treated with angiotensin II infusion (400ng/kg/min) via a subcutaneously implanted osmotic minipump (Alzet, model 2004, Durect Corp) and were sacrificed 2 weeks later. Intra-plaque hemorrhages were frequently observed (in 6 out of the 8 animals): (C) overview of an atherosclerotic lesion with intra-plaque hemorrhages in the low shear stress region; (D) overview of an atherosclerotic lesion in the oscillatory shear stress region. No intra-plaque hemorrhages can be detected; (E) detail from intra-plaque hemorrhage in the low shear stress atherosclerotic lesions; (F) the same detail as in (E) stained for iron deposits (arrowheads) with the Prussian blue reaction; (G): overview of a carotid artery with a large false lumen (FL); (H) detail showing the depressed lumen (arrowheads). 7 µm cryosections were stained

with eosin and hematoxylin. Representative pictures from 6 animals are shown. Original magnifications: 100 X (C, D, G); 400 X (A, B, F, G, H). Colour version of this figure is available in the full colour section.

Table 1: Distribution of cast induced atherosclerotic lesions showing the occurrence of intra-plaque hemorrhages without and with angiotensin II stimulation.

	control		angiotensin II	
animals in group	14		8	
shear stress regions	low	oscillatory	low	oscillatory
intra-plaque hemorrhages	4	0	6	0
% of intimal area	0	0	2	0
false lumen	5.5±3.2*	0	29.7±7.9*	0

Low shear stress (LSS), oscillatory shear stress (OSS). Shown are frequency of false lumens and intra-plaque hemorrhages, and the mean % ± sem of the area in the plaque occupied by intra-laminal bleeding in the animals with intraplaque hemorrhages. *P<0.05 versus OSS, #P<0.05 versus control group.

6.6 Discussion

In this study we provided evidence that variations in shear stress patterns profoundly affect the initiation of atherosclerosis and induces the development of atherosclerotic plaques with a vulnerable phenotype. We conclude that both low and oscillatory shear stress are highly pro-atherogenic, because: 1) well-developed lesions are present from the earliest time point (week 6) in all of the cast-treated animals under both hemodynamic conditions; 2) lesions are absent in the straight segments of the contra-lateral, non-treated carotid arteries; and 3) the high shear stress area in the carotid arteries treated with the cast is protected from atherosclerotic lesion formation. In addition, low shear stress is a key factor in induction of plaques with a vulnerable phenotype. Damage to the endothelium due to cast placement could have also elicited a non-specific atherogenic response and reduce shear stress responsiveness. However, immuno-histological staining with PECAM-1 showed that the endothelium was intact in all of the examined shear stress regions after 9 weeks of cast placement (Figure 2B). In addition, in a previous study, the cast was used in mice transgenic for an endothelial nitric oxide - green fluorescent (eNOS-GFP) fusion gene [18]. We examined the expression of eNOS, which is endothelial cell specific, by monitoring the GFP signal en face, and found continuity of the endothelium in the treated carotid arteries directly after 1 day of cast placement [8]. Taken together, these data clearly show that the cast does not induce a non-specific atherogenic response by damaging the endothelium.

No atherosclerotic lesions were present in the high shear stress regions at 6 weeks after cast placement. Only small sized lesions that were not significantly different in intima/media ratio compared with control developed at later time point in some but not all of the treated ApoE -/- mice. These findings are in agreement with the generally accepted notion that plaques do not develop in high shear stress conditions [19-21]. Upregulation in the expression of eNOS in response to the high shear stress stimulation could be part of the anti-atherogenic properties of high shear stress [22]. Indeed, in previous studies we observed that eNOS levels were increased in the high shear stress regions of the cast treated vessels [8], suggesting that these vessel areas are more protected from the development of atherosclerosis [22]. Placement of a non-constrictive sham-cast made of the same material as the tapered cast (polyetherketon) does not induce atherosclerosis in the up and down stream regions. Thus, cast material or design does not cause a non-specific inflammatory response in the vessel wall that might lead to atherosclerotic disease. It has been reported that placement of a perivascular, non-constrictive cuff can induce intima hyperplasia or atherosclerosis in the treated vessel area [23]. This is remarkable, as in our control experiments placement of the non-constrictive sham-casts does not induce such a response. The development of atherosclerosis in these cuff models could have been elicited either by the material or the surgical procedure itself. More importantly, the cuffs are placed around the femoral arteries, which could respond differently to the placement of the device than the carotid arteries, used in this study. The superficial location of the

123

femoral artery, and movement of the hind limps by the animals could have limited the blood flow in cuffed vessels for periods of time, resulting in low shear stress and the induction of atherosclerosis.

Although the relation between shear stress and atherogenesis has been well documented, to the best of our knowledge nothing is known about the effect of this hemodynamic force on the composition of the plaque. Vulnerable atherosclerotic lesions are characterized by high percentages of "destabilizing" components (lipids and macrophages), and low percentages of "stabilizing" components (vascular smooth muscle cells and collagen). Morphologically, the destabilizing components are accumulated in pools underneath a thin fibrous cap with little infiltration of vascular smooth muscle cells [24,25]. Shear stress could determine the vulnerability of the lesion by altering the gene expression of the endothelial cells (e.g. upregulation of adhesion molecules, pro-inflammatory factors, and factors that mediate vascular wall permeability), and by increasing the interaction of pro-atherogenic components in the blood (lipoproteins and monocytes) with the activated endothelium [26-28]. We quantified the lesion components of the different shear stress regions in order to test whether shear stress patterns indeed affect plaque vulnerability. Low shear stress lesions contained more lipids, less vascular smooth muscle cells, and less collagen compared with lesions in the oscillatory shear stress region. At the same time, the lesions present in the low shear stress region displayed lipid pools and foam cells underneath a thin fibrous cap containing little vascular smooth muscle cells. Conversely, in the lesions induced by oscillatory shear stress, a thick fibrous cap heavily infiltrated with vascular smooth muscle cells covers the lesion, which contain similar relative amounts of macrophages but less lipids than the lesions in the low shear stress regions. Furthermore, outward vascular remodeling, which is considered one of the characteristic features of vulnerable plaques [29], is more prominent in the low shear stress region. These findings indicate that oscillatory shear stress induces the growth of more stabilized plaques, whereas low shear stress initiates the development of lesions with a vulnerable phenotype.

This was further substantiated by the occurrence of intra-plaque hemorrhages (both before and after administration of angiotensin II) in the lesions located in the low shear stress region. Intra-plaque hemorrhages are considered prominent markers of plaque instability [17,25,30,31]. Without angiotensin II stimulation, the more extended lesions developed in the low shear stress regions showed small intra-plaque hemorrhages close to the internal elastic lamina in 28% of the treated animals. Those were never observed in the lesions located in the oscillatory shear stress region.

Angiotensin II administration increases the mechanical strain on the lesions by raising blood pressure. Recently, several groups have also shown that Angiotensin II infusion into hyperlipidemic mice profoundly augments lesion formation independent from elevated blood pressure. Angiotensin II could therefore also have augmented the inflammatory process by increasing the Th1 response [32] or by increasing angiogenic properties of the plaque [33], resulting in the observed effect on the plaques located in the low shear stress area. However, despite the multi-potent ability of

angiotensin II to affect plaque vulnerability, our data clearly demonstrated that only the plaques triggered by low shear stress were susceptible to more severe and increased occurrence of intra-plaque haemorrhages in response to angiotensin II stimulation.

In order to understand the mechanism by which shear stress determines lesion vulnerability, we hypothesized that different shear stress patterns elicit divergent pro-atherogenic inflammatory responses in the vascular wall. It has been reported that VCAM-1 and ICAM-1 expression respond to low shear stress and oscillatory shear stress conditions in cultured endothelial cells [34-36]. We could confirm these findings in vivo, and found that low shear stress induces higher expression levels of VCAM-1 and ICAM-1 than oscillatory shear stress. Therefore, leukocyte recruitment is probably elevated in these regions. Although there was no difference found in the relative lesion area occupied by macrophages, the larger lesions in the low shear stress region contain considerably higher number of macrophages than the lesions in the oscillatory shear stress regions. Consequently, differences in infiltration efficiency of monocytes induced by low and oscillatory shear stress could result in the observed differences in lesion size. We also found increased expression levels of the atherosclerosis markers IL-6 and CRP in the lesions of the low shear stress area, indicating enhanced pro-atherogenic inflammatory activity [9,10]. IL-6 is an important factor for increased plaque vulnerability, as it stimulates recruitment of macrophages and leukocytes, and is a crucial regulator of extracellular matrix remodeling (increasing activity of matrix metalloproteinases such as MMP-9). Actually, more MMP activity was observed in low shear stress compared to the oscillatory shear stress region. Macrophages have been shown to induce collagen breakdown in fibrous caps of human atherosclerotic plaques associated with cellular expression and zymographic evidence of MMP activity [37]. Increased Collagen breakdown in the low shear stress lesions by MMP activity contributes to weakening of the fibrous cap, increasing its vulnerability to rupture.

The augmented inflammatory response also causes a decline in vascular smooth muscle cells mainly due to inhibition of proliferation by interferon-γ (released by leukocytes) and increased apoptosis [25]. As a result, lesions induced by low shear stress contained relatively less vascular smooth muscle cells than lesions induced by oscillatory shear stress. Thus, low shear stress appears to induce larger plaques with a stronger inflammatory response, giving rise to lesions with characteristics of a vulnerable plaque.

In summary, the present study identifies shear stress patterns as an essential factor in atherosclerotic lesion development, size, composition and vulnerability. Future studies are needed to elucidate the pathways by which endothelial cells initially react to shear stress during the atherogenic process and will be important for our understanding of the development of the vulnerable plaque. With the pro-atherogenic shear stress fields induced by the cast, we have generated an animal model in which both stable and unstable lesions can be studied in one straight vessel segment. Intra-

plaque haemorrhages have been previously observed in other atherosclerosis-prone mousemodels (reviewed in [38]). In our model, however, intra-plaque hemorrhages occurred more frequently in a controlled fashion, even without additional stimuli such as angiotensin II. This will create opportunities to further study the molecular pathways involved and evaluate therapies aimed at plaque stabilization.

6.7 References

1.   Pedersen EM, Oyre S, Agerbaek M, Kristensen IB, Ringgaard S, Boesiger P, Paaske WP. Distribution of early atherosclerotic lesions in the human abdominal aorta correlates with wall shear stresses measured in vivo. *Eur J Vasc Endovasc Surg*. 1999;18:328-33.
2.   Wentzel JJ, Kloet J, Andhyiswara I, Oomen JA, Schuurbiers JC, de Smet BJ, Post MJ, de Kleijn D, Pasterkamp G, Borst C, Slager CJ, Krams R. Shear-stress and wall-stress regulation of vascular remodeling after balloon angioplasty: effect of matrix metalloproteinase inhibition. *Circulation*. 2001;104:91-6.
3.   Davies PF, Polacek DC, Shi C, Helmke BP. The convergence of haemodynamics, genomics, and endothelial structure in studies of the focal origin of atherosclerosis. *Biorheology*. 2002;39:299-306.
4.   Buchanan JR, Jr., Kleinstreuer C, Truskey GA, Lei M. Relation between non-uniform hemodynamics and sites of altered permeability and lesion growth at the rabbit aorto-celiac junction. *Atherosclerosis*. 1999;143:27-40.
5.   Stone PH, Coskun AU, Kinlay S, Clark ME, Sonka M, Wahle A, Ilegbusi OJ, Yeghiazarians Y, Popma JJ, Orav J, Kuntz RE, Feldman CL. Effect of endothelial shear stress on the progression of coronary artery disease, vascular remodeling, and in-stent restenosis in humans: in vivo 6-month follow-up study. *Circulation*. 2003;108:438-44.
6.   Shyy JY, Chien S. Role of integrins in endothelial mechanosensing of shear stress. *Circ Res*. 2002;91:769-75.
7.   Cheng C, de Crom R, van Haperen R, Helderman F, Gourabi BM, van Damme LC, Kirschbaum SW, Slager CJ, van der Steen AF, Krams R. The role of shear stress in atherosclerosis: action through gene expression and inflammation? *Cell Biochem Biophys*. 2004;41:279-94.
8.   Cheng C. Shear stress affects the intracellular distribution of eNOS: Direct demonstration by a novel in vivo technique. *Blood*. 2005.
9.   Paul A, Ko KW, Li L, Yechoor V, McCrory MA, Szalai AJ, Chan L. C-reactive protein accelerates the progression of atherosclerosis in apolipoprotein E-deficient mice. *Circulation*. 2004;109:647-55.
10.   Schieffer B, Selle T, Hilfiker A, Hilfiker-Kleiner D, Grote K, Tietge UJ, Trautwein C, Luchtefeld M, Schmittkamp C, Heeneman S, Daemen MJ, Drexler H. Impact of interleukin-6 on plaque development and morphology in experimental atherosclerosis. *Circulation*. 2004;110:3493-500.
11.   de Boer OJ, van der Wal AC, Teeling P, Becker AE. Leucocyte recruitment in rupture prone regions of lipid-rich plaques: a prominent role for neovascularization? *Cardiovasc Res*. 1999;41:443-9.
12.   Curfs DM, Lutgens E, Gijbels MJ, Kockx MM, Daemen MJ, van Schooten FJ. Chronic exposure to the carcinogenic compound benzo[a]pyrene induces

larger and phenotypically different atherosclerotic plaques in ApoE-knockout mice. *Am J Pathol*. 2004;164:101-8.

13. Weiss D, Kools JJ, Taylor WR. Angiotensin II-induced hypertension accelerates the development of atherosclerosis in apoE-deficient mice. *Circulation*. 2001;103:448-54.

14. von der Thusen JH, van Vlijmen BJ, Hoeben RC, Kockx MM, Havekes LM, van Berkel TJ, Biessen EA. Induction of atherosclerotic plaque rupture in apolipoprotein E-/- mice after adenovirus-mediated transfer of p53. *Circulation*. 2002;105:2064-70.

15. van Haperen R, Cheng C, Mees BM, van Deel E, de Waard M, van Damme LC, van Gent T, van Aken T, Krams R, Duncker DJ, de Crom R. Functional expression of endothelial nitric oxide synthase fused to green fluorescent protein in transgenic mice. *Am J Pathol*. 2003;163:1677-86.

16. Traub O, Berk BC. Laminar shear stress: mechanisms by which endothelial cells transduce an atheroprotective force. *Arterioscler Thromb Vasc Biol*. 1998;18:677-85.

17. Gimbrone MA, Jr., Topper JN, Nagel T, Anderson KR, Garcia-Cardena G. Endothelial dysfunction, hemodynamic forces, and atherogenesis. *Ann N Y Acad Sci*. 2000;902:230-9; discussion 239-40.

18. Cunningham KS, Gotlieb AI. The role of shear stress in the pathogenesis of atherosclerosis. *Lab Invest*. 2005;85:9-23.

19. van Haperen R, de Waard M, van Deel E, Mees B, Kutryk M, van Aken T, Hamming J, Grosveld F, Duncker DJ, de Crom R. Reduction of blood pressure, plasma cholesterol, and atherosclerosis by elevated endothelial nitric oxide. *J Biol Chem*. 2002;277:48803-7.

20. Lardenoye JH, Delsing DJ, de Vries MR, Deckers MM, Princen HM, Havekes LM, van Hinsbergh VW, van Bockel JH, Quax PH. Accelerated atherosclerosis by placement of a perivascular cuff and a cholesterol-rich diet in ApoE*3Leiden transgenic mice. *Circ Res*. 2000;87:248-53.

21. Virmani R, Kolodgie FD, Burke AP, Farb A, Schwartz SM. Lessons from sudden coronary death: a comprehensive morphological classification scheme for atherosclerotic lesions. *Arterioscler Thromb Vasc Biol*. 2000;20:1262-75.

22. Lutgens E, van Suylen RJ, Faber BC, Gijbels MJ, Eurlings PM, Bijnens AP, Cleutjens KB, Heeneman S, Daemen MJ. Atherosclerotic plaque rupture: local or systemic process? *Arterioscler Thromb Vasc Biol*. 2003;23:2123-30.

23. Topper JN, Gimbrone MA, Jr. Blood flow and vascular gene expression: fluid shear stress as a modulator of endothelial phenotype. *Mol Med Today*. 1999;5:40-6.

24. Truskey GA, Barber KM, Rinker KD. Factors influencing the nonuniform localization of monocytes in the arterial wall. *Biorheology*. 2002;39:325-9.

25. Dai G, Kaazempur-Mofrad MR, Natarajan S, Zhang Y, Vaughn S, Blackman BR, Kamm RD, Garcia-Cardena G, Gimbrone MA, Jr. Distinct endothelial

phenotypes evoked by arterial waveforms derived from atherosclerosis-susceptible and -resistant regions of human vasculature. *Proc Natl Acad Sci U S A*. 2004;101:14871-6.

26. Ivan E, Khatri JJ, Johnson C, Magid R, Godin D, Nandi S, Lessner S, Galis ZS. Expansive arterial remodeling is associated with increased neointimal macrophage foam cell content: the murine model of macrophage-rich carotid artery lesions. *Circulation*. 2002;105:2686-91.

27. Rosenfeld ME, Polinsky P, Virmani R, Kauser K, Rubanyi G, Schwartz SM. Advanced atherosclerotic lesions in the innominate artery of the ApoE knockout mouse. *Arterioscler Thromb Vasc Biol*. 2000;20:2587-92.

28. Takaya N, Yuan C, Chu B, Saam T, Polissar NL, Jarvik GP, Isaac C, McDonough J, Natiello C, Small R, Ferguson MS, Hatsukami TS. Presence of intraplaque hemorrhage stimulates progression of carotid atherosclerotic plaques: a high-resolution magnetic resonance imaging study. *Circulation*. 2005;111:2768-75.

29. Mazzolai L, Duchosal MA, Korber M, Bouzourene K, Aubert JF, Hao H, Vallet V, Brunner HR, Nussberger J, Gabbiani G, Hayoz D. Endogenous angiotensin II induces atherosclerotic plaque vulnerability and elicits a Th1 response in ApoE-/- mice. *Hypertension*. 2004;44:277-82.

30. Hilfiker A, Hilfiker-Kleiner D, Fuchs M, Kaminski K, Lichtenberg A, Rothkotter HJ, Schieffer B, Drexler H. Expression of CYR61, an angiogenic immediate early gene, in arteriosclerosis and its regulation by angiotensin II. *Circulation*. 2002;106:254-60.

31. Morigi M, Zoja C, Figliuzzi M, Foppolo M, Micheletti G, Bontempelli M, Saronni M, Remuzzi G, Remuzzi A. Fluid shear stress modulates surface expression of adhesion molecules by endothelial cells. *Blood*. 1995;85:1696-703.

32. Chappell DC, Varner SE, Nerem RM, Medford RM, Alexander RW. Oscillatory shear stress stimulates adhesion molecule expression in cultured human endothelium. *Circ Res*. 1998;82:532-9.

33. Mohan S, Mohan N, Valente AJ, Sprague EA. Regulation of low shear flow-induced HAEC VCAM-1 expression and monocyte adhesion. *Am J Physiol*. 1999;276:C1100-7.

34. Shah PK, Falk E, Badimon JJ, Fernandez-Ortiz A, Mailhac A, Villareal-Levy G, Fallon JT, Regnstrom J, Fuster V. Human monocyte-derived macrophages induce collagen breakdown in fibrous caps of atherosclerotic plaques. Potential role of matrix-degrading metalloproteinases and implications for plaque rupture. *Circulation*. 1995;92:1565-9.

35. Rekhter MD. How to evaluate plaque vulnerability in animal models of atherosclerosis? *Cardiovasc Res*. 2002;54:36-41.

36. Delsing DJ, Offerman EH, van Duyvenvoorde W, van Der Boom H, de Wit EC, Gijbels MJ, van Der Laarse A, Jukema JW, Havekes LM, Princen HM. Acyl-CoA:cholesterol acyltransferase inhibitor avasimibe reduces

atherosclerosis in addition to its cholesterol-lowering effect in ApoE*3-Leiden mice. *Circulation*. 2001;103:1778-86.

Chapter 7: Shear Stress-induced Plaque Vulnerability is Modulated by Chemokines

C. Cheng, D. Tempel, R. van Haperen, M. Huisman, F. Doran, P. Leenen, R. de Crom, and R. Krams,
submitted for publication

7.1 Abstract

Low and oscillatory shear stress are strongly correlated to atherosclerosis. Recent studies also designate a significant role for chemokines in atherogenesis. No studies have yet been performed in which the direct effect of shear stress on chemokine expression during atherogenesis is investigated. We studied the time dependent expression of chemkines/chemokine receptors in response to these hemodynamical forces in ApoE -/- mice.

Using an extravascular device, referred to as the cast, we induced regions of low, high, and low/oscillatory shear stress (LSS, HSS and OSS, respectively) in the carotid artery. We studied expression of MCP1, KC (mouse homologue of IL8), RANTES, eotaxin1, ELC, SDFα, NAP-2, IP10, fractalkine, and CCL14 by Q-PCR in the LSS and OSS vessel segments at different time points. No lesions were present after 1 week of shear stress modification. Shear stress alteration did induce expression of chemokines: Expression of IP10 was more observed in the LSS region, whereas MCP1 and IL8/KC were equally upregulated in both LSS and OSS regions. After 3 weeks, lesions start to develop in both shear stress areas, and specific upregulation of IL8/KC and IP10 was observed in under LSS stimulation. After 9 weeks, lesions with a vulnerable plaque phenotype (thin fibrous cap, large necrotic core) were found in the LSS region, whereas stable lesions were found in the OSS region. Equal levels of MCP1 expression were observed in both regions, while expression of fractalkine was only found in the LSS region. Placement of non-constrictive casts did not induce chemokine expression or lesion formation. Quantitative analysis of immunohistochemistry data confirmed these results: At 1 week MCP1 expression was detected in VSMCs in the media, and IP10 expression in ECS and VSMCs. Fractalkine could be detected at 9 weeks in the media and intima of the LSS lesions. At 9 weeks, CCR2 (MCP1 receptor) expression was only observed on a few monocytes located on top of the plaque in both the LSS and the OSS region, indicating that recruitment of monocytes via MCP1 was limited. Conversely, plaques in the LSS region contained more CX3CR1 (fractalkine receptor) expressing cells in the intima. Blockage of fractalkine using a neutralizing antibody inhibited the growth and the development of vulnerable plaque in the LSS regions.

We conclude that LSS or OSS triggers expression of chemokines (MCP1, IL8/KC) involved in atherogenesis. Increased expression of IP10 induced by LSS could be involved in the subsequent development of lesions with a vulnerable plaque phenotype. Upregulation of fractalkine during LSS induced atherogenesis is crucial for vulnerable plaque formation.

7.2 Introduction

Shear stress, the drag force per unit area acting on the endothelium as a result of blood flow, plays a critical role in plaque initiation, location, and progression. Both low shear stress and oscillatory shear stress have been implied as pro-atherogenic, while high shear stress protects against atherosclerosis. In previous studies, we demonstrate that low shear stress and oscillatory shear stress are both crucial conditions for the induction of atherosclerosis. However, important dissimilarities in their atherogenic abilities are present that results in the outcome of two different types of plaques. Low shear stress induces the development of large-sized lesions with a vulnerable plaque phenotype, whereas oscillatory shear stress triggers the growth of more stable lesions after 9 weeks of cast placement[1].

Several studies indicated the role of inflammatory cells in the pathogenesis of plaques with a vulnerable phenotype. Accumulation of inflammatory cells occurs through a cascade of mechanisms leading to rolling, arrest and migration. Shear stress plays an important role in this process: it exerts torque on the rolling cells[2,3], and it affects the density of adhesion factors[4,5]. Both in low shear and oscillatory shear stress, torque is low and expression of adhesion factors is increased.

Recent studies indicate that avidity and affinity of integrins plays an important role in the strength of receptor-ligand binding[6], thereby determining the possibility of accumulation of the inflammatory cells. These processes are initiated and modulated by chemokines[7,8]. Chemokines are a family of small, secreted proteins consisting roughly of C-C and C-X-C subgroups[9]. As studies in humans indicate a strict spatial localization of the inflammatory cells in plaques[10], we postulated that this could be due to a decisive role of chemokines in controlling this process. To the best of our knowledge, data depicting a role for low or oscillatory shear stress in the regulation of chemokines come from a limited number of *in vitro* studies, that point to a shear stress dependent expression of MCP1[11,12] , and IL8[13]. The role of shear stress regulated chemokine expression in atherosclerosis development still needs to be investigated. Therefore, the first aim of the study is to characterize the chemokine expression pattern induced by shear stress during atherogenesis. Furthermore, as chemokines could modulate the development of vulnerable plaques or inhibit stabilization of atherosclerotic lesions, the second aim of this study was to characterize the chemokine expression pattern that defined vulnerable or stable plaque development. For both purposes, we compared the response of the chemokines Monocyte Chemoattractant Protein 1 (MCP1), KC (mouse homologue of Interleukin 8 (IL8)), RANTES, eotaxin1, EBI1-ligand chemokine (ELC), stromal cell-derived factor 1 (SDFα), neutrophil-activating protein 2 (NAP-2), interferon γ-inducible protein 10 (IP10), fractalkine, and CCL14 (all known or suggested to be involved in atherosclerosis or to be regulated by shear stress[11,13,14]), on low and oscillatory shear stress stimuli at different time points. We analyzed two early time points (1 and 3 weeks after cast placement) and time point 9 weeks after cast

placement when the advanced lesions with the different plaque characteristics are present.

On basis of our findings we selected several candidate genes that were tested for their protein levels in the plaque, confirming the findings observed in the gene-expression analysis. Finally, one candidate gene – fractalkine – was selected, for its arrest properties and chemo-attracting properties[15]. Fractalkine is located in the membrane of several cells, including the endothelial cell, making it sensitive to shear stress. In addition, it was exclusively expressed in the by low shear stress induced lesions with the vulnerable plaque phenotype. The functional implication of this protein in this process was studied by treatment with a fractalkine neutralizing antibody.

7.3 Materials and Methods

Mice
Mice deficient in apolipoprotein E (apoE-/-) expression in a C57BL/6J background were obtained from Jackson Laboratories. Animals 15-20 weeks of age were assigned randomly to one of the 3 time points (see below). During the experimental period, all animals were fed a Western type diet consisting of 15% (w/w) cacoa butter and 0.25% (w/w) cholesterol (diet W, Hope Farms, Woerden, The Netherlands). After a two weeks period of Western diet, shear stress in the right common carotid artery was altered by cast placement as previously described. Animals with casts implants were sacrificed at 1, 3, and 9 weeks after surgery.
To study the effects of fractalkine blockage, ApoE-/- animals were injected in the tail artery three times a week with 25µg of neutralizing rabbit α-mouse fractalkine antibody (Ebioscience, Malden, The Netherlands) or rabbit IgG isotype control antibody (Ebioscience, Malden, The Netherlands). Mice received the injections after six weeks of cast placement up until the 9 weeks time point at which the animals were sacrificed. The Erasmus MC institutional review board approved all animal studies described in this manuscript.

Gene expression analysis
Freshly isolated vessel segments were each divided into three different regions (0.5 mm proximal from the cast, 1 mm in the cast, and 0.5 mm distal to the cast) and pooled per region (n=10). Total RNA from the samples was extracted using the RNAeasy kit and was linearly amplified following an Eberwine T7 protocol or, when necessary directly reversed transcribed into cDNA. QPCR reactions were performed using a real-time fluorescent determination in the iCycler iQ Detection System (Biorad, Veenendaal, The Netherlands). Primers were designed for MCP1, KC, RANTES, eotaxin1, ELC, SDFα, NAP-2, IP10, Fractalkine, and CCL14. Target gene mRNA levels were expressed relatively to the housekeeping gene HPRT.

Cholesterol analysis
Blood samples were taken under anaesthesia by orbital puncture at the time of sacrifice. Total plasma cholesterol concentrations were measured enzymatically using a commercially available kit (Boehringer Mannheim GmbH, kit 236691).

(Immuno)histological assessment
Both the right and the left common carotid arteries were harvested after in situ fixation and were subsequently imbedded in cubes of liver. These cubes were immersed in OCT compound, and frozen in liquid nitrogen. Subsequently, cryosections of 6 μm were obtained from the entire right carotid artery and each staining was performed on sections equally spaced throughout the arteries at 120 μm intervals. Macrophages were detected using anti CD68 antibody (Santa Cruz

Biotechnology, Santa Cruz, USA), and smooth muscle cells by antibodies against VSMC α-actin (Sigma, Chemical Co., Zwijndrecht, The Netherlands). Lipid deposition was analysed with Oil-red-O staining and collagen with picrosirus red. Fractalkine, MCP1, IP10 (Sigma Chemical Co., Zwijndrecht, The Netherlands), and CX3CR1 polyclonal antibodies (Santa Cruz Biotechnology, Santa Cruz, USA) and R594 or Fitch labeled second antibodies (Molecular Probes, Leiden, The Netherlands) were used for fluorescent detection by a Zeiss LSM510LNO inverted laser scanning confocal microscope (Carl Zeiss, Thornwood, USA). Haematoxylin/eosin staining was assessed by light microscopy.

Analysis and statistics
Data analysis was performed using a microscopy image analysis system (Impak C, Clemex vision Image analysis system; Clemex Technologies, Quebec, Canada). To assess intima formation in the different shear stress fields, the intima/media ratio was analysed on haematoxylin/eosin stained sections. The media area was defined as the layer between the internal and external elastic lamina. The intimal area was defined as the area between the endothelial lining and the internal elastic lamina. In order to quantify the expression of different chemokines in the vessel, the area of the entire arterial wall positive for the specific staining was expressed as a percentage of the total area enclosed by the external elastic lamina and the lumen. To assess the percentage of the different plaque components, the area within the intima positive for each staining was expressed as a percentage of the total intimal area. All cross sections stained were averaged per region of shear stress, i.e. low, oscillatory and high shear stress.
Gene expression was calculated after normalization on the house-keeping gene HPRT. Statistical analysis was performed using two-way ANOVA analysis of variance taking time and location as independent variables. Data are presented as mean ± SEM. P values <0.05 were considered significant.

7.4 Results

Extent of atherosclerosis
Cast placement around the common carotid artery induces low shear stress upstream, and oscillatory shear stress downstream from the cast. To study the effects of these shear stress fields on atherogenesis, a time series was performed (time points 1, 3, and 9 weeks, N = 5 mice per time point). No significant difference in intima/media ratio was observed between the different shear stress areas after 1 week of cast placement due to minimal atherogenesis (Fig. 1a,b). From 3 weeks on, intima/media ratio in the low shear stress region significantly increased (Fig. 1b), but the difference between oscillatory shear stress regions and control regions remained insignificant. Evaluation of the intima/media ratio at 9 weeks showed that lesions in the low shear stress area were larger in size compared to those in oscillatory shear stress and control regions. The intima/media ratio in the oscillatory shear stress region became significantly larger than in the control at the same time point. Furthermore, lesions that developed under low shear stress conditions showed a vulnerable plaque phenotype, containing large necrotic cores underneath a thin fibrous cap, whereas the lesions in the oscillatory shear stress had a more stable morphology (Fig. 1a).

Gene expression of specific chemokines in shear stress induced atherosclerosis
To investigate the effect of low shear stress and oscillatory shear stress on chemokine expression under pro-atherogenic conditions, we screened the linear amplified pools of antisense RNA from vessel segments exposed to the different shear stress conditions after 1, 3, and 9 weeks of cast placement in ApoE -/- mice. As indicated by the results described above, no plaques were observed in both shear stress regions after 1 week of cast placement. The results obtained from this time point will therefore show the effect of shear stress alteration on the vessel wall without an existing ahterosclerotic lesion. Furthermore, at time point 3 weeks, the effect of shear stress on the carotic artery with an early atherosclerotic lesion is studied. Finally, at 9 weeks after cast placment, the specific chemokine expression of advanced lesions is analysed. From the 10 chemokines assessed in this study, 4 of them (MCP1, IL8/KC, IP10, and fractalkine) were upregulated in response to alterations in shear stress at different time points. No shear stress responsive upregulation in the expression of the other chemokines (RANTES, eotaxin, ELC, NAP-2, SDF-α and CCL14) was observed (See online supplemented data, Table 1). After 1 week, quantitative RT-PCR showed an increase in expression of the chemokines: MCP1, and IL8/KC in the altered shear stress regions compared to control, and IP10 was more expressed in the low shear stress than in the oscillatory shear stress region (Fig. 2a). After 3 weeks of cast placement, the increased gene expression levels in MCP1 were maintained in both low shear stress and oscillatory shear stress regions, while. IL8/KC and IP10 were only upregulated in the low shear stress region (Fig. 2b). After 9 weeks of cast placement the expression of MCP1 and

IP10 returned to baseline levels (Fig. 2c). Remarkably, upregulation of fractalkine was detected in the low shear stress regions at this specific time point only.
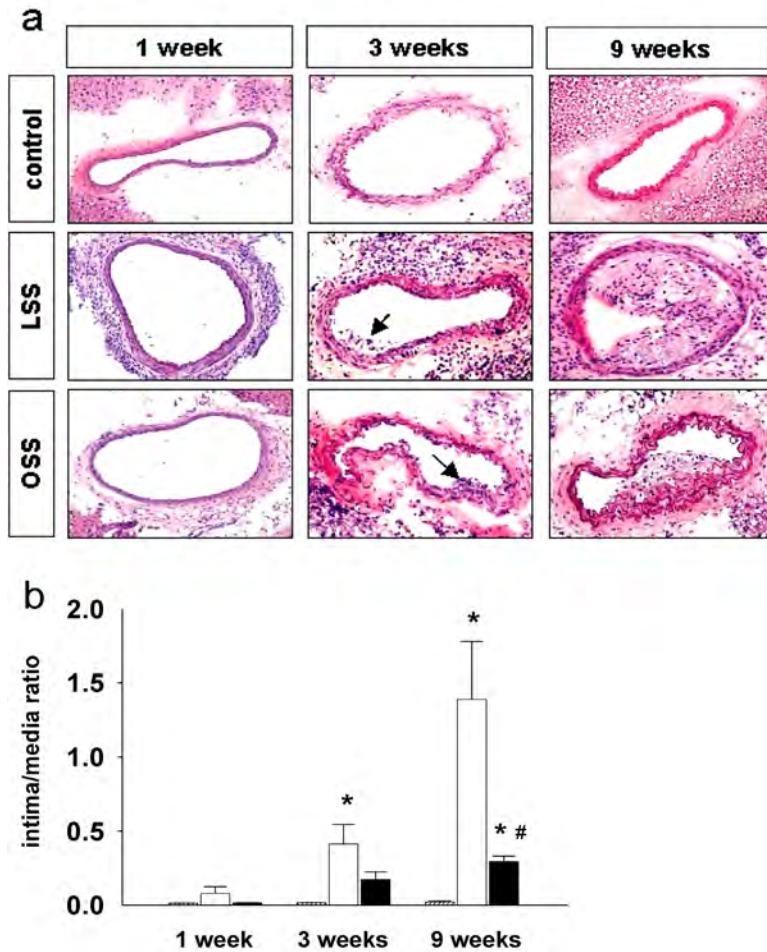

Figure 1: Representative hematoxylin and eosin-stained cross-sections of murine carotid arteries at different time points after cast placement in mice on western diet (20X magnification). Shown is the response of the vessel wall to oscillatory shear stress (OSS, lower panel), low shear stress (LSS, middle panel) versus control (undisturbed shear stress, upper panel) after one (right row), three (middle row), and nine weeks (left row) of cast placement. The arrows in the panel indicate to accumulation of macrophages in fatty streaks (a). Comparison of the intima/media ratio in the low shear stress region (white bar) with the oscillatory shear stress region (black bar) versus control (gray bar) at the three different time points (b). *P<0.05 versus control. #P<0.05 versus low shear stress.
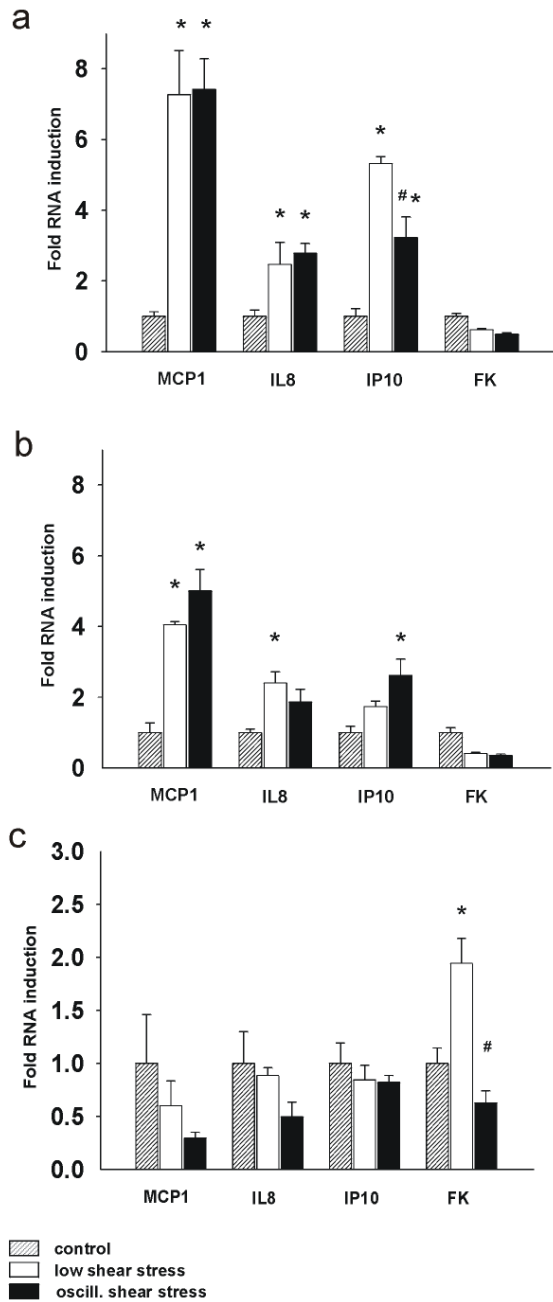
138

Figure 2: Expression levels of upregulated chemokines in carotid arteries at different time points after cast placement in mice on western diet measured by qPCR using pooled amplified RNA samples (10 animals per pool, N=3). Shown are the expression levels of MCP1, IL8/KC, IP10, and fractalkine after one week (a), three weeks (b), and nine weeks (c) of cast placement. *P<0.05 versus control. #P<0.05 versus low shear stress.

Validation of the gene expression profile of chemokines

To verify the results obtained from the linear amplified samples, we repeated the RT-PCR experiments for those chemokines that were significantly upregulated with pooled samples of non-linear amplified cDNA. In accordance with the linear amplified data we measured an increased expression of fractalkine in the low shear stress region compared to oscillatory shear stress after 9 weeks of cast placement, whereas at earlier time points, no fractalkine response was observed (Fig. 3a). In contrast to fractalkine, but in accordance with the amplified data, MCP1 expression levels were upregulated in both low and oscillatory shear stress regions at most of the studied time points (Fig. 3b). As expected, IL8/KC expression was increased in week 1 in both the low and the oscillatory shear stress regions (Fig. 3c), while it was differentially upregulated in low shear stress regions after 3 weeks of cast placement. Finally, the low shear stress region showed increased expression of IP10 after 1 week of cast placement compared to oscillatory shear stress (Fig. 3d), and IP-10 was differentially expressed at 3 weeks of cast placement in the low shear stress region. In order to exclude possible non-shear stress related effects of the cast on chemokine expression, we performed control experiments with sham-casts. These were made of the same material as the real cast, but did not induce the alterations in shear stress due to a non-constrictive luminal geometry. Placement of the sham-casts failed to cause lesion formation in both the upstream or downstream location from the device even after 9 weeks of instrumentation. Gene expression analysis on cDNA obtained from both locations did not reveal upregulation of MCP1 or fractalkine (Fig. 3e).

Total cholesterol levels were increased in animals on the atherogenic Western diet (1 week = 27.3± 2.0nM, 3 weeks = 22.4± 0.9nM, 9 weeks = 24.3± 2.4nM) compared to animals on chow (10.9± 3.0nM). However, total cholesterol concentrations between animals treated with the cast or the non-constricting sham-cast were not different (9 weeks cast = 24.3± 2.4nM versus 9 weeks sham-cast = 25.5± 3.0nM). This indicates that the response in chemokine expression observed with the cast is the result of low or oscillatory shear stress only.

Protein levels follow gene expression levels of selected chemokines.

Next, we evaluated the protein levels of a selected group of responsive chemokines. We studied fractalkine, because it was the only chemokine that was specifically expressed in the atherosclerotic lesions with a vulnerable plaque phenotype. More fractalkine was detected in the low shear stress region compared to the oscillatory shear stress and control regions (Fig. 4a,b, upper panel) at 9 weeks, which is the only time-point at which the gene was expressed. We also evaluated MCP1, as the relevance of this chemokine for the pathology of atherosclerosis is well-known. Immunohistological analysis of vessel segments at 1 week, which is the time-point with the highest MCP1 expression, confirmed the upregulation of MCP1 under both shear stress conditions (Fig. 4a,b, middle panel). In addition, we selected one of the chemokines that were early upregulated during low shear stress induced atherosclerosis development. Differential gene expression of IP10 between the low

140

shear stress and the oscillatory shear stress areas at 1 week, the only time-point at which this chemokine was significantly differentially expressed, was observed (Fig. 4a,b, lower panels).
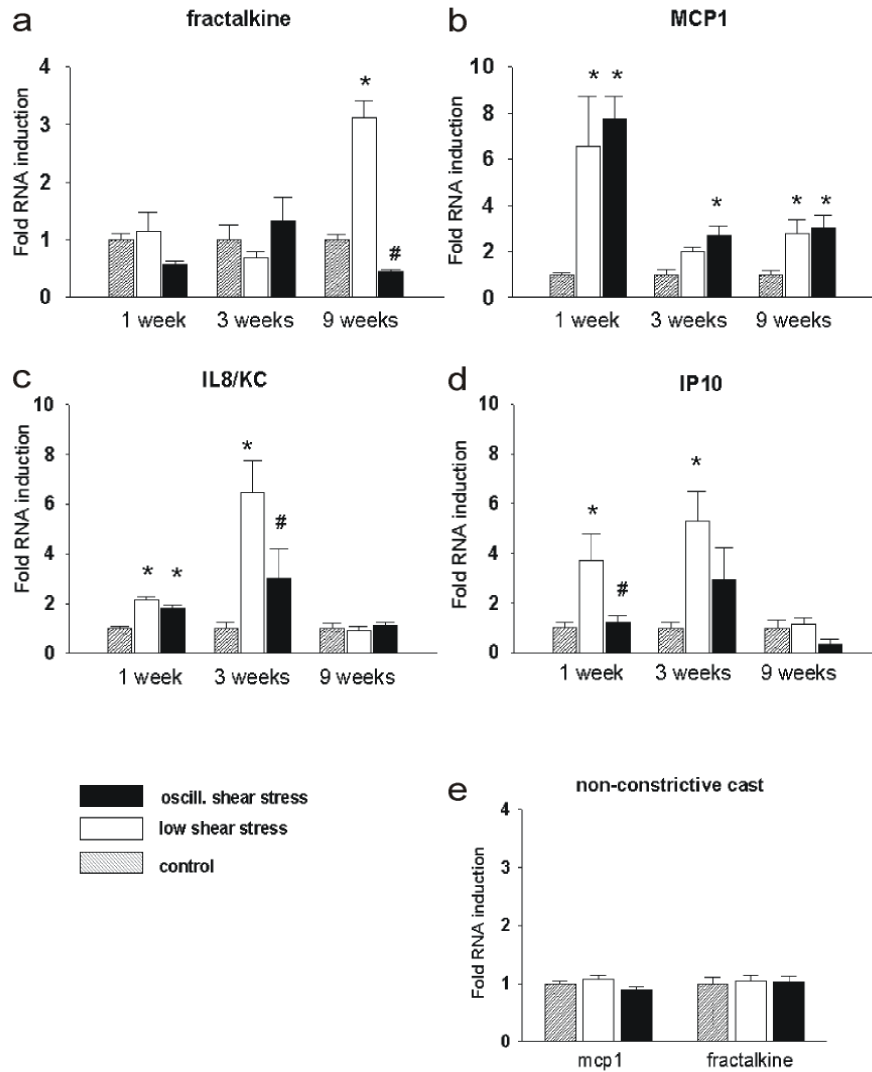
Figure 3: Validation of the expression levels of the upregulated chemokines by qPCR using pooled non-amplified CDNA samples (5 animals per pool, N=3). Shown are the expression levels of fractalkine (a), IL8/KC (b), MCP1 (C), and IP10 (d) at the three different time points assessed. Placement of a non-constrictive, control cast that does not alter the laminar shear stress, did not induce changes in gene expression. No difference (between control and the regions situated upstream and down stream from the control device) in expression of MCP1 or fractalkine was observed in the carotid arteries of ApoE -/- deficient mice, even after 9 weeks of cast placement and western diet (e). *P<0.05 versus control. #P<0.05 versus low shear stress.
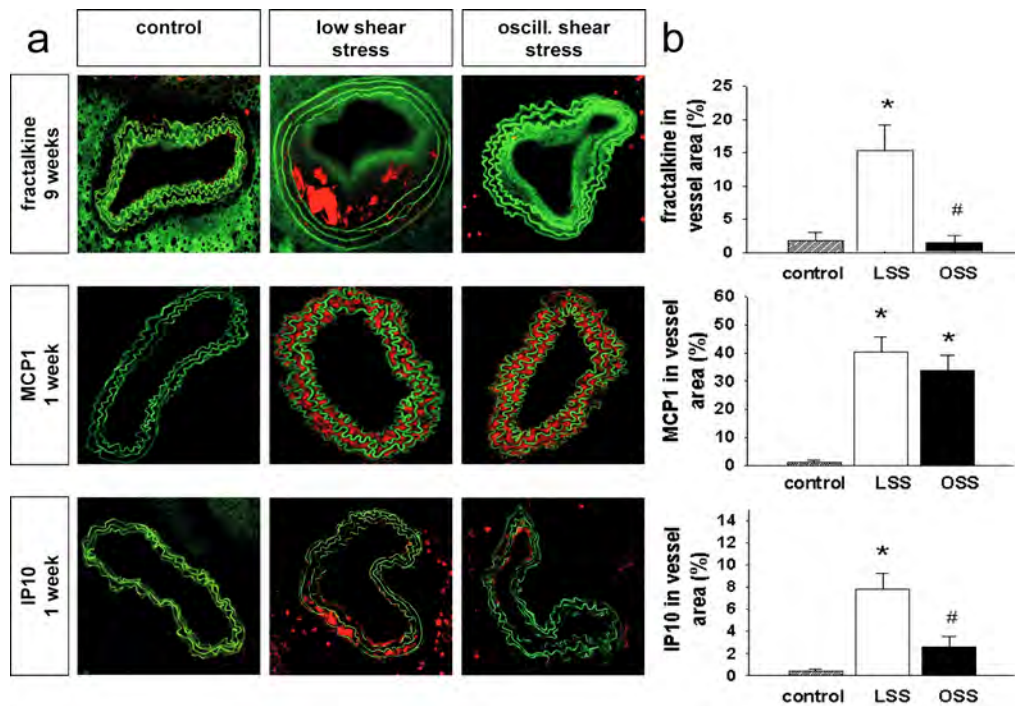
Figure 4: Validation of result of a selected group of chemokines by immuno-histological analysis of the protein levels in carotid arteries at different time points after cast placement in mice on western diet. Shown are representative cross-sections of murine carotid arteries stained for fractalkine after 9 weeks of cast placement (upper panel), and MCP1 (middle panel) and IP10 (lower panel after 1 week of cast placement, in the control, low and oscillatory shear stress regions (20X magnification) Chemokine expression is specified by a red signal. Green auto-fluorescence designates the intimal and medial areas (a). The results of the immuno-histological quantification of the chemokine signals. The percentages of fractalkine at time point 9 weeks (upper graph), MCP1 at time point 1 week (middle graph), and IP10 at time point 1 week (lower graph) in the vessel area of the low shear stress (LSS) and the oscillatory shear stress (OSS) regions are shown (b). N=5. *P<0.05 versus control. #P<0.05 versus low shear stress. Colour version of this figure is available in the full colour section.

The role of chemokines in advanced atherosclerotic lesions with stable and instable phenotypes: fractalkine expression and cell recruitment.
From our findings, we concluded that fractalkine is exclusively upregulated in the atherosclerotic lesions induced by low shear stress. These lesions were identified as lesions with a vulnerable phenotype at the 9 weeks time point. Fractalkine is therefore an interesting candidate to be evaluated as a potential target for treatment of vulnerable

plaques. We selected this chemokine for further studies, and assessed the effect of low and oscillatory shear stress on the accumulation of CX3CR1 (i.e. fractalkine receptor) positive cells accumulation in advanced lesions to determine its contribution on the pathology of vulnerable lesions. More CX3CR1 expressing cells were detected in the intima of lesions situated in the low shear stress region as compared to the oscillatory shear stress regions (Fig. 5a,b). Further analysis identified CX3CR1/CD11b double positive cells with rounded monocyte-like morphology in the lesions (Fig. 6, upper panel). In addition, small numbers of CX3CR1/CD68 double positive macrophages were found with the characteristics of foam cells (Fig. 6, middle panel). Double staining for CX3CR1 and VSMC α-actin, did not clearly show any smooth muscle cells expressing the fractalkine receptor (Fig. 6. lower panel). Thus cells expressing CX3CR1 in the vulnerable atherosclerotic lesions consist mainly of CD11b-positive monocytes and some CD68-positive macrophages/foam cells.
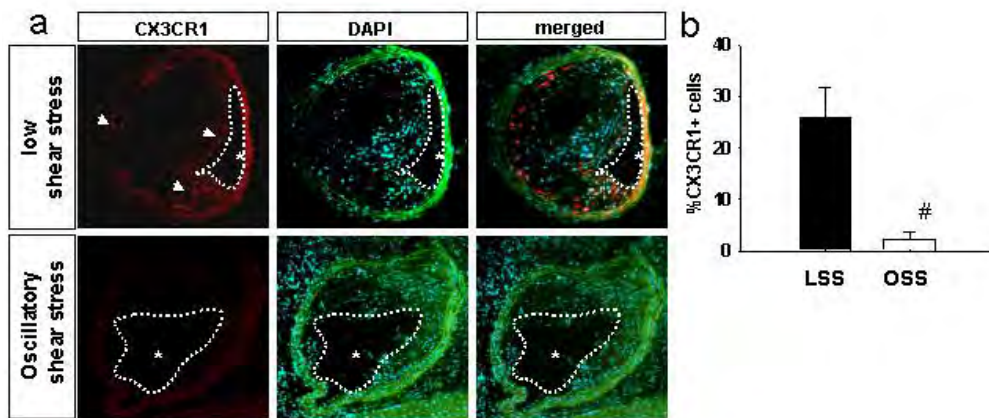

Figure 5: The effect of fractalkine expression on cell recruitment in the mature lesions. Shown are representative cross-sections of murine carotid arteries double stained for CX3CR1 (red signal) and nuclei (blue signal). In the upper panel, CX3CR1 positive cells in the low shear stress lesions (indicated by arrows) are shown. The lumen is indicated by an (*), and the intima contours are traced by a white line. In the upper panel, CX3CR1 positive cells in the oscillatory shear stress lesions are shown. The lumen is indicated by an (*), and the intima contours are traced by a white line (a). The results of the immuno-histological quantification of the chemokine signal. The percentages of CX3CR1 positive area at time point 9 weeks in the intima in the low (LSS) and the oscillatory shear stress (OSS) region (b). N=5. #P<0.05 versus low shear stress. Colour version of this figure is available in the colour section.

144

Figure 6: CX3CR1 expressing cells located in the advanced lesions are mainly monocytes and macrophages. Shown are representative cross-sections of murine carotid arteries double stained for CX3CR1 (middle column) and CD11b, CD68, and VSMC α-actin (left column, from upper to lower panels), respectively. In the third column, the (yellow) co-localization signal is shown. The lumen is indicated by a (*) and the intima contours are traced by a white line. Colour version of this figure is available in the full colour version.

The role of fractalkine in shear stress induced atherosclerosis: blocking study
Next, we studied the possible effect of fractalkine blockage on plaque composition and vulnerability. Macroscopic and microscopic analysis of hematoxin-eosin-stained sections of liver, lung, spleen and draining lymphnodes of the carotid artery did not reveal any abnormalities in animals treated with the rabbit polyclonal IgG neutralizing antibody against fractalkine in the fractalkine group or the rabbit polyclonal IgG control antibody in the control group. Furthermore, FACS analysis on spleen-derived and peripheral blood leukocytes showed no differences in the numbers of CD3+ cells or in the CD4+/CD8+ cell ratios between the two groups (data not shown). Animals in the fractalkine group showed a 50% reduction of plaque area in low shear stress regions (Fig. 7a), i.e. in the regions with a differential upregulation of fractalkine. Analysis of plaque composition showed roughly a doubling in collagen content in both the low and oscillatory shear stress regions in response to fractalkine blockage (Fig. 7b), which was only partly related to increments in vascular smooth muscle cells content, as VSMC content did not increase in the oscillatory regions of the fractalkine group (Fig. 7c). Further analysis revealed that the fractalkine-neutralizing antibody approximately halved CD68 positive macrophage content and lipid accumulation in the vulnerable plaques compared with the control group (fig. 7d). However, in the oscillatory shear stress regions, no differences between the fractalkine and the control group were observed (fig. 7e). Both shear stress regions showed no effect on the CX3CR1 positive area in response to fractalkine antibody treatment, although a trend toward increase was observed in the instable lesions of the low shear stress region (Fig. 7f).

146

low shear stress
+ control antibody

low shear stress
+ αfractakine antibody

A

*P<0.05

I/M ratio

low ss   oscill. ss

B

*P<0.001

%CD68+cells

low ss   oscill. ss

C

*P<0.05

*P=0.17

%lipids

low ss   oscill. ss

D

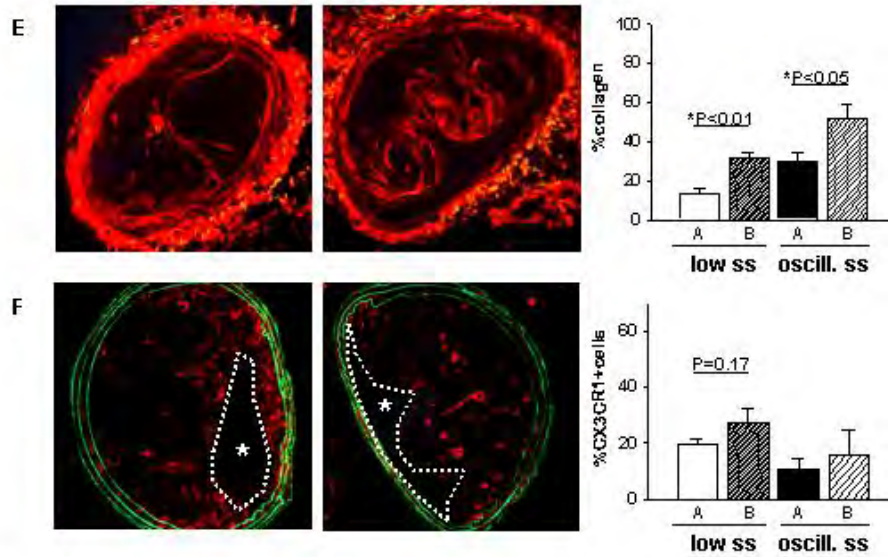*P<0.001

%VSMCs

low ss   oscill. ss

Figure 7: Fractalkine function was inhibited during cast-induced atherogenesis in ApoE KO mice by administration of a neutralizing antibody from week 6 till week 9. In the left column, Representative cross-sections are shown. These are stained for: (2a) lesion morphology by H/E, (2b) macrophages, (2c) lipids, (2d) VSMCs, (2e) collagen, and (2f) fractalkine receptor (CX3CR1). The lumen is indicated by a (*) and the intima contours are traced by a white line. In the right column, the lesion area is shown in the first graph, followed by results of the (immuno-) histological quantification of the different plaque components. The percentages of positive area at time point 9 weeks in the intima in the low (LSS) and the oscillatory shear stress (OSS) region are indicated, comparing the control antibody group (A) with the a-fractalkine antibody group (B). N=8. *P<0.05 versus control antibody group. Colour version of this figure is available in the full colour section.

7.5 Discussion

The high mortality accompanying atherosclerosis has been associated with rupture of vulnerable plaques. The morphology of vulnerable plaques consists of characteristic triage: large lipid core, think fibrous can and a large inflammatory component. The inflammatory component has been shown to be prominent in plaques with a vulnerable phenotype. Uptake and migration of inflammatory cells have been examined extensively and a cascade model has been emerged from these studies. This model describes rolling, arrest and migration as a sequential process[17]. Arrest of inflammatory cells on the endothelial layer is due to a force balance, where a balance exist between shear stress induced disruptive torque and the formation of adhesive bonds[2,3]. Shear stress has been shown to affect essential steps in this cascade model. Low shear stress enhances the expression of some of the selectins and integrins[18,19], thereby increasing their density on the endothelial layer. It also lowers the torque, favouring binding of blood cells to the endothelium. Furthermore, recent studies indicate that clustering and the activity of integrins affects the strength of these bonds, and that chemokines actively regulate these processes. Their role in shear stress induced plaque formation is presently unknown. In order to study their role in the formation of vulnerable plaque, we performed a literature based screening of 10 chemokines by applying qPCR. Interestingly, 4 of the selected genes: MCP1, IL8/KC, IP10 and fractalkine were upregulated, and these were further studied.

MCP1 has been shown to be present in human atherosclerotic lesions and in plaques induced in animal models. It is involved in monocyte/macrophage recruitment and knock out studies indicate an important role in atherogenesis. MCP1, in the present conditions, does not differ in expression levels between low and oscillatory shear stress stimulus. These findings are in accordance with cell culture studies showing a role for both low and oscillatory shear stress in MCP1 production by endothelial cells. This lack in differential expression and the decline in MCP1 expression after the first week of shear stress stimulation, may imply that the MCP1/CCR2 (MCP1 receptor) interaction is predominantly important during early atherogenesis, and may not play an important role in vulnerable plaque formation. Other mechanisms must be involved to affect the types of plaque that develop under these shear stress conditions.

Two genes (IP10 and IL8/KC) were indicated as differentially upregulated in the early phase of vulnerable plaque formation. IP10 is a chemoattractant for monocytes[20] and T-lymphocytes[21] and is induced by production of interferon-γ (IFN-γ). Only a small number of studies have yet identified this chemokine to play a role in vascular disease. However, as IFN-γ has been associated with vulnerable plaque formation, this chemokine may be of importance for this disease. Indeed, increased serum levels of IP10 have been associated to coronary artery disease in patients [22].

IL8/KC and its receptor CXCR2 are involved in the accumulation of neutrophils and macrophages during atherogenesis, and high expression of CXCR2 by macrophages

is detected in advanced lesions of patients and LDL receptor deficient mice[23]. In agreement with these findings, we found increased expression of CXCR2 in the mature lesions after 9 weeks of cast placement (data not shown). However, increased IL8/KC expression was only detected at the earlier time points. This implies that IL8/KC/CXCR2 interaction is mainly involved during the early events of atherogenesis. In mice, macrophage inflammatory protein 2 (MIP-2) and granulocyte chemotactic protein 2 (GCP-2) can also bind to the CXCR2 receptor[24], and these chemokines could have effected CXCR2 expression in the mature lesions, either by increasing the influx of CXCR2 expressing blood cells (neutrophils and macrophages for GCP-2 and MIP-2 respectively), or by inducing the expression of this chemokine receptor in the cells which are already situated in the intima.

From the upregulated chemokines, fractalkine is the only one that is exclusively expressed in the low shear stress induced vulnerable plaque. Fractalkine is a unique chemokine that not only acts as a chemoattractant, but also as an adhesion molecule expressed on endothelial cells upon stimulation[25]. The fractalkine receptor CX3CR1 is expressed on lymphocytes, macrophages, VSMCs[26] and ECs its expression is regulated by IFN-γ[27,28]. Functional studies with knock out mice indicate that CX3CR1 or fractalkine deficiency results in decreased atherosclerotic lesion growth, associated with a reduction in the accumulation of macrophages and foam cells[29,15,30]. In the present study, we observed more CX3CR1 positive cells in the plaques located in the low shear stress region compared to oscillatory shear stress plaques, suggesting that there is an effect of fractalkine expression on cell recruitment. Subsequent analysis of CX3CR1 positive cells identified predominantly monocytes and macrophages, and few VSMCs co-localizing with the fractalkine receptor. These findings were consistent with our functional studies where we blocked fractalkine/CX3CR1 interaction by administrating a fractalkine-neutralizing antibody. Inhibition of fractalkine function decreased plaque growth, and prevented the development of plaque with a vulnerable phenotype within the low shear stress region. The exact mechanism is presently unknown, but the reduced accumulation of lipids and macrophages, indicate a reduction in the number of foam cells. In addition, the lesions contained increased amounts of extracellular matrix (collagen) and VSMCs, thereby increasing collagen synthesis. Importantly, inhibition of fractalkine/CX3CR1 interaction had only limited effect on the by oscillatory shear stress induced stable lesions. This might indicate a role for shear stress in the fractalkine-mediated effects. However, as the by fractalkine induced effects were only observed after 9 weeks of cast placement, other factors maybe involved. For instance, inward vascular remodeling might have increased shear stress locally, or inflammatory mediators released from within the vessel wall during low shear stress induced atherogenesis (e.g. IFN-γ) might be responsible in upregulation of this chemokine. In spite of this, expression of fractalkine remains a distinctive (indirect) effect of low shear stress, and the findings presented in this (blocking) study are

important, for they clearly show the critical role of fractakine in the development of vulnerable plaque.

In conclusion, different shear stress fields have yielded different responses in chemokine expression. Low shear stress induces the development of lesions with a vulnerable plaque phenotype, characterized by increased expression of multiple chemokines (KC/IL8, and IP10) that may result in a more efficient recruitment of monocytes compared to the oscillatory shear stress induced lesions. This subsequently leads to the development of remarkably larger atherosclerotic lesions, with a more severe inflammatory response, resulting in the vulnerable plaque phenotype[1] with the observed characteristic fractalkine expression. Fractalkine determines plaque vulnerability, as blockage of fractalkine/CX3CR1 interaction in advanced lesions prevents the development of the vulnerable plaque phenotype. Stabilization of vulnerable plaques in patients by inhibiting fractalkine-fractalkine receptor interaction might provide an effective therapy, thereby preventing future acute coronary events as a result of sudden plaque rupture.

7.6 Supplemented data

Table S1: Expression levels of chemokines in carotid arteries at different time points after cast placement in mice on western diet.

chemokine	control			low shear stress			oscillatory shear stress		
	1 week	3 weeks	9 weeks	1 week	3 weeks	9 weeks	1 week	3 weeks	9 weeks
RANTES	1.00 ±0.10	1.00 ±0.18	1.00 ±0.69	0.68 ±0.12	0.15 ±0.06*	0.37 ±0.14	0.72 ±0.14	0.29 ±0.28*	0.32 ±0.06
eotaxin	1.00 ±0.15	1.00 ±0.05	1.00 ±0.30	0.39 ±0.09*	0.15 ±0.07*	0.31 ±0.03	0.23 ±0.01*#	0.44 ±0.16*	0.48 ±0.28
ELC	1.00 ±0.07	1.00 ±0.33	1.00 ±0.13	0.60 ±0.07*	0.47 ±0.03	0.41 ±0.16*	0.42 ±0.13*	0.33 ±0.01*#	0.12 ±0.03*
NAP-2	1.00 ±0.14	1.00 ±0.34	1.00 ±0.12	1.00 ±0.04	1.08 ±0.12	0.85 ±0.07	1.14 ±0.17	1.41 ±0.00	0.39 ±0.12 *#
SDF-α	1.00 ±0.09	1.00 ±0.15	1.00 ±0.24	0.91 ±0.11*	1.34 ±0.07	0.32 ±0.20	0.41 ±0.32#	1.82 ±0.34	0.34 ±0.25
CCL14	1.00 ±0.17	1.00 ±0.50	1.00 ±0.56	0.36 ±0.09*	0.34 ±0.22	0.48 ±0.24	0.49 ±0.05*	0.50 ±0.28	0.54 ±0.30

Shown are the expression levels of RANTES, eotaxin, ELC, NAP-2, SDF-α, and CCL14 after one, three, and nine weeks of cast placement. Data obtained by qPCR using pooled amplified RNA samples. (10 animals per pool, N=3). *$P<0.05$ versus control. #$P<0.05$ versus low shear stress.

7.7 References

1. Caroline Cheng DT, Rien van Haperen, Arjen van der Baan, Frank Grosveld, Mat J.A.P. Daemen, Rob Krams, and Rini de Crom. Atherosclerotic lesion size and vulnerability are determined by patterns of fluid shear stress. submitted.
2. Sugihara-Seki M. Flow around cells adhered to a microvessel wall. I. Fluid stresses and forces acting on the cells. *Biorheology*. 2000;37:341-59.
3. Gaver DP, 3rd, Kute SM. A theoretical model study of the influence of fluid stresses on a cell adhering to a microchannel wall. *Biophys J*. 1998;75:721-33.
4. Mohan S, Mohan N, Valente AJ, Sprague EA. Regulation of low shear flow-induced HAEC VCAM-1 expression and monocyte adhesion. *Am J Physiol*. 1999;276:C1100-7.
5. Chappell DC, Varner SE, Nerem RM, Medford RM, Alexander RW. Oscillatory shear stress stimulates adhesion molecule expression in cultured human endothelium. *Circ Res*. 1998;82:532-9.
6. Kucik DF. Rearrangement of integrins in avidity regulation by leukocytes. *Immunol Res*. 2002;26:199-206.
7. Weber C. Novel mechanistic concepts for the control of leukocyte transmigration: specialization of integrins, chemokines, and junctional molecules. *J Mol Med*. 2003;81:4-19.
8. Laudanna C, Kim JY, Constantin G, Butcher E. Rapid leukocyte integrin activation by chemokines. *Immunol Rev*. 2002;186:37-46.
9. Charo IF, Taubman MB. Chemokines in the pathogenesis of vascular disease. *Circ Res*. 2004;95:858-66.
10. Dirksen MT, van der Wal AC, van den Berg FM, van der Loos CM, Becker AE. Distribution of inflammatory cells in atherosclerotic plaques relates to the direction of flow. *Circulation*. 1998;98:2000-3.
11. Shyy YJ, Hsieh HJ, Usami S, Chien S. Fluid shear stress induces a biphasic response of human monocyte chemotactic protein 1 gene expression in vascular endothelium. *Proc Natl Acad Sci U S A*. 1994;91:4678-82.
12. Bao X, Lu C, Frangos JA. Temporal gradient in shear but not steady shear stress induces PDGF-A and MCP-1 expression in endothelial cells: role of NO, NF kappa B, and egr-1. *Arterioscler Thromb Vasc Biol*. 1999;19:996-1003.
13. Kato H, Uchimura I, Nawa C, Kawakami A, Numano F. Fluid shear stress suppresses interleukin 8 production by vascular endothelial cells. *Biorheology*. 2001;38:347-53.
14. Weber C, Schober A, Zernecke A. Chemokines: key regulators of mononuclear cell recruitment in atherosclerotic vascular disease. *Arterioscler Thromb Vasc Biol*. 2004;24:1997-2008.

15. Lesnik P, Haskell CA, Charo IF. Decreased atherosclerosis in CX3CR1-/- mice reveals a role for fractalkine in atherogenesis. *J Clin Invest*. 2003;111:333-40.

16. Moll PR, Duschl J, Richter K. Optimized RNA amplification using T7-RNA-polymerase based in vitro transcription. *Anal Biochem*. 2004;334:164-74.

17. Konstantopoulos K, Kukreti S, McIntire LV. Biomechanics of cell interactions in shear fields. *Adv Drug Deliv Rev*. 1998;33:141-64.

18. Urbich C, Walter DH, Zeiher AM, Dimmeler S. Laminar shear stress upregulates integrin expression: role in endothelial cell adhesion and apoptosis. *Circ Res*. 2000;87:683-9.

19. Urbich C, Dernbach E, Reissner A, Vasa M, Zeiher AM, Dimmeler S. Shear stress-induced endothelial cell migration involves integrin signaling via the fibronectin receptor subunits alpha(5) and beta(1). *Arterioscler Thromb Vasc Biol*. 2002;22:69-75.

20. Taub DD, Longo DL, Murphy WJ. Human interferon-inducible protein-10 induces mononuclear cell infiltration in mice and promotes the migration of human T lymphocytes into the peripheral tissues and human peripheral blood lymphocytes-SCID mice. *Blood*. 1996;87:1423-31.

21. Loetscher M, Gerber B, Loetscher P, Jones SA, Piali L, Clark-Lewis I, Baggiolini M, Moser B. Chemokine receptor specific for IP10 and mig: structure, function, and expression in activated T-lymphocytes. *J Exp Med*. 1996;184:963-9.

22. Kawamura A, Miura S, Fujino M, Nishikawa H, Matsuo Y, Tanigawa H, Tomita S, Tsuchiya Y, Matsuo K, Saku K. CXCR3 chemokine receptor-plasma IP10 interaction in patients with coronary artery disease. *Circ J*. 2003;67:851-4.

23. Boisvert WA, Santiago R, Curtiss LK, Terkeltaub RA. A leukocyte homologue of the IL-8 receptor CXCR-2 mediates the accumulation of macrophages in atherosclerotic lesions of LDL receptor-deficient mice. *J Clin Invest*. 1998;101:353-63.

24. Van Damme J, Wuyts A, Froyen G, Van Coillie E, Struyf S, Billiau A, Proost P, Wang JM, Opdenakker G. Granulocyte chemotactic protein-2 and related CXC chemokines: from gene regulation to receptor usage. *J Leukoc Biol*. 1997;62:563-9.

25. Mizoue LS, Bazan JF, Johnson EC, Handel TM. Solution structure and dynamics of the CX3C chemokine domain of fractalkine and its interaction with an N-terminal fragment of CX3CR1. *Biochemistry*. 1999;38:1402-14.

26. Lucas AD, Bursill C, Guzik TJ, Sadowski J, Channon KM, Greaves DR. Smooth muscle cells in human atherosclerotic plaques express the fractalkine receptor CX3CR1 and undergo chemotaxis to the CX3C chemokine fractalkine (CX3CL1). *Circulation*. 2003;108:2498-504.

27.   Ludwig A, Berkhout T, Moores K, Groot P, Chapman G. Fractalkine is expressed by smooth muscle cells in response to IFN-gamma and TNF-alpha and is modulated by metalloproteinase activity. *J Immunol*. 2002;168:604-12.

28.   Hatakeyama M, Imaizumi T, Tamo W, Yamashita K, Yoshida H, Fukuda I, Satoh K. Heparin inhibits IFN-gamma-induced fractalkine/CX3CL1 expression in human endothelial cells. *Inflammation*. 2004;28:7-13.

29.   Combadiere C, Potteaux S, Gao JL, Esposito B, Casanova S, Lee EJ, Debre P, Tedgui A, Murphy PM, Mallat Z. Decreased atherosclerotic lesion formation in CX3CR1/apolipoprotein E double knockout mice. *Circulation*. 2003;107:1009-16.

30.   Teupser D, Pavlides S, Tan M, Gutierrez-Ramos JC, Kolbeck R, Breslow JL. Major reduction of atherosclerosis in fractalkine (CX3CL1)-deficient mice is at the brachiocephalic artery, not the aortic root. *Proc Natl Acad Sci U S A*. 2004;101:17795-800.

Chapter 8: Summary, General Discussion, and Future Perspectives

8.1 Summary

Studies in the hemodynamic field point to a strong relation between shear stress and the onset to vascular diseases such as atherosclerosis. Data from *in vitro* studies using sheared endothelial cells have provided insight into the possible mechanisms involved. However, the lack of an appropriate *in vivo* model to introduce pro-atherogenic shear stress parameters has hampered investigation of the effects of this hemodynamic force on the vessel wall. In this thesis, we developed and validated a new shear stess model to be applied *in vivo*. We studied the effects of low, high and oscillatory shear stress on the pathology of atherosclerosis.

The Cast model
In **chapter 1**, a new method to study shear stress *in vivo* is introduced. We have developed a device (the cast), which is a cylinder with a cone shaped lumen made of the thermoplastic polyetherketon. Placement of the cast around the straight vessel segment of the common carotid artery of a mouse alters the normal laminar flow, creating controlled deviations in shear stress. Upstream from the cast, a region of low shear stress is created. In the vessel segment situated inside the cast, the tapered geometry creates a region with gradually increasing shear stress. Downstream from the cast, the stenosis created by the device induces oscillatory shear stress. With this unique model, we are able to look at the full response of the vessel wall to shear stress, complete with its (indirect) effects on the intima and the immune response. In addition, three significant shear stress fields (low shear stress, high shear stress and oscillatory shear stress) are examined in this causal system.

The effect of shear stress on eNOS expression
In the first study, we implanted the cast around the carotid artery of wild type (C57BL/6) and transgenic mice. The physiological effects of our method were successfully validated by Doppler echography. In order to evaluate if the method also triggers a biological response, we decided to study eNOS, which is a shear stress responsive gene that is known to be involved in cardiovascular disease [1,2]. We showed *in vivo* that the response in expression of eNOS to shear stress is dose-dependent using an in-house developed transgenic mouse **(chapter 3)**. In this mouse model, human eNOS expression and distribution can be easily monitored by virtue of a fusion of eNOS with green fluorescent protein (GFP). The fusion protein is driven by the human eNOS promoter, which is known from *in vitro* studies to be shear stress responsive **(chapter 2)**. Regulation of eNOS protein levels and activity is very complex and occurs both at transcriptional and post-transcriptional levels. Post-translational modification of eNOS by myristoylation and palmitoylation that targets the protein to the Golgi complex and the lipid rich domains of the cell membrane are both necessary for proper eNOS activation [3]. Shear stress activates eNOS predominantly through Akt dependent phosphorylation of eNOS at serine1177 [4].

Recently, it has been shown that the fraction of eNOS localized in the Golgi complex is responsive to phosphorylation by Akt [3]. This implies that shear stress activates eNOS when it is located in certain compartments of the endothelial cells. The effects of shear stress on the phosphorylation and the intracellular localization of eNOS *in vivo* are not known. We therefore analysed the phosphorylated state and intracellular distribution of eNOS to the Golgi compartment and the cell membrane in vessel regions exposed to the three different shear stress fields. Under high shear stress conditions, more eNOS protein (in absolute values) are located in the Golgi complex and the cell membrane, and the Golgi complex itself has become extended, probably in order to accommodate/process more proteins as the endothelial cells become more activated. Phosphorylation of eNOS has also increased after high shear stress stimulation. These results indicate that high shear stress is atheroprotective as it increases eNOS expression. The extra amount of eNOS protein is located in the correct cellular compartments where it can be phosphorylated and activated to produce NO. Remarkably, eNOS expression and phosphorylation is also increased under oscillatory shear stress conditions, pointing towards some degree of protection against vascular disease. Conversely, the vessel segments exposed to low shear stress show a significant reduction in eNOS expression and therefore are less protected against the onset of atherosclerosis. Measurements of the mRNA levels of the human eNOS trangene, the endogenous mouse eNOS and of a number of shear stress responsive genes (identified in *in vitro* studies [5-7], clearly indicate that the cellular response to the alterations in shear stress induced by the cast, is not limited to the eNOS transgene (**chapter 4**). In addition, we show with the placement of a non-constrictive cast (also made of polyetherketon), that the surgical procedure or the material of the device does not induce the observed biological response of the vascular wall. Taking together the evidence obtained from this study, we conclude that our new cast model is a suitable model to investigate shear stress responses *in vivo*.

In a follow-up study, we used the same experimental setup to study the effects of rapamycin on the shear stress responsiveness of the eNOS gene. Rapamycin is a well-known pharmaceutical compound that is frequently used in the clinic in coated stents. It prevents cell-cycle progression, and has anti-atherogenic and immunosuppressive properties. Recent publications suggest that rapamycin affects the shear stress responsiveness of the vessel wall . We show that oral administration of rapamycin increases the expression of eNOS in the low shear stress regions while in the high shear stress regions the maximal eNOS response is decreased (**chapter 5**). These results imply that rapamycin is mainly athero-protective in the low shear stress regions of the arterial system.

The effect of shear stress on atherosclerosis
Evidence for a relation between athersclerosis and shear stress is mainly deducted from observational studies where certain shear stress fields are correlated to the location of atherosclerotic lesions [8,9]. Additional evidence that also provides insight

into the possible mechanisms, come from experiments in which different cellular components of the plaque are tested on their shear stress response *in vitro* (reviewed in [10]). As the endothelium is directly exposed to the blood flow and should therefore be highly adapted to sense and react to shear stress, the most studied cell type is the endothelial cell. The many factors produced by endothelial cells in response to shear stress may be grouped into functional classes including vasoactive compounds (e.g. endothelin 1 (ET1), eNOS, and angiotensin converting enzyme (ACE)), growth factors (e.g. Platelet derived growth factors (PDGFs)), adhesion molecules and pro-inflammatory factors (e.g.VCAM1, ICAM1, E-selectin, MCP1 and PECAM1), coagulation/fibrinolysis/complement factors (e.g. tissue factor), and extracellular matrix (ECM) modifying factors (e.g. matrix metalloproteinase 2 and 9). Summarizing these findings and translating them into a vascular response, we can assume that low shear stress and oscillatory shear stress prime the endothelium to the development of atherosclerosis. We tested the pro-atherogenic properties of low and oscillatory shear stress directly in ApoE deficient mice on high cholesterol, high fat diet (Western diet). Low shear stress and oscillatory shear stress are indeed atherogenic. Six weeks after cast placement, plaques develop in both the low and oscillatory shear stress regions, whereas the high shear stress area remains protected from atherosclerosis. Further study at later time points reveals a remarkable morphological difference between the lesions developed under low shear stress and oscillatory shear stress. Nine weeks after cast placement atherosclerotic lesions induced under low shear stress conditions are more extensive than plaques developed under oscillatory shear stress. In addition, the plaque composition is very different. The atherosclerotic lesions that developed under a low shear stress stimulus contain less plaque stabilizing components, such as collagen fibers and VSMCs, and more plaque destabilizing components such as lipids than plaques from the oscillatory shear stress region. We also observed more outward remodeling, neo-vascularization and increased metallo proteinase activity in the low shear stress lesions. These findings suggest that these atherosclerotic lesions have a vulnerable plaque phenotype. High risk/vulnerable atherosclerotic lesions are strongly associated to thrombosis and the onset of acute coronary syndromes in patients. Several forms of plaques have currently been identified as vulnerable lesions: eroded plaques, inflamed thin cap atheromas (TCFA), and calcified plaques [11,12]. The plaques induced by the low shear stress stimulus in our cast model highly resemble the TCFA in morphology. The TCFA is described in the literature as a plaque with a thin fibrous cap containing only one or two layers of VSMCs covering a lipid-rich, necrotic core. The cap and shoulders of the plaque are heavily infiltrated with blood cells (mainly monocytes and macrophages). The plaques in the low shear stress region have indeed a thin fibrous cap with one to three layers VSMCs covering large lipid-rich, necrotic cores. In the shoulder areas of the plaque, accumulations of inflammatory cells are often observed. Conversely, lesions in the oscillatory shear stress region show a more homogenous distribution of VSMCs and collagen, resulting in an extensive cap, and contain only small lipid pools with little to no necrosis. More compelling evidence is

the exclusive occurrence of intra plaque-hemorrhages (IPH) in plaques of the low shear stress regions in 14% of all treated animals. Remnants of blood plasma and erythrocytes are found, mainly in the upstream area of the plaque, close to the internal elastic lamina. The frequency and the severity of these IPHs increase to 75% if angiotensin II is administered to the animals. Taking together the results from **chapter 6**, we conclude that low shear stress and oscillatory shear stress are both crucial conditions for the development of atherosclerosis. Low shear stress triggers the growth of more extensive and more instable lesions than oscillatory shear stress, with the characteristics of a vulnerable plaque.

The effect of shear stress on inflammation
Shear stress plays an important role in regulating the inflammatory processes that initiate and enhance the growth of the atherosclerotic lesions. Studies have also indicated that shear stress regulates the expression of chemokines [13-15]. Chemokines are an extensive family of small peptides that are potent activators and chemoattractants for leukocyte subpopulations and some non-haemotopoietic cells. They function by binding to G-protein coupled chemokine receptors that results in the initiation of different signaling cascades. *In vivo* and *in vitro* studies showed that chemokines are produced by a variety of cells and play important roles in the development and progression of many physiological and pathological conditions including atherosclerosis [16,17]. Although expression of adhesion molecules is crucial for the adhesion and migration of leucocytes into the inflamed vessel wall, chemokine expression is important as well because it determines the specificity of the immune response by selecting which type of blood cells are drawn into action. In our cast model, we studied the expression of chemokines in response to shear stress alterations during the early phase of atherosclerosis development, and compared that to their responses in mature atherosclerotic lesions. Ten candidate genes were selected from the literature on basis of identified shear stress responsiveness or association with atherosclerosis. They were studied in ApoE deficient mice after one (no detectable atherosclerosis present, endothelium consists of monolayer of rounded cells with decreased eNOS production in the low shear stress region, pointing towards endothelial dysfunction), three (onset of the formation of fatty streaks in both low and oscillatory shear stress regions), and nine weeks (advanced atherosclerotic lesions in both low and oscillatory shear stress regions) of cast placement. Our data showed the early upregulation of both MCP1 and IL8 in response to shear stress. MCP-1 plays a role in the recruitment of monocytes to sites of injury and infection. Mice genetically deficient for MCP-1 or its receptor, CCR2, are protected from vascular lesions in several atherosclerosis models [18,19]. In our model both low shear stress and oscillatory shear stress were capable in eliciting a strong response of MCP1 in the first week that declined at the later time points, suggesting that MCP1 mainly plays a role in recruiting monocytes in the early phase of plaque initiation. In the previous study, gene expression analysis of pro-inflammatory mediators has suggested that the difference in plaque phenotype results from an augmented

inflammatory response to low shear stress compared to oscillatory shear stress stimuli (chapter 6). In this study, we found that differential expression levels of interferonγ-inducible protein (IP10) and fractalkine characterized the development of vulnerable atherosclerotic lesions. IP10 expression was only induced in the low shear stress regions in the early time points, whereas fractalkine was not expressed till 9 weeks after cast placement, in the vulnerable plaques of the low shear stress region exclusively. Further study indicates that fractalkine receptor (CX3CR1) expressing cells are present in high numbers in the vulnerable lesions. Blockage of fractalkine using a neutralizing antibody reduces the growth of the by low shear stress induced vulnerable plaque and stabilizes these type of lesions. Because of their association to plaque instability, we identify IP10 and fractalkine as interesting candidates for more extensive studies to elicit their function in the pathology of the disease (**chapter 7**).

8.2 General discussion and future perspectives

The use of the new cast model enables us to study the direct effects of low, high and oscillatory shear stress on the vessel wall in mice. Low shear stress diminishes eNOS expression, whereas high and oscillatory shear stress increase basal eNOS expression levels. In ApoE-/- mice fed a high fat, high cholesterol diet, both low shear stress and oscillatory shear stress can trigger an inflammatory response by increasing the expression of the chemokines IL8 and MCP1, initiating the development of atherosclerosis. Low shear stress triggers an augmented inflammatory response compared to oscillatory shear stress, characterized by early upregulation of IP10, late upregulation of fractalkine, and the development of extensive atherosclerotic lesions with a vulnerable plaque phenotype. Oscillatory shear stress stimulates the growth of smaller plaques with a stable phenotype.

The remarkable observation that different shear stress fields trigger different types of plaques may be partially explained by the differential expression of the chemokines IP10 and fractalkine. IP10 is a chemoattractant for monocytes and lymphocytes, and promotes T-cell adhesion to endothelial cells. Only a small number of studies have yet identified this chemokine to be associated to vascular disease. Fractalkine is a unique chemokine that functions not only as a chemoattractant but also as an adhesion molecule and is expressed on endothelial cells activated by pro inflammatory cytokines, such as interferon-γ and tumor necrosis factor-α. The fractalkine receptor, CX3CR1, is expressed on lymphocytes and on macrophages. Soluble fractalkine causes migration of natural killer (NK) cells, cytotoxic T-lymphocytes, and macrophages, whereas the membrane-bound form captures and enhances the subsequent migration of these cells in response to secondary stimulation with other chemokines. High levels of fractalkine mRNA expression have been observed in some, but not all, human arteries with advanced atherosclerotic lesions. Combadiere *et al.* have reported that fractalkine expression is upregulated in atherosclerotic lesions of ApoE deficient mice. In addition ApoE combined with CX3CR1 deficiency results in decreased atherosclerotic lesion formation with reduced macrophage accumulation compared to ApoE-/- mice without the extra deficiency. Furthermore, gene polymorphisms at amino acids 249 and 280 of human CX3CR1 are a known genetic risk factor for coronary artery disease. CX3CR1-V249I/T280M heterozygosity is associated with a reduced risk of acute coronary events. This protective effect might be explained by the decreased ability of monocytes to adhere to vascular endothelium. Another intriguing aspect of this chemokine is that it is related to chemotaxis of certain sub-populations of monocytes with specific functions. It was demonstrated that fractalkine preferentially mediates arrest and migration of CD16 (+) monocytes. These cells produce high levels of proinflammatory cytokines and may represent dendritic cell precursors *in vivo*. The

CX3CR1-fractalkine pathway could therefore be one of the main recruitment strategies of dendritic cells into the intima during a strong inflammatory response. In contrast, MCP-1 was shown to be a potent chemokine for CD16 (–) but not CD16 (+) monocytes. Dendritic cells have been recently identified in vulnerable lesions in patients, where they might contribute to plaque destabilization through activation of T-cells. In a recent screening experiment conducted on our model, we detected higher numbers of CD11 (+) (dendritic cell marker) cells in the instable atherosclerotic lesions located in the low shear stress area (preliminary results not shown). Further investigation to identify which type of cells are drawn into the lesion by the IP10 and the fractalkine pathway, will help to elucidate the difference in pro-atherogenic effects of the low shear stress and oscillatory shear stress.

The observed difference in eNOS response elicited by alterations in shear stress could be a major   factor in the development of more stabilized lesions in the oscillatory shear stress field. Increased availability of NO by upregulation of the eNOS protein protects the vessel wall from inflammation by inhibiting platelet and inflammatory cell adhesion and activation. In addition, high concentrations of NO trigger apoptosis resulting in shutdown of the secretory pathways of pro-inflammatory cells, followed by cell death and non-inflammatory clearance by macrophages. Therefore, the increased NO production in the oscillatory shear stress area may provide an effective mechanism to remove harmful inflammatory blood cells from the intima, resulting in the development of small (less recruitment of monocytes means less growth) and stable (less inflammation, due to clearance of inflammatory cells) lesions observed with our cast model. Indeed, previous findings from our group indicate that increased eNOS expression in transgenic mice protects against atherosclerosis [20]. Conversely, the decrease in eNOS expression in the low shear stress area translates into a loss of this protection system. Additional studies in which NO production is actively inhibited (e.g. by using the non-specific NOS inhibitor L-NAME for the whole period of cast-induced atherosclerosis development) should abolish this protection mechanism, resulting in a destabilization of the lesions developing under oscillatory shear stress condition, providing evidence for this hypothesis. However, ENOS in atherosclerosis is uncoupled and produces peroxynitrite, which is harmful. It might therefore be that high eNOS expression is harmful in atherosclerosis (reviewed in [21]).

Placement of the cast around the carotid artery of ApoE deficient mice results in vulnerable plaque upstream and a stable plaque downstream from the device. This finding has two important aspects: 1) the vessel wall responds differently to different shear stress fields; and 2) it also provides a potential model for studying plaque vulnerability. The mechanisms that affect lesion stability and induce the growth towards a vulnerable lesion are still unclear. The progress is hampered by a lack of an adequate and reproducible animal model for vulnerable plaque. Comparisons of the

atherosclerotic lesions of ApoE deficient mice with human plaques show striking similarities. The mouse atherosclerotic lesions can contain large lipid cores, intra plaque haemorrhages, and thin fibrous caps that are capable of rupture. In addition, buried caps representing healed ruptures, have also been identified in mouse atherosclerotic lesions. However, these types of lesions resembling thin cap fibrous atheromas are rare in the aortic root and the thoracic aorta and have been mainly found in aged animals (older than 42 weeks), resulting in long and elaborate experiments. In literature, only a handful of additional murine models have been described that could be used for vulnerable plaque studies. Most of them are using ApoE deficient mice, crossed with a mouse line with a deficiency in an additional gene (e.g. SRB1) or overexpressing an atherogenic transgene (e.g. p53 [22]). These mouse models also provide reproducible methods to induce vulnerable lesions in a short period of time. However, compared to our cast model only one of these systems, the ApoE deficient/p53 transgenic mice, show frequent intraplaque haemorrhages. A drawback in these models is that they limit the scientist to study the mechanisms of the one gene that is altered, because the effects of a third genetic modification might be influenced by the overexpression or deficiency of the second gene. An efficient and reproducible murine model that does not require a second gene modification, has been described by Johnson *et al* [23]. His group studied the brachiocephalic artery in young ApoE deficient mice, and showed plaque rupture (defined as a visible breach in the cap with intra plaque haemorrhages intruding) in 68% of animals after 8 weeks of feeding a Western diet. Particularly noteworthy of this study is that it clearly shows that a murine model can be used to test the effect of pharmaceutical compounds on plaque rupture, as treatment with Pravastatin reduced incidents of acute plaque rupture to 36% in the brachiocephalic artery.

The cast model provides a highly reproducible method to induce vulnerable lesions within a short period of time (9 weeks). In addition, stable lesions develop downstream from the cast in the same vessel segment that can be used for comparison. Shear stress alteration is the only stimulus needed for these plaques to develop, and no additional expression of a pro-atherogenic transgene, or extra gene deficiency except for ApoE is required. The cast can therefore be implanted in any ApoE deficient line carrying a second deficiency or transgene of interest, thus providing a wide research potential, making this murine model suitable for basic and intervention studies.

In recent years, the rapid development of microarray technology has enabled scientists to study gene expression profiles in complex disease systems in high throughput. In relation to shear stress, most of these high throughput gene expression studies have been performed using HAECs or HUVECs. As indicated earlier in the introduction, although these studies are technically easy to perform, results obtained from cultured endothelial cells may not accurately reflect the molecular events that take place in the vessel wall. A more desirerable approach is the use the endothelium located at the areas exposed to variations in shear stress. However, these populations

of endothelial cells located at these specified predilection sites may have adapted early in development to the remarkable shear stress conditions dominating in these areas, resulting in a decrease of their shear stress response. Differential gene expression patterns identified by comparing these cells to cells located in areas of the arterial system with laminar flow conditions will highlight the genes that account for these cells' adaptation system. However, it will possibly conceal the genes responsible for the pathological events in the onset of vascular disease, as the endothelium would have already counteracted their expression. The cast model provides cause-effect studies from which shear stress alteration results in atherosclerosis. The effect of shear stress alteration on endothelial cells, which have been previously exposed to laminar shear stress, results in a gene expression profile that is directly related to early atherogenic events. A carefully prepared study in which only RNA material isolated from the treated endothelium is used for microarray analysis would provide a useful gene-profile of the endothelial shear stress response in the vessel wall. In addition, since we have also shown in the cast model that the different shear stress regions introduce different types of plaques, we could study the gene expression patterns that characterize the onset to vulnerable atherosclerotic lesions using the same technology.

Finally, the interpretation of the observed effects of shear stress on atherosclerosis in an *in vivo* situation remains, even with the use of our validated cast model, difficult. Although the placement of the cast creates well-controlled shear stress fields, continuous plaque growth will eventually alter the original shear stress conditions. For example, extensive plaques creating more than 50% stenosis might have a similar effect on the blood flow as the cast (depending on the angle at which the flow is separated) and create oscillatory shear stress in the downstream shoulder area. In the upstream shoulder of the plaque, shear stress levels are gradually increased depending on the size of the stenosis downstream. Currently, a protocol is developed in order to study blood flow in the mice during atherogenesis using micro CT (computer tomography). This provides the 3D *in vivo* dimensions needed to reconstruct the vessel in order to calculate the different shear stress fields. A better understanding of how the shear stress is altered during atherogenesis in our cast model will improve our understanding of the acquired data for future atherosclerosis studies.

8.3 References

1.   Ziegler T, Silacci P, Harrison VJ, Hayoz D. Nitric oxide synthase expression in endothelial cells exposed to mechanical forces. *Hypertension*. 1998;32:351-5.

2.   Tuttle JL, Nachreiner RD, Bhuller AS, Condict KW, Connors BA, Herring BP, Dalsing MC, Unthank JL. Shear level influences resistance artery remodeling: wall dimensions, cell density, and eNOS expression. *Am J Physiol Heart Circ Physiol*. 2001;281:H1380-9.

3.   Fulton D, Babbitt R, Zoellner S, Fontana J, Acevedo L, McCabe TJ, Iwakiri Y, Sessa WC. Targeting of endothelial nitric oxide synthase to the cytoplasmic face of the golgi or plasma membrane regulates Akt- versus calcium-dependent mechanisms for nitric oxide release. *J Biol Chem*. 2004.

4.   Dimmeler S, Fleming I, Fisslthaler B, Hermann C, Busse R, Zeiher AM. Activation of nitric oxide synthase in endothelial cells by Akt-dependent phosphorylation. *Nature*. 1999;399:601-5.

5.   Malek AM, Greene AL, Izumo S. Regulation of endothelin 1 gene by fluid shear stress is transcriptionally mediated and independent of protein kinase C and cAMP. *Proc Natl Acad Sci U S A*. 1993;90:5999-6003.

6.   Okahara K, Sun B, Kambayashi J. Upregulation of prostacyclin synthesis-related gene expression by shear stress in vascular endothelial cells. *Arterioscler Thromb Vasc Biol*. 1998;18:1922-6.

7.   Rieder MJ, Carmona R, Krieger JE, Pritchard KA, Jr., Greene AS. Suppression of angiotensin-converting enzyme expression and activity by shear stress. *Circ Res*. 1997;80:312-9.

8.   Stone PH, Coskun AU, Kinlay S, Clark ME, Sonka M, Wahle A, Ilegbusi OJ, Yeghiazarians Y, Popma JJ, Orav J, Kuntz RE, Feldman CL. Effect of endothelial shear stress on the progression of coronary artery disease, vascular remodeling, and in-stent restenosis in humans: in vivo 6-month follow-up study. *Circulation*. 2003;108:438-44.

9.   Buchanan JR, Jr., Kleinstreuer C, Truskey GA, Lei M. Relation between non-uniform hemodynamics and sites of altered permeability and lesion growth at the rabbit aorto-celiac junction. *Atherosclerosis*. 1999;143:27-40.

10.   Cheng C, de Crom R, van Haperen R, Helderman F, Gourabi BM, van Damme LC, Kirschbaum SW, Slager CJ, van der Steen AF, Krams R. The role of shear stress in atherosclerosis: action through gene expression and inflammation? *Cell Biochem Biophys*. 2004;41:279-94.

11.   Dickson BC, Gotlieb AI. Towards understanding acute destabilization of vulnerable atherosclerotic plaques. *Cardiovasc Pathol*. 2003;12:237-48.

12.   Virmani R, Kolodgie FD, Burke AP, Farb A, Schwartz SM. Lessons from sudden coronary death: a comprehensive morphological classification scheme for atherosclerotic lesions. *Arterioscler Thromb Vasc Biol*. 2000;20:1262-75.

13. Bao X, Lu C, Frangos JA. Temporal gradient in shear but not steady shear stress induces PDGF-A and MCP-1 expression in endothelial cells: role of NO, NF kappa B, and egr-1. *Arterioscler Thromb Vasc Biol*. 1999;19:996-1003.

14. Kato H, Uchimura I, Nawa C, Kawakami A, Numano F. Fluid shear stress suppresses interleukin 8 production by vascular endothelial cells. *Biorheology*. 2001;38:347-53.

15. Shyy YJ, Hsieh HJ, Usami S, Chien S. Fluid shear stress induces a biphasic response of human monocyte chemotactic protein 1 gene expression in vascular endothelium. *Proc Natl Acad Sci U S A*. 1994;91:4678-82.

16. Charo IF, Taubman MB. Chemokines in the pathogenesis of vascular disease. *Circ Res*. 2004;95:858-66.

17. Lutgens E, Faber B, Schapira K, Evelo CT, van Haaften R, Heeneman S, Cleutjens KB, Bijnens AP, Beckers L, Porter JG, Mackay CR, Rennert P, Bailly V, Jarpe M, Dolinski B, Koteliansky V, de Fougerolles T, Daemen MJ. Gene profiling in atherosclerosis reveals a key role for small inducible cytokines: validation using a novel monocyte chemoattractant protein monoclonal antibody. *Circulation*. 2005;111:3443-52.

18. Ni W, Egashira K, Kitamoto S, Kataoka C, Koyanagi M, Inoue S, Imaizumi K, Akiyama C, Nishida KI, Takeshita A. New anti-monocyte chemoattractant protein-1 gene therapy attenuates atherosclerosis in apolipoprotein E-knockout mice. *Circulation*. 2001;103:2096-101.

19. Boring L, Gosling J, Cleary M, Charo IF. Decreased lesion formation in CCR2-/- mice reveals a role for chemokines in the initiation of atherosclerosis. *Nature*. 1998;394:894-7.

20. van Haperen R, de Waard M, van Deel E, Mees B, Kutryk M, van Aken T, Hamming J, Grosveld F, Duncker DJ, de Crom R. Reduction of blood pressure, plasma cholesterol, and atherosclerosis by elevated endothelial nitric oxide. *J Biol Chem*. 2002;277:48803-7.

21. Slager CJ, Wentzel JJ, Gijsen FJ, Thury A, van der Wal AC, Schaar JA, Serruys PW. The role of shear stress in the destabilization of vulnerable plaques and related therapeutic implications. *Nat Clin Pract Cardiovasc Med*. 2005;2:456-64.

22. von der Thusen JH, van Vlijmen BJ, Hoeben RC, Kockx MM, Havekes LM, van Berkel TJ, Biessen EA. Induction of atherosclerotic plaque rupture in apolipoprotein E-/- mice after adenovirus-mediated transfer of p53. *Circulation*. 2002;105:2064-70.

23. Johnson J, Carson K, Williams H, Karanam S, Newby A, Angelini G, George S, Jackson C. Plaque rupture after short periods of fat feeding in the apolipoprotein E-knockout mouse: model characterization and effects of pravastatin treatment. *Circulation*. 2005;111:1422-30.

Nederlandse samenvatting (Summary in Dutch)

Atherosclerose is de belangrijkste doodsoorzaak in de westerse wereld. Atherosclerotische laesies ontwikkelen zich op specifieke plaatsen in slagaders, te weten in binnenbochten en aftakkingen. Dit wordt geassocieerd met veranderingen in het bloedstroomprofiel. "Shear stress" of afschuifspanning is de hemodynamische kracht die door de bloedstroom wordt uitgeoefend op het
"endotheel", de cellaag waarmee bloedvaten aan de binnenzijde zijn bekleed. In een recht stuk vat met een normaal laminair stromingsprofiel, wordt de shear stress actief gereguleerd en op een ingestelde waarde gehouden. Een verlaging in die shear stress waarde (lage shear stress) wordt in verband gebracht met het ontstaan van atherosclerose. Tevens wordt oscillatie in shear stress (oscillatoire shear stress), waarbij het endotheel een tijdelijke terugstroming ondervindt gedurende de hart cyclus, geassocieerd met atherosclerose. Onderzoek naar het effect van shear stress op gekweekte endotheelcellen heeft laten zien dat beide hemodynamische condities (dus zowel lage als oscillatoire shear stress) expressie van genen kan activeren die atherosclerose bevorderen. Ondanks deze waarnemingen is er nog weinig bekend van het onderliggende mechanisme van het door shear stress geïnduceerde atherosclerotische proces. Dit komt ten dele omdat er geen goed proefdiermodel bestaat, waardoor er slechts weinig in vivo studies zijn gedaan. In dit project bestuderen we de effecten van shear stress op de vaatwand die de ontwikkeling van atherosclerose beïnvloeden. Hierbij maken we gebruik van een door ons zelf ontwikkeld kunststof implantaat (hier cast genoemd), dat een cilinder is met een taps toelopende binnenzijde. Deze kan om het rechte deel van de arteria carotis communis (a.carotis, halsslagader) van het proefdier worden aangebracht en induceert dan veranderingen in het normaal laminaire stromingsprofiel, waardoor gecontroleerde veranderingen in het shear stress profiel ontstaan. In de richting van de bloedstroom ontstaat er voor de cast een verlaging van shear stress. In het deel van het bloedvat dat zich in de cast bevindt, wordt door de tapse vormgeving van de cast de shear stress geleidelijk verhoogd. Na de cast ontstaat door de versmalde uitstroomopening van de cast een gebied van oscillatoire shear stress (**Hoofdstuk 1**). Door gebruik te maken van dit unieke model, hebben we de volgende in vivo effecten van shear stress bestudeerd:

Het effect van shear stress op genexpressie: De cast werd geïmplanteerd rondom de a. carotis van wildtype en transgene muizen. We konden aantonen door middel van bloedstroommetingen met Doppler echografie dat de cast inderdaad de verwachte verlaging and oscillaties in shear stress induceerde. We toonden verder aan dat de expressie van het eiwit endothelial nitric oxide synthase (eNOS) dosis-afhankelijk reageerde op veranderingen in shear stress in vivo in een transgeen eNOS-GFP muismodel (**Hoofdstuk 3**). In deze muizen is het eNOS eiwit gefuseerd aan een tweede (markerings-)eiwit, genaamd green fluorescent protein (GFP), waardoor ieder eNOS eiwit is gelabeld met een groen fluorescerend signaal (beschreven in

Hoofdstuk 2). Tevens toonden we aan dat de cellulaire lokalisatie van eNOS ook afhankelijk is van shear stress: meer eNOS is gelokaliseerd in het Golgi complex en is gebonden aan het celmembraan wanneer de shear stress toeneemt. Ook de activatie van eNOS, gemeten in deze studie d.m.v. analyse van mate van fosforylering van het eiwit, is toegenomen. Metingen aan de mRNA niveaus van het transgene (humane) eNOS, het endogene (muizen) eNOS, en van een aantal aan shear stress gerelateerde genen (geselecteerd op basis van gepubliceerde resultaten van in vitro studies), toonden duidelijke effecten aan, die duiden op een algemeen shear stress effect dat niet beperkt is tot het transgen (**Hoofdstuk 4**). We concluderen uit deze studie dat het nieuwe cast model in staat is om veranderingen (lage shear stress en oscillatoire shear stress) te induceren in vivo, en dat het op effectieve wijze veranderingen in genexpressie induceert. In een vervolgstudie hebben we tevens gekeken naar het effect Rapamycine, dat in de kliniek wordt toegediend aan de vaatwand via gecoate stents om restenosis te verhinderen, op shear stress gevoeligheid van het eNOS eiwit. Wij toonden aan dat toediening van rapamycine een verhoging in eNOS expressie in lage shear stress gebieden induceert, terwijl in hoge shear stress gebieden de maximale eNOS respons wordt verlaagd (**Hoofdstuk 5**). Dit impliceert dat m.n. in de lage (meer atherosclerosis gevoelige) shear stress gebieden rapamycine een beschermende werking geeft.

Het effect van shear stress op atherosclerose: Vervolgens werd het atherosclerose bevorderende effect van lage en oscillatoire shear stress bestudeerd in apoE deficiënte muizen, het meest gebruikte diermodel in onderzoek naar atherosclerose. We toonden in deze dieren een causaal verband aan tussen veranderingen in shear stress en atherosclerose. Laesies ontwikkelden zich in de lage and oscillatoire shear stress gebieden binnen 6 weken na cast plaatsing, terwijl het hoge shear stress gebied vrij bleef van atherosclerotische plaques. Lage shear stress induceerde grotere laesies die na 9 weken cast plaatsing lagere percentages collageen en gladde spiercellen en een hoger percentage lipiden in de intima bevatten. Ook vertoonden de vaatsegmenten in het lage shear stress gebied meer outward remodelling (groei naar buiten), meer neo-vascularisatie, meer metallo-proteïnase activiteit (en dus afbraak van collageen) en een verhoogde expressie van pro-inflammatoire factoren. Verder induceerde infusie van angiotensine II verhoogde incidentie van bloedingen in de laesies van het lage shear stress gebied. We concluderen dan ook uit deze studies dat zowel lage als oscillatoire shear stress noodzakelijk zijn voor het ontstaan van atherosclerose en dat met name lage shear stress de groei van grotere, meer instabiele laesies stimuleert, die de kenmerken hebben van een onstabiele plaque (**Hoofdstuk 6**).

Het effect van shear stress op inflammatie: Lange tijd is al bekend dat bij het ontstaan van atherosclerose ontstekingsprocessen zijn betrokken. Veranderingen in shear stress kunnen hierbij als atherosclerose bevorderende stimulus werken omdat er

aanwijzingen zijn dat het de expressie van adhesie-moleculen en chemokinen kan beïnvloeden. Chemokinen zijn een familie van eiwitten die helpen om inflammatoire cellen uit de bloedstroom te "vangen" en deze vervolgens laten migreren in de vaatwand naar de ontstekingshaard. Deze gesecreteerde stoffen dragen hierdoor bij aan het atherosclerose proces. Hoewel de expressie van adhesiemoleculen cruciaal is voor adhesie en migratie van bloedcellen, wordt de specificiteit van de respons met name bepaald door de chemokinen. We bestudeerden chemokine-expressie gedurende de vroege fase van de shear stress respons van de vaatwand en vergeleken dat met de shear stress respons bij volledig ontwikkelde atherosclerotische laesies. Hiervoor bekeken we het expressiepatroon van 12 verschillende chemokinen en chemokinereceptors in ApoE deficiënte muizen na een (alleen endotheliale dysfunctie waarneembaar), drie (fatty streaks) en negen weken (gevorderde atherosclerotische laesies) na plaatsing van de cast. We vonden een aanzienlijke inductie in expressie van een aantal duidelijk aan atherosclerose gerelateerde chemokinen (o.a. monocyte chemoattracting protein (MCP1) en interleukine 8 (IL8)) wat duidt op een pro-inflammatoire respons opgewekt door zowel lage als oscillatoire shear stress. Tevens vonden wij expressiepatronen in de onderzochte chemokinen in de gebieden met lage shear stress die karakteristiek zijn voor de groei van instabiele laesies. Met name de chemokinen fractakine (alleen aanwezig in de vulnerable leasies) en Interferon-gamma-inducible Protein-10 (IP10, alleen aanwezig in de vroegere tijdspunten van het door lage shear stress gestimuleerde gebied) zijn door hun associatie met het plaque stabiliteit interessante kandidaten voor verder onderzoek (**Hoofdstuk 7**).

De conclusies van de voorafgaand beschreven studies kunnen als volgt worden samengevat (**Hoofdstuk 8**):

Door het gebruik van het cast model zijn we in staat de directe effecten op de vaatwand van lage, hoge en oscillatoire shear stress te bestuderen. Door lage shear stress vervalt de bescherming van eNOS op de vaatwand. Daarentegen verhoogt oscillatoire shear stress de basale eNOS expressie. Zowel lage als oscillatoire shear stress induceren een inflammatoire respons. Hierbij komen chemokinen vrij die het atherogene proces activeren en bevorderen. Een verlaging in shear stress resulteert in het ontstaan van een atherosclerotische laesie met een instabiel fenotype. Oscillatoire shear stress resulteert in het ontstaan van stabiele atherosclerotische laesies. Het uiteindelijke verschil in mate van stabiliteit kan mogelijk worden verklaard door het karakteristieke chemokinenexpressie patroon dat we hebben gevonden in het lage shear stress gebied. Vroege expressie van IP10, en late expressie van fractakine, kan door het beïnvloeden van de differentiatie van de monocyten/macrofagen in de plaque, de functie van deze cellen sturen en zo doende het inflammatieproces bevorderen. Het blocken van fractalkine resulteert in het stabiliseren van de ahterosclerotische plaque. Verder onderzoek naar de samenstelling van de in de

atherosclerotische laesie aanwezige macrofagenpopulatie kan de rol van deze shear stress gevoelige chemokinen verduidelijken.

Dankwoord (Acknowledgements)

Iemand bedanken is schijnbaar toch een kunst, aangezien veel mensen klagen dat ze onvoldoende gewaardeerd worden door hun collega's. Veel AIO's maken dan ook een hele waslijst van het dankwoord, onder het motto "Je zou maar iemand vergeten!" Ikzelf heb er minder moeite mee. Ere wie ere toekomt. Dat geldt ook voor het uiten van dank. Dus hierbij, de mensen die me met raad en daad hebben bijgestaan gedurende deze lange jaren AIO-zijn:

Beste Rob. Jij eerst, omdat je hoe dan ook de kapitein bent op dit onstuimige schip. Van jou heb ik geleerd dat origineel werk loont (en hoe!). Jouw creativiteit, grote kennis op fysiologisch gebied, nauwgezetheid en enthousiasme heb ik toch erg gewaardeerd, ook al laat ik dat niet altijd blijken. Jij hebt mij gestimuleerd om niet alleen hard door te werken, maar ook heel kritisch mijn resultaten te blijven bekijken. Soms verliep niet alles even gladjes, maar gelukkig loste de meeste problemen op als suiker in hete thee zodra dingen netjes konden worden besproken. Al met al heb ik de afgelopen vijf jaar met steeds meer plezier voor je gewerkt. Ik ben overtuigd dat het de komende jaren ook steeds beter zou gaan. Van onze trip naar Dallas heb ik in ieder geval zeer warme herinneringen overgehouden.

Beste Rini, mijn dank is groot. Niet alleen voor de begeleidende rol die je hebt gespeeld gedurende mijn promotie, maar ook heel erg bedankt voor het er simpelweg zijn voor me. Af en toe stoom afblazen, uithuilen of een IKEA kastje in elkaar zetten met elkaar (altijd de schroef met het pijltje naar buiten draaien!), daar hebben AIOs soms behoefte aan. Ook van jouw grote kennis op het gebied van atherosclerose, goede communicatieve eigenschappen, enthousiasme en (bijna pathologische) netheid heb ik veel geprofiteerd en geleerd (ook al heb ik thuis mijn collectie proefschriften nog lang niet op alfabetische volgorde staan). Dankzij je gratis theetjes van onze collectieve koffiekaart kom ik graag naar het werk. Onze trip naar Dallas was zeker prijsloos.

Mijn promotor professor van der Steen, en professor Grosveld, professor Poelman, en professor Simoons, hartelijk dank voor uw bereidheid om mijn thesis kritisch te beoordelen. Eveneens wil ik professor Grosveld bedanken voor zijn betrokkenheid bij dit onderzoek en de prettige werksfeer die ik ervaar op de afdeling celbiologie. Uw afdeling is erg groot, maar ondanks dat heeft het toch de sociale en behulpzame sfeer van een kleinere intieme groep. ***I never felt lost in this big city.***

Dr. Davies and Dr. Tedgui, thank you for travelling this far to attend the public defence of my thesis. Your contributions to the shear stress congress are also gratefully acknowledged. I also want to thank Dr. Davies for his tour around the Philadelphia University campus. I especially liked the squirrels the size of small cats.

Beste Dennie, alleen pipetteren is lang zo leuk nog niet als samen met jou. In mijn eentje op het lab kwam ik maar al te vaak handen te kort. Je bent de rots in de branding, wanneer ik weer eens dreig te verdrinken in het papierwerk. De afgelopen jaren waren een verademing en mede dankzij jou is er een boel afgekomen en kon het allemaal in dit boekje worden opgeschreven. Verder ben je mijn vaste lunchpartner, klaagpaal, benchcleaner ("*Carolien, je maakt echt een tering zooi van mijn bench!*"), meeting dummie (gedeelde smart is halve smart, voor mij dan wel te verstaan), en kaatsmuur (wetenschappelijk gezien dan, niet letterlijk). Kortom, je bent de beste collega die een AIO zich kan wensen. Maak je geen zorgen, je hebt niet alleen alle kwaliteiten van een uitmuntende analist, maar ook die van een goede AIO in je. Zet hem op! Over 4-5 jaartjes wil ik in je dankwoord staan!

Beste Rien, hoe druk je het ook had, altijd was je bereid om hulp te bieden wanneer er weer eens wat mis dreigde te gaan op het lab. Het aantal keren dat je me goed advies hebt gegeven is net zo talrijk als het nageslacht van je guppen thuis (tis altijd raak). Ook al kon ik je in het begin niet altijd goed verstaan (mompel de mompel), je hebt me veel onmisbare praktische kennis bijgebracht die de basis vormen voor al het werk dat omschreven wordt in dit boekje. Verder: je eNOS GFP muizen zijn absoluut prachtig, zeker onder de confocal.

Dan de rest van de mensen op het lab: Teus, bedankt voor het doen van de bestellingen en mijn mede AIO genoten Hanne en Matthijs, bedankt voor de gezelligheid en de hulp bij allerlei ditjes en datjes. Heel veel succes met jullie verdere promotie! Ik beloof in ieder geval weer vaker wat gezelliger te doen op het werk (en nieuwe planten te kopen en die beter te verzorgen) nadat de promotie achter de rug is.

Dan de mensen van de afdeling cel biologie die ik gedurende al die tijd meerdere keer heb aangesproken met: "Sorry, mag ik u even storen en een vraag stellen?": Rick, Sylvia, en Dubi (oud labgenoten), Pim (een van de aardigste collega's die ik ken) en de heren van de computerclub, Melle en de dames van het bestelkamertje, de mensen op Robbert Rotier's lab (hele ml's antilichamen worden er door ons "geleend"), Ton de Wit (voor de muizen en het leuke commentaar), en iedereen die ik vergeten ben, allen heel erg bedankt!

Gert, bedankt voor de hulp met bij confocal en Joop voor het maken van de castjes, zonder jullie waren er toch wel flinke gaten gevallen in het proefschrift.

De heren van de 22ste verdieping: Frank, je kunt fysiologie zo uitleggen dat ik het zelfs snap. Bedankt voor je theoretische bijdrage. Luc, je was altijd hulpvaardig en vriendelijk wat een heel fijne collega van je maakte. Veel succes met je nieuwe loopbaan (niet dat je die nodig zult hebben) en erg bedankt, m.n. voor je MMP werk. Dolf, succes met de AIO jaren die je nog voor de boeg hebt.

De studenten die hard hebben meegewerkt aan de verschillende studies: Laurens, Martin, Arjen, Rianne, Angela, Tariqe, en Fadime, allemaal heel erg bedankt voor jullie bijdrage! Ieder van jullie wens ik het allerbeste toe met jullie loopbaan!

De wetenschappers waarmee we goede samenwerkingen hebben:
Jolanda en Frank van de haemodynamiek (ook voor het organiseren van het shear stress symposium), Pieter Leenen en John Laman van de afdeling immunologie, Dirk Jan Duncker en de rest van de afdeling experimentele cardiologie, Rob Poelman, Berend Hierck en Marco de Ruiter uit Leiden, en Domique de Kleijn en Gerard Paterkamp uit Utrecht, bedankt voor de praktische hulp en/of de zeer gewaardeerde wetenschappelijke input.

Van de 23ste wil ik speciaal de volgende mensen een extra bedankje geven:

Monique, heel erg bedankt voor je hulp bij de muizen, zeker in het begin. Ik wens je nog veel succes toe met je verdere promotie en volgend jaar in Chicago ben ik *wel* bij je praatje, zeker weten!

Lieve Esther, het was echt een stuk gezelliger toen je nog beneden zat en ik mis je enorm. Zonder jou ben ik de enige die een tering zooi van zijn bench maakt en ga ik nog maar nauwelijks in de zomer even een ijsje halen in de baas zijn tijd. Gelukkig kun je mijn smart goed maken door je eens flink uit te sloven als mijn paranimf (wink wink). Zonder dollen: je was en bent echt een super fijne collega om "around" te hebben. Bedankt voor alles!

Annemarietje, ook met jou het ik stoom afgeblazen, uitgehuild en een IKEA kastje naar zijn grootje geholpen. Een oprechter en liever cardioloogje dan jij is er domweg niet op deze roterende aardkloot. Met zo'n huis van een karma kan het alleen maar goed komen met je. Nog even doorbijten, en dan mag jij ook het dankwoord schrijven.
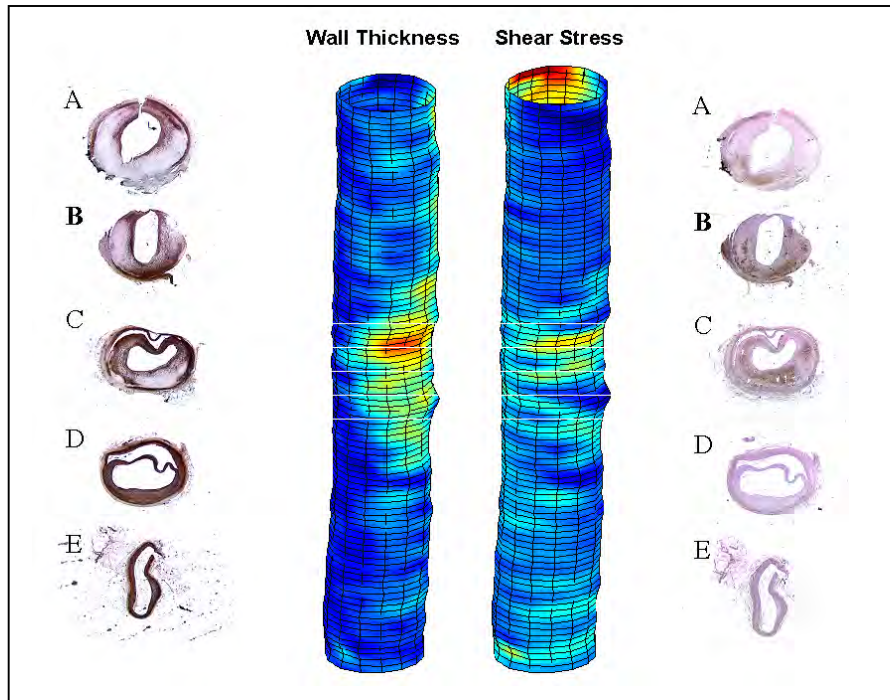
Desire, onze lieve, ultra nette, uiterst vis vriendelijke (jammer genoeg) ex-collega. Bedankt voor je gezelligheid en je goede tips. Ik kom langs zodra je je 500L aquarium (met guppen vretende haai!) geïnstalleerd hebt in je nieuwe woning.

Bedankt lieve mans en paps. Hoe druk ik het ook had met mijn werk, ik kon naderhand altijd bij jullie weer terecht als jullie kleine meid. Thuis in Eindhoven was het altijd warm en gezellig (en het eten (ge)weldadig veel). Bedankt Kawah en Wing, zonder jullie is een spelletje monopolie spelen toch wel erg saai. Lief (rijk) zusje van me, wil je ophouden mijn spullen te lenen zonder het terug te geven!
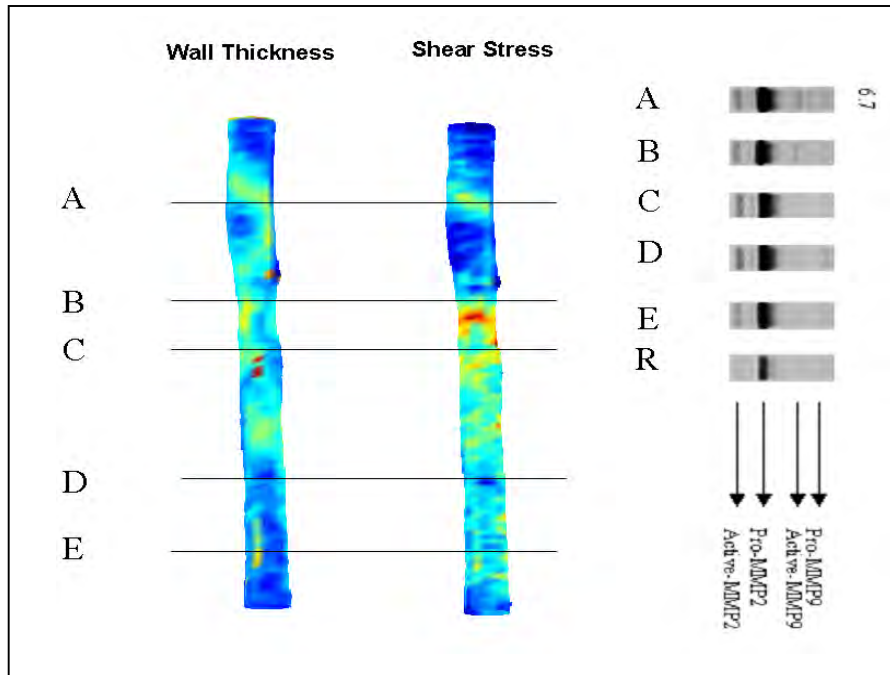
Lieve David, zonder jou geen lieve Caroline. We hebben samen al heel veel leuke dingen gezien en meegemaakt (Slecht Vlaams eten(!) in Brugge, ultra snob doen in

Londen, Venetiaans rioleringswater, "doggie-bags" en eikeltjes in New Orleans, sub zero Toronto, *Beter dan gij* Franse bediening in Parijs, een deinende Star ferry in Hong Kong, met rauw billen door de donkere landweggetjes van Texas, en Kou Kleumen op Keulse Kerstmarkten). Het leukste van dit alles is dat ik iedere keer weer het dierbaarste van al die plekken weer mee naar Rotterdam mocht nemen, n.l. jou. Ik hou van je. Bedankt lief, bedankt voor alles.
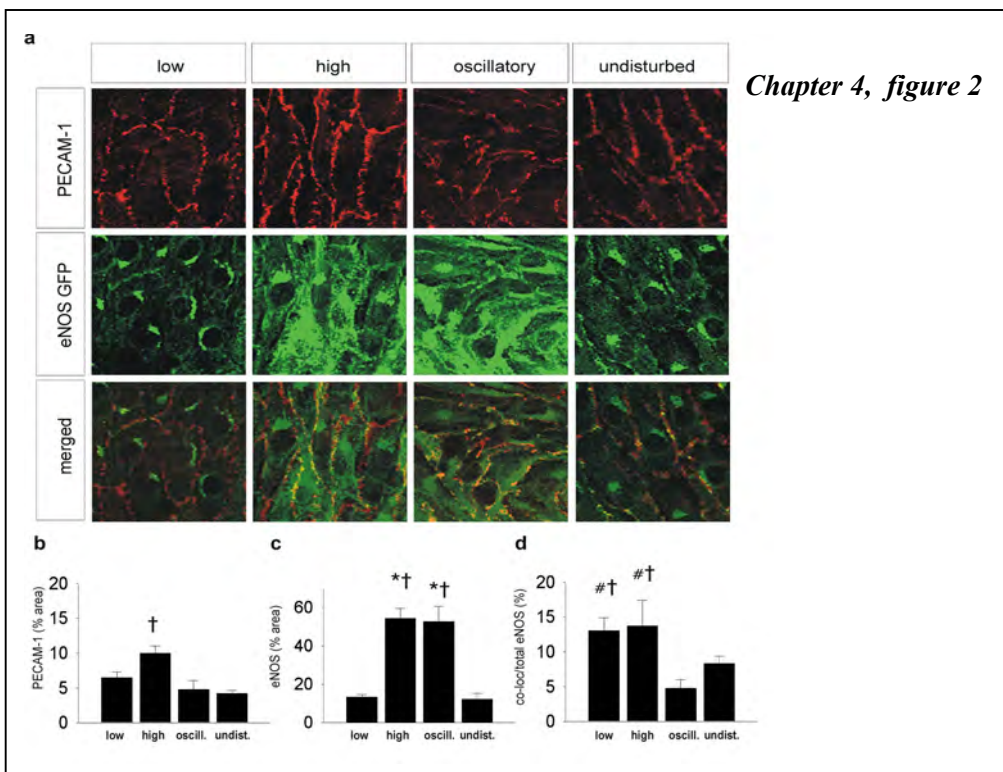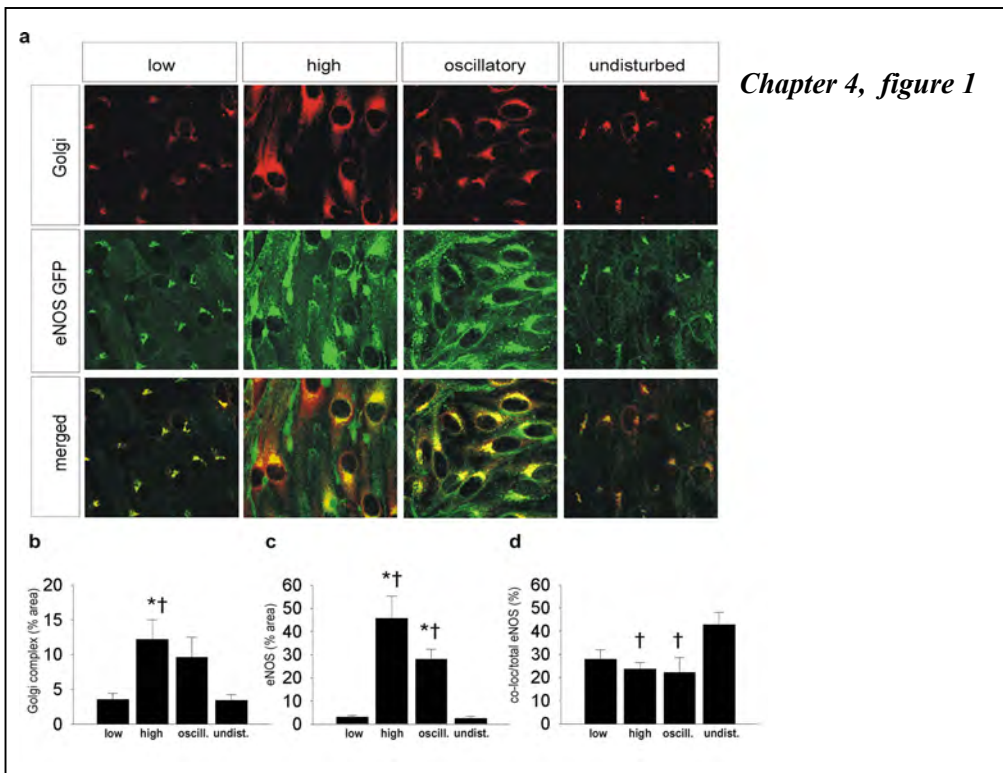
Full Colour Section

Chapter 1, figure 1

Chapter 1, figure 2
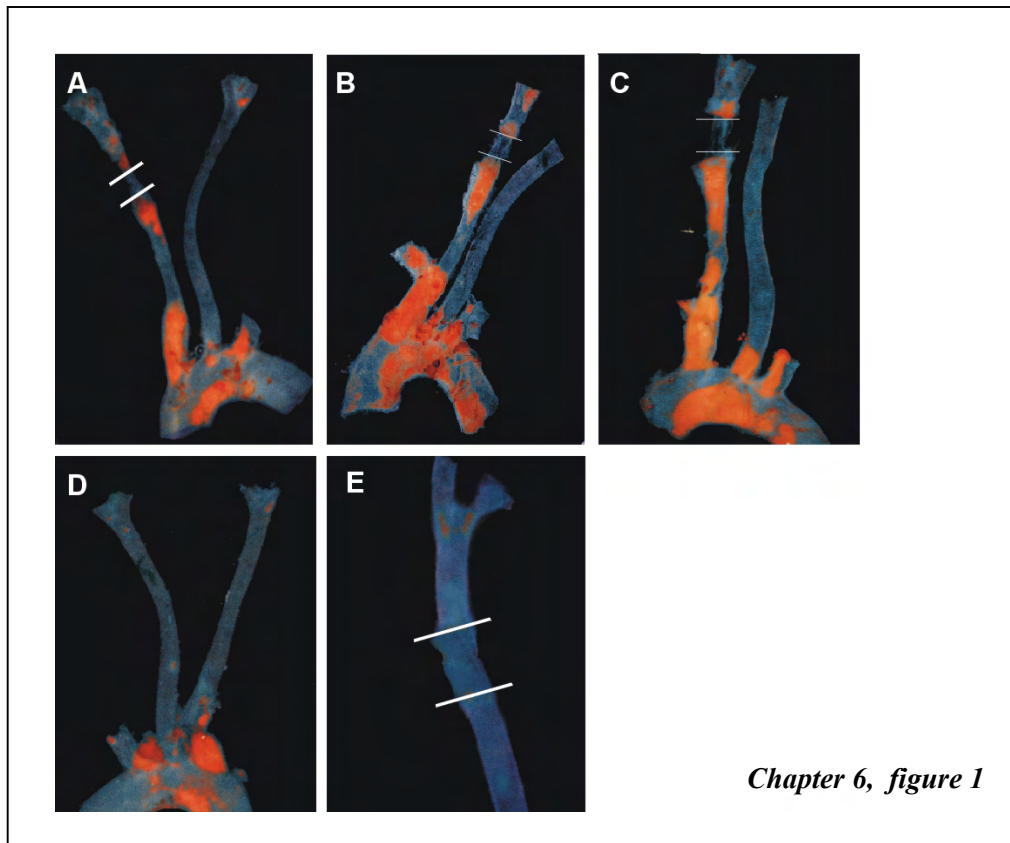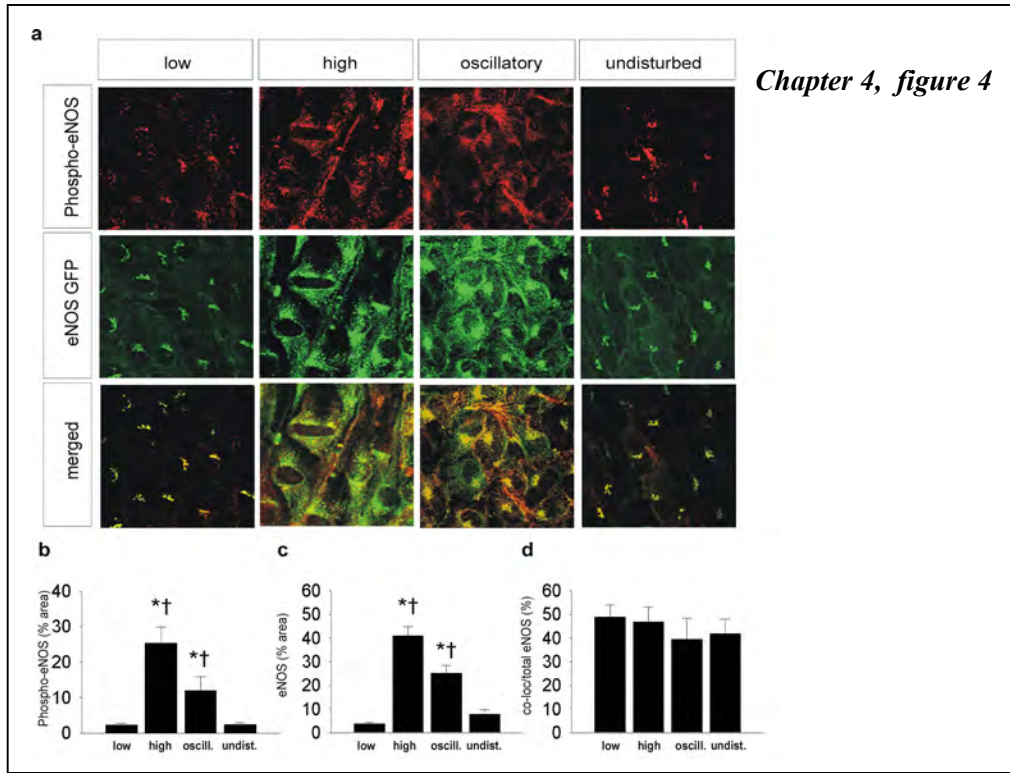
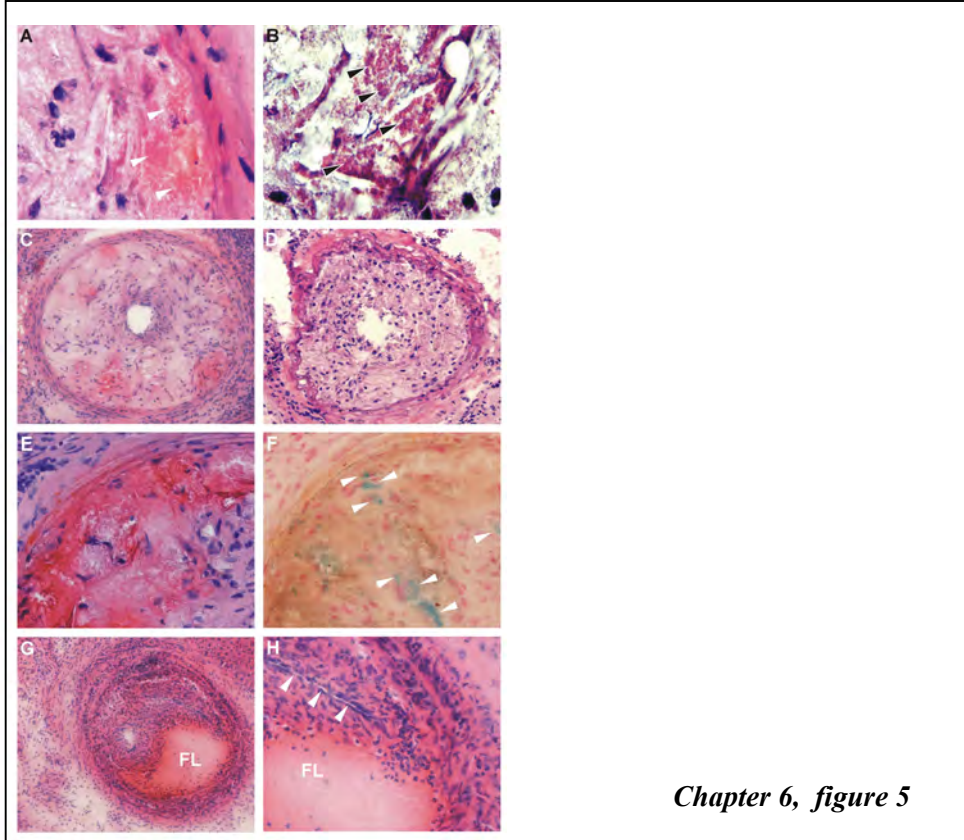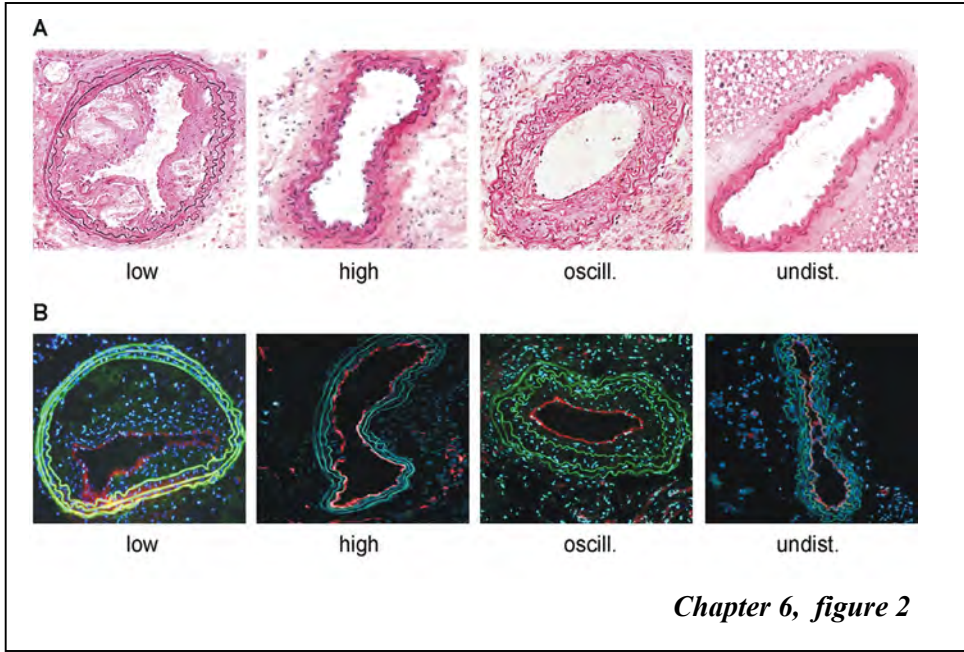*Chapter 4, figure 1*

Chapter 4, figure 2

Chapter 1, figure 1: 3D reconstruction of an atherosclerotic rabbit aorta with IVUS, allowing the projection of wall thickness on the 3D lumen reconstruction. Indicated is also the shear stress distribution obtained by CFD. Atherosclerosis was induced in New Zealand White rabbits by a combination of denudation (surgical removal of the endothelium) and high cholesterol diet for two months. CFD modeling was based upon a commercially available finite element package as described before. On the left and right sides are indicated the macrophage distribution and the smooth muscle cell distribution. Lines in the figure indicate the approximate location of the histological cross sections. The position of these cross sections was determined by measurement at sacrifice. Note that upstream, where the shear stress is high, the macrophages accumulate. Full colour image of this figure is available in the colour section.

Chapter 1, figure 2: Relationship between metalloproteinase activity as determined by zymography, plaque location and shear stress distribution mapped upon the 3D reconstruction of the blood vessel. CFD was used as described in figure 1. Mapping of location was performed by selection on basis of shear stress distribution and correction for shrinkage after dissection. Note that the location of MMP9 activity is upstream of the plaque and associates with high shear stress values. MMP-2 is activated through the entire plaque region. A-E represent samples from the sections in different locations of the atherosclerotic vessel. R stands for the control sample. Full colour image of this figure is available in the colour section.

Chapter 4, figure 1: Intracellular localization of eNOS-GFP and Golgi complex in areas of the carotid artery experiencing different shear stress patterns after 2 days of cast placement. (a) In the upper panel: Golgi complex in corresponding vascular regions visualized by en face immunofluorescence staining. Indicated are: the low shear stress region (low), the high shear stress region (high), the oscillatory shear stress region (oscillatory), and the control region (undisturbed). Fluorescence was monitored by en face confocal microscopy in stacks of 500 μm x 500 x 40 μm each. In the middle panel: Fluorescence of eNOS-GFP in endothelial cells located in the three different shear stress regions and in the contra-lateral carotid artery. In the lower panel the upper and middle panels are merged, showing the co-localization signal in yellow. (b-d) Quantification of the localization of (b) the Golgi complex, (c) the eNOS-GFP and d) the co-localization signals in response to the different shear stress fields in percentages of the total area (b,c) or of the total eNOS-GFP signal (d). n = 4, * P<0.05 versus low shear stress. † P<0.05 versus undisturbed shear stress. Full colour image of this figure is available in the colour section.

Chapter 4, figure 2: Intracellular localization of eNOS-GFP and PECAM-1 in regions of the carotid artery experiencing different shear stress patterns after two days cast placement. (a) In the upper panel: PECAM-1 in corresponding vascular regions visualized by en face immunofluorescence staining. Indicated are: the low shear stress region (low), the high shear stress region (high), the oscillatory shear stress region (oscillatory), and the control region (undisturbed). Fluorescence was monitored by en face confocal microscopy in stacks of 500 μm x 500 x 40 μm each. In the middle panel: Fluorescence of eNOS-GFP in endothelial cells located in the three different shear stress regions and in the contra-lateral carotid artery. In the lower panel the upper and middle panels are merged, showing the co-localization signal in yellow. (b-d) Quantification of the localization of (b) the PECAM-1, (c) the eNOS-GFP and d) the co-localization signals in response to the different shear stress fields in percentages of the total area (b,c) or of the total eNOS-GFP signal (d). n = 5, † P<0.05 versus undisturbed shear stress. # P<0.05 versus oscillatory shear stress. Full colour image of this figure is available in the colour section.
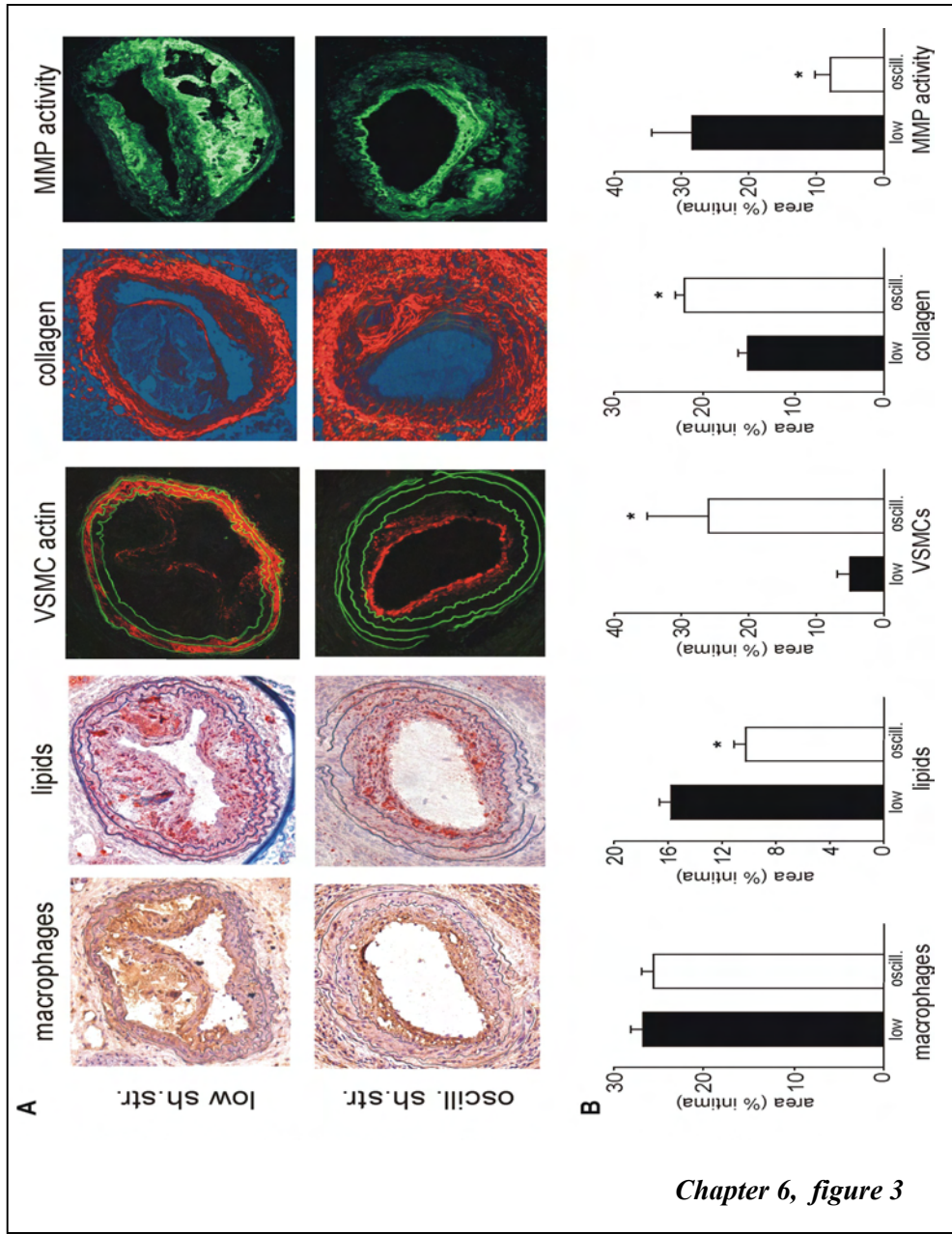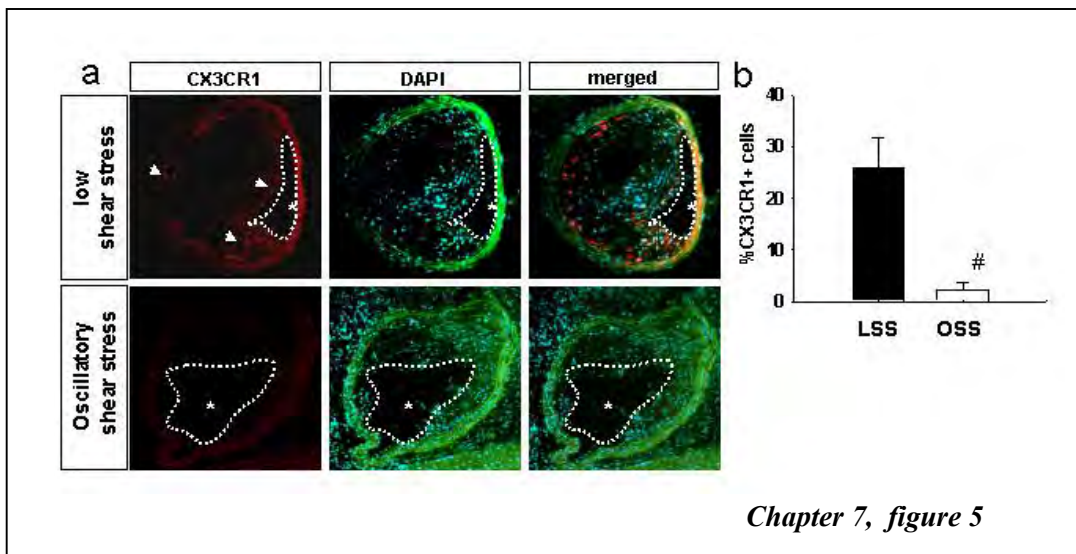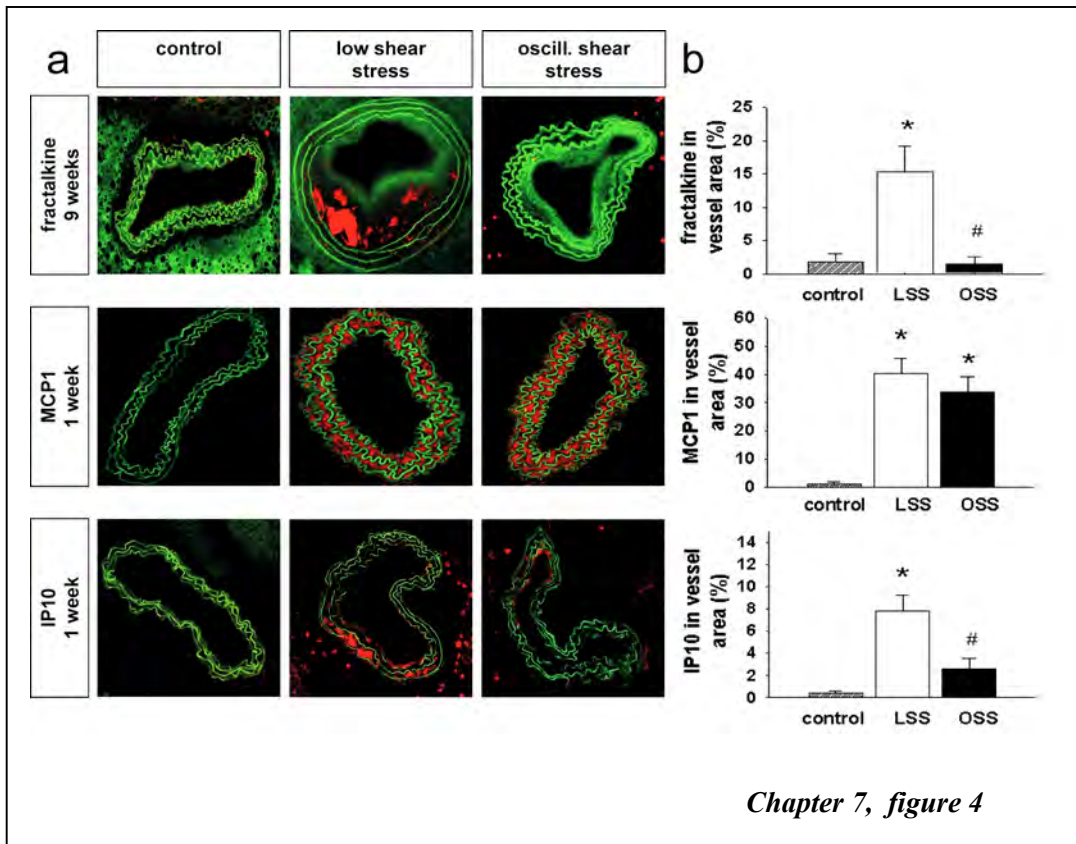
Chapter 4, figure 4

Chapter 6, figure 1

A

low   high   oscill.   undist.

B

low   high   oscill.   undist.

Chapter 6, figure 2

Chapter 6, figure 5

Chapter 4, figure 4: Intracellular localization of eNOS-GFP and phospho-eNOS in areas of the carotid artery experiencing different shear stress patterns after two days of cast placement. (a) In the upper panel: Phospho-eNOS in corresponding vascular regions visualized by en face immunofluorescence staining. Indicated are; the low shear stress region (low), the high shear stress region (high), the oscillatory shear stress region (oscillatory), and the control region (undisturbed). Fluorescence was monitored by en face confocal microscopy in stacks of 500 μm x 500 μm each. In the middle panel: Fluorescence of eNOS-GFP in endothelial cells located in the three different shear stress regions and in the contra-lateral carotid artery. In the lower panel the upper and middle panels are merged, showing the co-localization signal in yellow. (b-d) Quantification of the localization of (b) thePhospho-eNOS, (c) the eNOS-GFP and d) the co-localization signals in response to the different shear stress fields in percentages of the total area (b,c) or of the total eNOS-GFP signal (d). n = 5, * P<0.05 versus low shear stress. † P<0.05 versus undisturbed shear stress. Full colour image of this figure is available in the colour section.

Chapter 6, figure 1: Low shear stress and oscillatory shear stress induce atherosclerosis in apoE –/– mice fed an atherogenic Western diet. Whole mount aortic arches and carotid arteries were stained with Oil-red-O for atherosclerotic lesions. The white lines demarcate the previous position of the cast with the high shear stress region. Upstream from the cast is the low shear stress region, and downstream from the cast is the oscillatory shear stress region. Animals were instrumented with a cast after 2 weeks of the beginning of the diet and sacrificed after 6 (A), 9 (B), or 12 (C-E) weeks of cast placement. No lesions are detected in the carotid arteries of sham operated mice (D) or in the carotid arteries of animals instrumented with a non-constrictive cast (E). Representative images are shown from groups consisting of 6-8 animals. Colour version of this figure is available in the full colour section.

Chapter 6, figure 2: Histological analyses of carotid arteries at 9 weeks after cast placement in apoE–/– mice fed a Western diet. (A) Representative images are shown from the low, high, and oscillatory shear stress regions as well as from the contra-lateral non-treated carotid artery (undisturbed shear stress) (hematoxylin and eosin staining, original magnifications 100X). (B) Representative images showing PECAM-1 staining (red) of the intact endothelium in the four different shear stress regions. Auto-fluorescence of the elastic lamellae is in green and the cell nuclei stained with DAPI are in blue. Original magnifications: 100 X. Histological analyses were performed by quantification of the intima/media ratio (C), and of the relative cross-sectional area of the vessel wall (D), which was obtained by measuring the area confined by the external elastic lamina of the instrumented carotid artery and expressed as percentage of the cross-sectional area of the contra-lateral non-treated carotid artery. * P<0.05 versus low shear stress. † P<0.05 versus oscillatory shear stress. Colour version of this figure is available in the full colour section.

Chapter 6, figure 5: Intra-plaque hemorrhages in the lesions located in the low shear stress region. ApoE–/– mice were fed a Western diet and instrumented with a cast around the carotid artery. (A,B) After nine weeks, intra-plaque hemorrhages were found in approximately 28% of the animals analyzed. Arrowheads point at accumulations of red blood cells near the internal elastic lamina (A) or in the necrotic core (B). (C-H) After 7 weeks of cast placement, the animals were treated with angiotensin II infusion (400ng/kg/min) via a subcutaneously implanted osmotic minipump (Alzet, model 2004, Durect Corp) and were sacrificed 2 weeks later. Intra-plaque hemorrhages were frequently observed (in 6 out of the 8 animals): (C) overview of an atherosclerotic lesion with intra-plaque hemorrhages in the low shear stress region; (D) overview of an atherosclerotic lesion in the oscillatory shear stress region. No intra-plaque hemorrhages can be detected; (E) detail from intra-plaque hemorrhage in the low shear stress atherosclerotic lesions; (F) the same detail as in (E) stained for iron deposits (arrowheads) with the Prussian blue reaction; (G): overview of a carotid artery with a large false lumen (FL); (H) detail showing the depressed lumen (arrowheads). 7 µm cryosections were stained with eosin and hematoxylin. Representative pictures from 6 animals are shown. Original magnifications: 100 X (C, D, G); 400 X (A, B, F, G, H). Colour version of this figure is available in the full colour section.
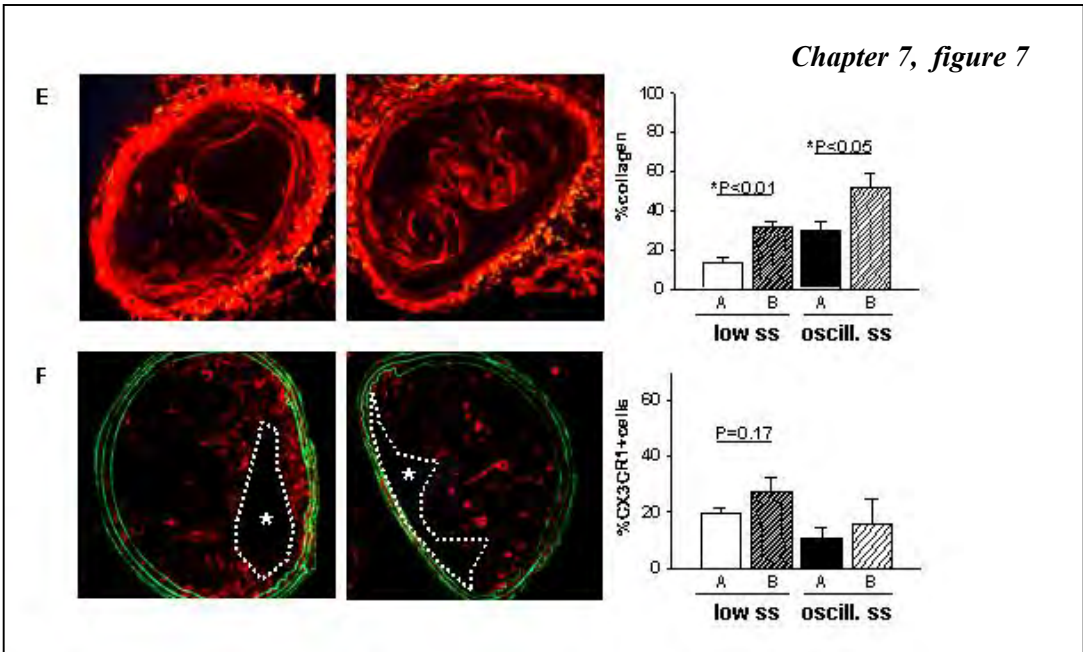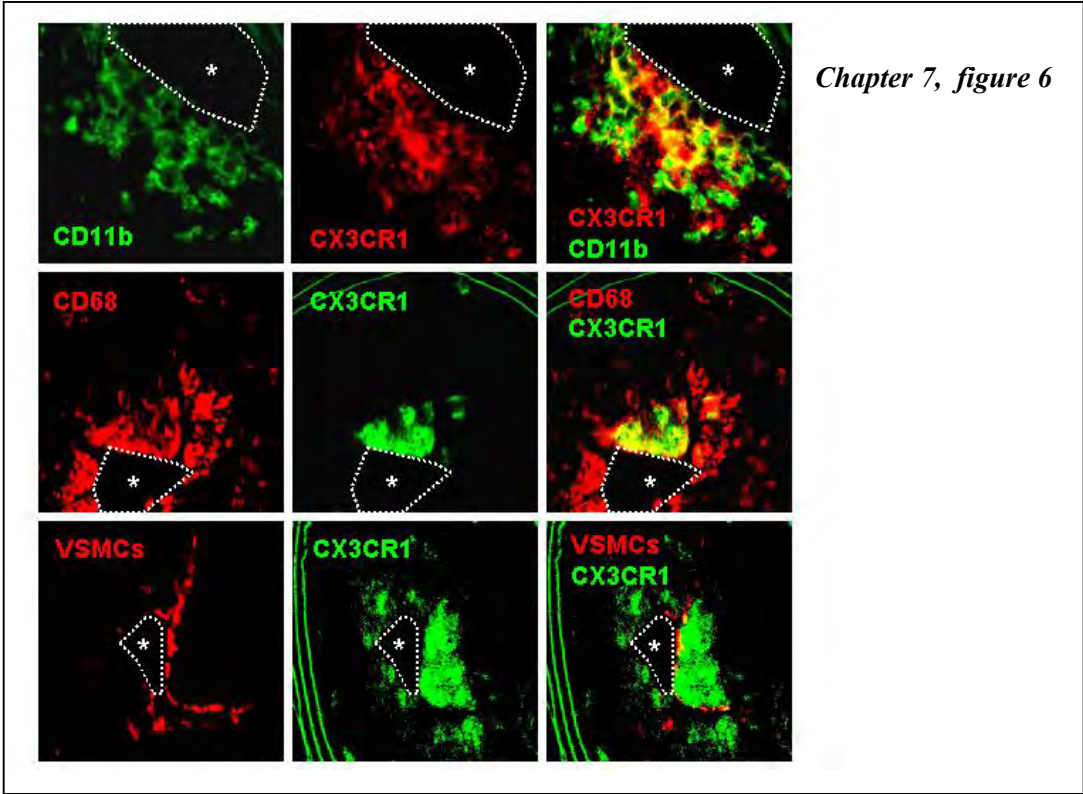
Chapter 6, figure 3

Chapter 7, figure 4

Chapter 7, figure 5

187

Chapter 6, figure 3: (A) Cross-sections of carotid arteries 9 weeks after cast placement in apoE–/– mice on a Western diet (100X magnification) stained for macrophages [15], lipids (Oil red-O), vascular smooth muscle cells (anti α-actin), or collagen (picrosirius red) in the low shear stress and the oscillatory shear stress region. MMP activity was studied by DQ gelatinase assay. (B) Quantification of macrophages, lipids, vascular smooth muscle cells, and collagen in the intimal area of the low shear stress and the oscillatory shear stress region, and of MMP activity. Data are the average values of sections from 5 different animals. * $P<0.05$ versus low shear stress. Colour version of this figure is available in the full colour section.
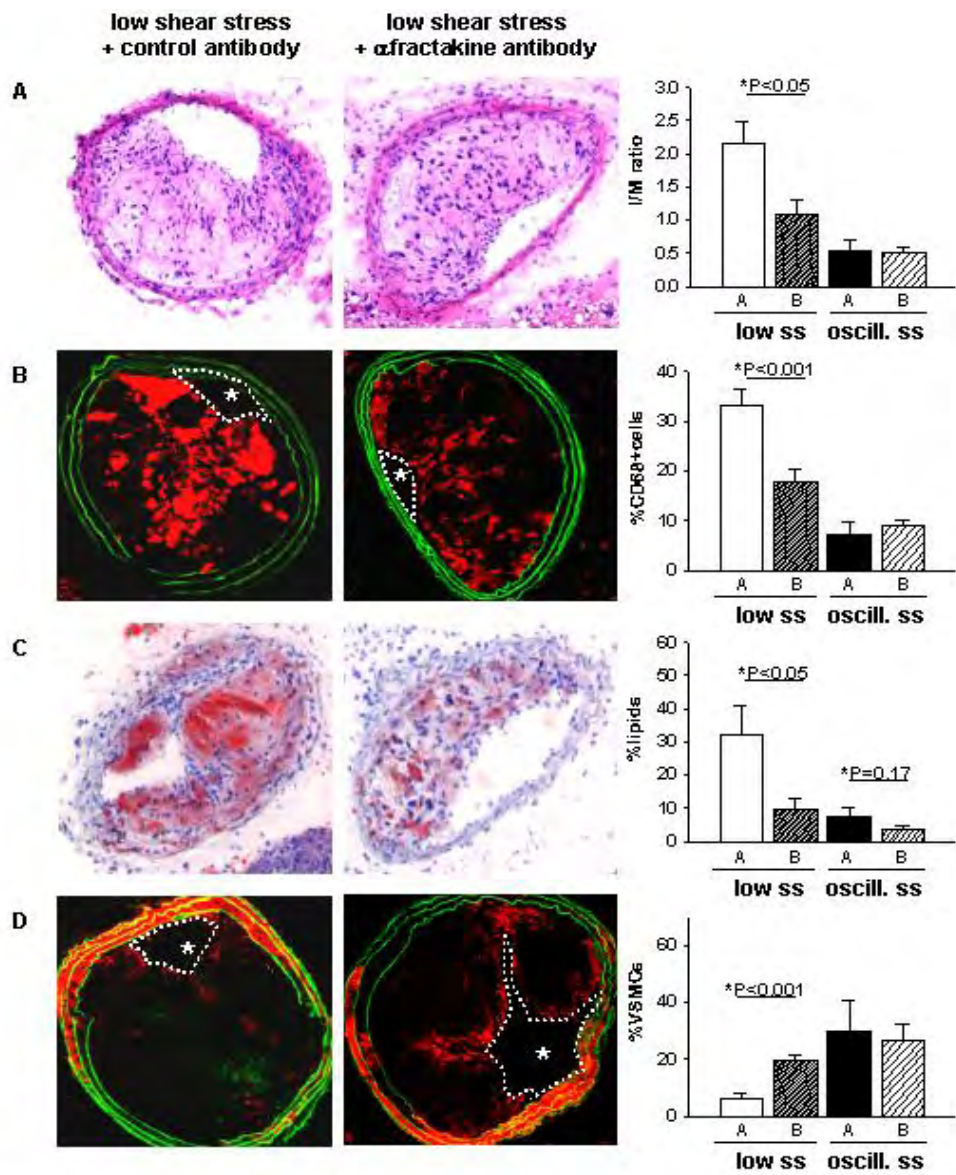
Chapter 7, figure 4: Validation of result of a selected group of chemokines by immuno-histological analysis of the protein levels in carotid arteries at different time points after cast placement in mice on western diet. Shown are representative cross-sections of murine carotid arteries stained for fractalkine after 9 weeks of cast placement (upper panel), and MCP1 (middle panel) and IP10 (lower panel after 1 week of cast placement, in the control, low and oscillatory shear stress regions (20X magnification) Chemokine expression is specified by a red signal. Green auto-fluorescence designates the intimal and medial areas (a). The results of the immuno-histological quantification of the chemokine signals. The percentages of fractalkine at time point 9 weeks (upper graph), MCP1 at time point 1 week (middle graph), and IP10 at time point 1 week (lower graph) in the vessel area of the low shear stress (LSS) and the oscillatory shear stress (OSS) regions are shown (b). N=5. *$P<0.05$ versus control. #$P<0.05$ versus low shear stress. Colour version of this figure is available in the full colour section.

Chapter 7, figure 5: The effect of fractalkine expression on cell recruitment in the mature lesions. Shown are representative cross-sections of murine carotid arteries double stained for CX3CR1 (red signal) and nuclei (blue signal). In the upper panel, CX3CR1 positive cells in the low shear stress lesions (indicated by arrows) are shown. The lumen is indicated by an (*), and the intima contours are traced by a white line. In the upper panel, CX3CR1 positive cells in the oscillatory shear stress lesions are shown. The lumen is indicated by an (*), and the intima contours are traced by a white line (a). The results of the immuno-histological quantification of the chemokine signal. The percentages of CX3CR1 positive area at time point 9 weeks in the intima in the low (LSS) and the oscillatory shear stress (OSS) region (b). N=5. #$P<0.05$ versus low shear stress. Colour version of this figure is available in the colour section.

Chapter 7, figure 6: CX3CR1 expressing cells located in the advanced lesions are mainly monocytes and macrophages. Shown are representative cross-sections of murine carotid arteries double stained for CX3CR1 (middle column) and CD11b, CD68, and VSMC α-actin (left column, from upper to lower panels), respectively. In the third column, the (yellow) co-localization signal is shown. The lumen is indicated by a (*) and the intima contours are traced by a white line. Colour version of this figure is available in the full colour version.

Chapter 7, figure 7: Fractalkine function was inhibited during cast-induced atherogenesis in ApoE KO mice by administration of a neutralizing antibody from week 6 till week 9. In the left column, Representative cross-sections are shown. These are stained for: (2a) lesion morphology by H/E, (2b) macrophages, (2c) lipids, (2d) VSMCs, (2e) collagen, and (2f) fractalkine receptor (CX3CR1). The lumen is indicated by a (*) and the intima contours are traced by a white line. In the right column, the lesion area is shown in the first graph, followed by results of the (immuno-) histological quantification of the different plaque components. The percentages of positive area at time point 9 weeks in the intima in the low (LSS) and the oscillatory shear stress (OSS) region are indicated, comparing the control antibody group (A) with the a-fractalkine antibody group (B). N=8. *P<0.05 versus control antibody group. Colour version of this figure is available in the full colour section.

Chapter 7, figure 6

Chapter 7, figure 7

190

low shear stress + control antibody **low shear stress + αfractalkine antibody**

A

*P<0.05

I/M ratio

low ss   oscill. ss

B

*P<0.001

%CD68+cells

low ss   oscill. ss

C

*P<0.05

*P=0.17

%lipids

low ss   oscill. ss

D

*P<0.001

%VSMCs

low ss   oscill. ss

Chapter 7, figure 7

191

Curriculum vitae

Caroline (Ka Lai) Cheng was born on the 20th of January 1978 in Hong Kong (China). She moved to the Netherlands in 1981 and graduated from the VWO in 1996 at the Christian Huygens College in Eindhoven. She studied Medical Biology at the Free University (Vrije Universiteit) in Amsterdam where she graduated in 2000. In September 2000, she started as a Ph.D. student in the Erasmus MC in Rotterdam under the guidance of Dr. Rob Krams (department of Cardiology) and Dr. Rini de Crom (department of Cell Biology and Genetics). Her main interests are the effects of shear stress on the vessel wall during atherosclerosis development. At this moment, she remains at the department of cardiology, working as a post-doc in close collaboration with the department of cell biology and genetics.

Scientific Awards:

Finalist poster awards American Heart Association Congress 2005

Fellowship from the Dutch Atherosclerosis Society, at the Dutch Atherosclerosis Society Symposium 2005

"Best presentation award" awarded by ICIN 2004

Finalist poster awards European Heart Congress 2004

"Best presentation award" at the Dutch Atherosclerosis Society Symposium 2003

"Best presentation award", at the 14th endothelium research symposium 2003

List of publications

Full papers:

C. Cheng, R. van Haperen, M. de Waard, L.C.A. van Damme, D. Tempel, L. Hanemaaijer, G.W.A. van Cappellen, J. Bos, Cornelis J. Slager, D.J. Duncker, A.F.W. van der Steen, R. de Crom, and R. Krams. Shear stress affects the intracellular distribution of eNOS: direct demonstration by a novel in vivo model.
Blood. 2005;1;106(12):3691-8

C. Cheng, R. de Crom, R. van Haperen, F. Helderman, B.M. Gourabi, L.C.A. van Damme, S.W. Kirschbaum, C.J. Slager, A.F.W. van der Steen, and R. Krams. The role of shear stress in atherosclerosis: action through gene expression and inflammation?
Cell Biochem Biophys. 2004;41(2):279-94.

C. Cheng, D. Tempel, R. van Haperen, A. van der Baan, F. Grosveld, M.J.A.P. Daemen, R. Krams, and R. de Crom. Atherosclerotic lesion size and vulnerability are determined by patterns of fluid shear stress.
Circulation, in review

C. Cheng, D. Tempel, A. Oostlander, F. Helderman, F. Gijsen, J. Wentzel, R. van Haperen, P.W. Serruys, A. F. W. van der Steen, R. de Crom, and R. Krams. Rapamycin affects eNOS expression through a shear stress dependent mechanism.
Submitted

C. Cheng, D. Tempel, R. van Haperen, M. Huisman, R. de Crom, and R. Krams. Shear stress affects chemokine expression during atherogenesis: difference in pro-inflammatory abilities between low and oscillatory shear stress.
Submitted

R. van Haperen, *C. Cheng*, B.M. Mees, E. van Deel, M. de Waard, L.C.A. van Damme, T. van Gent, T. van Aken, R. Krams, D.J. Duncker, R. de Crom. Functional expression of endothelial nitric oxide synthase fused to green fluorescent protein in transgenic mice.
Am J Pathol. 2003;163(4):1677-86.

F. Helderman, *C. Cheng*, L.C.A. van Damme, D. Segers, B. Mousavi Gourabi, N. Stergiopulos, M.M. Kockx, M. W. M. Knaapen, P.W. Serruys and R. Krams. The role of shear stress and wall stress after balloon angioplasty and stent placement.
Recent Res Development in Biomechanics, 2003;1:99-109.

D. Segers, *C. Cheng*, R. de Crom, S.W.M. Kirschbaum, A.E. Oostlander, F. Helderman, A. van Wamel, C.J. Slager, P.W. Serruys, A.F.W. van der Steen and R. Krams. Monocyte Adhesion in Atherosclerosis: A Biomechanical Approach.
Vascular Disease Prevention. 2005; 2(3):227-235.

R. Krams, D. Segers, B.M. Gourabi, W. Maat, *C. Cheng*, C. van pelt, L.C.A. van Damme, P. de Feyter, A. F. W. van der Steen, C.L. de Korte, P.W. Serruys. Inflammation and atherosclerosis: mechanisms underlying vulnerable plaque.
J Interv Cardiol. 2003 Apr;16(2):107-13.

S.G. Calier, L.C.A. van Damme, C.P. Blommerde, J.J. Wentzel, G. van Langehove, S. Verheye, M.M. Kockx, M.W. Knaapen, *C. Cheng*, F. Gijsen, D.J. Duncker, N. Sterngiopulos, C.J. Slager, P.W. Serruys, R. Krams. Augmentation of wall stress inhibits neointimal hyperplasia after stent implantation: inhibition through reduction of inflammation?
Circulation. 2003 Jun 3;107(21):2741-6.

Abstracts and Presentations:

C. Cheng, D. Tempel, L. van Damme, K van Gaalen, R. van Haperen, R. de Crom, R. Krams. Angiotensin II induces severe intra-plaque hemorrhages in lesions with a vulnerable plaque phenotype in apoE KO mice.
Circulation 2005; 112:II-165.
Presented at the American Heart Association Congress, Dallas 2005

C. Cheng, D. Tempel, L. van Damme, R. van Haperen, R. Krams, R de Crom.Vunerable lesions induced by low shear stress are characterized by expression of specific inflammatory chemokines.
Circulation 2005; 112:II-82.
Presented at the American Heart Association Congress, Dallas 2005

C. Cheng, D. Tempel, L. van Damme, R. van Haperen, R. Krams, R de Crom. Patterns of fluid shear stress determine atherosclerotic lesion size and vulnerability.
Circulation 2005; 112:II-292.
Presented at the American Heart Association Congress, Dallas 2005

C. Cheng, D. Tempel, L.C.A. van Damme, R. van Haperen, R. Krams, R. de Crom. Patterns of fluid shear stress determine atherosclerotic lesion size and vulnerability.
Vasculaire Geneeskunde 2005; 2:30.
Presented at the Dutch Atherosclerosis Society Symposium, Ermelo 2005

C. Cheng, R. van Haperen, M. de Waard, R. de Crom, R. Krams. In vivo induced changes in shear stress patterns affect the expression and the intracellular localization of endothelial nitric oxide synthase.
Eur. Heart. J. 2004; 25:58.
Presented at the European Heart Congress, München 2004

C. Cheng, M. de Waard. R. van Haperen, D. Tempel, A. van der Baan, R. Krams, R. de Crom. In vivo induction of low shear stress and oscillatory shear stress causes atherosclerosis.
Circulation 2004; 110:III-39.
Presented at the American Heart Association Congress, New Orleans 2004

C. Cheng, R. van Haperen, M. de Waard, R. de Crom, R. Krams. ENOS expression responds to changes in shear stress: direct demonstration in a novel in vivo mouse model.
Circulation 2003; 108: IV-151.
Presented at the American Heart Association Congress, Orlando 2003

C. Cheng, R. van Haperen, M. de Waard, R. de Crom, R. Krams. ENOS expression responds to changes in shear stress: direct demonstration in a novel mouse model.
Presented at the 14th endothelium research symposium, Amsterdam 2003

C. Cheng, R. van Haperen, M. de Waard, R. de Crom, R. Krams. ENOS expression responds to changes in shear stress: direct demonstration in a novel mouse model.
Vasculaire Geneeskunde 2003; 2:14.
Presented at the Dutch Atherosclerosis Society Symposium, Ermelo 2003